

**A biomimetic collagen membrane for delivery of
mesenchymal stem cells and growth factors for large
fracture repair**

Katrina Marie Moisley

Submitted in accordance with the requirements for the degree of
Doctor of Philosophy as part of the integrated PhD with MSc in
Tissue Engineering and Regenerative Medicine.

The University of Leeds
Institute of Biological and Medical Engineering

May 2019

The candidate confirms that the work submitted is her own and that appropriate credit has been given where reference has been made to the work of others.

This copy has been supplied on the understanding that it is copyright material and that no quotation from the thesis may be published without proper acknowledgement.

© 2019 The University of Leeds and Katrina Marie Moisley

Acknowledgements

I would first like to thank my thesis advisors Peter Giannoudis, Elena Jones, Stephen Russell and Giuseppe Tronci. In particular, I am gratefully indebted to Elena Jones, whose office door was always open for help and guidance.

I would also like to acknowledge my fellow researchers at the Leeds Institute of Rheumatic and Musculoskeletal Medicine; Thomas Baboolal, Richard Cuthbert, Ola Altaie, Heather Owston, Jehan El Jawhari, Payal Ganguly, Dragos Ilas, Daniel Perez Witzke, Zoe Wigston and Rekha Parmar. My thanks also goes to the Engineering and Physical Science research council (EPSRC) for my studentship.

And last but not least, to my steadfast parents; Anne-Marie and Michael, and to my Grandmother Poppy, who always encouraged me to be better and to whom I owe it all.

Abstract

This study aimed to engineer a collagen membrane scaffold for the delivery of platelet rich plasma (PRP) and bone marrow derived mesenchymal stem cells (BM-MSCs) for complex fracture repair. The design of the guided bone regeneration device was based on the microarchitecture of the induced membrane which was found to be rich in high organised collagen fibres and have less distinct bi-layer organisation than expected. This contributed towards the design, optimisation and manufacturing of a working prototype made of 70% collagen and 30% polycaprolactone (PCL) using novel needleless-electrospinning technology. The scaffolds produced had substantial mechanical properties and were found to be biocompatible. The scaffold was also found to be made up of nano-scale fibres and sub-micron pores which acted as a barrier. The scaffold can be tailored using laser cutting to incorporate pores as well as folding and heat-treating the scaffold to increase the construct's thickness. PRP was also optimised as a biological signalling product to maximise BM-MSCs migration and proliferation at the site of injury. Removal of leukocytes was not found to improve cell migration or proliferation as expected and all platelet products tested induced significantly more cell migration than fetal calf serum (FCS). Most promising was the experiments that combined the platelet products, BM-MSCs and scaffolds, which found that the loaded scaffolds were effectively able to support rare BM-MSCs colony formation from bone marrow aspirate. These promising findings indicate that this scaffold could be effectively translated in future treatment of bone reconstruction alongside clinical standard PRP.

Abbreviations

Abbreviation: **Full form:**

ACD-A	Acid citrate dextrose
BCA	Bicinchoninic acid
BSA	Bovine serum albumin
BMA	Bone marrow aspirate
BM-MSC	Bone marrow derived mesenchymal stem cell
BMP	Bone morphogenic protein
CFU-F	Colony forming units- fibroblast
C-PL	Commercial platelet lysate
C-PRP	Commercial platelet rich plasma
DMSO	Dimethyl sulfoxide
DMEM	Dulbecco's Modified Eagle Medium
ECO	Endochondral ossification
EDTA	Ethylenediaminetetraacetic acid
EM	Expansion media
ES	Electrospinning
fPL	Filtered platelet lysate
fPRP	Filtered platelet rich plasma
GBR	Guided bone regeneration
GFs	Growth factors
H&E	Haematoxylin and Eosin
HFIP	Hexafluoroisopropanol
IM	Induced membrane
LEUK	Leukocytes
OD	Optical density
PBS	Phosphate buffered saline

PCL	Polycaprolactone
PL	Platelet lysate
PLT	Platelets
PPP	Platelet poor plasma
PRP	Platelet rich plasma
PSR	Picro Sirius red
SBF	Simulated body fluid
SEM	Scanning electron microscope
TGF- β1	Transforming growth factor beta 1
VEGF	Vascular endothelial growth factor

Table of Contents

Acknowledgements	iii
Abstract	iv
Abbreviations	v
Table of Contents	vii
1 Introduction	1
1.1 Bone physiology:	1
1.2 Fracture Repair:	2
1.3 Clinical need:	3
1.4 Adult Stem cells and MSCs:	4
1.4.1 Mesenchymal Stem Cells:	5
1.4.2 BM-MSc variability:	5
1.5 Growth Factors and Chemokines:	6
1.5.1 Main GFs and chemokines involved in bone fracture repair:	7
1.6 Platelets and platelet-rich plasma (PRP):	8
1.7 Induced Membrane and Biomimetic Scaffolds:	10
1.7.1 Biomimetic Scaffolds:	10
1.8 Electrospinning a collagen scaffold:	11
1.9 Mechanical Stability:	13
1.10 Other factors affecting bone regeneration:	14
1.11 Hypothesis and aims:	15
1.12 References:	16
2 Materials and Methods	21
2.1 Sample collection:	21
2.2 Bone marrow aspirate (BMA) sample collection	21
2.3 Whole blood sample collection:	22
2.4 C-PRP sample collection:	23
2.5 Induced membrane and periosteum samples	24
2.6 Processing bone marrow nucleated cells (NCs) for storage:	25
2.7 Processing BM nucleated cells for culture:	25
2.8 Colony-forming unit-fibroblast (CFU-F) assay:	26
2.9 XTT assay:	26
3 Characterising the naturally induced membrane	28
3.1 Introduction:	28
3.2 Chapter specific methods:	31

3.2.1	Tissue processing for histology:.....	31
3.2.2	Fixing:	32
3.2.3	Embedding and sectioning:.....	32
3.2.4	Tissue staining:.....	33
3.2.5	Haematoxylin and eosin stain	34
3.2.6	Picro sirius red stain.....	35
3.2.7	Verhoeff van gieson stain.....	36
3.2.8	Microscopy and imaging:	37
3.2.9	Histology measurements:.....	37
3.2.10	Polarized light microscopy:.....	38
3.2.11	Statistics.....	39
3.3	Results	39
3.3.1	Characterisation of the bilayer membrane structure:	39
3.3.2	Polarised light microscopy:	44
3.3.3	Elastin content of IM:	47
3.3.4	Characterisation of IM's maturity:.....	49
3.4	Discussion:	51
3.5	References:	54
4	Manufacture and process-structure relationships of the collagen-poly(ϵ-caprolactone) membrane	56
4.1	Introduction:.....	56
4.2	Specific methods	60
4.2.1	Isolation of type I collagen from rat tail tendons:	60
4.2.2	Electrospinning solutions:	61
4.2.3	Free-surface electrospinning:.....	61
4.2.4	Gas liquid displacement porometry using the Porolux:.....	62
4.2.5	Post-manufacture processing (folding and laser cutting):.....	63
4.2.6	Scanning electron microscopy (SEM):	65
4.2.7	SEM microarchitecture analysis:	65
4.2.8	Energy-dispersive X-ray spectroscopy (EDS):	65
4.2.9	Thickness measurement:.....	66
4.2.10	Tensile testing:.....	66
4.2.11	Scaffold degradation assay:	68
4.2.12	Statistics.....	68
4.3	Results:	68
4.3.1	Optimising electrospinning parameters:	69

4.3.2	Optimising spinning blended collagen and PCL solutions	71
4.3.3	Pore size analysis:	74
4.3.4	Mechanical properties of the laser cut scaffolds	76
4.3.5	Comparing the properties of 70:30 scaffolds with different laser cut pore densities	79
4.3.6	Comparing the properties of PCL scaffolds with different laser cut pore densities	80
4.4	Discussion	83
4.5	References:	87
5	Biological products.....	90
5.1	Introduction:.....	90
5.2	Specific methods:	91
5.2.1	Blood collection and generation of PRP:	91
5.2.2	Generating commercial PRP (C-PRP):	92
5.2.3	Generating filtered PRP (fPRP):.....	93
5.2.4	Leukocyte and platelet stability assay:	93
5.2.5	Analysing blood and PRP samples:	94
5.2.6	Generating PL and C-PL and fPL:.....	94
5.2.7	BM-MSX XTT Proliferation assay:	94
5.2.8	Migration assays:	95
5.2.9	Statistics	96
5.3	Results:	97
5.3.1	Cellular composition of PRP and fPRP:	97
5.3.2	PRP stability:	99
5.3.3	Optimising XTT proliferation assay:	101
5.3.4	Comparing PL's vs fPL's ability to induce BM-MSX proliferation:.....	108
5.3.5	Developing a migration assay towards PL supplemented media using the IncuCyte device:	111
5.3.6	Comparing PL's and fPL's ability to induce migration in BM- MSCs:.....	119
5.3.7	In-house and commercial PRP cell compositions:.....	123
5.3.8	Comparing PL's and C-PL's ability to induce BM-MSX proliferation:.....	127
5.3.9	Comparing PL and C-PL's ability to induce BM-MSX migration:.....	130
5.4	Discussion:	133
5.5	References:	136

6	Functionality testing of scaffolds	140
6.1	Introduction:.....	140
6.2	Specific Methods:	142
6.2.1	Scaffold eluate XTT cytotoxicity assay:.....	142
6.2.2	Scaffold eluate proliferation assay:	142
6.2.3	Scaffold absorbance of PL:.....	143
6.2.4	Scaffold release of PL:.....	143
6.2.5	Scaffold release of PL – sample collection.....	144
6.2.6	Scaffold release of PL – Bicinchoninic acid (BCA) assay:	144
6.2.7	Scaffold release of PL – Analysis.....	145
6.2.8	Protein quantification in 10% PL:	146
6.2.9	Degradability:.....	147
6.2.10	PRP loaded scaffold CFU-F proliferation assay:.....	147
6.2.11	Statistics.....	148
6.3	Results:	148
6.3.1	Cytotoxicity:	149
6.3.2	Effect of the scaffold on BM-MSc proliferation:.....	150
6.3.3	Measuring the scaffold’s ability to absorb PRP:	151
6.3.4	Release:	151
6.3.5	Assessment of the scaffold’s degradation profile:	154
6.3.6	Loaded scaffold ability to support colony formation:	156
6.4	Discussion:	159
6.5	References:	161
7	Conclusions	164
7.1	References:.....	167
8	Appendix 1	169
8.1	Standard solutions:.....	169
9	Appendix 2:	170
9.1	Consumables:	170
9.2	Equipment:	171
9.3	Solutions:	173
10	Appendix 3	175
10.1	Patient Consent form.....	175

1 Introduction

The designing and engineering of a collagen membrane scaffold for the delivery of platelet rich plasma (PRP) and bone marrow derived mesenchymal stem cells (BM-MSCs) for fracture repair is an interdisciplinary project that encompasses various fields of research including, engineering, materials and textiles, anatomy and biology. To bring these research areas together for this project, this introductory review provides an outline of the current understanding of bone fractures and the factors involved in their repair.

1.1 Bone physiology:

The human skeleton constantly remodels itself to maintain a homeostasis between its main functions; providing strong mechanical support to the body and supplying the body with calcium via resorption of old bone and laying down new bone. This process is carried out by three main cell types; osteoclasts, osteoblasts and osteocytes. Detection of increased hormone and cytokine levels activate pre-osteoclast cells to differentiate into osteoclasts ^[2] and attach to the bone. Once attached, osteoclasts break down the bone matrix via acidification and enzymatic breakdown to re-release the ions. Osteoblasts are similarly activated to differentiate from osteoblast precursor cells, also termed mesenchymal stem cells (MSCs), by stimulants such as in full bone morphogenetic protein-2 (BMP-2) to form new bone ^[2]. Osteoblasts deposit bone by secreting type 1 collagen and osteocalcin, the building blocks essential for mineral deposition ^[3]. The deposited bone accumulates around the osteoblast trapping it whilst it differentiates into an osteocyte. The embedded osteocyte forms long processes along the canaliculi network of the osteons which help it to detect and communicate mechanical and chemical signals ^[4] as well as release its own signals to stimulate and inhibit bone growth ^[5]. These cells interact constantly to create tissue, which in turn supports the cell attachment, proliferation and differentiation necessary for bone remodelling.

With regards to the anatomy of bone, they are usually composed of three main regions; the periosteum, cortical bone, and trabecular bone. Firstly, surrounding the bone is the periosteum tissue with its superficial fibrous layer and inner cellular layer ^[6] this tissue is highly vascularised and a rich source of osteogenic progenitor cells required for regeneration ^[7]. Periosteum also has a specialised mechanosensory role and is able to activate osteogenic differentiation of local

MSCs when under strain, for example when damaged during fracture [8]. Cortical bone is made up of the hydroxyapatite bone matrix secreted by osteoblasts which accumulate to form densely packed concentric mineralised osteons interspersed with lacunae and haversian canals. It is the cortical bone's solid structure which allows bone to function as a mechanical support system to the body. Trabecular (or cancellous) bone is found toward the centre of long bones such as the femur and flat bones like the skull and iliac crest of the pelvis. It consists of mineralised trabeculae that align in the direction of stress into the bone marrow, it is less dense than cortical bone and its porous structure provides a high-surface area for cell attachment and proliferation [9] Because of their porous structure and large surface area, trabecular bones (the iliac crest in particular) are a rich source of bone marrow derived MSCs (BM-MSCs) for clinical and research applications [10, 11].

1.2 Fracture Repair:

Despite bone's strong structure, it is still susceptible to damage and fracture. Most fractures are small in size and the body is able to repair them via two mechanisms: intramembranous ossification (IMO) and endochondral ossification (ECO). IMO occurs in mechanically stable fractures and is characterised by MSCs migrating from the periosteum or the bone marrow to the fracture [12] and differentiating into osteoblasts [13] to develop new bone. ECO occurs in non-stabilised sites and sees MSCs initially differentiate into chondrocytes which lay down a hyaline cartilage template around the defect forming a protective callus [14]. After an initial loss of blood flow to the injury, vascularisation to the callus increases due to the hypertrophic chondrocytes secreting the angiogenic growth factors; vascular endothelial growth factor (VEGF) and platelet derived growth factor (PDGF) which stimulates angiogenesis and allows the infiltration of osteogenic committed MSCs. These progenitor cells differentiate into osteoblasts and secrete the extracellular matrix to first form an immature poorly-mineralised bone which is later remodelled into mechanically competent bone tissue [12].

Immature bone is first rapidly secreted in a coarse, woven structure with a non-uniform collagen arrangement to partially restore the bone's functional properties and is later resorbed and restructured into highly organised lamellar bone. Once the cartilage callus has completely ossified, osteoclasts resorb the excess bone, returning the defect to its original shape. However, some fractures are too large or the patient has co-morbidities that prevent the defect from healing, known as complex fractures and require clinical intervention.

1.3 Clinical need:

Arising from injury and age-related diseases, fractures are highly prevalent in all societies and are a particular burden on public health services, costing an estimated £726 million in the UK in 2000 alone ^[15]. Furthermore, despite the significant improvements in treatment and fracture healing techniques, it has been estimated that 5–10% of all patients with long bone fractures will develop impaired fracture healing processes, such as delayed healing and non-union ^[15]^[16, 17]. A range of techniques currently exist to minimise complications and increase bone healing, examples include internal fixation using metal plates and screws, and external fixation using the Ilizarov technique (extending an external frame to distract the fracture ends) ^[18, 19] for critical sized defects (CSD). A CSD is defined as bone loss greater than 2.5cm ^[20] or as a defect that will not heal unaided. In conjunction with these fixation devices, cancellous bone autografts are often used to fill the defect site and provide a scaffold for regeneration. Commercial scaffolds such as decellurised allogeneic, xenogeneic bone chips and synthetic materials are also used for larger defects but autografts are considered the gold standard because of their efficacy and safety ^[11].

If the fracture site is infected an antibiotic loaded bone cement is first used to stabilise the bone whilst the infection is treated. It was observed that by using this technique, a naturally induced membrane (IM) forms around the fracture. By carefully removing the cement and retaining the IM, the defect gap can be filled with autograft bone and a commercial scaffold material loaded with autologous bone marrow (BM) aspirates, this two-step process is known as the Masquelet technique ^[21]. It has been shown that the IM which forms around the cement spacer can be used as a protective membrane to retain the grafted material and act as a guided bone regeneration device. However, this technique is limited not only by the need of a cement spacer, and therefore two surgeries, but also by the rarity of MSCs in the grafted material which is poorly controlled and also varies significantly between patients. All these techniques described aim to manage and repair bone defects by incorporating basic tissue engineering principles that utilise stem cells, growth factors (GFs), scaffolds and mechanical stability as outlined in the diamond concept ^[1] shown in figure 1.

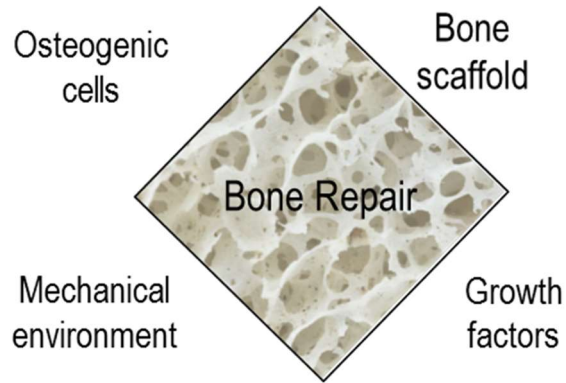


Figure 1: Adapted from Giannoudis et al. The diamond concept [1] which outlines the fundamental principles of bone regeneration.

Specifically for bone healing, the presence of stem cells with osteogenic potential, osteo-inductive GFs, osteo-conductive scaffolds and sufficient mechanical stability around the defect site initiates a range of complex pathways which facilitate bone healing. However, despite the wide range of products and techniques available, there is still significant room for optimisation of the bone regeneration process. This review will cover each principle of the diamond concept to outline our current understanding and identify key areas of further research.

1.4 Adult Stem cells and MSCs:

Stem cells are defined as undifferentiated cells which are able to remain unspecialised and self-renew indefinitely during the organism's lifetime. Once activated, they can differentiate into a range of cell lineages depending on their classification. Totipotency is a rare characteristic only found in zygotes and allows these cells to differentiate into any and every cell in the human body. Pluripotency is limited to embryonic stem cells and enables them to differentiate into any somatic cell type except cells forming extra-embryonic tissues [22]. Multipotent cells have the most limited differentiation abilities of the stem cell classes as they can only differentiate down the cell lineage they are a progenitor for, for example, bone resident mesenchymal stem cells (BM-MSC) can only differentiate into chondrogenic, osteogenic and adipogenic cells [23, 24]. BM-MSCs, although a rare population of cells making up just ~0.001–0.01% cells in the bone marrow aspirates [25], their trilineage potential and role in laying down new bone has made them the focus of bone tissue engineering and regeneration research.

1.4.1 Mesenchymal Stem Cells:

Mesenchymal stem cells (MSCs), which are also sometimes referred to as 'stromal cells' are characterised by their ability to adhere to plastic ^[25], differentiate into osteoblasts, adipocytes and chondroblasts *in vitro* ^[26], express CD73, CD90 and CD105 and lack the expression of CD45, CD34, CD14 or HLA-DR surface markers ^[27]. They were first identified as a result of experiments throughout the 1960's and 1970's by Alexander Friedenstein who extracted them from bone marrow aspirate (BMA) and discovered their ability to differentiate down multiple lineages depending on experimental *in vitro* influences ^[28]. Since their initial discovery and characterisation, MSC-like cells have been found in essentially all post-natal human tissues ^[29] although their differentiation potentials differ depending on the host tissue's location. The cell's differences in differentiation potential has been demonstrated by Kellner *et al.* who used a calcium deposition stain (alizarin red) and found that although the cells are morphologically similar they vary in functionality ^[30]. This work has more recently been superseded by, and enhanced, by numerous *in vivo* studies that support MSCs unique differentiation potential and demonstrate their self-renewal capabilities ^[31, 32].

However, the current understanding of MSCs and their differences is inadequate because of a majority of the evidence is based on experiments using cultured-expanded MSCs which is known to alter their gene expression ^[33, 34], cell surface markers ^[35], morphology ^[36], and functionality ^[34, 37] as they adapt to the *in vitro* environment. This is not only a misleading representation of the *in vivo* environment, but also almost impossible to replicate in the clinic because of current health and safety regulations of the Medicines and Healthcare Products Regulatory Agency's (MHRA). Once a patient's bone marrow or blood sample leaves the theatre and enters the lab for culture expansion of MSCs it becomes an advanced therapeutic medicinal product (ATMP) and its use is highly restricted. To overcome these restrictions, current research is focusing on using uncultured bone marrow which has been aspirated from a patient's iliac crest during surgery and can be concentrated to enrich BM-MSC s for delivery to the fracture site.

1.4.2 BM-MSC variability:

BM-MSCs make up between 0.001- 0.01% of aspirated mononuclear cells in adult humans ^[25, 38] and it is thought there are even less in donors whose health is

compromised, particularly those with systemic bone diseases such as osteoporosis. This is based on animal data from osteoporotic mice which suggests that bone diseases causes a change in the BM-MSCs' morphology and slows their growth and proliferation rate [39], but no significant difference has been found in humans in other diseases such as leukemia [40] or neurodegenerative disorders such as amyotrophic lateral sclerosis [41]. Another factor which can cause variation in BM-MSCs between patients is age. A recent review by Ganguly et al. describe how not only the quantity, but also the quality of BM-MSCs declines with age having knock-on effects linked to osteoarthritis and osteoporosis [42] number and "fitness" of mesenchymal stromal cells (MSCs) in the bone marrow (BM) niche has been suggested as one of the factors contributing to bone abnormalities in OP and OA. Their work summarised that for older donors, their cells could be 'rejuvenated' following exposure to a younger donor's blood serum.

The quality of the sample is also cause of variation as it can be prone to dilution with peripheral blood (haemodilution) as bleeding into the extraction site is unavoidable [40]. To minimize contamination with blood, it is recommended that small volumes (<5 ml) are aspirated, ideally only 1 ml as this has been found to be the most MSC abundant volume [43, 44]. Because of this variability in an already rare cell population, bone regeneration therapies have historically focused on providing more autogenous BM-MSCs directly from aspirates by concentrating MSCs using various volume reduction techniques. Recently however, there has been a shift in attention to attracting neighbouring MSCs to the site of repair through the use of chemokines and GFs most notably released from platelets.

1.5 Growth Factors and Chemokines:

GFs are proteins which are manufactured and secreted by nucleated cells and platelets which can bind to specific transmembrane receptors on target cells. Once bound, they initiate a range of cell signalling pathways activating target genes such as the osteogenic transcription factor *Runx2* which are responsible for cell fate changes including proliferation, migration and differentiation. Specific GFs which have already been linked to bone regeneration include insulin-like growth factor 1 (IGF-1), platelet-derived GFs (PDGFs), vascular endothelial growth factor (VEGF), bone morphogenic protein 2 (BMP-2) and transforming growth factor-beta 1 (TGF- β 1) to name a few.

1.5.1 Main GFs and chemokines involved in bone fracture repair:

IGF-1 is a small 'growth-promoting' peptide which regulates signalling pathways resulting in the production of insulin receptor substrate one and two (IRS2) [45] which knockout studies in mice found reduced overall bone mass suggesting their role in bone maintenance [46]. PDGF is a family of dimeric proteins which include the isoforms: AA/AB/BB/CC and are released in high concentrations from platelets at the site of trauma [47]. PDGF's role in bone repair is to activate MSC proliferation [48] as well as act as a chemoattractant to recruit other cells to the site of fracture [49]. VEGF regulates vascularisation and angiogenesis during bone formation to provide nutrients and transport for the migrating cells [50]. BMP-2 is a key growth factor which regulates osteoblast differentiation and bone repair and disruption of its expression is an underlying contributor to many adult bone pathologies such as osteopenia, osteoarthritis and calcification of the vasculature [51]. TGF- β 1 protein has also been closely linked to bone repair since several studies in human patients have found significantly elevated TGF- β 1 concentrations circulating in the peripheral blood following injury and have stayed elevated for months after [52]. Knock-out studies of these GFs have found that not only are all these GFs involved in bone remodelling and repair, but that they also work in combination and enhance each other's function. Single knock-outs results in some decrease in function but rarely function is completely lost [53].

These GFs also act alongside chemokines, a sub-set of a cytokines whose role it is to induce chemotaxis in nearby cells and include interleukin-8 (IL8), chemokine ligand 5 (CCL5/RANTES), tumor necrosis factor alpha (TNF α), soluble intracellular adhesion molecule (sICAM) and stromal cell-derived factor 1 (SDF-1). SDF-1, sometimes referred to as CXCL12, is particularly important in recruiting MSCs by binding to the CXCR4 receptor [54]. As a whole, these molecules also work by exacerbating inflammation to the site of injury by additionally attracting innate and adaptive immune cells as well as aiding migration and MSC adhesion to the trauma site. Immune cell response at the fracture site is necessary to remove necrotic cells and debris as well as to activate osteoclasts to remove dead bone, however, excessive production of immune cell-produced cytokines such as TNF α and interferon gamma (IF γ) is also known to inhibit MSC osteogenesis.

The majority of these GFs and chemokines are readily distributed where needed by platelets, but due to the down regulation of chemokine receptors in culture expanded BM-MSCs their exact mechanisms of action is difficult to study *in vitro* [55]. For example, a study in rats found that expression levels of the chemokine

receptors CCR1, CCR2, and CXCR4 in BM-MSCs was four times lower after four passages than in freshly cultured BM-MSCs [56]. Because of this down regulation, some research groups are focusing on first over-expressing chemokine receptors before culturing as a novel way to increase MSC sensitivity to chemotactic signals. This method involves first isolating the BM-MSCs and then increasing gene expression of their chemokine receptors using either recombinant protein or viral vectors. However, despite findings of improved MSC migration and accelerated wound-healing [57], this technique is extremely costly, time-consuming and labour intensive so is yet to be perfected as a treatment strategy.

1.6 Platelets and platelet-rich plasma (PRP):

Platelets are small fragments of megakaryocytes found in abundance (150–400×10⁹ platelets/L) in the peripheral blood. These anucleate cells are the smallest in the blood, 0.5 – 3 µm in size and discoid in shape [58]. Their major function is to generate and release proteins by means of their secretory granules when chemically activated via their numerous and highly sensitive membrane receptors. One of the most common activators following trauma is thrombin which acts on the platelets' PAR1 and PAR4 receptors prompting them to change shape and release GFs [59]. Platelets' capacity to produce a range of proteins, their significant concentration in the peripheral blood and ease of collection makes them an ideal source of GFs and chemokines alongside other fracture repair techniques. Platelets can be utilised as an orthopaedic therapy in the form of autologous platelet rich plasma (PRP) which can be generated in the laboratory and in surgery from a patient's whole peripheral blood. In the clinical setting, whole blood is collected using the BioCUE device and centrifuged at 1100g for 15 min. Following centrifugation, supernatant is removed and the platelet containing fraction can be extracted using a syringe resulting in reported increases in platelet concentrations up to 4-fold greater than baseline [60, 61].

DeLong *et al.* classified PRP into four groups depending on their fold increase and end platelet concentration whereby; low PRP was anything below a two fold increase, moderate PRP was between a one to four fold increase, high PRP was between four to six fold and very high was anything greater than a six fold increase [62]. However this system is limited by the lack of a definitive 'optimum' platelet concentration and therefore assumes that the more platelets, the better despite some papers finding that osteoblast proliferation plateaus after 2.5 fold increase

and diminishes at greater concentrations indicating potentially biologically adverse effects ^[63]. The DeLong study also developed the PAW system (platelets, activation, and white blood cells (WBCs)) which categorises PRP based on platelet quantity, mechanism of activation and the presence of leukocytes. This is an improved system because despite the absence of an optimal platelet quantity, it includes the fixed activation and leukocyte parameters and so considers the ongoing debate about the presence of WBCs.

Whether or not WBCs should be totally depleted to produce 'pure' PRP (pPRP) or concentrated as leukocyte-rich-PRP (L-PRP) is still not clear. The argument for purifying PRP is based on findings that high leukocyte concentrations induce necrotic and inflammatory effects at the site of application ^[64] however some findings are contradictory to this and have found that pPRP's significant anabolic effects increases the formation of scar tissue ^[65] as well as evidence that culture of BM-MSCs in L-PRP increases proliferation compared to in pPRP and PPP ^[66]. The differences in opinion stem from the unclear characterisation of all large cells found in PRP as 'leukocytes' despite the wide range of cells that come under that category. Some of these cells can be beneficial for bone regeneration whereas others can have more harmful effects, so to simply include or exclude all WBCs limits PRP's effectiveness. Polymorphonuclear cells (PMN) for example have catabolic effects on various tissues whereas macrophages have been found to promote MSC's osteoblastic differentiation and fracture repair ^[67]. It may therefore be beneficial to concentrate macrophages in the PRP whilst removing all PMNs. This is just one example of how further research and standardisation is needed to better define each cell type and its role in fracture regeneration.

The lack of understanding comes partly from the lack of standardisation between researchers generating PRP. There is variation in the number and length of centrifugation steps, in platelet extraction techniques, in inclusion or exclusion of WBCs and in their activating methods. The lack of standardisation makes PRP's clinical efficacy unpredictable and *in vitro* findings less translatable to patients.

Activation of the PRP is important to maximise the release of GFs from the platelets which can either be released quickly using high concentrations of thrombin, sodium citrate (SC) or calcium chloride, or slowly with just the intrinsic mechanical and biochemical stimuli of environment. Both release techniques have their advantages and disadvantages. Fast release for example, may only induce a short lived but potent response which has been found *in vitro* to improve osteoblast viability ^[68] and neovascularization ^[69], whereas a slow release brings about a more sustainable but less active response due to clots suppressing growth factor release.

There is still a lot of debate about how to best optimise PRP but it clearly has significant potential to even replace autologous bone marrow in improving bone regeneration in patients by creating an optimal niche for cell proliferation as well as an effective attractant for endogenous MSCs. However, platelets aren't entirely responsible for generating all the proteins necessary for bone repair since they lack factors such as BMP-2 and parathyroid hormone (PTH) which knock-out studies have found to be upregulated in the osteogenic processes of fracture healing [70, 71]. These proteins will have to come from another cellular source and could be a limiting factor in the efficiency of platelets if used unaccompanied with another treatment.

1.7 Induced Membrane and Biomimetic Scaffolds:

A limiting factor of both PRP and autologous BM-MSCs is their tendency to diffuse away from the site of application which has led to attempts to retaining as much of the GFs and stem cells as possible to the defect site. The natural formation of the induced membrane (IM) as a result of the masquelet technique lends itself perfectly for this use. The IM has a bilayer structure similar to that of periosteum with a deep cellular layer which a study by Cuthbert *et al.* found to stain positive for BM-MSCs [72]. Superficially to the cellular layer is fibrous-collagen layer which seems to act as protection from soft tissue infiltration into the defect site. Both layers are well vascularised and stain well for important GFs and chemokines such as VEGF and SDF-1 [72]. The IM's structure, together with the added PRP and osteogenic cells, which has been shown to induce regeneration [72], creates an enriched environment for guided bone regeneration. This forms the basis of a novel treatment option for fractures using biocompatible scaffolds.

1.7.1 Biomimetic Scaffolds:

For bone, several types of scaffold have been developed; with hard scaffolds being designed to mimic the properties of cancellous bone, and soft scaffolds, which are more flexible and can adhere to or wrap around bone, emulating the environment of the extracellular matrix found in periosteum [6, 73, 74]. Hard scaffolds are usually made up from hydroxyapatite or decellurised xenogenic or allogenic bone which can be mixed with autologous MSCs and PRP and packed into fracture sites to allow new bone growth. Products such as Orthoss (derived from decellurised bovine bone) are already widely available commercially and used regularly in orthopaedic surgery. Soft scaffolds, which usually exist as membranes, are relatively new and only

currently used in dentistry because of their small size and weak mechanical properties. However; since the discovery of the IM, larger stronger membranes are now being developed for fractures. They can be generated from a range of material sources including synthetic polymers such as polyester, natural polymers such as alginate and proteins such as collagen. Because of its biocompatibility, abundance in bone and extracellular matrix ^[75], collagen is the favoured choice for membrane scaffolds. Collagen also has a unique structure hierarchy of triple helices which combine to form fibrils which further combine to form fibres which allows for better control over its final arrangement and degradation rate. Another benefit of collagen is that when it does degrade, its by-products are also biocompatible unlike synthetic polymers which can breakdown into acids and cause oxidative stress ^[76, 77]. Collagen is not without its drawbacks; so far, existing scaffolds of pure collagen lack mechanical strength needed for large orthopaedic applications and the strengthening methods available often involve toxic chemicals and can make the scaffold brittle ^[78]. Due to its protein structure, collagen is also relatively sensitive to temperature and chemical exposure which can cause microscopic alterations and denaturation to its fibres, weakening the final construct. This limits the sterilisation options available by excluding all heat treatments (autoclaving and steam), most chemical treatments (ethylene oxide) and physical treatments (low dose γ -radiation) ^[79] and so as of yet, no perfect option exists. However, despite these disadvantages, the benefits of using collagen are still thought to outweigh the risks, making it the optimal material to manufacture a biomimetic scaffold from.

1.8 Electrospinning a collagen scaffold:

Whilst many methods exist to manufacture scaffolds including additive manufacturing, tissue decellurisation and injection moulding, none offer such fine control over the final micro-architecture of the scaffold as electrospinning (ES). ES is a nano- and micro- fibre forming method from a range of natural and synthetic polymers dissolved in a solvent system ^[80]. As shown in figure 2, the technology involves charging a polymer solution through a needle at high voltage (typically between 20-60kV) until the electrostatic forces cause the polymer solution droplet at the needle tip to deform into a cone shape (taylor cone). From the taylor cone, the charged solution forms a jet and is attracted towards the earthed collector. During this process, the solvent evaporates from the polymer solution leaving a dry mesh of fibres on the collector. This technique enables the production of sub-

micron fibres which are known to possess enhanced mechanical properties compared to the bulk material from which they were processed due to their being stretched in the charged jet ^[81]. Constructs made using this process offer remarkably high surface-area to volume ratios, interconnected pores and a tuneable porosity of up to 90% ^[82]. These properties render a scaffold with vast biomedical applications due to their mechanical properties and resemblance to the extra cellular matrix. Because of this, ES as a manufacturing process has become a vibrant research area in the last decade, particularly in the areas of tissue engineering and regenerative medicine. However, despite its low cost and simplicity, ES's notoriously low fibre production rate is well documented in the literature ^[83], restricting sufficient industrial scale production, as well as the translation of research into 'real world' products and its commercial exploitation. The traditional set-up of a syringe solution container connected to a single needle spinneret are thought responsible for holding back the out-put of this technology as the incorporation of multiple jets isn't possible due to repulsion of the charged jets. A recent advancement in the technology overcomes its limited output by replacing the needle-based setup with an open bath setup – allowing multiple jets to form ^[84]. Furthermore, using needle-less ES (or free-surface ES) increases not only the rate of output through the increased number of jets, but also the volume produced as the volume is no-longer restricted to the volume of a syringe. Free-surface ES has successfully been demonstrated as a practical approach to the mass production of sub-micron fibre containing constructs.

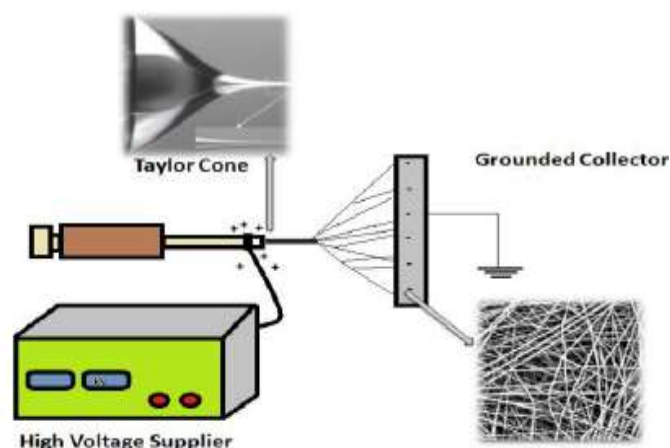


Figure 2: Demonstrating the formation of a Taylor cone from the syringe which separates into multiple jets towards the grounded collector. As the jets evaporate mid-air, a mesh of nano- and micro-fibres form. Figure of needle-based ES adapted from a paper by Yalcinkaya and Callioglu [85].

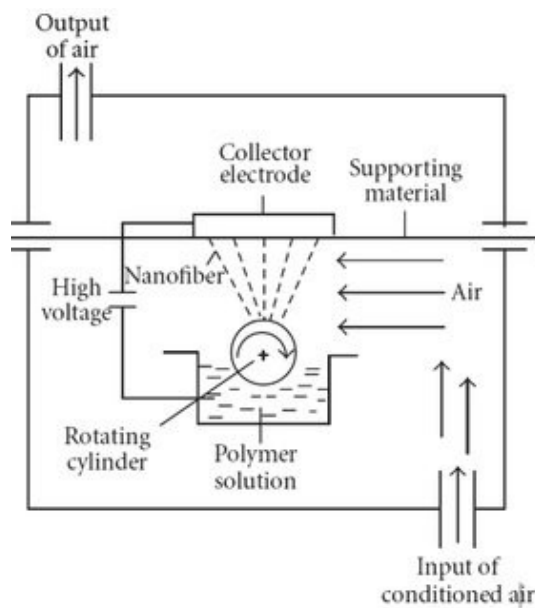


Figure 3: Demonstration of needleless ES using a bath set-up to charge the polymer solution which is attracted towards a grounded collector. This method forms multiple Taylor cones and jets increasing the fibre output. Image adapted from Niu et al [86]

Due to the relatively recent development in this technology, its application in tissue engineering is still in its infancy and, as of yet, its potential for manufacturing biomaterials, particularly collagen-based biomaterials has still been largely unexplored. Optimising the process and parameters is one of the key aims of this work.

1.9 Mechanical Stability:

For optimal regeneration of bone, as well as supplementary stem cells, GFs and scaffolds, the fracture site also needs to be mechanically stable. Stability is vital to facilitate callus formation by ECO in the correct alignment, as well as prevent excessive movement and reduce further tissue damage [87]. There are several options of providing stability to a fracture including intramedullary nailing, external fixation devices and plates, each with their advantages and disadvantages. The choice of fixation device used depends on the location of injury, mechanical stresses and strains carried by the bone and the degree of bone loss. The first option, intramedullary nailing, uses a metal rod inserted into the intramedullary cavity of bone to bridge defects with significant diaphyseal bone loss. This technique preserves the bone's length and allows some micromotions, stresses and

strains which have been found to improve bone regeneration ^[88]. Nailing cannot be used for epiphyseal or metaphyseal fractures or for fractures of the forearm, nor can it be used when the fracture site requires distraction. However an advantage to their use is their application alongside external fixation methods like the Ilizarov technique.

External fixation devices involve frames to distract, lengthen or shorten the bone. It is thought to be a more versatile technique than intramedullary nailing, however the pins used to attach the frame to the bone are prone to infection and require regular, thorough cleaning. These factors, as well as the frame's size and external placement, make it an obtrusive treatment option with poor patient acceptance only used for more extreme cases. An alternative to external fixation is internal plates, a more common choice of treatment for surgeons which uses metal screws to attach metal plates to bones. These plates stabilise the defect site in cases where most of the bone has been preserved. It is also used to prevent and treat non-union and malunion fractures but is less adaptable than the other techniques as it doesn't accommodate any lengthening or shortening.

Ensuring mechanical support of the fracture site is the fourth aspect of the diamond concept; however other factors also play a role in the success of bone healing.

1.10 Other factors affecting bone regeneration:

So far, the main contributors to bone healing have been described; as long as there are cells and GFs available, a scaffold for them to adhere to and a mechanically stable environment, the bone should repair itself. However, the rate at which the bone heals, and the quality of the end result can vary greatly on a range of factors which aren't covered by the diamond concept.

Vascularisation of the tissue plays a key role in determining the success of bone regeneration as it not only provides nutrients and removes waste but also acts as a transport conduit for osteoprogenitors, GFs and importantly, inhibitors of osteoclast activity such as osteoprotegerin ^[65].

Immediately after a fracture, the intraosseous blood supply to the bone is disrupted and pro-inflammatory cascades stimulate the blood vessels in the soft tissue to vasodilate. This increased blood supply to the fracture site not only increases red blood cell delivery of oxygen and nutrients to prevent tissue necrosis, but also initiates the deposition of fibrin and collagen in the formation of a haematoma to

provide mechanical stability and a natural scaffold for cells to adhere and new blood vessels to form [89, 90]. Angiogenesis after fracture is vital in the recruitment of macrophages and other white blood cells in aiding the removal of bone debris, as well as MSCs to form the initial callus and red blood cells to ensure cell and tissue survival. Its importance in bone regeneration is such that, supporting new blood vessel growth is a key characteristic in designing scaffolds that can aid angiogenesis and support the new blood vessels [50, 91].

Other factors to take into account are the patient's health profile and includes their age, physical fitness, health and co-morbidities e.g diabetes or osteoporosis and whether or not the patient smokes. The age of the patient is well understood to impact bone healing. A study in 'juvenile', 'middle-aged' and 'old' mice found that the older mice's tibial fractures expressed fewer angiogenic factors (indicative of diminished vascularisation) and healed slower than the younger mice [92]. Reduced healing is mostly thought to be due to the ageing of MSCs and changes in their morphology and functioning, supported by findings that younger donor's MSCs had better differentiation capacities and are a better source of MSCs than older donors [93]. However, another study also found that the decrease in bone repair in elderly patients may not be due to the decreased functioning of MSCs and osteoblasts, but instead due to the lack of environmental cues for them to differentiate and begin laying down new bone [94]. Elderly patients are also more likely to have co-morbidities which may affect bone regeneration, the most common and detrimental being type 2 diabetes, obesity and osteoporosis [95]. Osteoporosis is a disease that modulates osteoblast activity causing inadequate bone formation and excessive bone resorption resulting in brittle and weak bones. This makes stabilising the injury difficult as well as finding enough autologous graft material to fill the defect. Diabetes mellitus is even more problematic as it also causes brittle bones as well as weaker calluses and delayed healing post-fracture which have been related to reduced expression of TGF- β 1 and BMP-2 [96].

It is clear then that, when thinking about bone trauma, vascularisation and patient characteristics are as significant as the use of osteogenic cells, GFs, scaffolds and mechanical stability in treating fractures and must be carefully considered.

1.11 Hypothesis and aims:

The hypothesis for this study is to develop and test a biomimetic collagen-based membrane to act as a guided bone regeneration device in the treatment of long bone fracture repair when loaded with BMA and PRP.

To address the hypothesis, this project aims to fully characterise the naturally-formed IM (chapter 3), specifically its collagen orientation and architecture; to design and engineer a collagen-based membrane scaffold which mimics the IM (chapter 4); to optimise PRP for supporting BM-MSC survival and migration (chapter 5), and finally to test the interaction and functionality between the cells, PRP and scaffold (chapter 6).

Collectively, the aim of this work is to further the treatment of complex bone fractures and lead to the translation of a clinically relevant medical device.

1.12 References:

1. Giannoudis, P.V., T. Einhorn, and D. Marsh, *Fracture healing: the diamond concept*. Injury 2007. **4**: p. 3-6.
2. Hankenson, K.D., K. Gagne, and M. Shaughnessy, *Extracellular signaling molecules to promote fracture healing and bone regeneration*. Advanced Drug Delivery Reviews, 2015. **94**: p. 3-12.
3. Kular, J., et al., An overview of the regulation of bone remodelling at the cellular level. Clinical Biochemistry, 2012. **45**(12): p. 863-873.
4. Graham, J.M., et al., The Role of Osteocytes in Targeted Bone Remodeling: A Mathematical Model. PLoS ONE, 2013. **8**(5): p. e63884.
5. Neve, A., A. Corrado, and F.P. Cantatore, *Osteocytes: central conductors of bone biology in normal and pathological conditions*. Acta Physiologica, 2012. **204**(3): p. 317-330.
6. Dwek, J.R., The periosteum: what is it, where is it, and what mimics it in its absence? Skeletal Radiology, 2010. **39**(4): p. 319-323.
7. Knight, M.N. and K.D. Hankenson, *Mesenchymal Stem Cells in Bone Regeneration*. Advances in Wound Care, 2013. **2**(6): p. 306-316.
8. Evans, S.F., H. Chang, and M.L. Knothe Tate, Elucidating multiscale periosteal mechanobiology: a key to unlocking the smart properties and regenerative capacity of the periosteum? Tissue Eng Part B Rev, 2013. **19**(2): p. 147-59.
9. Hankenson, K.D., G. Zimmerman, and R. Marcucio, *Biological Perspectives of Delayed Fracture Healing*. Injury, 2014. **45**(0 2): p. S8-S15.
10. Bianco, P., et al., Bone Marrow Stromal Stem Cells: Nature, Biology, and Potential Applications. STEM CELLS, 2001. **19**(3): p. 180-192.
11. Dimitriou, R., et al., Complications following autologous bone graft harvesting from the iliac crest and using the RIA: A systematic review. Injury, 2011. **42**, **Supplement 2**: p. S3-S15.
12. Percival, C.J. and J.T. Richtsmeier, *Angiogenesis and intramembranous osteogenesis*. Dev Dyn, 2013. **242**(8): p. 909-22.
13. Colnot, C., Skeletal cell fate decisions within periosteum and bone marrow during bone regeneration. J Bone Miner Res, 2009. **24**(2): p. 274-82.
14. Thompson, E.M., et al., *Recapitulating endochondral ossification: a promising route to in vivo bone regeneration*. Journal of Tissue Engineering and Regenerative Medicine, 2015. **9**(8): p. 889-902.
15. Donaldson, L., et al., *The epidemiology of fractures in England*. J Epidemiol Community Health 2008. **62**(2): p. 174-180.
16. Tzioupis, C. and P. Giannoudis, *Prevalence of long-bone non-unions*. Injury, 2007. **38**, **Supplement 2**: p. S3-S9.

17. Panteli, M., et al., Biological and molecular profile of fracture non-union tissue: current insights. *J Cell Mol Med*, 2015. **19**(4): p. 685–713.
18. Iacobellis C, Berizzi A, and A. R, *Bone transport using the Ilizarov method: a review of complications in 100 consecutive cases*. . *Strategies in Trauma and Limb Reconstruction*. , 2010. **5**(1): p. 17-22.
19. Ilizarov, G.A., The tension stress effect on the genesis and growth of tissues .1. the influence of stability of fixation and soft-tissue preservation. *Clinical Orthopaedics and Related Research*, 1989(238): p. 249-281.
20. Hossain, N.M., Barry, *Management of traumatic bone loss*. Bone and Joint Research, 2011. **British Editorial Society of Bone and Joint Surgery**.
21. Giannoudis, P.V., et al., Masquelet technique for the treatment of bone defects: Tips-tricks and future directions. *Injury*, 2011. **42**(6): p. 591-598.
22. Li, M. and J.C.I. Belmonte, *Ground rules of the pluripotency gene regulatory network*. *Nature Reviews Genetics*, 2017. **18**: p. 180.
23. Jones, E. and D. McGonagle, *Human bone marrow mesenchymal stem cells in vivo*. *Rheumatology (Oxford)*, 2008. **47**(2): p. 126-31.
24. Jones, E.A., et al., Isolation and characterization of bone marrow multipotential mesenchymal progenitor cells. *Arthritis Rheum*, 2002. **46**(12): p. 3349-60.
25. Malgieri, A., et al., *Bone marrow and umbilical cord blood human mesenchymal stem cells: state of the art*. *International Journal of Clinical and Experimental Medicine*, 2010. **3**(4): p. 248-269.
26. Dominici, M., et al., Minimal criteria for defining multipotent mesenchymal stromal cells. The International Society for Cellular Therapy position statement. *Cytotherapy*., 2006. **8**(4): p. 315-317.
27. Dominici M, et al., Minimal criteria for defining multipotent mesenchymal stromal cells. The International Society for Cellular Therapy position statement. *Cytotherapy*, 2006. **8**(4): p. 315-7.
28. Friedenstein, A., et al., Stromal cells responsible for transferring the microenvironment of the hemopoietic tissues. Cloning in vitro and retransplantation in vivo. *Transplantation*., 1974. **17**(4): p. 331-340.
29. Meirelles, L.d.S., P.C. Chagastelles, and N.B. Nardi, *Mesenchymal stem cells reside in virtually all post-natal organs and tissues*. *Journal of Cell Science*, 2006. **119**(11): p. 2204-2213.
30. Kellner, J., S. Sivajothi, and I. McNiece, Differential properties of human stromal cells from bone marrow, adipose, liver and cardiac tissues. *Cytotherapy*, 2015. **17**(11): p. 1514-1523.
31. Méndez-Ferrer, S., et al., Mesenchymal and haematopoietic stem cells form a unique bone marrow niche. *Nature*, 2010. **466**: p. 829.
32. Sacchetti, B., et al., Self-renewing osteoprogenitors in bone marrow sinusoids can organize a hematopoietic microenvironment. *Cell*, 2007. **131**(2): p. 324-36.
33. Churchman, S.M., et al., Transcriptional profile of native CD271+ multipotential stromal cells: Evidence for multiple fates, with prominent osteogenic and Wnt pathway signaling activity. *Arthritis & Rheumatism*, 2012. **64**(8): p. 2632-2643.
34. Alves, H., et al., A link between the accumulation of DNA damage and loss of multipotency of human mesenchymal stromal cells. *Journal of Cellular and Molecular Medicine*, 2010. **14**(12): p. 2729-2738.
35. Qian, H., K. Le Blanc, and M. Sigvardsson, *Primary Mesenchymal Stem and Progenitor Cells from Bone Marrow Lack Expression of CD44 Protein*. *The Journal of Biological Chemistry*, 2012. **287**(31): p. 25795-25807.
36. Wagner W, Ho AD, and Zenke M, *Different facets of aging in human mesenchymal stem cells*. *Tissue Eng B*, 2010 **16**(4): p. 445-53.

37. Rombouts, W.J.C. and R.E. Ploemacher, Primary murine MSC show highly efficient homing to the bone marrow but lose homing ability following culture. *Leukemia*, 2003. **17**(1): p. 160-170.
38. Rosset, P., F. Deschaseaux, and P. Layrolle, *Cell therapy for bone repair*. *Orthopaedics & Traumatology: Surgery & Research*, 2014. **100**(1, Supplement): p. S107-S112.
39. Goergen, J., et al., Characterization of Bone-Marrow-Derived Stem Cells in Osteoporotic Models of the Rat. *ISRN Stem Cells*, 2013. **2013**: p. 9.
40. Li, J., et al., *Factors Affecting Mesenchymal Stromal Cells Yield from Bone Marrow Aspiration*. *Chinese Journal of Cancer Research*, 2011. **23**(1): p. 43-48.
41. Ferrero, I., et al., Bone Marrow Mesenchymal Stem Cells From Healthy Donors and Sporadic Amyotrophic Lateral Sclerosis Patients. *Cell Transplantation*, 2008. **17**(3): p. 255-266.
42. Ganguly, P., et al., Age-related Changes in Bone Marrow Mesenchymal Stromal Cells: A Potential Impact on Osteoporosis and Osteoarthritis Development. *Cell transplantation*, 2017. **26**(9): p. 1520-1529.
43. Fennema, E.M., et al., The effect of bone marrow aspiration strategy on the yield and quality of human mesenchymal stem cells. *Acta Orthopaedica*, 2009. **80**(5): p. 618-621.
44. Veyrat-Masson, R., et al., Mesenchymal content of fresh bone marrow: a proposed quality control method for cell therapy. *British Journal of Haematology*, 2007. **139**(2): p. 312-320.
45. Hernández-Sánchez, C., et al., The Role of the Tyrosine Kinase Domain of the Insulin-like Growth Factor-I Receptor in Intracellular Signaling, Cellular Proliferation, and Tumorigenesis. *Journal of Biological Chemistry*, 1995. **270**(49): p. 29176-29181.
46. Ogata, N., et al., Insulin receptor substrate-1 in osteoblast is indispensable for maintaining bone turnover. *The Journal of Clinical Investigation*, 2000. **105**(7): p. 935-943.
47. Hart, C.E. and D.F. Bowen-Pope, *Platelet-Derived Growth Factor Receptor: Current Views of the Two-Subunit Model*. *J Investig Dermatol*, 1990. **94**(s6): p. 53s-57s.
48. Tan, H.B., et al., The systemic influence of platelet-derived growth factors on bone marrow mesenchymal stem cells in fracture patients. *BMC Medicine*, 2015. **13**: p. 6.
49. Beckermann, B.M., et al., VEGF expression by mesenchymal stem cells contributes to angiogenesis in pancreatic carcinoma. *British Journal of Cancer*, 2008. **99**(4): p. 622-631.
50. Gerstenfeld, L.C., et al., Fracture healing as a post-natal developmental process: Molecular, spatial, and temporal aspects of its regulation. *Journal of Cellular Biochemistry*, 2003. **88**(5): p. 873-884.
51. Fotinos, A., et al., Competing Repressive Factors Control Bone Morphogenetic Protein 2 (BMP2) in Mesenchymal Cells. *J Cell Biochem*, 2016. **117**(2): p. 439-47.
52. Sarahrudi, K., et al., Elevated transforming growth factor-beta 1 (TGF- β 1) levels in human fracture healing(). *Injury*, 2011. **42**(8): p. 833-837.
53. Cho, T.-J., L.C. Gerstenfeld, and T.A. Einhorn, Differential Temporal Expression of Members of the Transforming Growth Factor β Superfamily During Murine Fracture Healing. *Journal of Bone and Mineral Research*, 2002. **17**(3): p. 513-520.
54. Kitaori, T., et al., Stromal cell-derived factor 1/CXCR4 signaling is critical for the recruitment of mesenchymal stem cells to the fracture site during skeletal repair in a mouse model. *Arthritis & Rheumatism*, 2009. **60**(3): p. 813-823.
55. Wynn, R.F., et al., A small proportion of mesenchymal stem cells strongly expresses functionally active CXCR4 receptor capable of promoting migration to bone marrow. *Blood*, 2004. **104**(9): p. 2643-2645.
56. Alexeev, V., et al., Analysis of chemotactic molecules in bone marrow-derived mesenchymal stem cells and the skin: Ccl27-Ccr10 axis as a basis for targeting to cutaneous tissues. *Cytotherapy*, 2013. **15**(2): p. 171-184.e1.

57. Yang, D., et al., Stromal cell-derived factor-1 receptor CXCR4-overexpressing bone marrow mesenchymal stem cells accelerate wound healing by migrating into skin injury areas. *Cell Reprogram*, 2013. **15**(3): p. 206-15.
58. Semple, J.W., J.E. Italiano, and J. Freedman, *Platelets and the immune continuum*. *Nat Rev Immunol*, 2011. **11**(4): p. 264-274.
59. Coughlin, S.R., *Thrombin signalling and protease-activated receptors*. *Nature*, 2000. **407**(6801): p. 258-264.
60. Dhurat, R. and M.S. Sukesh, *Principles and Methods of Preparation of Platelet-Rich Plasma: A Review and Author's Perspective*. *Journal of Cutaneous and Aesthetic Surgery*, 2014. **7**(4): p. 189-197.
61. Oh, J.H., et al., Comparison of the Cellular Composition and Cytokine-Release Kinetics of Various Platelet-Rich Plasma Preparations. *Am J Sports Med*, 2015. **43**(12): p. 3062-70.
62. DeLong, J.M., R.P. Russell, and A.D. Mazzocca, *Platelet-Rich Plasma: The PAW Classification System*. *Arthroscopy: The Journal of Arthroscopic & Related Surgery*, 2012. **28**(7): p. 998-1009.
63. Graziani, F., et al., *The in vitro effect of different PRP concentrations on osteoblasts and fibroblasts*. *Clinical Oral Implants Research*, 2006. **17**(2): p. 212-219.
64. Sundman, E., B. Cole, and L. Fortier, Growth Factor and Catabolic Cytokine Concentrations Are Influenced by the Cellular Composition of Platelet-Rich Plasma. *Am J Sports*, 2011. **39**: p. 2135-2140.
65. Zhou, Y., et al., The differential effects of leukocyte-containing and pure platelet-rich plasma (PRP) on tendon stem/progenitor cells - implications of PRP application for the clinical treatment of tendon injuries. *Stem Cell Research & Therapy*, 2015. **6**(1): p. 173.
66. Perut, F., et al., Preparation method and growth factor content of platelet concentrate influence the osteogenic differentiation of bone marrow stromal cells. *Cytotherapy*, 2013. **15**(7): p. 830-839.
67. Vi, L., et al., Macrophages promote osteoblastic differentiation in-vivo: implications in fracture repair and bone homeostasis. *J Bone Miner Res*, 2015. **30**(6): p. 1090-102.
68. Slapnicka, J., et al., Effects of Activated and Nonactivated Platelet-Rich Plasma on Proliferation of Human Osteoblasts In Vitro. *Journal of Oral and Maxillofacial Surgery*, 2008. **66**(2): p. 297-301.
69. Fernandez-Moure, J.S., et al., *Platelet rich plasma enhances tissue incorporation of biologic mesh*. *Journal of Surgical Research*, 2015. **199**(2): p. 412-419.
70. Kidd, L.J., et al., Temporal pattern of gene expression and histology of stress fracture healing. *Bone*, 2010. **46**(2): p. 369-378.
71. McBride-Gagyi, S.H., et al., Bmp2 conditional knockout in osteoblasts and endothelial cells does not impair bone formation after injury or mechanical loading in adult mice. *Bone*, 2015. **81**: p. 533-543.
72. Cuthbert, R.J., et al., Induced periosteum a complex cellular scaffold for the treatment of large bone defects. *Bone*, 2013. **57**(2): p. 484-492.
73. Haddo, O., et al., The use of chondroglide membrane in autologous chondrocyte implantation. *Knee*, 2004. **11**(1): p. 51-5.
74. Stankovic, D., et al., *Use of acellular collagen matrix for the closure of the open oral wound in bone regeneration*. *Journal of Stomatology, Oral and Maxillofacial Surgery*, 2018. **119**(5): p. 446-449.
75. Meyers, M.A., J. McKittrick, and P.Y. Chen, *Structural biological materials: critical mechanics-materials connections*. *Science*, 2013. **339**(6121): p. 773-9.
76. Gentile, P., et al., *Polymeric membranes for guided bone regeneration*. *Biotechnol J*, 2011. **6**(10): p. 1187-97.
77. Ren, T.B., et al., *Absorbable Guided Tissue Regeneration Membranes*. *Progress in Chemistry*, 2010. **22**(1): p. 179-185.

78. Thakur, V. and M. Thakur, Collagen-based materials for pharmaceutical applications, in Handbook of Polymers for Pharmaceutical Technologies, Volume 3, Biodegradable Polymers, V. Thakur and M. Thakur, Editors. 2015, John Wiley & Sons. p. 608.
79. Wiegand, C., et al., Effect of the sterilization method on the performance of collagen type I on chronic wound parameters in vitro. J Biomed Mater Res B Appl Biomater, 2009. **90**(2): p. 710-9.
80. Fang, J., et al., *Applications of electrospun nanofibers*. Chinese Science Bulletin, 2008. **53**(15): p. 2265-2286.
81. Jiang, S., et al., *Electrospun nanofiber reinforced composites: a review*. Polymer Chemistry, 2018. **9**(20): p. 2685-2720.
82. Casanova, M.R., et al., The Use of Electrospinning Technique on Osteochondral Tissue Engineering, in Osteochondral Tissue Engineering: Nanotechnology, Scaffolding-Related Developments and Translation, J.M. Oliveira, et al., Editors. 2018, Springer International Publishing: Cham. p. 247-263.
83. Leach, M.K., et al., *Electrospinning fundamentals: optimizing solution and apparatus parameters*. Journal of visualized experiments : JoVE, 2011(47): p. 2494.
84. Bhattacharyya, I., et al., *Free surface electrospinning of aqueous polymer solutions from a wire electrode*. Chemical Engineering Journal, 2016. **289**: p. 203-211.
85. Yalcinkaya, B. and F. Cengiz Çalloğlu, Fabrication of electrospun PVB/epoxy/MWCNT composite nanofibers. 2012.
86. Niu, H., X. Wang, and T. Lin, Needleless Electrospinning: Developments and Performances. 2011.
87. Keating, J.F., A.H.R.W. Simpson, and C.M. Robinson, *The management of fractures with bone loss*. Bone & Joint Journal, 2005. **87-B**(2): p. 142-150.
88. Braun, B.J., et al., *Fracture healing redefined*. Medical Hypotheses, 2015. **85**(6): p. 940-943.
89. Buza, J.A., 3rd and T. Einhorn, *Bone healing in 2016*. Clin Cases Miner Bone Metab, 2016. **13**(2): p. 101-105.
90. Dimitriou, R., et al., *Bone regeneration: current concepts and future directions*. BMC Medicine, 2011. **9**: p. 66-66.
91. Street, J., et al., *Vascular endothelial growth factor stimulates bone repair by promoting angiogenesis and bone turnover*. Proceedings of the National Academy of Sciences of the United States of America, 2002. **99**(15): p. 9656-9661.
92. Lu, C., et al., *Effect of age on vascularization during fracture repair*. Journal of orthopaedic research : official publication of the Orthopaedic Research Society, 2008. **26**(10): p. 1384-1389.
93. Brohlin, M., et al., Aging Effect on Neurotrophic Activity of Human Mesenchymal Stem Cells. PLoS ONE, 2012. **7**(9): p. e45052.
94. Baht, G.S., et al., Exposure to a youthful circulation rejuvenates bone repair through modulation of [beta]-catenin. Nat Commun, 2015. **6**.
95. Khan, T.S. and L.A. Fraser, Type 1 Diabetes and Osteoporosis: From Molecular Pathways to Bone Phenotype. J Osteoporos, 2015. **2015**.
96. Xu, M., Diabetes mellitus affects the biomechanical function of the callus and. 2016. **49**(1).

2 Materials and Methods

Details of the brands and manufacturers used for the reagents, consumables, equipment and software can be found in the appendices 1, 2, 3 and 4 respectively.

2.1 Sample collection:

Patients undergoing elective orthopaedic surgery with no underlying disease were recruited and gave informed written consent in compliance with the Helsinki Declaration. Ethics committee approval was obtained from the local National Health Service Research & Development Department, National Research Ethics Service, Leeds East Research Ethics Committee for the harvesting of these samples under the NHS Leeds east ethics code: 06/Q1206/127.

2.2 Bone marrow aspirate (BMA) sample collection

BMA was collected from recruited patients (n=11, 5 females and 6 males, median age 40, range 17-63) as outlined in table 1. 4mL of bone marrow were aspirated from the anterior iliac crest using an 11-gauge, bevel-tipped trocar and 10 ml syringe flushed with 1000 U/mL sodium heparin solution. The samples were collected in EDTA vacuettes and inverted to prevent clot formation. Once collected, samples were kept at 4°C and processed within 24 hours before being used in CFU-F assays, proliferation assays, and migration assays.

Table 1: BMA donors

Bone marrow aspirate		
Patient Number	Gender	Age (years)
1	M	63
2	F	54
3	F	39
4	F	69
5	F	23
6	M	19
7	M	49
8	F	45
9	M	26
10	M	17
11	M	31

2.3 Whole blood sample collection:

Whole blood was also collected from patients (n=12, 4 females and 8 males, median age 49, range 19-80) as outlined in table 2. 20-30 mL of blood in 10% ACD-A was drawn in an ACD-A flushed 30 mL syringe and inverted to prevent clotting. The syringe was sealed and stored at 4°C before processing within two hours of collection. The whole blood samples were used to generate 'in-house' PRP and PL in proliferations assays, migration assays and for loading the scaffold.

Table 2: Whole blood donors

Sample ID	Age	Sex	Used to generate
A	30	M	PRP, C-PRP
B	22	M	PRP, C-PRP
C	23	F	PRP, C-PRP
D	34	F	PRP, C-PRP
E	40	M	PRP
F	24	F	PRP, fPRP
G	28	F	PRP
H	28	M	PRP, fPRP
I	44	M	PRP, fPRP
J	33	M	PRP
K	30	M	PRP
L	36	M	PRP

*Platelet rich plasma (PRP, fPRP (filtered PRP), C-PRP (commercial PRP)

2.4 C-PRP sample collection:

C-PRP was also collected from patients (n=4, 2 females and 2 males, median age 27, range 22-34) as outlined in table 2. C-PRP was made in theatre by first drawing 60 mL of whole blood into two 30mL syringes, each containing 3 mL ACD-A to give a final anticoagulant concentration of 10%. The anticoagulated blood was then transferred to the platelet concentration system and centrifuged at 1100 xg for 15 minutes spin step in a specialised in-theatre centrifuge.

Following centrifugation, the PPP fraction is first removed by inverting the device and extracting 25 mL using a syringe at the outlet, then the C-PRP fraction is removed by agitating the device and extracting the remaining 5 mL of C-PRP from the outlet. A 1 mL sample of the C-PRP fraction was collected from each donor in EDTA vacuettes, as well as 1mL of donor-matched whole blood, for analysis using the Hematology-Analyzer. The C-PRP samples were used in BM-MSK proliferation and migration assays as well as for loading onto the scaffolds (chapters 5 and 6). Three patients also donated 20mL of whole blood for the production of 'in-house'

PRP as outlined in section 5.2.1 to enable donor matched comparisons between the two platelet products.

2.5 Induced membrane and periosteum samples

Induced membrane and periosteal biopsies were collected from patients undergoing second stage masquelet surgery specifically with no underlying disease (n=7, 4 females and 3 males, median age 43yrs, range 32-58yrs from the ulna=1, femur=3 and tibia=3) outlined in table 4. The surgical procedure involves debridement of the polymethyl methacrylate cement spacer that was placed during the first surgery from the defect site to expose the IM tissue. An area of 1 cm² IM tissue was carefully harvested adjacent from the muscle followed by careful dissection of 1 cm² periosteal tissue harvested at least 10 cm from the area of the bone defect. Tissues were placed in 5 mL sterile PBS and stored at 4°C until processing up to 4 hours later. Samples were processed for histological analysis, SEM imaging, and polarised light imaging.

Table 3: IM and periosteum donors:

Sample ID	Age	Gender	Location of defect	Weeks in situ
Donor 1	32	M	Femur	14
Donor 2	40	F	Ulna	7
Donor 3	34	F	Tibia	8
Donor 4	44	M	Femur	3
Donor 5	58	M	Femur	17
Donor 6	47	F	Tibia	7
Donor 7	45	F	Tibia	11

2.6 Processing bone marrow nucleated cells (NCs) for storage:

BMA samples were first filtered through a 70 µm filter to remove large debris before being diluted in a 4:1 ratio of ammonium chloride solution to bone marrow. The suspension was mixed until homogenous thoroughly and cooled on ice for 10 minutes to lyse contaminating red blood cells. The cell suspension was then centrifuged (500 xg, 5 min), before washing in 10 mL DMEM and being resuspended in 10 mL DMEM and counted using a haemocytometer. To count the cells, 10 µL of cell suspension was mixed with 10 µL of Trypan blue and 10 µL of the stained cell solution was pipetted onto the haemocytometer. Live cells in the peripheral 4x4 squares were counted. To calculate the number of NCs/mL and in total, the following equation was used:

$$NC \text{ count per mL} = Total \text{ no of cells} \times 10,000 \times dilution \text{ factor } (2)$$

$$Total \text{ NC count} = NC \text{ count per ml} \times volume$$

Equation 1: Calculating number of nucleated cells in bone marrow aspirate

Freezing mix (10%DMSO, 45% FCS, 45% DMEM) was then added to the cells (approximately 1 mL of freezing mix per 20×10^6 cells) and frozen in cryovials using a freezing container at -80°C . After 24 hrs at -80°C vials were moved to liquid nitrogen tanks for long term storage at -175°C .

2.7 Processing BM nucleated cells for culture:

Cells purified from the lysed bone marrow aspirate were seeded into T-25 tissue culture grade flasks at a density of 2.5×10^4 cells/mL in 8 mL Stem Macs media containing 100µg/mL of Penicillin/Streptomycin. Unless stated otherwise, all cell incubations were carried out at 37°C in humidified 5% CO_2 /air. Following a PBS wash after 48 hrs to remove unattached cells, the media was replenished. Adherent cells were expanded with half media changes twice a week and trypsinised when they reached 80% confluence. For expansion, the trypsinised cells were re-plated at a density of 1×10^4 cells/mL up to passage four. Expanded BM-MSCs were used in chapter 5 to assay the proliferative and migratory effects of PRP, and to assess

the quality of BMA of the target population based on BM-MSC number. Expanded BM-MSCs were also used in chapter 6 to investigate the cytotoxic potential of the scaffolds as well as test the scaffold's functionality based on how they support BM-MSC proliferation.

2.8 Colony-forming unit-fibroblast (CFU-F) assay:

To enumerate BM-MSCs, the samples that were collected in up to 4 vacuettes (depending on volume aspirated) were pooled into a single falcon tube and filtered using a 70 μm cell strainer to remove clots. 80 μL of each sample was plated onto duplicate 60 mm x 15 mm dishes with 5 mL of Stem Macs media and kept in an incubator at 37°C. After 48 hours, dishes were washed with 10 mL PBS to remove red blood cells other unattached BM cells and replaced with 5mL Stem Macs media followed by a bi-weekly half media change. After two weeks, the dishes were washed with PBS and fixed in 3 ml of 3.7% formaldehyde for 15 minutes at RT. After fixing, the dishes were covered in 8 mL 1% (w/v) methylene blue solution for 30 minutes at RT, washed with distilled water and left to air dry. Visible colonies made up of at least 50 cells were counted, averaged and multiplied by 12.5 to get the number of colonies/mL.

2.9 XTT assay:

The XTT assay was used to quantify BM-MSC proliferation in the presence of different platelet lysate (PL) products (chapter five) as well as to assay the potential cytotoxicity of the scaffolds (chapter six) whereby a decrease in the number of living cells results in a decrease in the total activity of mitochondrial dehydrogenases in the sample. This decrease directly correlates to the amount of orange formazan formed, as monitored by the optical density at 450nm. In general, cells were seeded in triplicate in a 96 well plate (densities varied depending on specific assay) in 200 μL stem macs media and incubated to allow cell attachment. After 24 hours incubation, the stem macs media was removed, the wells gently rinsed in PBS, and the cells were treated with 200 μL of the treatment media (either PL based for chapter 5 or containing scaffold eluate for chapter 6). Following exposure to the treatment medias (exposure duration depends on whether proliferation or cytotoxicity are being assessed) the wells are replaced with 100 μL of DMEM with 10% FCS and 50 μL of the XTT solution and incubated for 4hrs at 37°C. An aliquot of 100 μL is transferred from each well into the corresponding well of a new plate

which is read on a microplate reader at 450nm and 630nm (reference wavelength). The value for the reference wave at 630nm is deducted from the 450nm reading to give the final optical density (OD).

3 Characterising the naturally induced membrane

3.1 Introduction:

Fracture non-union (sometimes referred to as “delayed union”) is a common complication of a fracture affecting 2-12% of all fracture patients ^[1, 2]; characterised by the absence of fracture healing after 6 months ^[3]. As previously described, for severe non-unions of a critical sized defect the current ‘gold-standard’ treatment involves a two-stage surgical procedure known as the Masquelet technique. In the first surgery, all loose and nonviable tissue is removed and the fracture void is filled with a polymethylmethacrylate (PMMA) cement. Exposure to the cement induces a response from the surrounding tissues which leads to the formation of a bioactive IM. After 4-12 weeks, in a second surgery, the surgeon incises the IM to remove the PMMA cement, the defect void is then filled with osteogenic graft material and internally fixed with metalwork. While this technique has been found to have widespread clinical success, it still requires at least two separate surgeries – which is costly in time and finance and does not always guarantee the induction of a robust membrane [10, 13]. One solution to address these limitations would be to engineer a synthetic biomimetic membrane based on the tissue which is thought to be the key player in the Masquelet techniques’ success; the IM. The IM was chosen as the foundation for the biomimetic scaffold based on its unique structure and role in 1) acting as a guided bone regeneration device, 2) retaining the grafted material to the defect site and 3) acting as a protective layer. Some of its characteristics have already been determined through the study of animal models and human samples, the key findings of which have been outlined in table 6, but there has been little examination carried out on human samples due to the precious nature of the tissue ^[4-6]. Fundamental differences between animal and human tissues such as their size, composition and healing pathways necessitate the need for further analysis of human samples to better understand what its key characteristics are that contribute to its role as a guided bone regeneration tissue. Collectively, the studies describe the IM’s bilayer structure as composed of a thin, densely populated cell layer as well as a larger fibrous layer synonymous to that seen in periosteum tissue which is highly vascular initially but this, and its overall thickness, decrease over time ^[7, 8]. However, as it stands, there is still uncertainty surrounding the development of the tissue, better understanding how it develops will help identify the key features to its success.

Table 4: Induced membrane literature review

Study	Species	IM exposure to PMMA	Main findings
Henrich <i>et al.</i> . 2016	Rat	6 weeks	<ul style="list-style-type: none"> - IM vascularity decreases after 1 month - IM has a bilayer similar to the periosteum, only thicker
Wang <i>et al.</i> . 2015	Rabbit	8 weeks	<ul style="list-style-type: none"> - IM has a bilayer similar to the periosteum, only thicker - Thickness and vascularity of the IM decreases over time
Liu <i>et al.</i> . 2014	Rabbit	8 weeks	<ul style="list-style-type: none"> - IM has a bilayer - Thickness and vascularity decreased after 1 month
Aho <i>et al.</i> . 2013	Human	22 months	<ul style="list-style-type: none"> - Optimal time for performing second-stage surgery is 1 month after PMMA implantation - Tissue vascularity decreased over time
Cuthbert <i>et al.</i> . 2013	Human	8 weeks	<ul style="list-style-type: none"> - IM is a thick, vascularised bilayered structure that resembles periosteum
Viateau <i>et al.</i> . 2006	Sheep	6 months	<ul style="list-style-type: none"> - IM is a highly vascularised collagenous tissue positive for type I collagen
Pelissier <i>et al.</i> . 2004	Rabbit	8 weeks	<ul style="list-style-type: none"> - IM has a distinct bilayer which is highly vascular - IM reaches 'peak' maturity with regard to growth factor release at 1 month

The recent focus on biomimetics in tissue engineering stems from the theory that each tissue's distinctive microarchitecture are critical to their specific functions and therefore need to be fully understood [9, 10]. In non-union fractures especially, there is a need to create an IM surrogate that acts as a focal point for BM-MSc proliferation and migration to the site of injury.

The purpose of this chapter is to characterise the human IM samples (alongside periosteum from the same anatomical location as a comparison), particularly its collagen structure and composition, the findings of which will contribute to the design of a novel biomimetic membrane. When combined with appropriate internal fixation and autologous osteogenic stem cells and growth factors, the simulated biological tissue has the potential to negate the need for the second surgery, and streamline the current two-step reconstructive process. As well as reducing the number of surgeries required, use of a synthetic IM could also reduce the risk of complications as well as accelerate bone healing.

3.2 Chapter specific methods:

3.2.1 Tissue processing for histology:

To characterise the structure and microarchitecture of the natural IM and periosteal tissues, the biopsied samples (figure 4) were fixed in paraformaldehyde, before being dehydrated and embedded in paraffin wax as outlined in 3.2.2 . The embedded samples were sectioned in 5 μm thin slices and mounted onto glass slides before staining with haematoxylin and eosin, masons trichrome, picro sirius red (PSR) and verhoeff van gieson stain. Seven IM samples were fixed and stained for imaging as well as two periosteal samples.

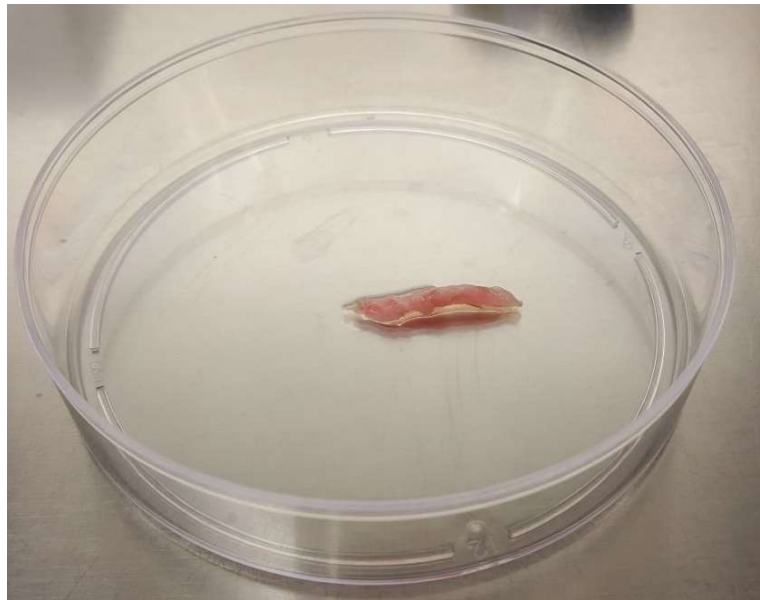


Figure 4: An example IM tissue biopsy harvested from the femur before fixing and processing for histology. Figure shows tissue in a 15 cm petri dish.

3.2.2 Fixing:

After harvesting, the IM and periosteum samples were transferred to 3.7% formaldehyde for 7 days at room temperature. The fixed samples were then placed into individual cases and processed overnight using an automated vacuum tissue processor the solutions and durations of each step are outlined in table 5.

Table 5: Tissue processing protocol

Step	Solution and reagents	Time (hr:min)	Temperature (°C)
1	70% ethanol	0:30	37
2	80% ethanol	0:30	37
3	90% ethanol	0:30	37
4	95% ethanol	0:30	37
5	100% ethanol	1:00	37
6	100% ethanol	1:00	37
7	100% ethanol	1:30	37
8	Xylene	1:00	37
9	Xylene	1:30	37
10	Xylene	1:30	37
11	Paraffin wax	1:00	65
12	Paraffin wax	1:00	65
13	Paraffin wax	1:00	65

3.2.3 Embedding and sectioning:

The samples were orientated in a cassette to allow a full cross-section of the tissue and covered in paraffin wax at 70°C. Once hardened the tissues could be sectioned using a microtome set to 5 µm thickness. Sections were floated in a water bath set at 40°C and mounted on glass slides before heat-treating on a hot plate at 60°C for 2 hours prior to staining.

3.2.4 Tissue staining:

To gain an accurate understanding of the IM's microarchitecture, a range of histology stains were utilised to identify the various structures. Haematoxylin and eosin was used to give a general overview of the tissues' morphology by staining nuclei blue and extracellular proteins, such as collagen, varying degrees of pink. To gain better definition of the individual collagen fibres, picro sirius red stain was used which stains collagen fibres red, extracellular matrix pale yellow and nuclei black. Picro Sirius red stain was also used to image the tissue sections under polarised light to gain insight into the collagen fibrils maturity based on their structure, thickness, and orientation. Finally, verhoeff van giesons stain was used to identify the presence of elastin fibres by staining elastin and cell nuclei black, collagen fibres red and cytoplasm yellow.

3.2.5 Haematoxylin and eosin stain

Table 6: Haematoxylin and eosin stain

Process	Step	Solutions and reagents	Time (min:s)
Dewaxing	1	Xylene	3:00
	2	Xylene	3:00
	3	Xylene	3:00
	4	Xylene	3:00
Rehydration	5	100% ethanol	3:00
	6	100% ethanol	3:00
	7	100% ethanol	3:00
	8	100% ethanol	3:00
	9	75% ethanol	3:00
	10	50% ethanol	3:00
	11	25% ethanol	3:00
	12	Running tap water	1:00
Staining	13	Mayer's haematoxylin	2:00
	14	Running tap water	1:00
	15	Scott's tap water	2:00
	16	Running tap water	1:00
	17	Eosin	2:00
	18	Running tap water	1:00
Dehydration	19	100% ethanol	0:15
	20	100% ethanol	1:00
	21	100% ethanol	5:00
	22	100% ethanol	5:00
Clearing	23	Xylene	3:00
	24	Xylene	3:00
	25	Xylene	3:00
Coverslip	26	DPX (to adhere coverslip to slide)	N/a

3.2.6 Picro sirius red stain

Table 7: Picro sirius red stain

Process	Step	Solutions and reagents	Time (min:s)
Dewaxing	1	Xylene	3:00
	2	Xylene	3:00
	3	Xylene	3:00
	4	Xylene	3:00
Rehydration	5	100% ethanol	3:00
	6	100% ethanol	3:00
	7	100% ethanol	3:00
	8	100% ethanol	3:00
	9	75% ethanol	3:00
	10	50% ethanol	3:00
	11	25% ethanol	3:00
	12	Running tap water	1:00
Staining	13	Weigerts solution A & B	8:00
	14	Running tap water	10:00
	15	Picro sirius red	60:00
	16	Acidified water	0:15
	17	Acidified water	0:15
Dehydration	18	100% ethanol	0:15
	19	100% ethanol	1:00
	20	100% ethanol	5:00
	21	100% ethanol	5:00
Clearing	22	Xylene	3:00
	23	Xylene	3:0
	24	Xylene	3:00
Coverslip	25	DPX (to adhere coverslip to slide)	N/a

3.2.7 Verhoeff van gieson stain

Table 8: Verhoeff van gieson stain

Process	Step	Solutions and reagents	Time (min:s)
Dewaxing	1	Xylene	3:00
	2	Xylene	3:00
	3	Xylene	3:00
	4	Xylene	3:00
Rehydration	5	100% ethanol	3:00
	6	100% ethanol	3:00
	7	100% ethanol	3:00
	8	100% ethanol	3:00
	9	75% ethanol	3:00
	10	50% ethanol	3:00
	11	25% ethanol	3:00
	12	Running tap water	1:00
Staining	13	Acid potassium permanganate	5:00
	14	Running tap water	0:15
	15	1% oxalic acid	2:00
	16	Running tap water	1:00
	17	95% ethanol	0:15
	18	Running tap water	1:00
	19	Weigert's haematoxylin	10:00
	20	Running tap water	1:00
	21	Picro Sirius red	10:00
	22	Running tap water	1:00
Dehydration	23	100% ethanol	0:15
	24	100% ethanol	1:00
Clearing	25	Xylene	3:00
	26	Xylene	3:00
Coverslip	27	DPX (to adhere coverslip to slide)	N/a

3.2.8 Microscopy and imaging:

Stained tissue sections were examined by bright field microscopy using an inverted microscope and captured using the camera function. The images were then processed using the image acquisition software Imagescope (see appendix 2, section 9.2) to measure the different sections of the tissues which was calibrated using a haemocytometer with known dimensions.

3.2.9 Histology measurements:

To measure the lumen diameter of blood vessels, H&E stained IM samples were imaged. Once imaged, blood vessels perpendicular to the vessel path were measured using a 10 x objective. The mean lumen diameter from a minimum of 20 characteristic blood vessels, which were selected randomly using three observation grids, was calculated. The mean lumen diameter was plotted against the duration of exposure of the IM to the PMMA cement (referred to as 'age of IM') to identify any trend of changing lumen size. It has already been described in previous literature that the IM is made up of two layers [7], the thicknesses of these layers were measured using a 10x objective at three depths of the tissue block (superficial, intermediate, and deep – each region was approximately 30 sections apart) and at a minimum 20 points across the length of each section (figure 5) . The mean thickness for each sample's cellular and fibrous layer was also plotted against the age of the IM to identify any trend in size change.

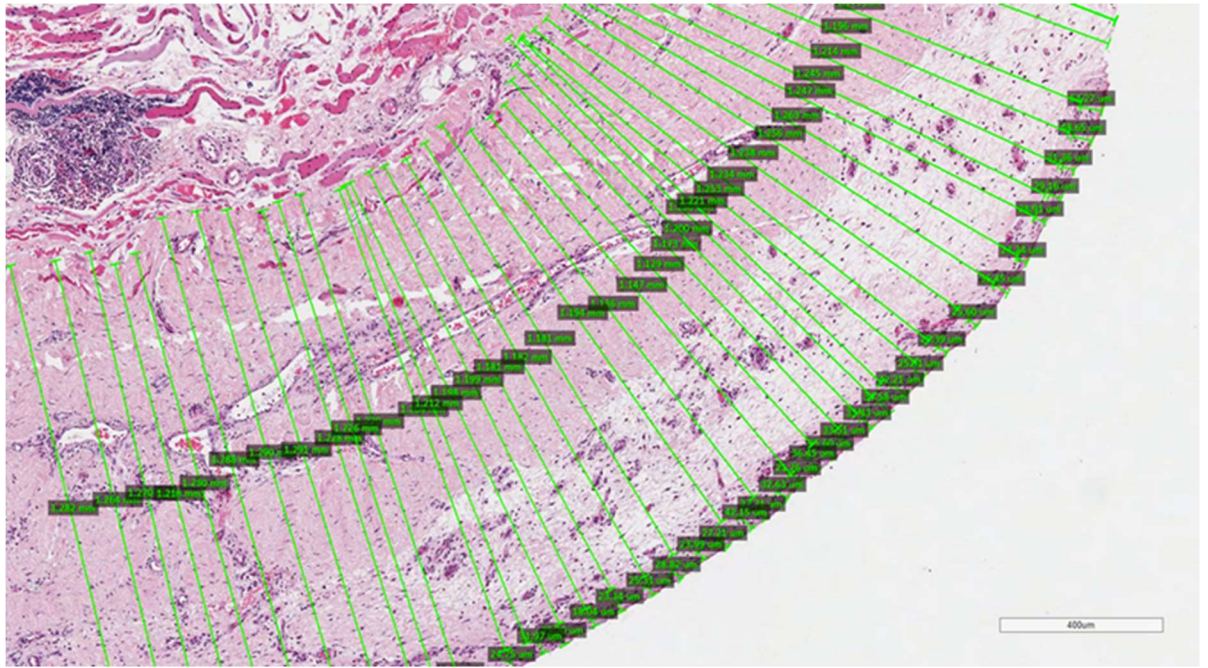


Figure 5: An example of how the IM bilayers were measured along the length of each cross section using ImageScope software before exporting the data into a GraphPad document for analysis. Scale bar indicates 400µm

3.2.10 Polarized light microscopy:

Tissue sections were cut 5µm thick and stained with picro sirius red according to section 3.2.6. Collagen molecules are known to be rich in basic amino acids, which strongly interact with the six sulfonate groups in sirius red [11]. Binding between the amino acids and sulfonates enhances the birefringence of the collagen fibrils that can be viewed under light waves from a single plane: polarized light. Due to differences in density between mature and newly formed collagen fibrils, mature collagen appears red-yellow under polarised light, whilst thinner, newly formed collagen appears green. Following staining, a Zeiss Axioplan microscope with circularly polarized microscopy filters aligned to 0° so that the background in the field of view was as dark as possible. Images were captured under an exposure time of 130 ms using a light path of 5V.

3.2.11 Statistics

All statistical analyses were carried out using GraphPad Prism software (GraphPad software). Data is expressed as mean \pm standard deviation for each parameter, the non-parametric Mann-Whitney U test was used to examine differences in cellular and fibrous IM layer thickness at different time points. A P-value of < 0.05 was considered significant.

3.3 Results

Gaining insight into the structure and morphology of the IM and how they contribute to its success as a guided bone regeneration device is a crucial step towards designing a novel biomimetic membrane. Histological techniques were primarily used as the principal technique to visualise and characterise the bilayer (figure 6 and 7), collagen content (figure 8), elastin content (figure 9) as well as analysis of the lumen diameter (figure 10) and bilayer thickness (figure 11).

3.3.1 Characterisation of the bilayer membrane structure:

Whilst the IM in animal models has been well characterised as sharing some morphological characteristics with periosteum [4-6] such as the presence of a bilayer structure, there is less known about human IM due to scarcity of samples. The human IM and periosteum samples collected from patients undergoing second stage masquelet surgery and were characterised using haematoxylin and eosin (figure 6) to elucidate their structure. Haematoxylin stains basophilic structures, primarily found in nuclei and is used to identify cell distribution. Eosinophilic structures, such as cytoplasm and extracellular matrix stain with different degrees of intensity – keratin fibres in muscle will stain a dark pink whilst collagen fibres will appear a much fainter pink [12].

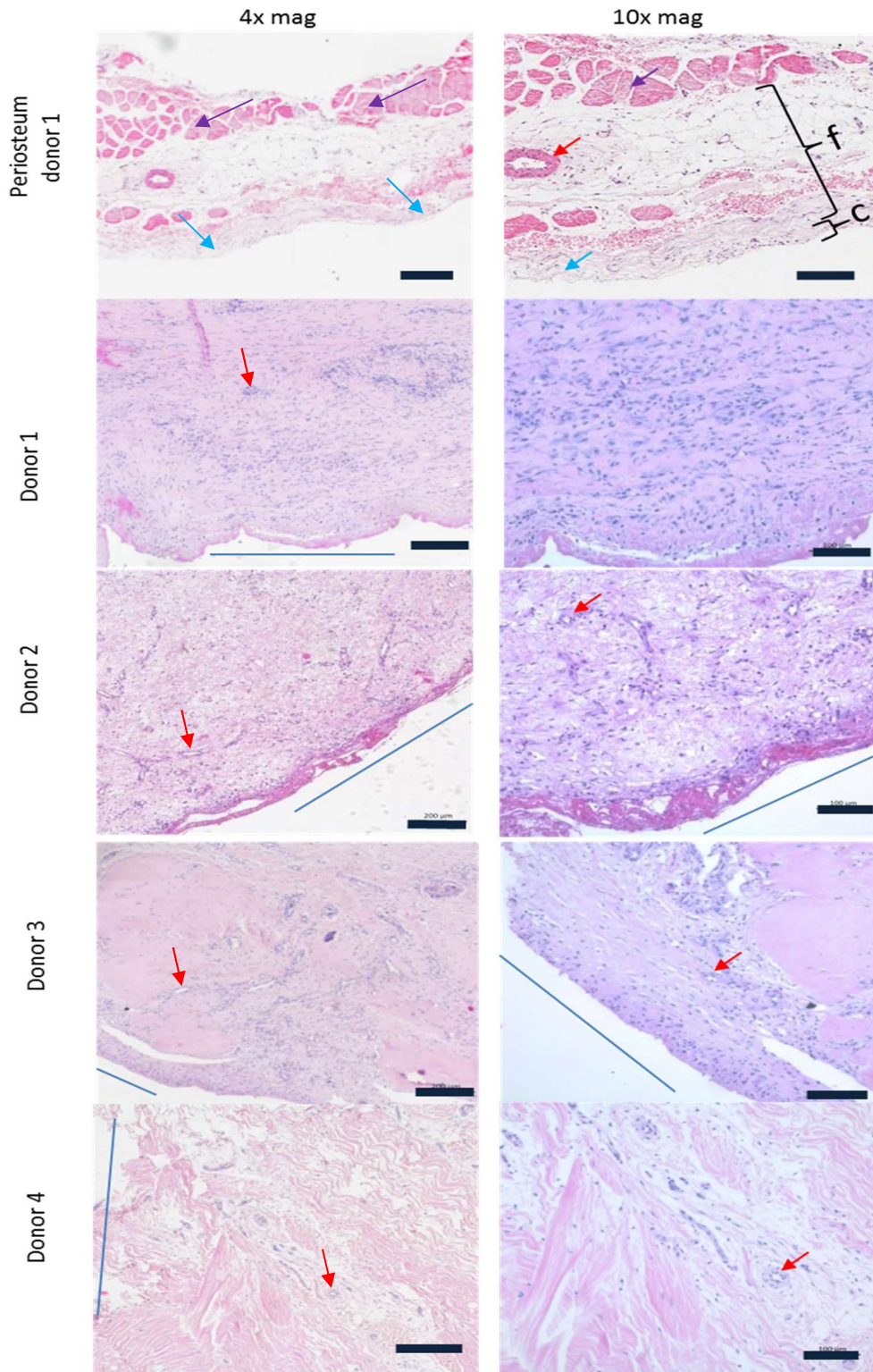


Figure 6: Basic features of periosteum and IM tissues stained with H&E. Left column 4 x magnification, scale bar represents 200μm. Right column 10 x magnification, scale bar represents 100 μm. The blue line indicates where the cement resided, whilst arrows indicate muscle fibres (purple arrows), regions of damaged cambium (blue arrow), and blood vessels (red arrows). The cambium (c) and fibrous (f) layer of the periosteum are also identified separately.

Looking first at the control periosteum sample, the stain revealed a loose outer fibrous layer and a more cellular cambium layer at the bone interface indicated in the figure by the blue line. The cambium layer was not found to be completely intact due to connective sharpeys fibres attaching the tissue to the bone, a phenomenon which has also been described in the literature [13, 14]. Severing these fibres during sample collection caused the observable damage to the cambium layer (blue arrows, figure 6). The tissue also appears to be highly vascular (red arrows), contributing to its role in supplying nutrients to the bone and the surrounding muscle layer is also visible (purple arrows).

Of the 7 IM samples stained for H&E, all showed some degree of variation in morphology, due to either age of IM or anatomical location, therefore 5 samples representative of the range will be discussed. IM from donor 1, which was exposed to PMMA for 14 weeks, had distinct collagen staining throughout the tissue as well as an equal distribution of cells that infiltrated the whole tissue rather than being localised as a cellular layer adjacent to where the cement spacer resided (blue line). IM from donors 2 and 3, which were both exposed to PMMA for 7 weeks, had a cellular organisation that correlated the most to what has been described in the literature with an intact cellular layer beside a much larger fibrous layer. Interestingly, IM from donor 4, which was exposed to the PMMA for only 3 weeks has the starkest contrast in morphology. Whereas donors 1-3 had some resemblance of cellular and fibrous organisation, the more immature IM from donor 4 has no observable structural arrangement. The lack of organisation is likely due to the initial inflammatory reaction to the PMMA spacer with MSC, and fibroblast cell infiltration contributing to the IM formation. The unusual morphology of donor 4's tissue supports findings in the literature that the second stage of the masquetelet procedure should be carried out after a minimum of 4 weeks to ensure full IM development before grafting [15, 16].

As expected, all the IM samples were distinctly thicker and denser than the periosteum and were mostly made up of fibrous matrix. Interestingly, with regard to the IM's bilayer, the different donors all displayed varying degrees of distinction between the layers and some samples lacked any observable bilayer at all (IM from donor 4). This absence of an obvious cellular layer which is described as putative in the literature [4, 7] is likely to stem from either differences in age of the IM (with regards to its exposure to PMMA), or its anatomical location, as the different mechanical forces on the tissue could bring about different morphological characteristics. Furthermore, as is often seen in periosteum histology where the cambium layer is lost due to its attachment to the bone and subsequent damage

during collection, the IM could be exposed to similar damage following dissection from the PMMA. Injuries in different anatomical locations may result in cement spacers that are more or less difficult to remove resulting in varying degrees of cell layer preservation. Damage to the IM's innermost layer in-contact with the PMMA could explain its varying presence across donors. This variation isn't seen in animal IM studies whereby the whole IM capsule is extracted and dissection from the cement spacer can be carried out more carefully. This is a limitation of using human tissues that is difficult to overcome due to the need to preserve as much of the tissue for the patients treatment as possible. It is also of note that the images taken at 10 x magnification lacked white balance, a technical issue that would be addressed in future work.

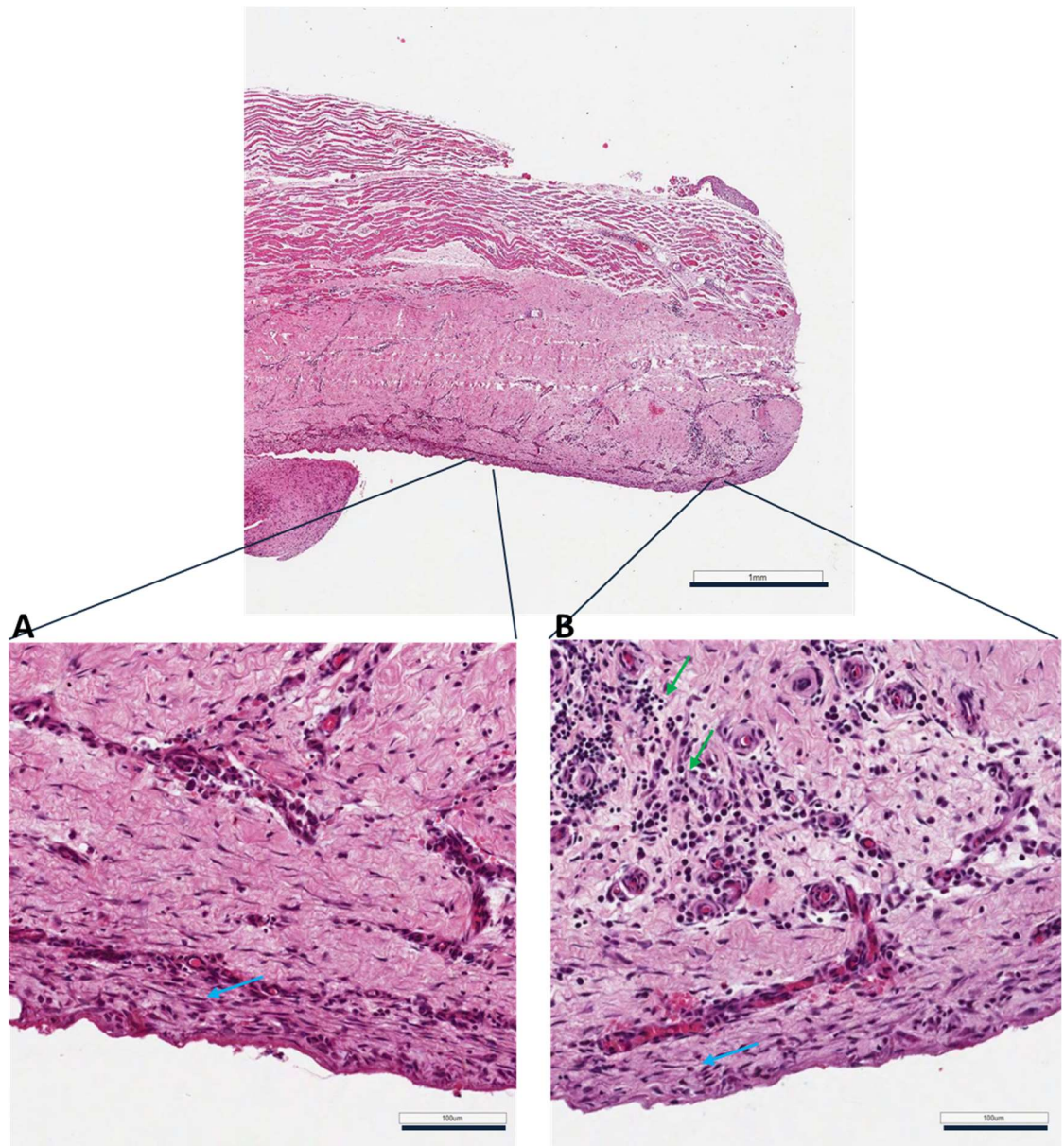


Figure 7: Detailed imaging of donor 5's IM tissue histoarchitecture using H&E stain, highlighted in A and B are two regions of the bilayer at x 20 magnification, scale bars indicate 1mm (top) and 100µm (bottom). Green arrows indicate region of acute inflammation and blue arrows indicate elongated fibroblast cells.

The IM from donor 5 was exposed to PMMA the longest of all the samples (17 weeks) and had the most intact bilayer. This sample was imaged separately (figure 7) under 20 x magnification to allow better characterisation. It can be seen that the innermost component adjacent to the PMMA is made up of densely packed elongated fibroblast-like cells orientated parallel to the PMMA (figure 4A and B, blue arrows). Deeper into the tissue, and further from the cement interface, the cells generally become more dispersed. An exception to this reduction in cells is a

region of acute inflammation (figure 7B, green arrows) which appears to be made up of multinucleated giant cells consistent with foreign body reactions and IM's role as an inflammatory response tissue [17].

3.3.2 Polarised light microscopy:

Whilst haematoxylin and eosin is capable of staining collagen, it isn't able to differentiate between the fibrous proteins of the extracellular matrix such as collagen, elastin, laminin and reticulin, therefore, to enable more accurate characterisation of the IM's structure, samples were fixed and stained with picro sirius red (figure 8). Under bright field microscopy, picro sirius red stains collagen red and muscle and cytoplasm yellow [18, 19]. To get more definition, the slides can also be viewed under polarised light whereby closely compacted and thick collagen fibres appear strongly birefringent (red-yellow) whilst thinner, loosely connected thinner collagen fibres appear faintly birefringent (green).

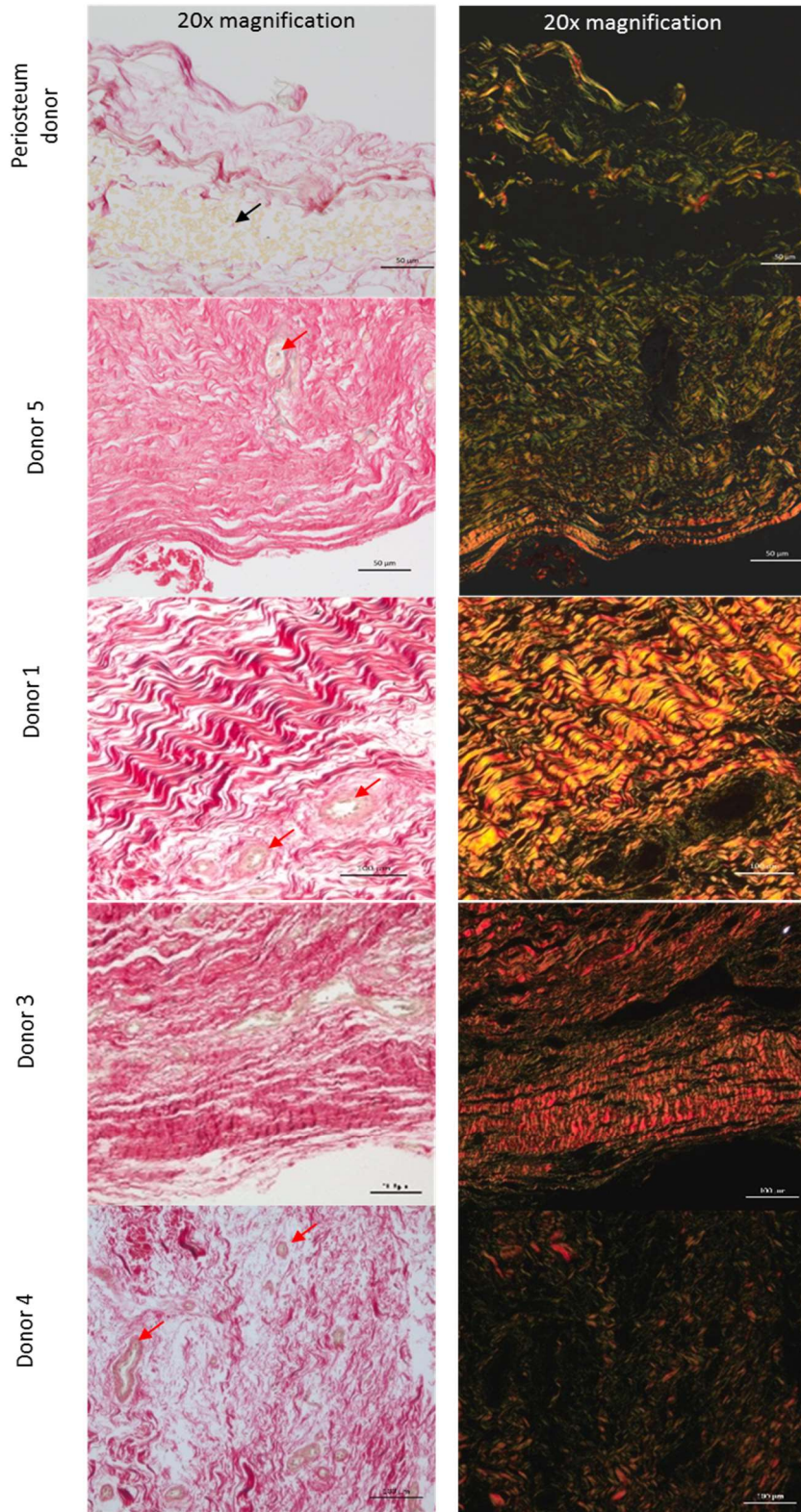


Figure 8: Picro sirius red staining of periosteum and IM biopsies under brightfield microscopy (left column) and polarised light (right column) both at 20x magnification. Scale bars indicates 50µm and arrows identify blood vessels (red arrows) and red blood cells (black arrows). Under bright field microscopy collagen fibres appear dark pink and under polarised light they appear green, yellow and red depending on their thickness and maturity.

Looking first at the collagen structure of periosteum, under bright field microscopy the picro sirius red stain has stained positively for collagen fibres (red) and it is clear that the fibres are not densely arranged. Furthermore, the stain highlights a region rich in red blood cells in yellow (black arrows), which is seen commonly in the literature due to periosteum's highly vascular nature. Under polarised light, the network of collagen fibres can be seen more clearly, and their sparsity as seen under bright field is confirmed by a majority of green birefringence. Although an occasional thick fibre is seen at the cambium layer, no overall gradient or change in collagen thickness was seen along the periosteum's cross-section, this indicates a generally homogenous tissue.

Demonstrated in previous stains, all four of the IM samples stained with picro Sirius red showed a degree of donor variation so were analysed individually. Donor 5, which was exposed to PMMA the longest of all the IM samples stained much more intensely for collagen than periosteum when viewed under bright field microscopy indicating denser and thicker collagen fibres. This was confirmed under polarised light which showed the IM was evidently more birefringent proximal to PMMA with a trend of decreasing density away from the cement spacer suggestive of a reduction in the secretion of fibrous, protective collagen. This further supports the notion that the IM is formed as a reactive response to the PMMA. The collagen fibres were clearly highly organised as bundles that were aligned parallel to the where PMMA resided. Analysis of donor 1, under both bright field and polarised light showed intensely dark collagen staining of fibres that also found to be highly stratified along where initially was the open defect. Unusually, no distinct gradient of birefringence was observed across the tissue as the whole tissue appeared to be made up of dense, thick fibres, with the only non-birefringent regions being blood vessels (red arrows). Donor 3 also stained more intensely for PSR than periosteum under bright field. Under polarised light donor 3 presented consistently intense birefringence (red) with no clear gradient, the weaker birefringence bisecting the sample is due to large blood vessels and adjacent to the PMMA is likely due to damage following harvesting. Despite this damage, the fibres' parallel alignment in bundles is still clearly visible. Finally, donor 4, which had the shortest exposure to the PMMA (3 weeks) demonstrated the most disordered collagen alignment supporting the H&E staining results. This tissue in particular was of interest as it appeared to grow perpendicular to the PMMA demonstrating the chaotic production of collagen following the initial response to the injury and cement spacer.

Overall, although there is some degree of donor variation, all samples to some extent showed significantly darker collagen staining and birefringence than

periosteum. In addition, all samples demonstrated the IM's organisation of collagen fibres into crimped bundles, and with the exception of the underdeveloped IM tissue from donor 4, all appeared to lay down collagen parallel to the PMMA spacer. The absence of this uniformity in IM from donor 4 suggests that during weeks 0-3 the IM is composed of randomly orientated collagen bundles which begin to align some point after week 3. This change in orientation is likely caused by both an increase in density (as more cells migrate to the site and more collagen is produced over time), as well as external musculoskeletal forces compressing the tissue into alignment.

3.3.3 Elastin content of IM:

The Verhoeff-van Gieson stain was used to elucidate the presence of elastic fibres which are involved in providing flexibility and elasticity to tissues such as skin and ligaments as well as to high-volume blood vessels (figure 9). High volume blood vessels are demonstrative of 'mature' blood vessels and can be used to identify tissue maturation. As expected, there was very little positive staining for elastic fibres (black staining) throughout the tissues indicating a general lack of elasticity and flexibility. The little staining that was observed was concentrated around larger blood vessels and was found in almost all IM donors. Interestingly, the only IM sample where elastin staining was completely absent was donor 4, which had the shortest exposure to the PMMA. Elastin's absence in this tissue supports the findings that IM tissues take at least 4 weeks to fully develop [4, 20].

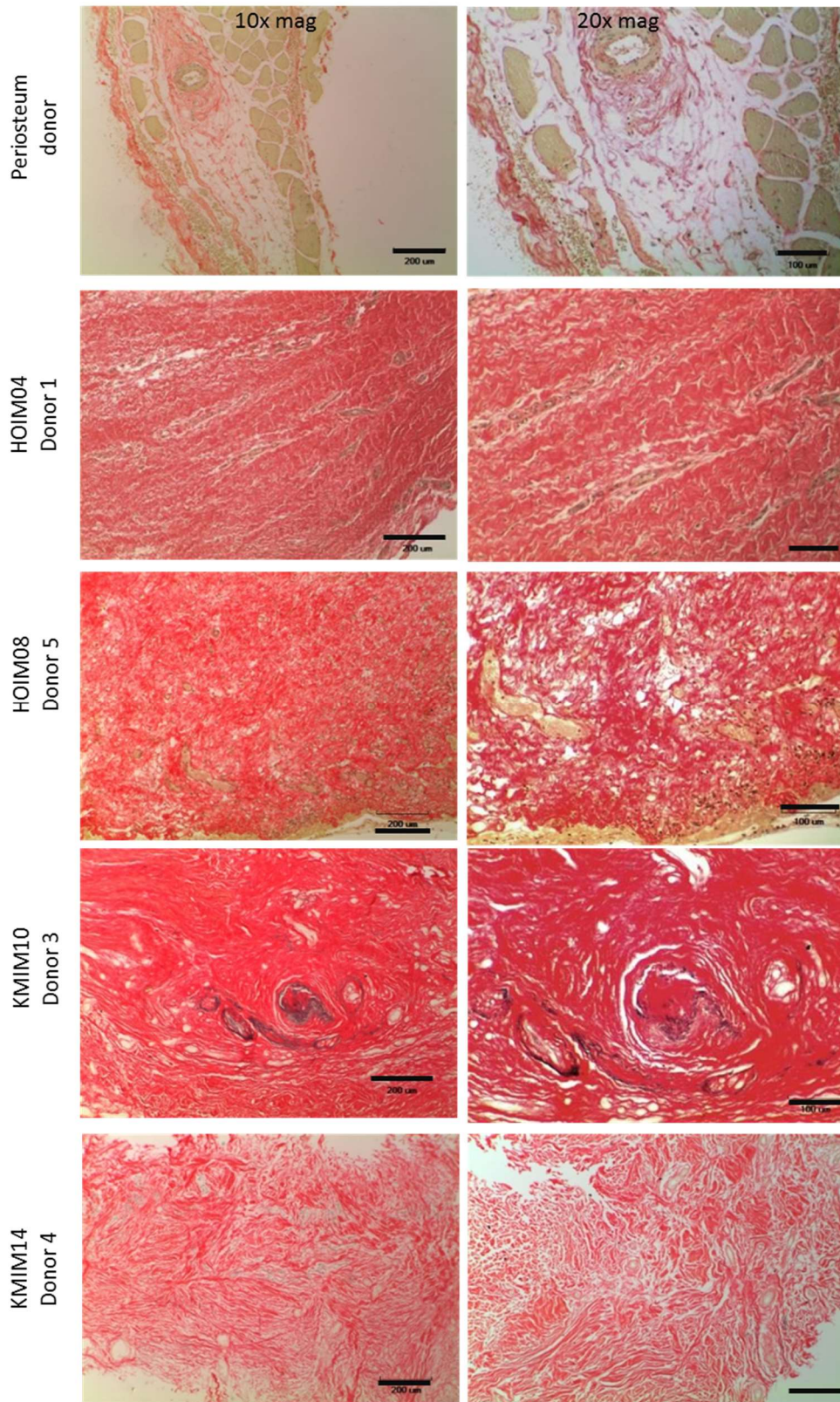


Figure 9: Elastin staining of periosteum and IM biopsies under brightfield microscopy at 10x magnification (left column) with scale bars indicating 200μm, and 20x magnification (right column) with scale bars indicating 100μm. Verhoeff-van gieson stain identifies collagen fibres (red), elastin fibres (black), muscle and cytoplasm (yellow).

3.3.4 Characterisation of IM's maturity:

After characterising the IM's histoarchitecture, it appeared that the lumen diameter varied between donors, and the overall size of the IM varied between donors. It was hypothesised that both these characteristics had a correlation to duration of exposure to PMMA ('age of IM'), whereby lumen diameter and IM thickness would be higher in mature IMs. To investigate whether these changes were related to the age of IM or donor variation seven samples were processed, stained and measured throughout the sample block to identify any correlation in donor age and IM maturity (figure 10).

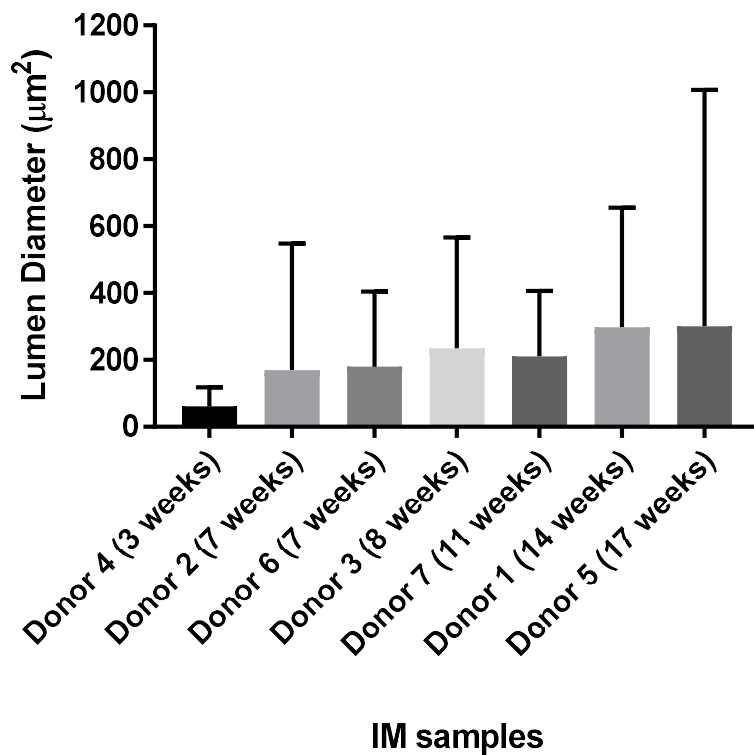


Figure 10: Mean lumen diameter of samples stained with H&E before imaging on Imagescope for analysis. Lines indicate standard deviation.

Analysis of the lumen diameter results indicate some degree of interrelationship between the age of the IM and increased lumen diameter with linear regression analysis of the data points revealing an R^2 value of 0.73 and the greatest increase occurring between 3 and 7 weeks. By 8 weeks, the average lumen diameter appears to plateau between 200 – 250 µm with the only observable change being an increase in diversification of blood vessel size demonstrated by an increased standard deviation at 17 weeks.

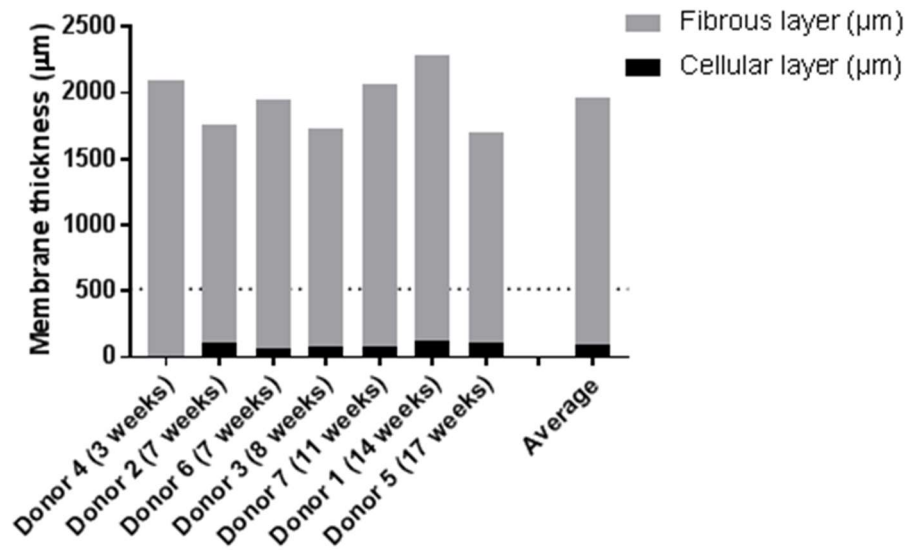


Figure 11: Membrane thickness for IM biopsies collected from patients 3-17 weeks after the initial surgery. Where present, both the cellular and fibrous layers were measured. The dotted line indicates the measurement of the periosteum.

Another key characteristic of the IM tissue is the thickness of the layers which were measured and plotted against their respective IM's age (figure 11). For samples that lacked a distinct cellular layer, only their fibrous layer was measured. This data effectively demonstrated the regularity in the IM's total thickness and how there was no significant time point at which thickness peaked, nor was there any significant degradation in size over time. Despite collecting samples from different IM ages (3-17 weeks) and anatomical locations (femur, ulna and tibia), the individual bilayers and total thickness were found to be generally consistent between donors. The cellular layer on average was found to measure $95 \pm 23 \mu\text{m}$ and the fibrous layer was found to be measure $1861 \pm 227 \mu\text{m}$. The overall thickness was $1942 \pm 220 \mu\text{m}$ on average (range: 1706-2286 μm). Consistently, every IM sample, at every time point was found to be thicker than periosteum which measured 516 μm (dotted line figure 11). These measurements correlate to previous work by Cuthbert *et al* on human samples who found periosteal samples to measure 860 μm [7]. Interestingly, there was little change in IM thickness from 3 weeks onwards, indicating that it has reached maximal thickness by this time point and can be considered a 'mature' tissue. This supports findings in rat femurs whereby, once fully formed, the IM's size remained static for up to 6 weeks [21]. However, longer studies in rabbits observed

degradation in size from 8 – 16 weeks [6]. As was seen in lumen measurements, more samples from more time points, particularly at the extremities, are necessary to identify any reliable trend of changing IM thickness.

3.4 Discussion:

The aim of this chapter was to address the lack of human IM tissue characterisation in the literature and to better understand its key structural characteristics in order to design a novel biomimetic GBR device. Previous work on characterising the IM has used animal tissues and generally focused on identifying the cells and growth factors present rather than the microarchitecture of the tissue [22]. This study enhanced the clinical characterisation of the IM in the literature by investigating the structure, collagen distribution and organisation, elastin content, lumen diameter and tissue thickness.

Analysis of the structure found that all the donor IMs were noticeably thicker and denser than periosteum confirming published research by Cuthbert *et al* and Pelissier *et al* on human [7] and animal studies [21] respectively that describe the IM as a reactive protective tissue [17]. Interestingly, although the presence of the IM's bilayer (analogous to the periosteum's fibrous and cambium layers) is described in the literature as putative [23], the samples stained for this chapter demonstrated varying degrees of distinction between the layers. Furthermore, the IM's bilayer, when present, seems to possess a more gradual transition between the layers. The absence of an obvious cellular layer which is described in the literature [4, 7] could be caused by damage during tissue harvesting as is often seen in periosteum histology where the cambium layer is lost due to its attachment to the bone. The IM's innermost layer in-contact with the PMMA could be exposed to similar damage following dissection especially when considering that injuries in different anatomical locations may also result in IM biopsies that are more or less difficult to extract, resulting in varying degrees of cell layer preservation. This variation isn't seen in animal IM studies whereby the whole IM capsule is extracted and dissection from the cement spacer can be carried out more carefully. This is a limitation of using human tissues that is difficult to overcome due to the need to preserve as much of the tissue for the patients treatment as possible. It is also of note that due to the precious nature of the tissue, the biopsies collected for histological analysis were small in size and often taken from the edges of the tissue that were surplus for the masquelet technique. Biopsies 1cm² in size taken from the

edge of the tissue are useful for giving an insight into the tissue's histoarchitecture but may not reflect the whole tissue.

Analysis of the collagen structure identified the IM tissue supports previous literature on the IM possessing some similar characteristics to periosteum, such as the presence of a bilayer [24], as well highlights their differences, such as the IM being made up of dense organised collagen bundles than periosteum. Although both tissues are predominantly collagen-based, their organisation and composition distinguishes them as two distinct tissues demonstrating the importance of using a range of histological techniques. Periosteum was found to be composed of thin, loosely connected collagen fibres whilst the IM samples were composed of thicker fibres that are tightly connected. Despite being found in very similar anatomical locations it is clear from this stain that they're biologically very different, suggestive of their different roles. Collagen's relatively high tensile strength and inextensible properties [25] suggest that the IM is mechanically stronger than periosteum.

With regards to elastin content of the tissue, as expected very little positive staining was observed across all samples indicating a general lack of elasticity in the tissue. The presence of elastin was appeared to be localised exclusively around large blood vessels, the only sample that lacked any elastin staining was donor 4, which had the shortest exposure to the PMMA. Elastin's absence in this tissue supports findings in the literature that the IM tissues take at least 4 weeks to fully develop [4, 20]. Despite the lack of positive staining from this data, it is still useful to inform the clinical understanding of the tissue.

Analysis of the lumen diameter discovered a plateau in lumen diameter around 200 – 250 μm by 8 weeks which opposes the reported decrease in vascularity described in animal studies after 1 month [4, 20, 21, 26, 27]. Although the results were not found to be significant, they suggest some disparity between human and animal tissues and highlights the need for additional characterisation of the former. Due to the nature of the masquetelet surgery, most tissue harvesting is carried out between weeks 4 to 12; therefore it is rare to get samples outside or even at the extremities of this range which is likely to be the cause of the disparity between this study's findings and previously published data. Aho *et al* who described the strongest trend of decreasing vascularity did so in human biopsies up to 22 months, a time point which is considerably anomalous to the ordinary treatment window and would be difficult to reproduce in future human studies [20].

Analysis of the 7 IM samples' thickness found them to measure $1942 \pm 220 \mu\text{m}$ on average which supports previous work on human by Cuthbert *et al* who found total

median thickness of IM to measure 1422 μm and which were also distinctly thicker than periosteum samples [7]. Interestingly, there was little change in total IM thickness from 3 weeks onwards, indicating that it reaches maximal thickness by this time point supporting findings whereby, once fully formed from 2 weeks, the IM's size remained static for up to 6 weeks in rat models [21] and 8 weeks in rabbit models [4]. Longer studies in rabbits did eventually observe a reduction in size from 8 – 16 weeks [6] but this could be due to the smaller size of the original defect (compared to human studies) and the basic anatomical and physiological differences between humans and rabbits.

Whether or not the human IM's structure changed over time was not clear based on the literature, and so, to create a biomimetic tissue based on the IM there was a demand for more certainty that the structural features observed in the histological 'snapshots' were representative of the tissue. To address this, samples were often discussed in relation to their duration of exposure to PMMA or 'age of IM'. However, often there were other significant variations between the samples other than 'age of IM', for example age of donor (24 to 61 years), anatomical location (femur, tibia and ulna) as well as the severity and size of defect. These factors undoubtedly influenced important features such as vascularisation since the vascularity and healing potential in a younger subject is presumed to be greater than that of an older subject. Further age- and site-controlled studies would increase the power of this data. The precious nature of the IM also limited the biopsy size available for analysis and was often harvested from the extremities of the defect which may not be representative of the whole tissue. To better understand the tissue as a whole, a much larger sample size would be necessary as well as multiple biopsies from the same tissue. Despite its limitations, the variability in this study reflects the clinical population and range of trauma patients with severe bone defects who would be the target population for this guided bone regeneration (GBR) device.

As the aim of this work was to further characterise the structure of the human IM and use the findings to mimic its role in bone repair, how these factors will inform the manufacturing process need to be considered. Based on the literature, it is understood that the key functions behind the IM's success as a GBR device is its ability to contain grafted material to the defect site and to provide GF to non-autologous bone grafts [22]. Therefore when considering the biomimetic membrane's size there may need to be compromise between thickness, mechanical strength and plasticity (with regards to it being capable of being molded into a desired form). A membrane that is too thick will act more like a sponge and be less moldable, whilst a membrane that is too thin won't absorb as much BMA

and GF (discussed in chapter 5) and may not be mechanically strong enough for function. Our data and the literature also collectively point to the inclusion of regular pores around 200-250 µm to allow blood vessel ingrowth, nutrient transport and MSC infiltration. Furthermore the bilayer was not found to be so distinct in the samples assayed in this chapter and will not play an integral part in the design process, instead the membrane will be populated with autologous bone marrow aspirate and growth factors which will serve as an interim tissue.

Overall these findings contribute towards a better understanding of the IM's unique structure and properties to aid the design and manufacture of a biomimetic guided bone regeneration device in chapter 4.

3.5 References:

1. Tzioupis, C. and P. Giannoudis, *Prevalence of long-bone non-unions*. Injury, 2007. **38**, Supplement 2: p. S3-S9.
2. Panteli, M., et al., Biological and molecular profile of fracture non-union tissue: current insights. J Cell Mol Med, 2015. **19**(4): p. 685–713.
3. Giannoudis, P.V., et al., Restoration of long bone defects treated with the induced membrane technique: protocol and outcomes. Injury, 2016. **47**: p. S53-S61.
4. Pelissier, P.H., et al., Induced membranes secrete growth factors including vascular and osteoinductive factors and could stimulate bone regeneration. Journal of Orthopaedic Research, 2004. **22**(1): p. 73-79.
5. Viateau, V., et al., Induction of a barrier membrane to facilitate reconstruction of massive segmental diaphyseal bone defects: an ovine model. Vet Surg, 2006. **35**(5): p. 445-52.
6. Liu, H., et al., Histological characteristics of induced membranes in subcutaneous, intramuscular sites and bone defect. Orthop Traumatol Surg Res, 2013. **99**(8): p. 959-64.
7. Cuthbert, R.J., et al., Induced periosteum a complex cellular scaffold for the treatment of large bone defects. Bone, 2013. **57**(2): p. 484-492.
8. Pountos, I., et al., How the Induced Membrane Contributes to Bone Repair: A Scientific-based Analysis. Techniques in Orthopaedics, 2016. **31**(1): p. 9-13.
9. Kim, H.D., et al., Biomimetic Materials and Fabrication Approaches for Bone Tissue Engineering. Adv Healthc Mater, 2017. **6**(23).
10. O'Brien, F.J., *Biomaterials & scaffolds for tissue engineering*. Materials Today, 2011. **14**(3): p. 88-95.
11. Lattouf, R., et al., Picrosirius red staining: a useful tool to appraise collagen networks in normal and pathological tissues. J Histochem Cytochem, 2014. **62**(10): p. 751-8.
12. Fischer, A.H., et al., *Hematoxylin and eosin staining of tissue and cell sections*. CSH Protoc, 2008. **2008**: p. pdb.prot4986.
13. Chang, H. and M.L. Knothe Tate, *Concise Review: The Periosteum: Tapping into a Reservoir of Clinically Useful Progenitor Cells*. Stem Cells Translational Medicine, 2012. **1**(6): p. 480-491.
14. Brownlow, H.C., et al., *Anatomical effects of periosteal elevation*. J Orthop Res, 2000. **18**(3): p. 500-2.

15. Masquelet, A.C. and T. Begue, *The concept of induced membrane for reconstruction of long bone defects*. Orthop Clin North Am, 2010. **41**(1): p. 27-37; table of contents.
16. Wong, T.M., et al., *Masquelet Technique for Treatment of Posttraumatic Bone Defects*. The Scientific World Journal, 2014. **2014**: p. 5.
17. Yee, M.A., et al., Scientific Understanding of the Induced Membrane Technique: Current Status and Future Directions. Journal of orthopaedic trauma, 2017. **31 Suppl 5**: p. S3-S8.
18. Junqueira, L.C.U., G. Bignolas, and R.R. Brentani, Picrosirius staining plus polarization microscopy, a specific method for collagen detection in tissue sections. The Histochemical Journal, 1979. **11**(4): p. 447-455.
19. Kiernan, J.A., Methods for connective tissue, in Histological and histochemical methods : theory and practice, 3rd ed, Butterworth-Heinemann, Editor. 1999, Oxford;.
20. Aho, O.-M., et al., *The Mechanism of Action of Induced Membranes in Bone Repair*. The Journal of Bone & Joint Surgery, 2013. **95**(7): p. 597-604.
21. Henrich, D., et al., Establishment and characterization of the Masquelet induced membrane technique in a rat femur critical-sized defect model. J Tissue Eng Regen Med, 2016. **10**(10): p. E382-e396.
22. Christou, C., et al., The Masquelet Technique for Membrane Induction and the Healing of Ovine Critical Sized Segmental Defects. PLOS ONE, 2014. **9**(12): p. e114122.
23. Gaio, N., et al., Masquelet technique: The effect of altering implant material and topography on membrane matrix composition, mechanical and barrier properties in a rat defect model. Journal of Biomechanics, 2018. **72**: p. 53-62.
24. Cuthbert, R., et al., Single-platform quality control assay to quantify multipotential stromal cells in bone marrow aspirates prior to bulk manufacture or direct therapeutic use. Cytotherapy, 2012. **14**(4): p. 431-40.
25. Lodish H, B.A., Zipursky SL, Collagen Fibrils Form by Lateral Interactions of Triple Helices Section 22.3, in Collagen: The Fibrous Proteins of the Matrix, A.f. W. H. Freeman; 2000. , Editor. 2000, Molecular Cell Biology. : New York:.
26. Wang, X., et al., Induction of granulation tissue for the secretion of growth factors and the promotion of bone defect repair. Journal of Orthopaedic Surgery and Research, 2015. **10**: p. 147.
27. Hankenson, K.D., G. Zimmerman, and R. Marcucio, *Biological Perspectives of Delayed Fracture Healing*. Injury, 2014. **45**(0 2): p. S8-S15.

4 Manufacture and process-structure relationships of the collagen-poly(ϵ -caprolactone) membrane

4.1 Introduction:

In the clinical setting, the gold-standard masquelet treatment for fracture non-union results in the formation of an induced membrane (IM) around the defect. This membrane-like tissue is believed to actively contribute towards guided bone regeneration through its protective role, preventing soft tissue ingrowth, and acting as an osteogenic niche. However, the current gold-standard clinical treatment for non-union requires two separate surgeries, whereby the formation of the IM is not always guaranteed. The debilitating pain associated with non-union, the extended recovery time for patients and the increasing medical and socioeconomic costs is making the development of a new membrane-based bone regeneration strategy a global priority. In order to address this, the design of multifunctional systems for orthopaedics and scalable manufacturing routes has received growing attention, whereby either synthetic or natural polymers have been employed [1] [2].

The membrane-forming multifunctional system should induce bone regeneration and accelerated healing in non-union fractures. As described by Giannoudis *et al* [3], the membrane building block must; 1) support osteogenic cell proliferation, 2) be compatible with growth factors and act as a vehicle for their localised delivery, 3) enable osteoconductivity, and 4) be mechanically stable to provide support and protect the defect site from soft-tissue ingrowth. Additionally, the specific design criteria for a successful cell-homing membrane architecture has been described by Matassi *et al* to include; 1) high porosity to provide space for cell adhesion and appropriate pore distribution to minimise diffusion constraints and facilitate homogenous tissue formation, 2) a controllable degradation profile, 3) cyto and immune compatibility of both the bulk material and its degradation by-products, and finally, 4) manufacturability and reproducibility at industrial scale [4].

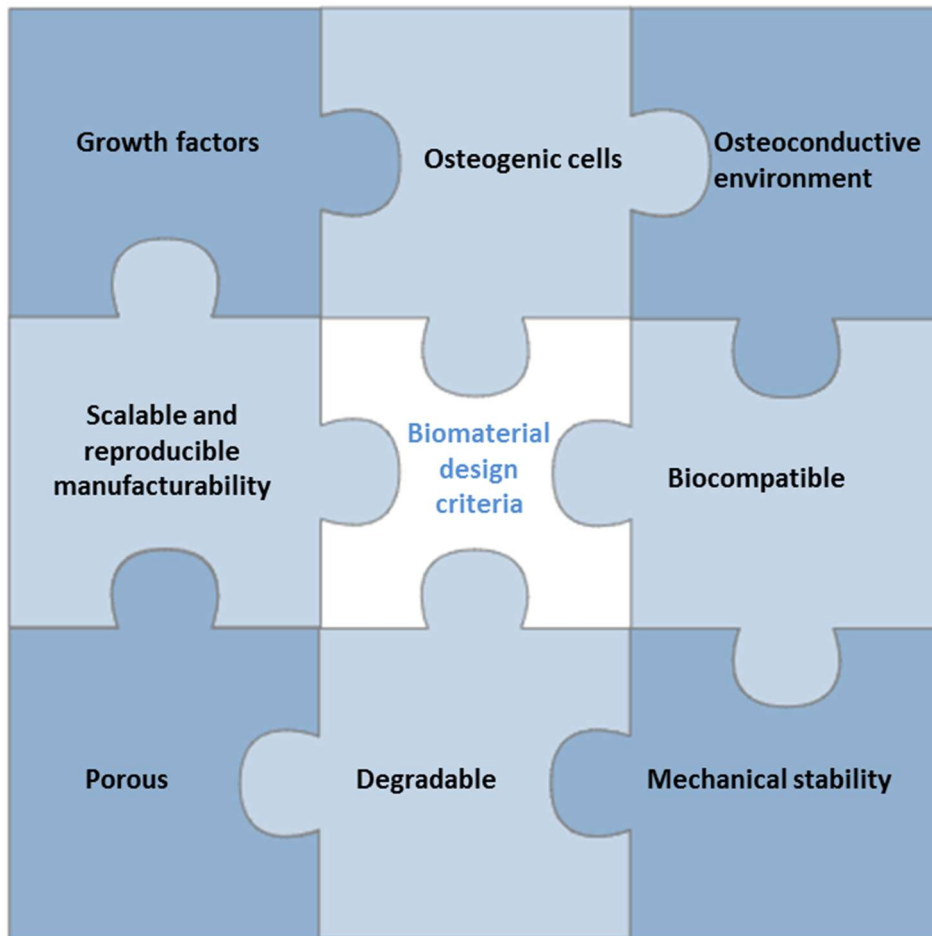


Figure 12: Schematic outlining the key characteristics and properties to aim for as part of the biomaterial design strategy.

These 8 design criteria informed the choice of material and the methods used to make the biomimetic membrane. The most common synthetic materials used are polyesters such as polylactide (PLA), polyglycolide (PGA), copolymers of PLA and PGA (PLGA), and poly(ϵ -caprolactone) (PCL). For engineering bone specifically, PCL is the most common choice as not only has it been found to be biocompatible, biodegradable, and with enhanced mechanical properties such as high mechanical strength and low rigidity [1, 5]; but also because PCL degradation, whilst breaking down into ϵ -hydroxycaproic acid [5], does not produce as much of an acidic local environment as PLA and PGA do [6, 7]. Furthermore, it is a comparatively low-cost material and can be processed easily using a wide range of industrial manufacturing methods. Despite its processability and appropriate mechanical properties, it is a highly hydrophobic material which limits its ability to absorb and deliver growth factors [1], it isn't known for its ability to induce osteogenesis and osteogenic cell proliferation and degrades very slowly (the absorption time of PCL in vivo can take up to 3 years [6, 1]).

In contrast, biological 'natural' polymers such as collagen, chitosan, hyaluronic acid, and silk fibres possess a range of versatile properties that also make them potential candidates for orthopaedic applications. In contrast to PCL, whilst the biological polymers listed possess biological cues to some extent that support osteogenic cell proliferation, collagen is the only extracellular matrix component involved during healing and the main building block of the IM, making it ideal to realise tissue-like biomimetic analogues. Alternatives to collagen became popular following concerns over immunogenicity and the potential risk of disease transmission depending on its source [8], however, since medical grade (atelo)collagen has recently become commercially available, its manufacturability at industrial scale is becoming realistic for orthopaedic applications [6]. Using a biopolymer such as collagen, which resided in the tissue prior to injury, has several relevant biofunctionalities in addition to being biomimetic; collagen possesses an innate ability to induce healing through initiation of the clotting cascade [9] as well as inducing localised chemotaxis. Collagen is the most biocompatible option and its ability to support cell survival and proliferation means it is already being used extensively in tissue culture. Compared to PCL, collagen is significantly more hydrophilic and allows increased oxygen and nutrient permeability [10]. Despite these advantages, its application is largely restricted due to its poor mechanical properties and proteolytic stability.

A material system capable of integrating the functionalities of both PCL and collagen could be envisaged in the form of a mechanically-competent, cell-homing membrane. In this application, PCL could be used to provide mechanical stability to the membrane, whilst collagen will provide the resulting prototype with inherent biological cues to induce cell migration and proliferation.

Various manufacturing methods are available to generate a membrane-like material including techniques such as electrospinning (ES), bioprinting, and decellurisation. Each technique has its advantages, but the ease of industry scale-up and the ability to produce a dense mesh of non-woven fibres in the nano- and micro-scale, with a high surface-to-volume ratio, makes ES a promising option aiming to realise multifunctional membrane prototypes with defined process-structure-function relationships [11].

The basic principle behind ES involves charging a viscoelastic polymer solution through an electrically charged metal needle. The subsequently charged solution is attracted to and propelled towards an electrode charged collector plate. The electrical field between the needle and collector deforms the polymer solution into a jet, as it does so, the solvent evaporates and a matrix of solid fibres is deposited.

As described, this method traditionally uses needles to charge the solution and contain the solvent – the benefit of this being it prevents excess solvent evaporation.

Although spinning of collagen only [12, 13, 14] leads to matrices with limited thickness and mechanical competence [12], the collagen nanofibres were found to support MSC viability and provide favourable growth conditions. Some attempts have been made to develop a stronger product by spinning collagen-PCL composites. These composites have been used in vascular grafts [15], showing collagen coated PCL was better than PCL fibres alone with regard to inducing cell viability and proliferation; as well as skin grafts [16] which also found enhanced cell proliferation in both collagen coated PCL scaffold. Interestingly, the latter study that developed PCL-collagen scaffolds for skin grafts also investigated the design of coaxial collagen-PCL matrices, where the PCL and collagen were spun together to create fibres with a PCL core and collagen shell, and found even greater cell proliferation and cell-scaffold interactions. These structure-function relationships were thought to be due to better replication of the ECM and the presence of more facets for cells to interact with and adhere to than the collagen coated PCL matrix [16]. As well as PCL, other researchers successfully electrospun a collagen and PLA scaffold demonstrating its use for sustained antibiotic release [17]. Despite their preliminary success, all these methods are restricted by their low-throughput (usually 0.1–1 g/hr/needle[18, 19]) from progressing further towards clinical translation.

One way to increase the output of electrospun fibres would be to use 'needle-free' or 'free-surface' ES, which until now has not been utilised for creating collagen-based membranes for orthopaedic reconstruction. Free-surface ES is a technique that creates multiple jets from a liquid charged directly onto an electrode - usually a rotating wire electrode into a liquid-filled trench or a spike with a concave surface that is able to contain small volumes of solution. The increased number of jets, the larger volumes of solutions, and the use of a rolling-collector mechanism are extensions of traditional syringe-ES that drastically increase the potential output of this technique. However, due to the novelty of this method for the application of creating a biomaterial, the process parameters need optimising including; humidity, solution concentration, solution composition, distance between the electrode and the collector, electric potential, flow rate, molecular weight of the polymers and the wire spinning rate, among others. To limit the variables as much as possible a spike electrode was used in this research.

This chapter aims to optimise the free-surface ES method to manufacture a range of biomimetic PCL-collagen membranes for guided bone regeneration.

4.2 Specific methods

4.2.1 Isolation of type I collagen from rat tail tendons:

Due to the expense of using commercially-available medical grade collagen, for initial prototyping, collagen was extracted in house from rat tail tendons via acid treatment [20]. First, frozen rat tails were thawed in 100% ethanol for 20 minutes, skinned and then individual tendons were removed from the tendon sheath. The tendons were then placed in 17.4 mM acetic acid solution (50mL/rat tail) and stirred for 48 hours at 4°C to extract the collagen. After extraction, the mixture was centrifuged at 10,000 xg for 40 minutes. The pellet was discarded, and the collagen-containing supernatant was neutralised with 0.1 M sodium hydroxide and stirred for 12 hours at 4°C, before being centrifuged at 10,000 xg for 45 minutes. The supernatant was then replaced with an equal volume of 17.4 M acetic acid to re-solubilise the pellet fraction. This solution was then freeze-dried for 48 hours and stored in air-tight 50mL falcon tubes at 4°C.

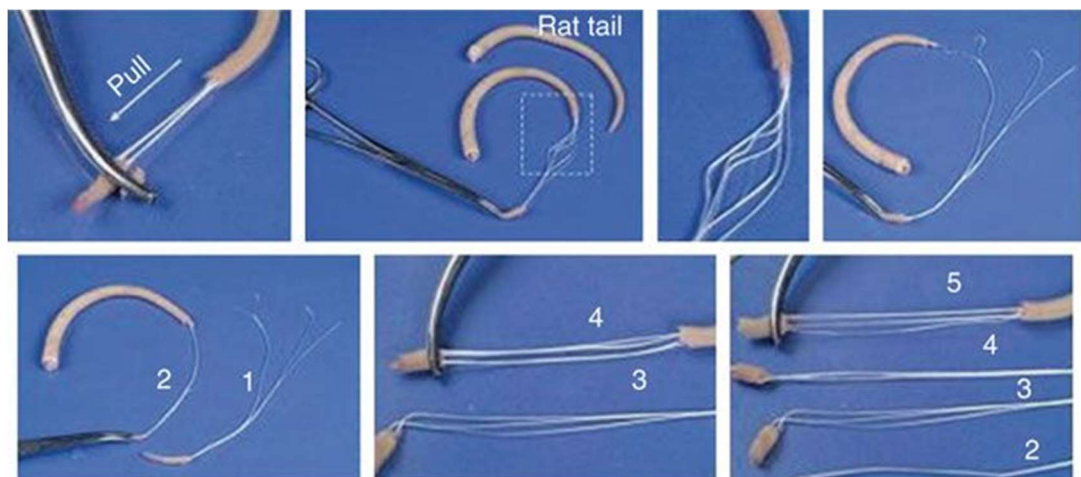


Figure 13: Isolation of rat tail tendons: the skin of the rat tail is ripped off several times with a clamp to reveal the collagen-rich tendons (white filaments). Image sourced from Nature Protocols [20] with permission from the Springer Nature and Copyright Clearance Centre.

4.2.2 Electrospinning solutions:

To identify the optimal composition of collagen to PCL for manufacturing the GBR prototype, a series of solutions were made up. Using freeze-dried in-house synthesised collagen and PCL with an average molecular weight of 80 kDa, a series of solutions with ratios of 50:50, 60:40, 70:30 and 80:20 were made up in 1,1,1,3,3,3-Hexafluoro-2-propanol (HFIP). 20mL of each solution was made up to a final concentration of 6% (w/v) and stirred over-night at room temperature to ensure the solution was homogenous.

4.2.3 Free-surface electrospinning:

Using a needle-less electrospinning set-up (Nanospider, figure 14 A) with a spike electrode (figure 14 B), single drops of 200 μ L of solution were charged with increasing voltage up to 60 kV until the drop had been used up (< 1 minute). The spike electrode was cleaned between drops to prevent residue build up. To give the solvent enough time to evaporate before reaching the grounded electrode, the distance between the electrode and the collector was set to the maximum height of 19.5 cm. The temperature of the ES environment was $19 \pm 5^{\circ}\text{C}$ and the air humidity $45 \pm 5\%$.

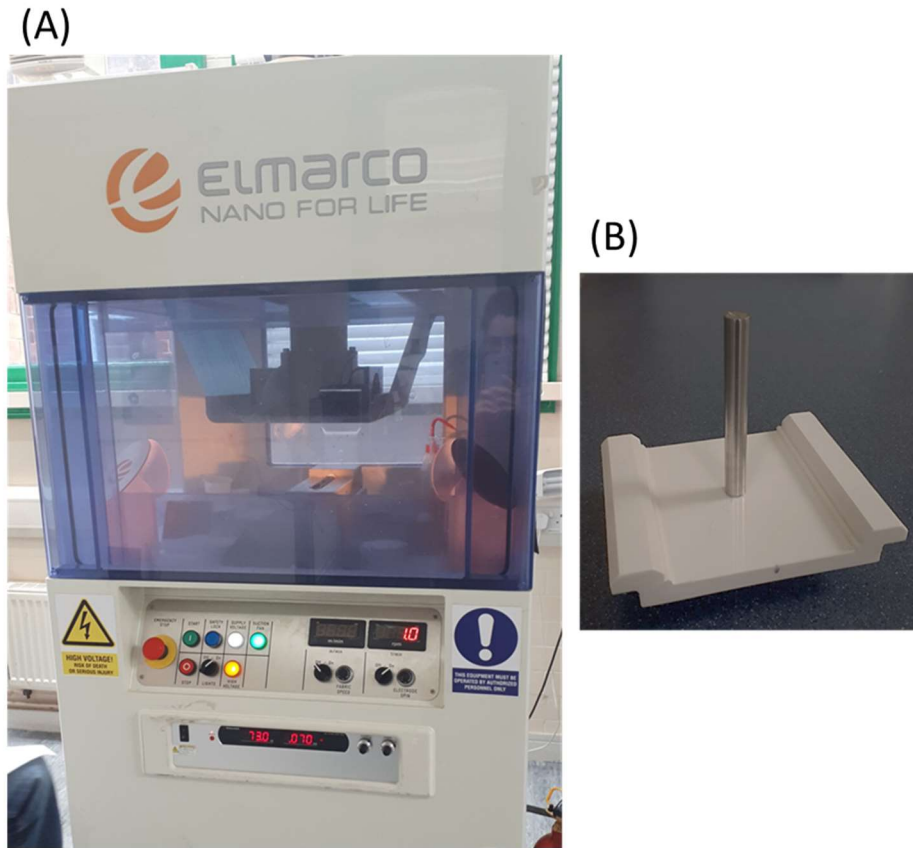


Figure 14: Nanospider needlefree ES apparatus (A) and its accompanying spike electrode (B).

4.2.4 Gas liquid displacement porometry using the Porolux:

To measure the material's inherent pore size distribution, the Porolux liquid displacement porometer was used. The equipment works by expelling the wetting fluid from the saturated scaffold by increasing the gas pressure, whereby pores with decreased diameter require increased gas pressure to expel the fluid. First scaffolds were cut to size to fit the 25mm diameter sample holder before being saturated in perfluoroether which acted as the wetting fluid. Perfluoroether is an inert liquid with a low surface tension (15.6 mN/m) and a contact angle of zero. The hydrated scaffolds were placed in the sample holder and the chamber was sealed before air was introduced into the chamber at increasing pressure until all the liquid was expelled. This initial run is referred to as the 'wet-run' and is followed by a subsequent 'dry-run' which is carried out once all the wetting fluid has been removed. The flow rates are then compared to measure the first bubble point (maximum pore size), mean flow pore size, minimum pore size and average pore size distribution.

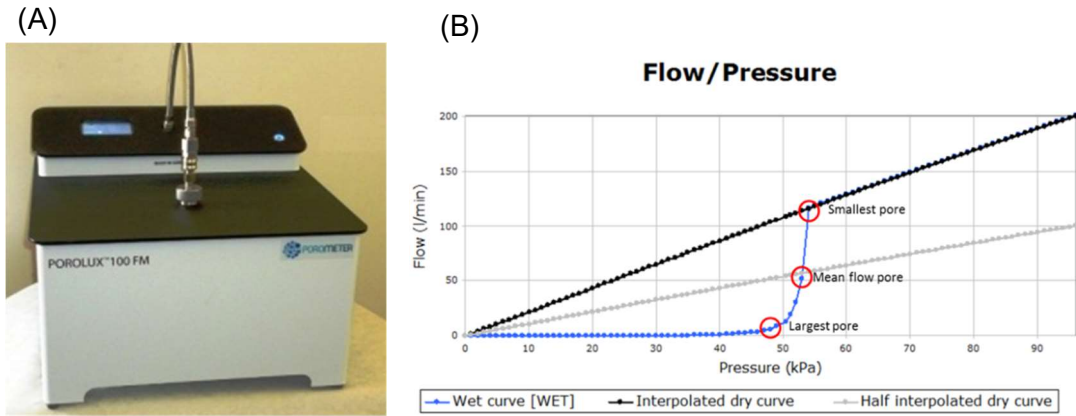


Figure 15: The Porolux 100 device (A) used for porometry analysis of scaffolds, an example of the data collected from the device is also shown (B) where the scaffold's smallest, mean, and largest pore can be easily identified from the wet curve (blue).

4.2.5 Post-manufacture processing (folding and laser cutting):

10 mL of spinning solutions were electrospun onto the collection fabric and folded to the desired thickness (0.5 mm and 1 mm) by briefly warming on a hot-plate set to 40°C and applying even pressure to bond the layers. Using ApS-Ethos control software, three scaffolds with distinct microarchitectures were designed: (1) no laser cut pores, (2) pore diameter of 200 μm and distance between pores of 4 mm (open area space of 0.01 cm^2/cm^2), and (3) pore diameter of 200 μm and distance between pores of 2mm (open area space of 0.04 cm^2/cm^2). The pores were cut into the folded scaffolds using a commercial 100-watt CO_2 air-cooled laser cutter. Full cut-through of the pores was achieved using a single pass at 10% power and a velocity of 600mm/s.



Figure 16: Demonstrates the laser cutter device in operation perforating pores into a scaffold which is held in place with weights.

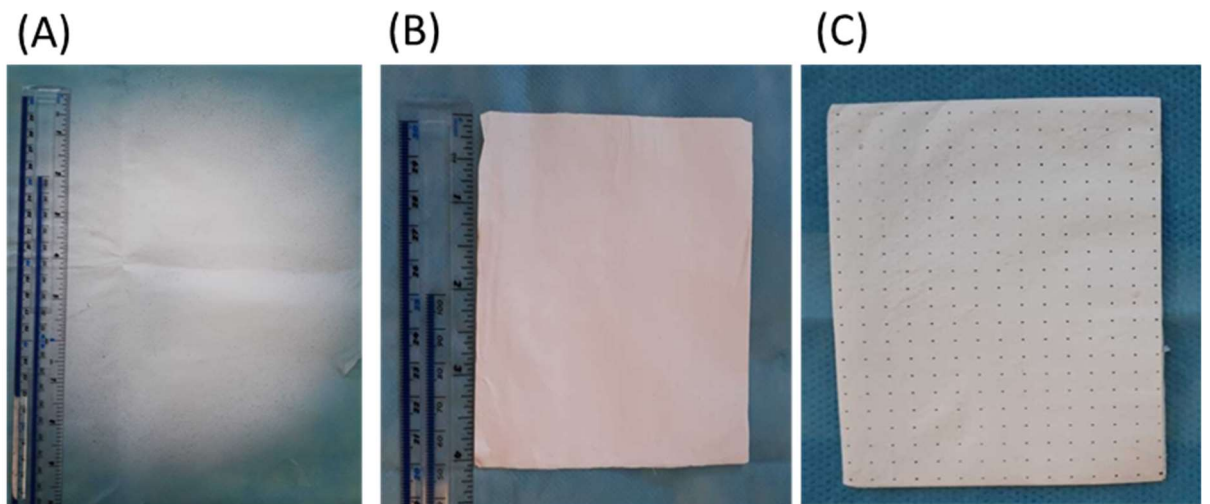


Figure 17: The three stages of post-manufacture processing: (A) the initial electrospun fibre mesh (white material) directly onto the collector fabric (blue material), (B) the electrospun material after folding and heat-setting on a hot plate to bond the layers, (C) the material after laser cutting (this example shows $200\ \mu\text{m}$ pores spaced $4\ \text{mm}$ apart)

$$\text{Inherent porosity (\%)} = 1 - \left(\frac{\text{apparent density}}{\text{bulk density}} \right) \times 100$$

$$\text{Apparent density (g.cm}^{-3}\text{)} = \frac{\text{mass (g)}}{(\text{thickness (cm)} \times \text{area (m}^2\text{)})}$$

Bulk density values for PCL: 1.14, 0.68 for rat tail collagen and 0.82 for 70:30 collagen:PCL.

$$\text{Open area/cm}^2 = 1 - ((\text{area of single pore}) \times \text{no. of pores/cm}^2)$$

$$\text{Area of a pore} = 2\pi rh + 2\pi r^2$$

Equation 2: Formulas used to calculate the inherent porosity of the scaffolds and the open areas produced by laser cutting per scaffold. Inherent porosity used published bulk density values; 1.14 for PCL [21], 0.68 for rat tail collagen [22], and 0.82 for 70:30 collagen:PCL

4.2.6 Scanning electron microscopy (SEM):

To capture the microarchitecture of the commercial and manufactured scaffolds, cell-free dry samples were imaged via SEM. Specimens were individually mounted onto sample stubs using adhesive mounting tabs and, to improve image resolution, sputter coated with gold using an automatic sputter coater under argon atmosphere with a vacuum set to 3×10^{-2} mbar. Brightness and focus were adjusted, and images were captured at a voltage of 20 kV, over 80 seconds, at a pixel rate of 2560 x 1920 using Hitachi S-3400N image processing software.

4.2.7 SEM microarchitecture analysis:

To quantify the scaffold's microarchitecture characteristics such as pore size and fibre diameter, SEM analysis was used. For measuring fibre diameter, samples were imaged at 10,000 x magnification and the diameter of a minimum of 20 fibres were randomly selected and measured. The diameter of the laser cut pores was measured at four points across the cross-section of the pore using SEM images of a minimum of three pores per sample.

4.2.8 Energy-dispersive X-ray spectroscopy (EDS):

The EDS function of the SEM was used for surface elemental analysis to identify the presence of collagen in the scaffolds by mapping the location of nitrogen and

carbon elements. The microscope operated under the following conditions: voltage 20 kV, current 10 nA, beam diameter 6 μm , and a vacuum pressure of 100 Pa.

4.2.9 Thickness measurement:

Scaffolds thickness measurements were carried out using a thickness tester with a nonwoven pressure foot. With the sample placed on the bottom anvil platform, the foot applies 0.5kPa of pressure to each sample and the thickness is measured through a digital gauge. Three samples were measured from each group and reported as mean \pm standard deviation.



Figure 18: The ProGage thickness gauge used to measure the thickness of the samples.

4.2.10 Tensile testing:

The tensile modulus and tensile strength samples were measured using a Titan 5 Universal strength tester with a 100 N load cell at a rate of 20.00 mm/min. The testing was carried out in a controlled environment with a room temperature of 18°C and relative humidity of 38% on samples measuring 30 x 20 mm. Samples were tested dry and hydrated in PBS which involved saturating the samples in 10 mL of PBS for 5 mins before testing. T27 clamp was used as the jaw with a gauge length of 20 mm. A minimum of four individual samples were tested from each group and measurements were reported as mean \pm standard deviation. Tensile strength,

strain at break and Young's modulus were calculated using the linear, plastic and failure regions of the stress-strain curves.

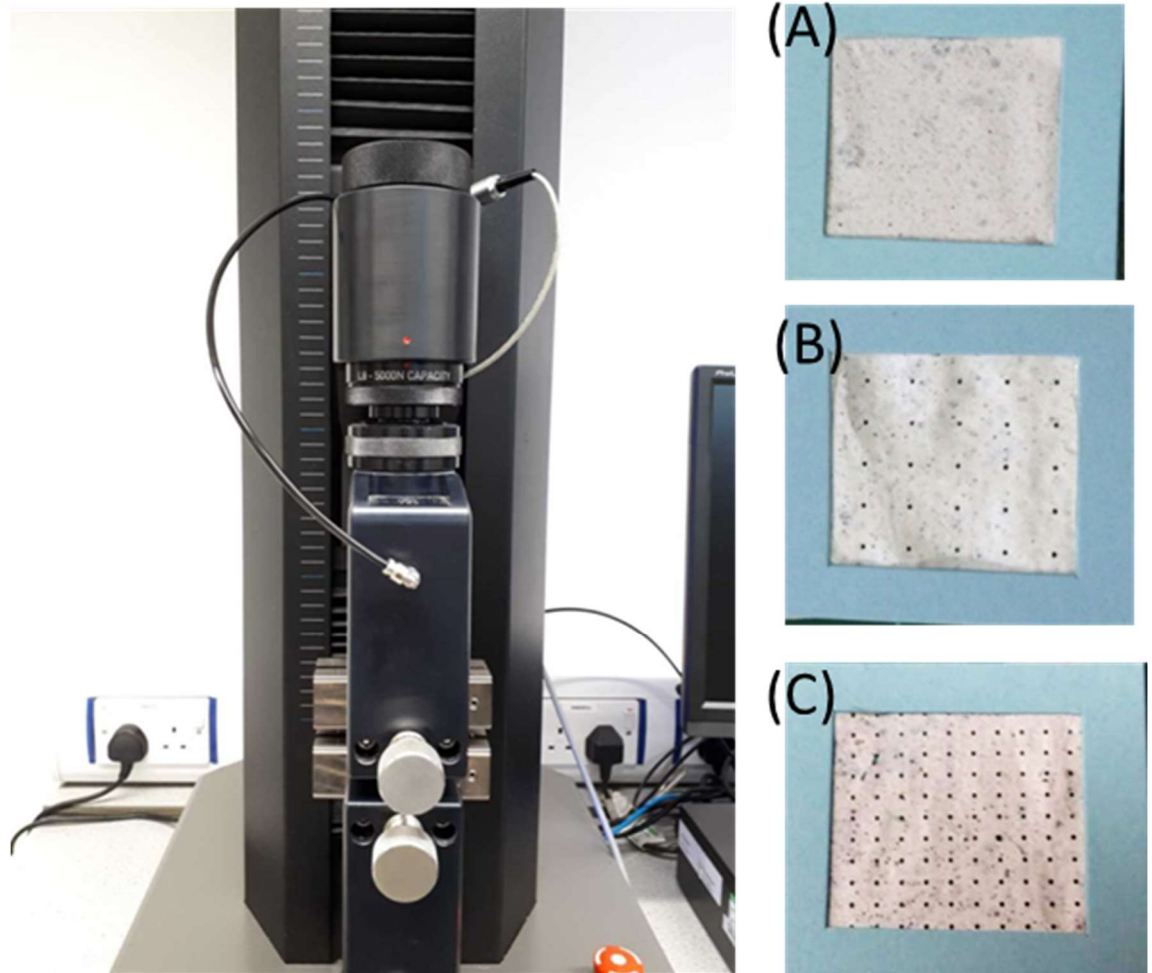


Figure 19: The Titan 5 Universal strength tester with a 100 N load cell used to measure the tensile properties of the scaffolds. Also shown are the examples of the single sheets of scaffolds (not folded), (A) intact with no laser cut pores, (B) 200 μm cut pores spaced 4 mm apart, and (C) 200 μm cut pores spaced 2 mm apart.

$$\text{Stress (MPa)} = \left(\frac{\text{force (N)}}{\text{area (m}^2\text{)}} \right)$$

$$\text{Strain (\%)} = \frac{\text{length (mm)}_{\text{new}} - \text{length (mm)}_{\text{original}}}{\text{length (mm)}_{\text{original}}}$$

Equation 3: Formulas used to calculate the tensile mechanical properties of scaffolds. The formulas used to calculate force (N), stress (MPa), and strain (%).

4.2.11 Scaffold degradation assay:

1cm² samples of scaffolds were placed in 5ml PBS with 1% Penicillin/Streptomycin in 6 well plates at 37°C for one month and imaged via SEM on day 0 and day 28 to compare any changes in their microarchitecture.

4.2.12 Statistics

Using GraphPad Prism software, statistical analyses were carried out on datasets that consisted of at least three independent experiments using a ANOVA with multiple comparisons to detect significant differences between the scaffold's tensile properties. All data are expressed as mean ± standard deviation. *P<0.05, **P<0.01, ***P<0.001, and ****P<0.0001 defined statistical significance.

4.3 Results:

For the creation of an orthopaedic collagen-based membrane prototype, it is essential to control the micro- and macroscopic physical morphology to enable optimal physiological functioning. This chapter used free surface ES to manufacture membranes from a range of PCL and collagen compositions and spinning parameters to achieve reliable process-structure relationships. The scaffolds were then analysed based on their fibre size (section 4.3.1-4.3.2), pore size (section 4.3.3) and tensile properties (4.3.4). Ensuring the membranes were biocompatible and not cytotoxic was investigated as well as its ability to MSC support proliferation.

4.3.1 Optimising electrospinning parameters:

To achieve the desired mechanical stability, fibre diameter and porosity as well as uniform and bead-free fibres, optimization of ES parameters such as electrode-to-collector distance and applied voltage was done whilst other ES variables such as concentration and temperature were set at constant values in all the experimental runs. Figure 20 demonstrates the scaffolds produced from 6% PCL at two different electrode-to-collector distances (120 and 155 mm) and five different applied voltages (20-60 kV). At the lower distance of 120 mm, whilst the lower applied voltages were able to produce a matrix on the collector; significant solvent damage was also seen at all voltages. The damage can be referred to as solvent 'spitting' and is caused by not enough time for the solvent to evaporate before reaching the collector, it was found to be more prevalent at higher voltages. To conserve material, higher voltages past 40 kV were not tested at 120 mm. To reduce the effect of solvent spitting, the electrode-to-collector distance was increased to the maximum setting of 155 mm. Optimal scaffold production was found at 155 mm and 40 kV, below this voltage, very little scaffold was produced and at higher voltages (50-60 kV) solvent spitting increased. SEM analysis of samples produced at 40 kV and 60 kV (both at 155 mm) also demonstrate the effect of solvent spitting. It is clear that solvent spitting damages the fibre structure and scaffold as a whole and so should be minimised to produce a high-quality biomaterial.

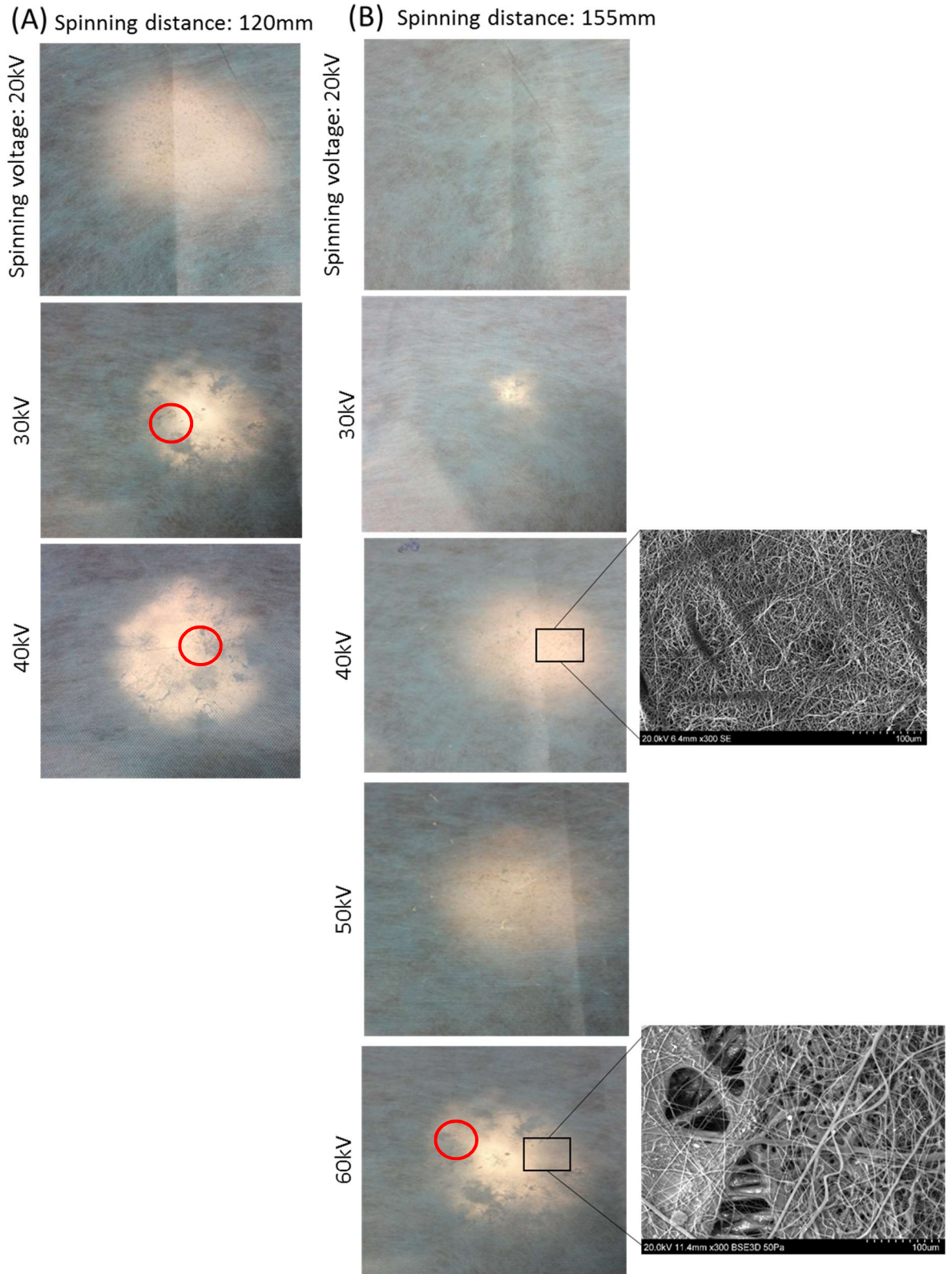


Figure 20: Membrane formation via free-surface ES 6% PCL with an electrode-to-collector distance of either 155 or 120 mm and varied voltage. At 120 mm, voltages 20-30 kV, significant spitting was seen, circled in red in column A. At 155 mm 40-50kV increased fibre deposition and minimal spitting was observed (column B). SEM images of membranes electrospun at 155 mm of electrode-to-collector distance and both 40 kV and 60 kV were also captured to demonstrate the effect of solvent spitting.

4.3.2 Optimising spinning blended collagen and PCL solutions

The spinning parameters were then further optimised using an equal blend of collagen and PCL (50:50). It was clear that at all the voltages tested, this solution spun more consistently and with fewer defects (spitting and beading) than the pure PCL despite the solution concentration being 6% (w/v) for both. This hinted at a decreased solution viscosity in the case of the 50:50 collagen:PCL solution compared to the PCL solution control at the same concentration, likely related to the hydrogen bonding interactions between PCL's repeating units and collagen's amino groups. Considering the increased spinnability of the PCL-collagen mixture, it was decided that this blend would be spun at 6% (w/v) concentration, whilst pure PCL solutions would be spun at reduced polymer concentration, i.e. 3% (w/v), aiming to achieve PCL control fibres with comparable homogeneity and fibre diameter. The optimised spinning parameters were kept consistent at a voltage of 40 kV and a spinning distance of 155 mm.

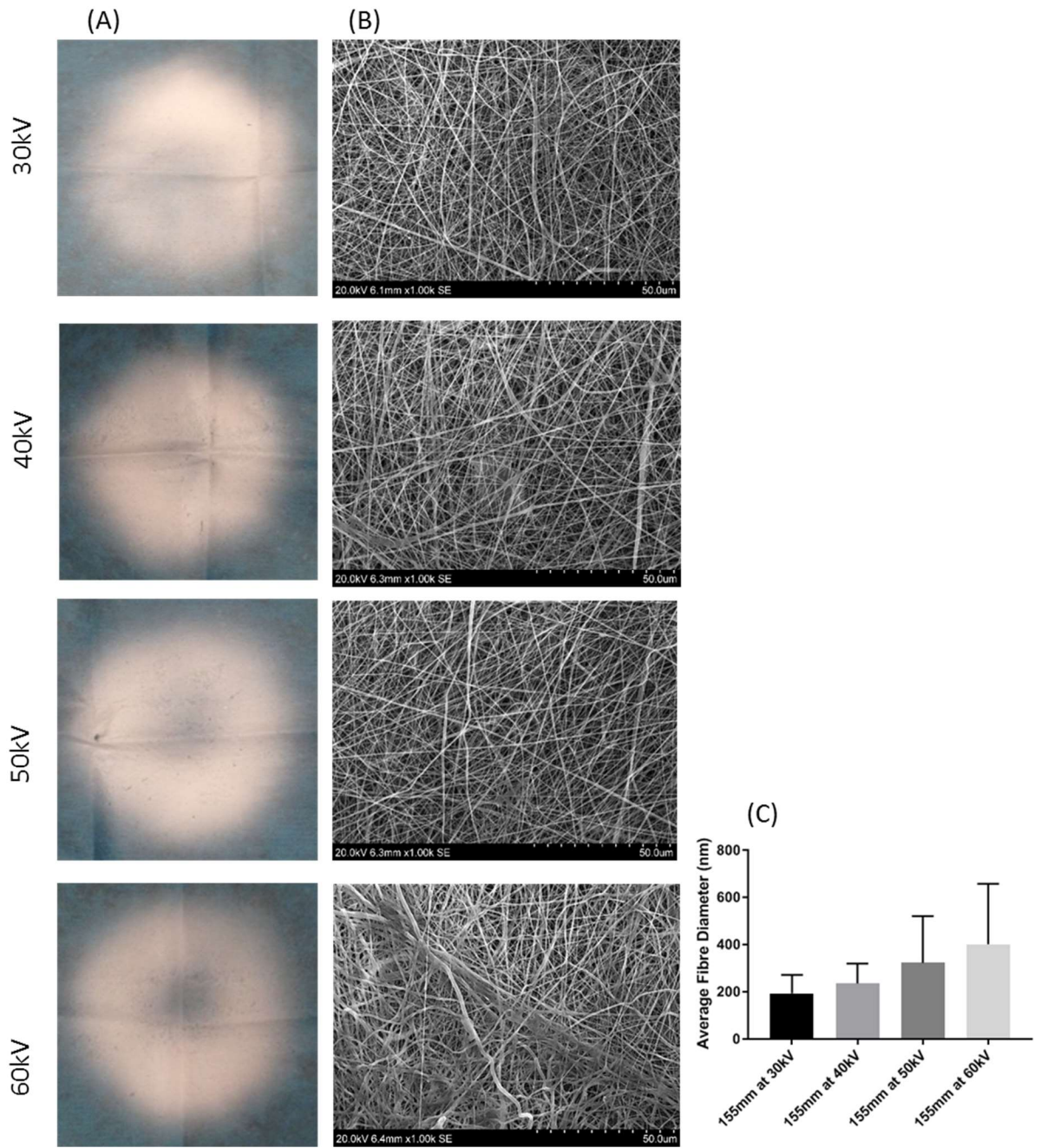


Figure 21: Membrane formation via free-surface ES 6% Collagen:PCL (50:50) with an electrode-to-collector distance of 155 mm and a range of applied voltages (30-60 kV). Column A shows the macroscopic view of the scaffolds spun at each voltage, whilst column B shows the microscopic image collected from SEM analysis. The average fibre diameter is also shown (C) with error bars indicating technical variation between replicates.

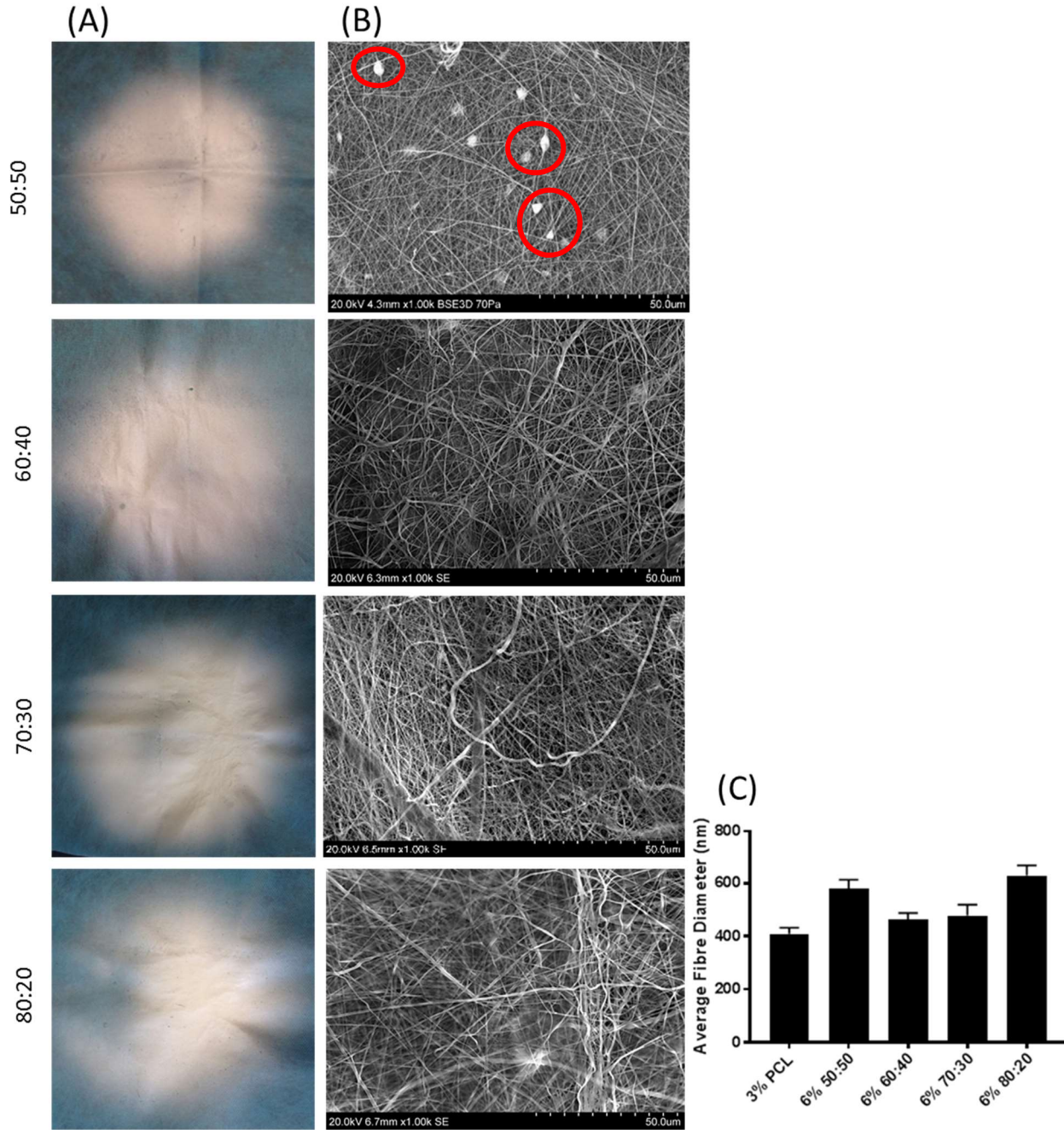


Figure 22: Membrane formation via free-surface ES of 6% Collagen:PCL at various compositions (50:50-80:20) with an electrode-to-collector distance of 155 mm and an applied voltages of 40 kV. Column A shows the macroscopic view of the scaffolds spun at each voltage, whilst column B shows the microscopic image collected from SEM analysis. Red circles indicate regions of beading. The average fibre diameter is also shown (C) with error bars indicating technical variation between replicates.

Once the spinning parameters were optimised for both the control PCL scaffold and the collagen:PCL blended scaffolds, different compositions were spun with the aim of ES collagen:PCL mixtures with increased collagen content whilst ensuring the formation of membranes with increased mechanical integrity. A range of membranes with increasing concentrations of collagen (50-80% w/v) were generated (figure 22). Interestingly, SEM analysis of the 50:50 scaffold revealed the presence of beads on some of the fibres, possibly due to unequal mixing of the solution. Despite distinct differences in the solution's composition, no clear trend of fibre diameter was observed (figure 22 C). Whilst the 80:20 solution was able to successfully spin, resulting membrane was brittle and too delicate to handle. Therefore, the membrane made with 70:30 collagen:PCL was selected for further analysis, alongside the electrospun PCL control.

4.3.3 Pore size analysis:

Using porometry, the pore size distribution for membranes made of both the PCL and 70:30 collagen:PCL was determined (figure 23, A and B respectively) and revealed that over 80% of the pores were smaller than 4 μm . The maximum pore size of membranes of either PCL or 70:30 collagen:PCL was 36 μm and 44 μm respectively, although these larger pores were rare occurrences in the latter case. Knowing that cells need a pore size of at least 8 μm to be able to migrate through [23] suggests that these scaffolds will likely act as a barrier to cell infiltration, angiogenesis, and possibly even nutrient transport.

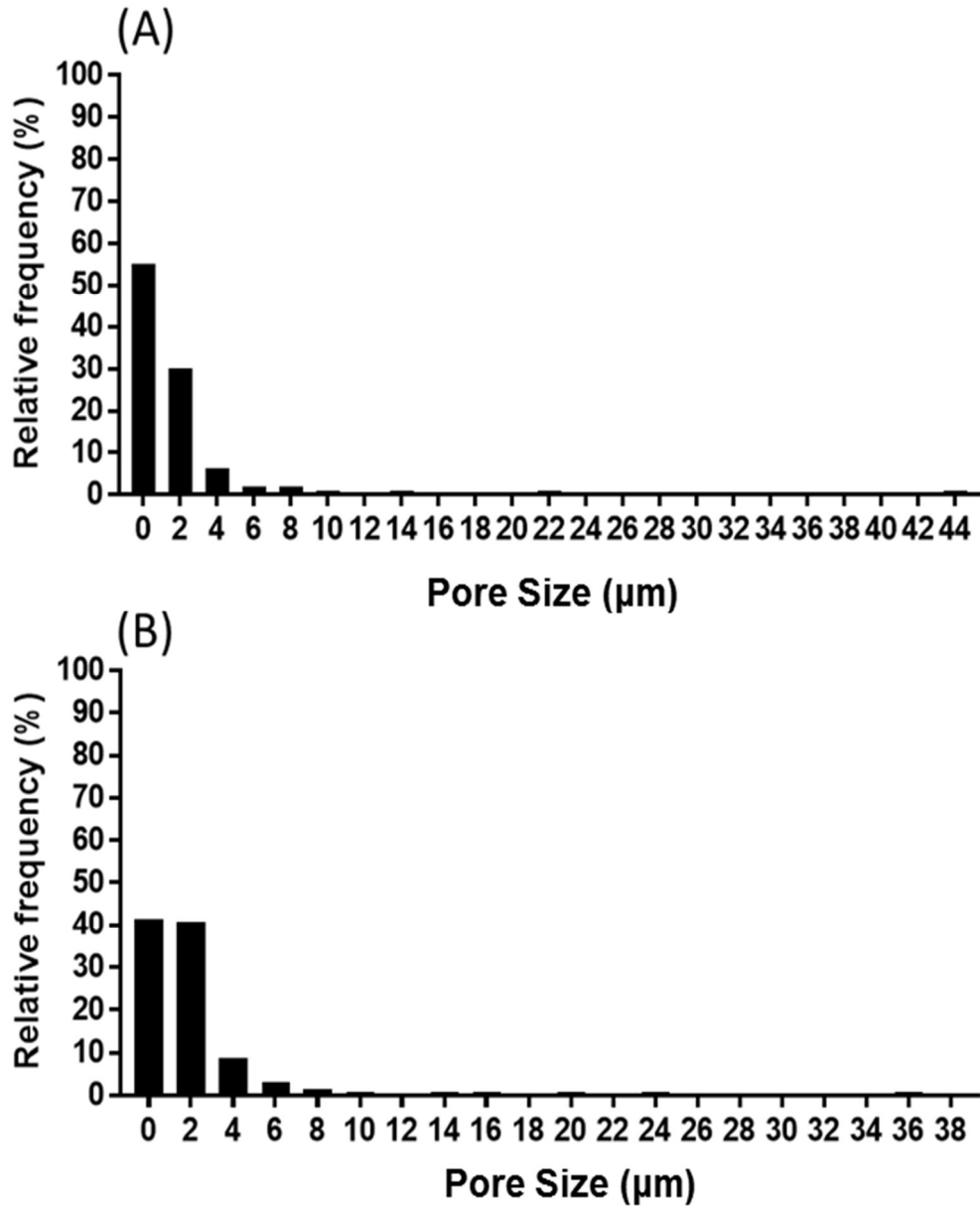


Figure 23: Pore size distribution from the porometry analysis, the top panel shows the relative frequency of pores in 6% 70:30 (A), the bottom panel shows the relative frequency of pores in 3% PCL (B).

To overcome the inherently-small pore size measured in the electrospun membranes, a laser cutter was used to create larger pores. Pores with a diameter of 200 μm was chosen as this was found previously to be the average lumen diameter of the IM, as well as being linked to osteogenesis in the literature [24], and it is the smallest pore the laser cutter can create. Because the pores were too large to be measured using the porometer, SEM images were used instead for pore diameter analysis (figure 24). Despite using the lowest power settings of the laser cutter, the three PCL membranes displayed larger pores (around 500 μm in

diameter) compared to the expected value ($\sim 200 \mu\text{m}$), likely due to the laser-induced melting of the PCL phase. The presence of collagen in the 70:30 collagen:PCL membrane resulted in the formation of smaller pores ($\sim 280 \mu\text{m}$) following laser cutting, likely due to the decreased content of the thermoplastic polymer in corresponding fibres, ultimately resulting in reduced fibre melting during laser cutting. Despite both membranes displayed larger than expected pores, insignificant differences in pore size were measured across membrane batches (figure 24).

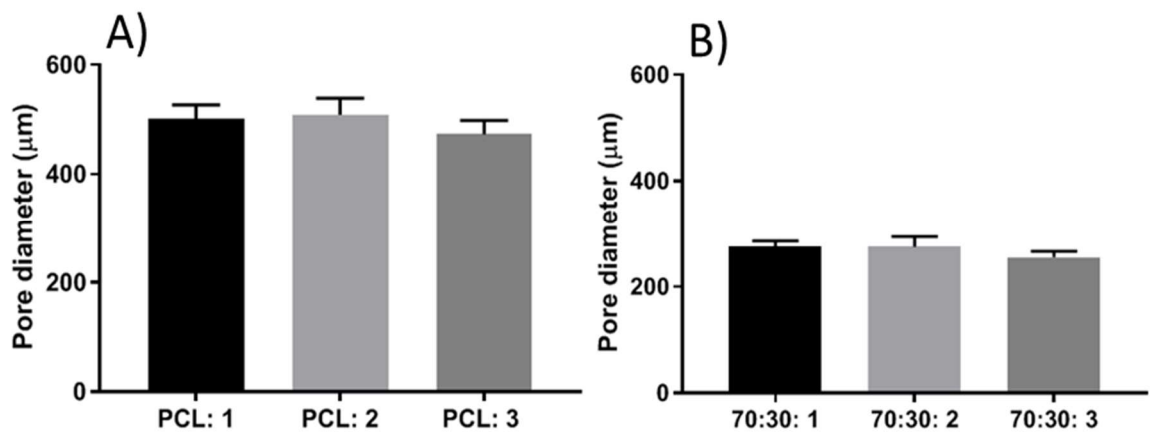


Figure 24: Results from the SEM analysis of laser cut pores in the 3% PCL scaffold (A) and 6% 70:30 scaffold (B). Each bar represents an individual sheet tested with a minimum of 4 pores tested from each sheet, error bars show replicate variation between pores.

4.3.4 Mechanical properties of the laser cut scaffolds

To investigate the effect of laser cutting on scaffold mechanical properties, tensile tests were carried out on membranes prepared with either reduced or increased pore frequency and compared against the pristine electrospun control with no laser cut pores. Details of the different scaffolds that underwent tensile testing are outlined in table 9. As described in equation 2 (section 4.2.5), the open area was calculated from the area and number of pores, whilst total porosity was calculated as a percentage of the apparent density of the scaffold and bulk density of the components. It is of note that even the intact scaffolds are still $>90\%$ porous due to the electrospun morphology of the scaffolds and high surface area.

Table 9: Outline of the open area (area of laser cut pores) and the total porosity (inherent porosity plus laser cut pores) for each scaffold type. Three variations of each material (PCL and 70:30) were included; intact control (no laser cut pores), sparse pores and dense pores.

		Open area (cm ²)	Total porosity – (%)
PCL	Intact scaffold	0	94
	Sparse pores	0.1	96
	Dense pores	0.4	97
70:30	Intact scaffold	0	93
	Sparse pores	0.1	95
	Dense pores	0.4	96

Representative stress-strain curves of the intact scaffolds are shown in figure 25A demonstrating how the data was plotted to extract maximum stress at break (ultimate strength), strain at break and the elastic modulus. Both scaffold types show similar ultimate strengths of 1.1 ± 0.2 and 1.0 ± 0.2 MPa for 70:30 and PCL respectively (figure 25B). Interestingly, PCL shows a significantly higher strain at break point of 0.54 ± 0.05 mm/mm compared to the decreased values measured on 70:30 scaffolds (strain at break: 0.37 ± 0.07 mm/mm) indicative of brittle properties (figure 25C). This finding is confirmed by the decreased elastic modulus measured on 70:30 scaffolds in comparison to electrospun PCL controls (figure 25D).

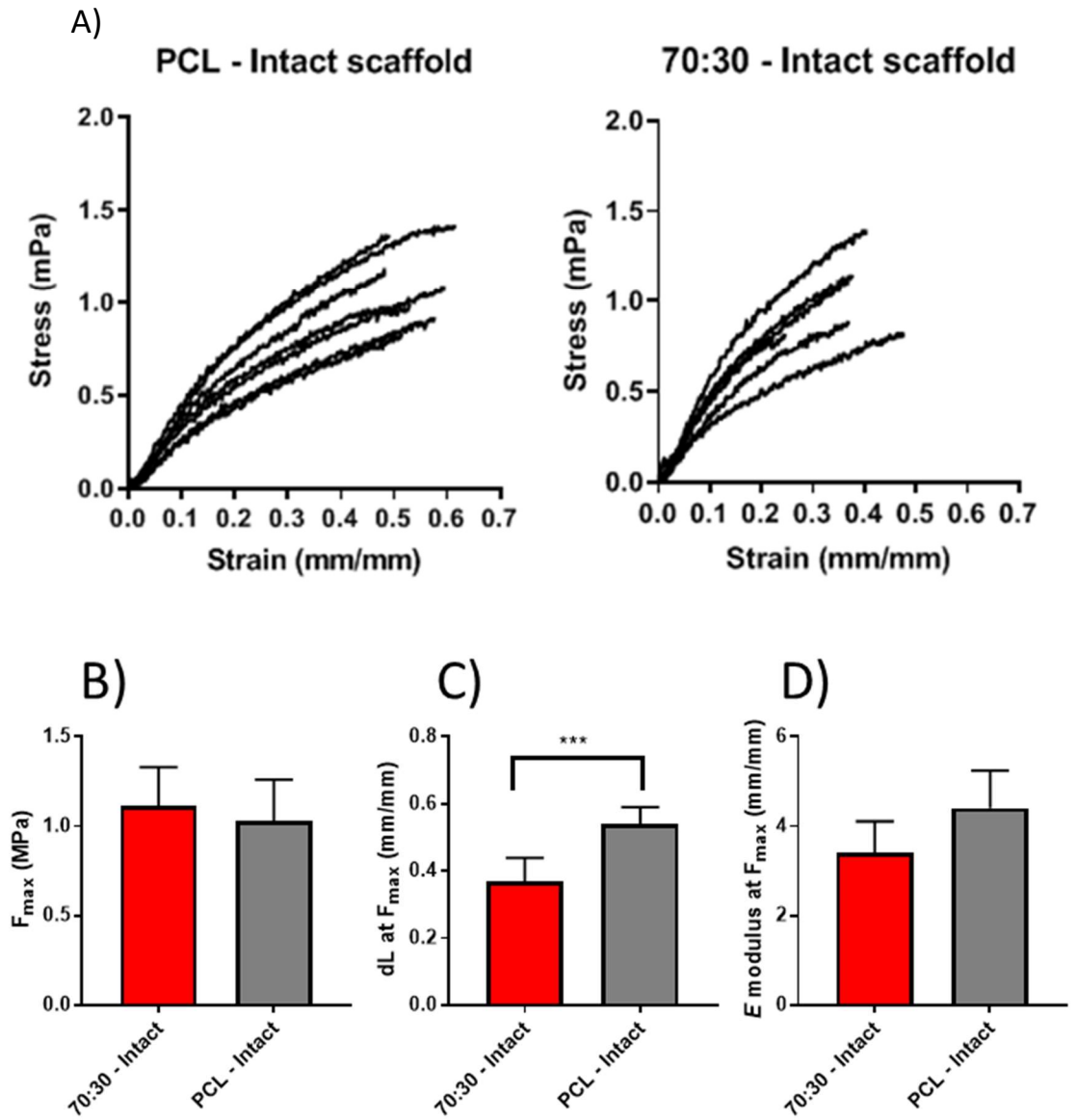


Figure 25: Representative stress-strain curves for intact 3% PCL and 6% 70:30 scaffolds (no laser cut pores) (A), from these curves the breaking stress (ultimate strength) (B), breaking strain (C) and the elastic modulus (D) can be extracted. The error bars represent the standard errors of the technical replicates ($n=6$), whilst an unpaired t-test was used to measure significance; $**P < 0.01$.

4.3.5 Comparing the properties of 70:30 scaffolds with different laser cut pore densities

Comparison of the different laser cut pore densities and their effect on the mechanical properties of the 70:30 scaffolds are shown in figure 26. Interestingly, the most unexpected result introducing sparse pores into the membrane was had on the maximum break point (figure 26A), whereby a significant increase was observed in the ultimate strength of the scaffold compared to the ultimate strength of the intact control. Furthermore, the introduction of more pores (dense pore scaffold) resulted in a significant reduction in ultimate strength. Analysis of the strain at break (figure 26B) demonstrated how the introduction of both sparse and dense pores resulted in a significant reduction in strain at break from the intact control. This reduction in strain at break is indicative of an increased brittleness of the scaffolds. This is mirrored by the elastic modulus (figure 26C) being significantly increased following the introduction of sparse pores compared to the intact control. Although not significant, the elastic modulus also appeared higher in the dense pore scaffold compared to the intact control.

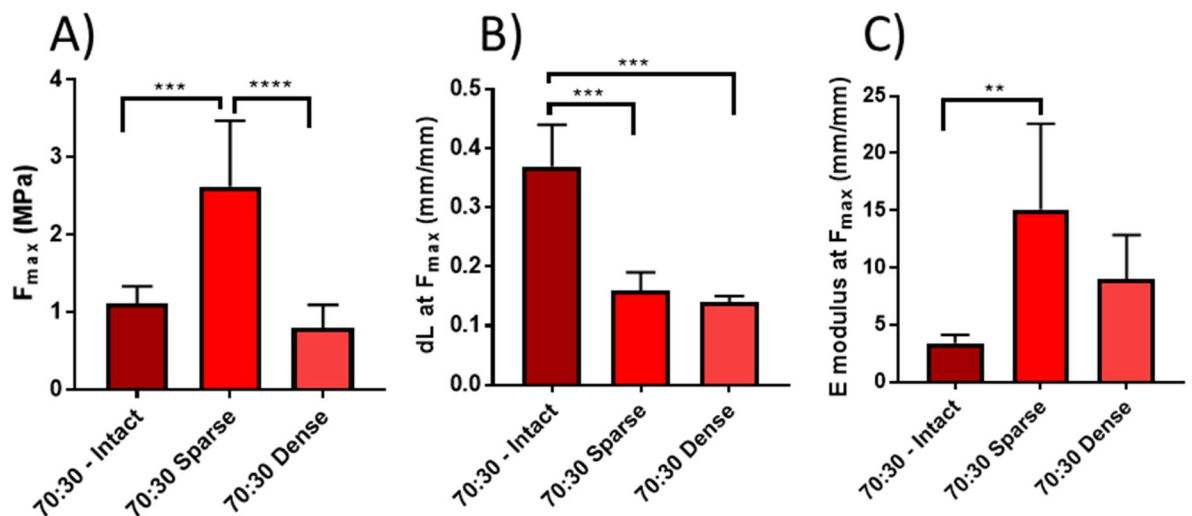


Figure 26: Results show the maximum breaking stress (ultimate strength) (A), breaking strain (B), and the elastic modulus (C) of 6% 70:30 scaffolds. The error bars represent the standard errors of the technical replicates (n=6), whilst ANOVA was used to measure significance; ** $P < 0.01$, *** $P < 0.001$.

4.3.6 Comparing the properties of PCL scaffolds with different laser cut pore densities

Comparison of the different laser cut pore densities and their effect on the mechanical properties of the PCL scaffolds are shown in figure 27. Interestingly, the same unexpected increase in maximum break point that was observed following the introduction of sparse pores in the 70:30 scaffold was also observed in the PCL scaffold (figure 27 A). As well, the introduction of more pores in the dense pore PCL scaffold resulted in a significant decrease in maximum break point. Analysis of the PCL scaffold's strain at break (figure 27 B) demonstrated how the introduction of dense pores resulted in a reduction in maximum strain at break, indicative of increased brittleness, whilst the introduction of sparse pores had no effect. The elastic modulus results (figure 27 C) again showed how PCL with sparse pores performed similarly to the intact PCL control, but the introduction of dense pores unexpectedly showed a significant reduction in elastic modulus indicative of reduced stiffness. Overall, whilst some reduction in strain at break and elastic modulus, was observed following the introduction of pores, the PCL scaffolds appear less brittle and stiff than the 70:30 scaffolds and appear to have a lower ultimate strength.

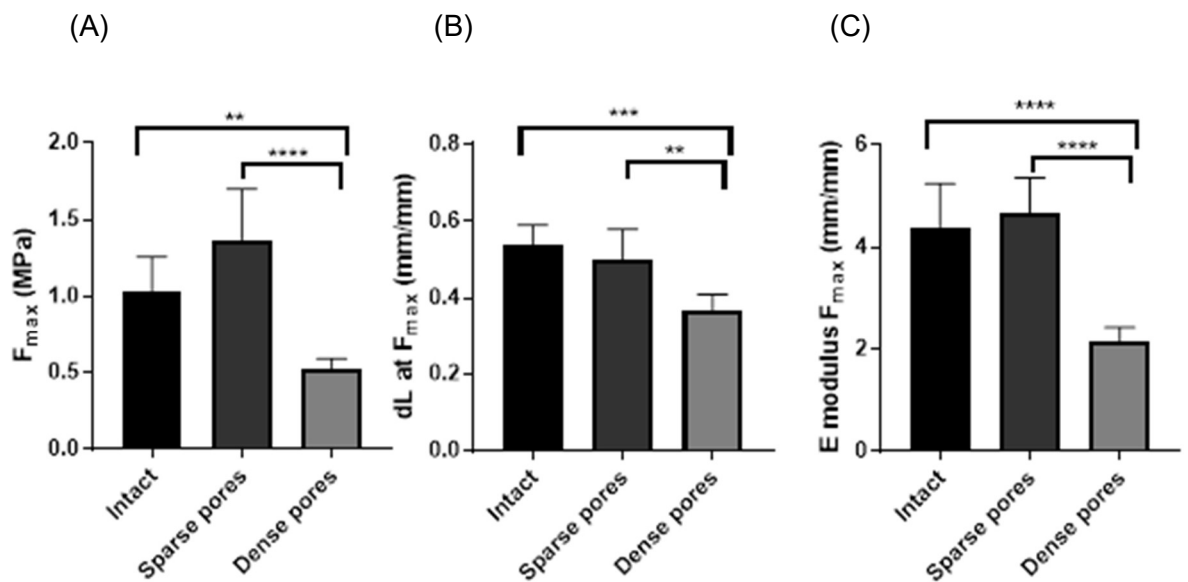


Figure 27: Results show the maximum breaking stress (ultimate strength) (A), breaking strain (B), and the elastic modulus (C) of 3% PCL scaffolds. The error bars represent the standard errors of the technical replicates (n=6), whilst ANOVA was used to measure significance; * $P < 0.05$, ** $P < 0.01$, *** $P < 0.001$.

Once the PCL-Collagen solutions have been spun, it was investigated whether or not they could be further tailored by folding and heat treating to increase their final thickness. Figure 28 demonstrates how both PCL and 70:30 membranes thickness can be increased by 4-fold after folding in half twice . Spinning 20 mL of solution resulted in a scaffold thickness of $90\pm 4\ \mu\text{m}$ for 70:30 , which increased to $408\pm 43\ \mu\text{m}$ after folding; PCL scaffold controls displayed a similar thickness of either $97\pm 13\ \mu\text{m}$ (in the electrospun format) or $408\pm 43\ \mu\text{m}$ (after folding and thermal bonding). Increasing the number of folds will result in a thicker tissue and this demonstrates how post-manufacture scaffold processing can be conveniently employed to achieve macroscopic scaffold customisation.

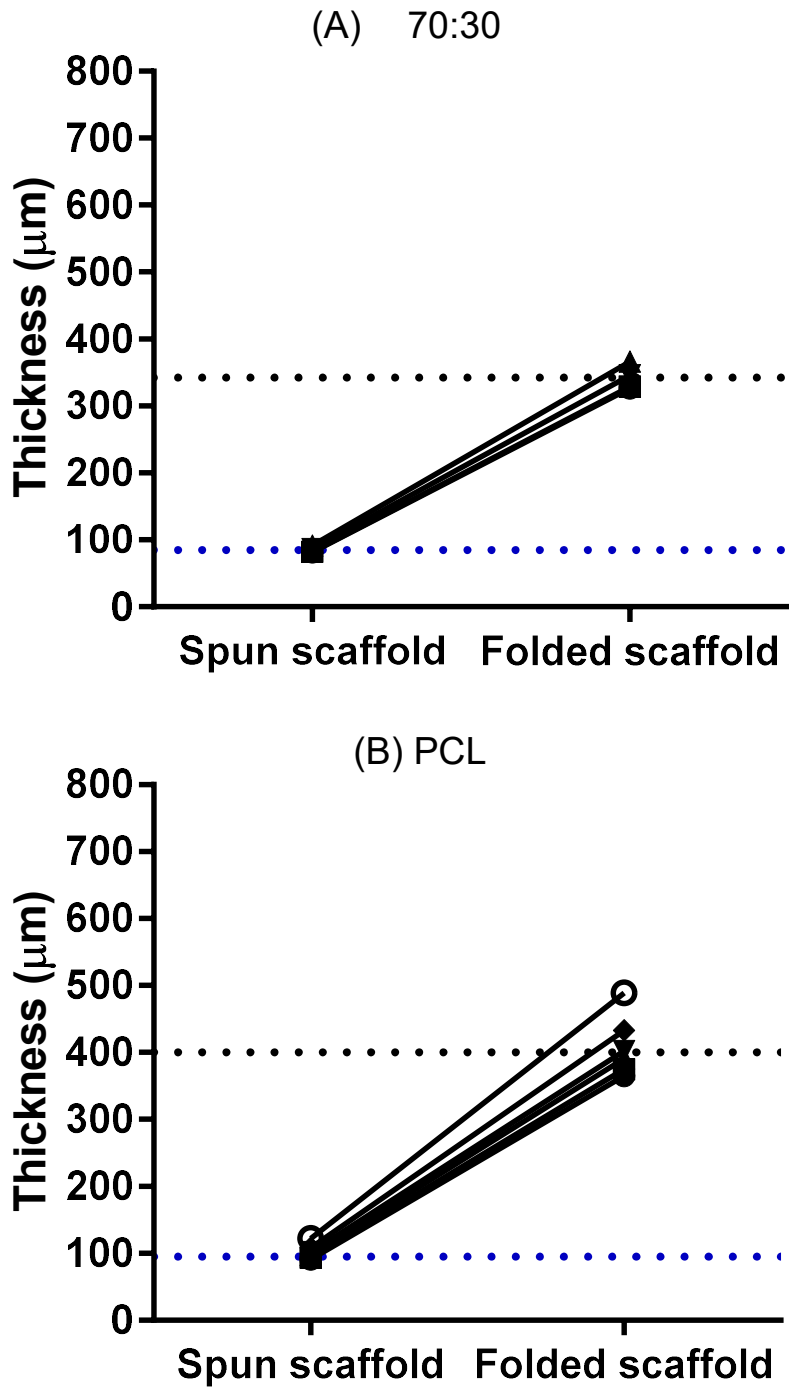


Figure 28 scaffold thickness for 70:30 scaffolds (A) and PCL scaffolds (B) in their unfolded 'spun' form and folded form. The blue lines indicate the average original thickness of spun scaffolds and the black lines indicate the average thickness of the folded scaffolds. $N=3$ for 70:30 and $n=5$ for PCL.

The intact folded 70:30 scaffolds were also tested after being hydrated in PBS and compared to the dry 70:30 control scaffolds (figure 29). It was shown that hydrating the scaffold decreased its ultimate strength, although this trend was mostly found to be insignificant (figure 29A). The only significant difference between the dry and hydrated samples was seen in the strain at break (figure 29B) whereby the hydrated scaffold was found to have a higher breaking strain indicative of a less brittle structure compared to the dry scaffold. This finding is further reinforced by the lower elastic modulus of the hydrated sample, whilst not a significant difference, is also indicative of a less stiff structure.

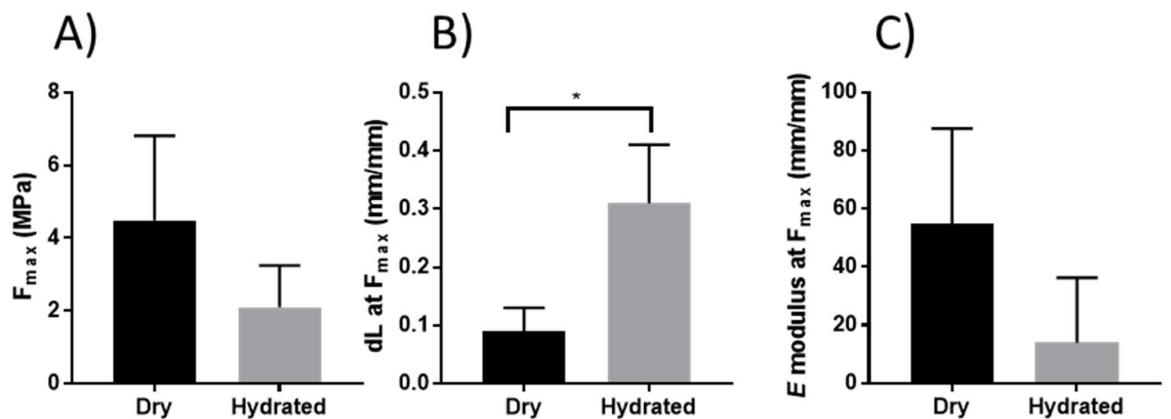


Figure 29: Results show the maximum breaking stress (ultimate strength) (A), breaking strain (B), and the elastic modulus (C) of 6% 70:30 folded scaffolds both dry and hydrated with PBS. The error bars represent the standard errors of the technical replicates ($n=3$), whilst an unpaired t -test was used to measure significance; * $P < 0.05$.

4.4 Discussion

To address the need for a guided bone regeneration device in long bone fracture, a novel collagen-PCL prototype scaffold was manufactured, and its microstructure and mechanical properties were characterised.

In the field of tissue engineering, whilst a wide range of manufacturing techniques exist, ES is a favoured option due to its ability to produce scaffolds with consistent nanofibers, interconnected pores as well as considerable surface to volume ratio. However, the ES manufacturing yield is typically restricted by the syringe volume with a maximum output of up to 1 g/h of fibre per syringe. These low yields make commercialisation and industrial scale up of electrospun scaffold challenging to realise. Free surface ES or 'needle-free' ES has therefore sparked interest by

increasing the yield output and production speed by using baths rather than syringes. A bath setup has a much higher volume capacity, and, when a roller electrode is used, results in multiple jets along its length which further increase the rate of fibre formation. Although synthetic polymers are usually the material of choice (such as PCL or PLGA) for ES due to their low cost and structural stability, they lack the biological cues necessary for stem cell migration, attachment and proliferation. Therefore, when synthetic polymers are used, their surface is often conjugated with collagen or other natural polymers [26]. One of the most advanced applications of this method has been demonstrated by Ramakrishna *et al*, who used coaxial spinning to create fibres with a PCL core coated in a collagen 'shell'. Although this method proved to be successful for improving cell migration into the scaffold, this coating technique comes with the risk of rapid leeching and degradation due to the superficial presence of collagen [16][25, 26].

Whilst pure collagen scaffolds exist in dentistry, their role is to act as sponges for plugging defects. This makes their required structural properties very different to what is needed for orthopaedic translation. For guided bone regeneration, the scaffold needs structural integrity as a membrane to wrap around the fracture, contain the grafted material whilst still be permeable to cell migration and nutrient transport. Pure collagen scaffolds for dentistry are often manufactured from decellularised porcine and equine tissues (such as Mucograft), which are associated with high manufacturing costs, risk of disease transmission, and challenging industrial scale up. Access to novel needle-free ES technology and using the extraction method for affordable and stable collagen from rat tails resulted in a unique opportunity to address the limitations of previous techniques and materials. Clinical grade collagen reduces the risk of xenogenic contamination, whilst the structural design is tailored with specific functionality in mind, and the equipment and materials were chosen based on ease of industrial scale-up.

Due to the novelty of this approach there was little published research on needle-free ES collagen scaffolds therefore, one of the aims of this work was to optimise the protocol for generating scaffolds from collagen containing solutions. HFIP was the solvent chosen due to its sufficient volatility (boiling point of 61°C) to maintain a consistent solution concentration in the open bath setup, as well as its ability to dissolve both collagen and PCL into a homogenous solution [27]. In the literature, the normal working concentrations for solutions is between 2-10% and initial trial and error (data not shown) brought the starting polymer solution concentration for this work to 6%. Ideally more extensive factorial design of the spinning parameters would have been part of the research but were limited due to time constraints.

For 6% PCL a spinning distance of 155 mm and a voltage of 40 kv were found to be the best spinning parameters both macroscopically and microscopically however spinning of 6% 50:50 collagen:PCL appeared to improve the consistency and fibre quality at all spinning voltages. It was observed that the 6% 50:50 solution was less viscous than the 6% PCL solution likely caused by the difference in the intrinsic viscosity of collagen and PCL as well as the different molecular interactions present [28]. Collagen's triple helix molecules are more sensitive to the HFIP solvent which results in denaturation of their conformation as well as lower viscosity [29]. Although other solvents such as acetic acid and ethanol may better preserve collagen's triple helical structure, they are too volatile for needle-free ES leading to the formation of highly variable material. The open bath arrangement of needle-free ES limits the number of solvents that can be used; however this has recently been addressed in the development of a continuous feed which coats the electrode with spinning solution instead of coating by directly rolling in a bath. Considering scaffold production was improved following the reduction in solution viscosity, collagen and PCL blends were spun at 6% whilst pure PCL blends were spun at 3%.

After spinning different blends of collagen and PCL, 70:30 was found to have the highest collagen content whilst still being structurally sound and easy to handle. Above this concentration, the scaffolds were too brittle and fragile and so weren't taken forward for further characterisation. Porometric analysis of the 70:30 and PCL scaffolds revealed that the majority of pores in both are smaller than 8 μm and are therefore likely to act as a barrier to cell migration and nutrient transport. To preserve the structural integrity of the scaffold, whilst improving its ability to allow nutrient and cell transport, pores were incorporated using a laser cutter [30]. The distribution of 200 μm pores, with either 2 or 4 mm gaps, was chosen as this design was simple to control and replicate. Smaller gaps of 1 mm between pores were also briefly tested and excluded because of their fragility when handling. Whilst laser cutting pores into scaffolds has been successfully used in the development of corneal scaffolds, to regulate their strength and transparency [30], its incorporation into the post-manufacture processing of an orthopaedic membrane remains novel. Before pores were introduced, both the intact 70:30 and PCL scaffolds possess similar tensile properties with regards to their breaking points and elastic modulus, the only significant difference found was between the two material's strain at break which was lower in the 70:30 blend. Due to the novelty of this device, there is no consensus in the literature regarding tensile requirements; therefore, the tensile properties of comparable devices and tissues were used instead to inform scaffold design. As the device is not envisaged to be weight-bearing or undergo much

manipulation once sutured in place, tensile properties were investigated at the breaking point. Analysis of 120 rat IM samples by Gaio *et al.* found their ultimate stress ranged from 0.1-0.4 MPa depending on the surface of the cement spacer used to induce their formation [31]. Other ES collagen-containing scaffolds, for example PLGA-collagen blend using needle-based ES, found their scaffolds to have breaking points of 1.1 MPa dry and 0.6 MPa hydrated [32] whilst pure PCL scaffolds were found to be stronger at 2 MPa (hydrated) [33]. This was supported by other research which found PCL to have a tensile strength of 2 MPa which decreased when blended with gelatine to 0.4 MPa [34].

Ideally, analysis of human IM sample's tensile properties would be carried out for comparison and would be one of the priorities of future work in this area. Despite the lack of specific guidelines, both scaffolds were found to be comparable to other scaffolds currently being developed and even exceed the properties of rat IM 10 fold. Furthermore, handling of the scaffolds for this research found them to be resilient and easy to manipulate, meeting the initial qualitative criteria for basic handling necessary during surgery.

The influence of pores and their spacing on tensile strength was clearly demonstrated during this research, interestingly, it was seen that the introduction of sparse pores increased the ultimate strength of the scaffold compared to the intact versions. This finding contradicts work by Li-Ping Lee *et al* [35] who describe how increasing the open area of the structure (either by increasing pore size or number) reduces the amount of connective material that supports the scaffold, resulting in decreased tensile strength. This negative correlation of decreasing tensile strength with increasing pore number was also described by Kong *et al* who conclude that decreasing the number of fibres per unit area that contribute to the force of the membrane would in-turn decrease the ultimate strength of the scaffold [23]. The discrepancy between the findings in this work and the previously published data is likely due to the incorporation of PCL whereby the heat of the laser cutter melted the layers of fibre around the pores creating regular anchor points which resulted in an overall increase in tensile strength. This interaction is easily offset by the presence of too many pores as demonstrated by the tensile strength of the scaffolds with dense pores, whereby the open area was too great to be supported by the remaining connective material resulting in an overall weaker scaffold.

As well as laser cutting pores, heating and folding the scaffolds was another method used to demonstrate the range of post-manufacture processing techniques that can be utilised to tailor the scaffold for specific applications. The aim of this

work is to mimic the functionality of the IM and so the scaffold will require thickness to enable PRP absorption and mechanical stability (properties which will be tested in chapter 6). As expected, both PCL and 70:30 proved to be highly malleable by demonstrating how the initial spun scaffolds thickness can be easily increased.

As these scaffolds are envisaged to be soaked in bone marrow aspirate or PRP, it was important to collect pilot data on the scaffolds hydrated state. It was clear that the hydrated scaffold appeared weaker than the dry scaffold but no significant difference was observed. The only significant difference hydrating the scaffolds made was increasing their strain at break. It is also of note that both the folded dry and hydrated scaffolds had higher tensile strength following folding and laser cutting than the single sheets (4 MPa compared to 1 MPa). This promising finding demonstrates how the scaffold's properties can be tailored depending on the specific orthopaedic requirement.

As well as optimising the collagen and PCL ratios and spinning voltage and distance, future work would also involve factorial design of all parameters [36] such as concentration, humidity, temperature and viscosity etc. to fully optimise the process as is the industry standard [37].

Next research steps will focus on the material's ability to absorb and release proteins as well as support cell viability and proliferation.

4.5 References:

1. P. Gentile, V. Chiono, C. Tonda-Turo, A. M. Ferreira and G. Ciardelli, *Polymeric membranes for guided bone regeneration*, *Biotechnology journal* **6** (2011), no. 10, 1187-1197.
2. M. S. Carvalho, A. A. Poundarik, J. M. S. Cabral, C. L. da Silva and D. Vashishth, *Biomimetic matrices for rapidly forming mineralized bone tissue based on stem cell-mediated osteogenesis*, *Scientific reports* **8** (2018), no. 1, 14388.
3. P. V. Giannoudis, T. Einhorn and D. Marsh, *Fracture healing: The diamond concept.*, *Injury* **4** (2007), 3-6.
4. F. Matassi, L. Nistri, D. Chicon Paez and M. Innocenti, *New biomaterials for bone regeneration*, *Clinical cases in mineral and bone metabolism : the official journal of the Italian Society of Osteoporosis, Mineral Metabolism, and Skeletal Diseases* **8** (2011), no. 1, 21-24.
5. T. Barrows, *Degradable implant materials: A review of synthetic absorbable polymers and their applications*, *Clinical Materials* **1** (1986), no. 4, 233-257.
6. R. Shi, J. Xue, M. He, D. Chen, L. Zhang and W. Tian, *Structure, physical properties, biocompatibility and in vitro/vivo degradation behavior of anti-infective polycaprolactone-based electrospun membranes for guided tissue/bone regeneration*, *Polym. Degrad. Stabil.* **109** (2014), 293-306.
7. F. Batool, D. N. Morand, L. Thomas, I. M. Bugueno, J. Aragon, S. Irusta, L. Keller, N. Benkirane-Jessel, H. Tenenbaum and O. Huck, *Synthesis of a novel electrospun*

polycaprolactone scaffold functionalized with ibuprofen for periodontal regeneration: An in vitro and in vivo study, *Materials* **11** (2018), no. 4.

8. S. Browne, D. I. Zeugolis and A. Pandit, *Collagen: Finding a solution for the source*, *Tissue Eng Part A* **19** (2013), no. 13-14, 1491-1494.

9. D. Brett, *A review of collagen and collagen-based wound dressings*, *Wounds : a compendium of clinical research and practice* **20** (2008), no. 12, 347-356.

10. M. A. Meyers, J. McKittrick and P. Y. Chen, *Structural biological materials: Critical mechanics-materials connections*, *Science (New York, N.Y.)* **339** (2013), no. 6121, 773-779.

11. T. D. Brown, P. D. Dalton and D. W. Hutmacher, *Melt electrospinning today: An opportune time for an emerging polymer process*, *Progress in Polymer Science* **56** (2016), 116-166.

12. J. A. Matthews, G. E. Wnek, D. G. Simpson and G. L. Bowlin, *Electrospinning of collagen nanofibers*, *Biomacromolecules* **3** (2002), no. 2, 232-238.

13. B. Dong, O. Arnoult, M. E. Smith and G. E. Wnek, *Electrospinning of collagen nanofiber scaffolds from benign solvents*, *Macromol. Rapid Commun.* **30** (2009), no. 7, 539-542.

14. Y. R. V. Shih, C. N. Chen, S. W. Tsai, Y. J. Wang and O. K. Lee, *Growth of mesenchymal stem cells on electrospun type i collagen nanofibers*, *Stem Cells* **24** (2006), no. 11, 2391-2397.

15. J. Venugopal, L. L. Ma, T. Yong and S. Ramakrishna, *In vitro study of smooth muscle cells on polycaprolactone and collagen nanofibrous matrices*, *Cell Biol. Int.* **29** (2005), no. 10, 861-867.

16. Y. Z. Zhang, J. Venugopal, Z. M. Huang, C. T. Lim and S. Ramakrishna, *Characterization of the surface biocompatibility of the electrospun pcl-collagen nanofibers using fibroblasts*, *Biomacromolecules* **6** (2005), no. 5, 2583-2589.

17. I. J. Hall Barrientos, E. Paladino, P. Szabó, S. Brozio, P. J. Hall, C. I. Oseghale, M. K. Passarelli, S. J. Moug, R. A. Black, C. G. Wilson, R. Zelkó and D. A. Lamprou, *Electrospun collagen-based nanofibres: A sustainable material for improved antibiotic utilisation in tissue engineering applications*, *International Journal of Pharmaceutics* **531** (2017), no. 1, 67-79.

18. I. Bhattacharyya, M. C. Molaro, R. D. Braatz and G. C. Rutledge, *Free surface electrospinning of aqueous polymer solutions from a wire electrode*, *Chemical Engineering Journal* **289** (2016), 203-211.

19. O. O. Dosunmu, G. G. Chase, W. Kataphinan and D. H. Reneker, *Electrospinning of polymer nanofibres from multiple jets on a porous tubular surface*, *Nanotechnology* **17** (2006), no. 4, 1123.

20. N. Rajan, J. Habermehl, M. F. Cote, C. J. Doillon and D. Mantovani, *Preparation of ready-to-use, storable and reconstituted type i collagen from rat tail tendon for tissue engineering applications*, *Nature protocols* **1** (2006), no. 6, 2753-2758.

21. S. Aldrich, "Sigma aldrich catalog," Merck (Editor), vol. 2019, <https://www.sigmaaldrich.com/catalog/product/aldrich/440744?lang=en®ion=GB>, 2019.

22. A. Shamloo, N. Mohammadaliha, S. C. Heilshorn and A. L. Bauer, *A comparative study of collagen matrix density effect on endothelial sprout formation using experimental and computational approaches*, *Annals of biomedical engineering* **44** (2016), no. 4, 929-941.

23. M. R. Lindy O'Clair, Maria Tikhonenko, Clare Syzbut, Nicola Bevan, Kirk Schroeder and Daniel M. Appledorn "Quantification of cell migration and invasion using the incuCyte® chemotaxis assay," *Essen BioScience - Application Note*, M. Ann Arbor, USA and Welwyn Garden City, Hertfordshire, UK (Editor), Michigan, USA, 2017.

24. V. Karageorgiou and D. Kaplan, *Porosity of 3d biomaterial scaffolds and osteogenesis*, *Biomaterials* **26** (2005), no. 27, 5474-5491.

25. M. Kim and G. H. Kim, Electrohydrodynamic direct printing of pcl/collagen fibrous scaffolds with a core/shell structure for tissue engineering applications, *Chemical Engineering Journal* **279** (2015), 317-326.
26. P. Gentile, K. McColgan-Bannon, N. C. Gianone, F. Sefat, K. Dalgarno and A. M. Ferreira, *Biosynthetic pcl-graft-collagen bulk material for tissue engineering applications*, *Materials (Basel, Switzerland)* **10** (2017), no. 7, 693.
27. E. D. Boland, J. A. Matthews, K. J. Pawlowski, D. G. Simpson, G. E. Wnek and G. L. Bowlin, *Electrospinning collagen and elastin: Preliminary vascular tissue engineering*, *Frontiers in bioscience : a journal and virtual library* **9** (2004), 1422-1432.
28. J. Dulnik, D. Kolbuk, P. Denis and P. Sajkiewicz, The effect of a solvent on cellular response to pcl/gelatin and pcl/collagen electrospun nanofibres, vol. 1042018.
29. T. Liu, W. K. Teng, B. P. Chan and S. Y. Chew, *Photochemical crosslinked electrospun collagen nanofibers: Synthesis, characterization and neural stem cell interactions*, *Journal of biomedical materials research. Part A* **95** (2010), no. 1, 276-282.
30. B. Kong, W. Sun, G. Chen, S. Tang, M. Li, Z. Shao and S. Mi, *Tissue-engineered cornea constructed with compressed collagen and laser-perforated electrospun mat*, *Scientific reports* **7** (2017), no. 1, 970.
31. N. Gaio, A. Martino, Z. Toth, J. T. Watson, D. Nicolaou and S. McBride-Gagyi, Masquelet technique: The effect of altering implant material and topography on membrane matrix composition, mechanical and barrier properties in a rat defect model, *Journal of Biomechanics* **72** (2018), 53-62.
32. A. Sadeghi-Avalshahr, S. Nokhasteh, A. M. Molavi, M. Khorsand-Ghayeni and M. Mahdavi-Shahri, *Synthesis and characterization of collagen/plga biodegradable skin scaffold fibers*, *Regen. Biomater.* **4** (2017), no. 5, 309-314.
33. A. P. Rameshbabu, S. Datta, K. Bankoti, E. Subramani, K. Chaudhury, V. Lalzawmliana, S. K. Nandi and S. Dhara, *Polycaprolactone nanofibers functionalized with placental derived extracellular matrix for stimulating wound healing activity*, *J. Mat. Chem. B* **6** (2018), no. 42, 6767-6780.
34. I. Rajzer, E. Menaszek, R. Kwiatkowski, J. A. Planell and O. Castano, *Electrospun gelatin/poly(ϵ -caprolactone) fibrous scaffold modified with calcium phosphate for bone tissue engineering*, *Materials Science and Engineering: C* **44** (2014), 183-190.
35. B. L. Lee, H. Jeon, A. Wang, Z. Yan, J. Yu, C. Grigoropoulos and S. Li, *Femtosecond laser ablation enhances cell infiltration into three-dimensional electrospun scaffolds*, *Acta Biomater* **8** (2012), no. 7, 2648-2658.
36. Levin A, Sharma V, Hook L and García Gareta E, The importance of factorial design in tissue engineering and biomaterials science: Optimisation of cell seeding efficiency on dermal scaffolds as a case study, *Journal of Tissue Engineering* **9** (2018), 1-14.
37. I. Y. Enis, H. Sezgin and T. G. Sadikoglu, *Full factorial experimental design for mechanical properties of electrospun vascular grafts*, *Journal of Industrial Textiles* **47** (2018), no. 6, 1378-1391.

5 Biological products

5.1 Introduction:

Fracture non-union persists as a prevalent complication, with the incidence in long bones reported to range between 5-10% [1, 2]. Its etiopathogenesis remains multifactorial with a recent review identifying over 20 factors to be implicated in this process [3]. To address impaired fracture healing, Giannoudis PV et al. proposed the diamond conceptual framework for bone repair highlighting that, for a successful healing response both mechanical stability and biological factors must be present [4]. For biological stimulation, while autologous bone graft remains the gold standard, recently, other forms have gained popularity including bone marrow aspirates (BMA) and/or growth factors [5, 6]. Since their introduction to the clinical setting, bone morphogenetic proteins (BMPs) have been extensively used for the treatment of non-union fractures [7]. There are numerous publications reporting on the clinical results of BMP-2 and BMP-7 [8-10]. However, since the withdrawal of BMP-7 from the market and the license limitation of BMP-2 to be used for the management of open tibial fractures, other inductive molecules gained popularity such as demineralised bone matrix (DBM)[11], teriparatide [12] and platelet rich plasma (PRP) [13, 14].

PRP is a highly enriched source of autologous growth factors and cytokines that acts as a biological stimulant [15] and is applied either with the cells intact, or more recently, as platelet lysate (PL) where only the growth-factor containing plasma is used [16]. Both forms have been found to be highly effective in the treatment of orthopaedic trauma [17] and several studies into PRP loaded membranes are already proving to be successful at promoting regeneration via the delivery of growth factors in cartilage and bone repair [18, 19]. When using PRP loaded membranes for guided bone regeneration, maximising BM-MSc proliferation and migration is key. By ensuring these functions are enhanced, more viable cells are available to differentiate, as well as inducing more resident BM-MSc homing to the site of injury. Whilst some studies found that the presence of leukocytes in PRP is advantageous due to their antimicrobial properties [20] as well as their high concentration of cytokines that are involved in bone repair such as VEGF [21, 22], there are also concerns related to leukocytes' role of inducing excessive inflammatory and necrotic pathways from the surrounding tissue – providing a strong case for their depletion [23, 24]. Therefore it was hypothesised that producing PRP using a two-step centrifugation method that could be tailored for

theatre application, will be purer in platelets than a clinical standard PRP made using a commercial device and will therefore stimulate more BM-MSC proliferation and migration.

This chapter investigates the *in vitro* effect of platelets and leukocytes on the proliferation and migration of BM-MSCs from BMA by studying a range of PRP compositions including a clinical-standard PRP. A laboratory-standard PRP made using a two-spin centrifugation protocol to enrich platelets but deplete leukocytes was also used as control [17, 25]. To investigate the specific importance of leukocytes, PRP was processed further by syringe-filtration to remove leukocytes and produce a pure filtered PRP (fPRP). These products were then lysed to ensure product consistency over the course of *in vitro* assays; thereafter referred to as clinical-standard platelet lysate (C-PL), platelet lysate (PL) and filtered PL (fPL). These PLs were then evaluated *in vitro* utilising primary BM-MSCs, including autologous BM-MSC-PL combinations. The aim was to assess if high numbers of leukocytes would impede BM-MSC proliferation and migration and whether their depletion from clinical PRPs would be desirable for bone regenerative approaches. The results will ensure the manufactured collagen-membrane is loaded with optimum PRP to stimulate bone repair by maximising autologous BM-MSCs migration to the fracture site as well as facilitate BM-MSC proliferation.

5.2 Specific methods:

5.2.1 Blood collection and generation of PRP:

Under the regulation of the Leeds East Research Ethics Committee, as outlined in section 2.1, healthy donors (n=12, 4 females and 8 males, age range 22-44yrs, median =30) were invited to donate 20ml of blood in dipotassium ethylenediaminetetraacetic acid (EDTA) and acid-citrate-dextrose (ACD) vacuette tubes. These anticoagulants were chosen because of their already widespread use in clinics and surgery as well as their existing use in generating C-PRP [26, 27]. Prior to processing, each donor's pooled blood was incubated at RT for 1 hr to achieve a clear separation between the layers.

The blood was centrifuged at 400 xg for 10 minutes at RT (figure 30 B) and then the platelet-containing supernatant was collected and further centrifuged at 2700 xg for 10 minutes (figure 30 C). The pellet was finally resuspended in 1/5 of the supernatant (considered the PPP fraction) to produce PRP (figure 30 D). Analysis of the sample was carried out using the Hematology-Analyzer as described in

section 5.2.5. The time between blood collection and processing was approximately 2 hours.

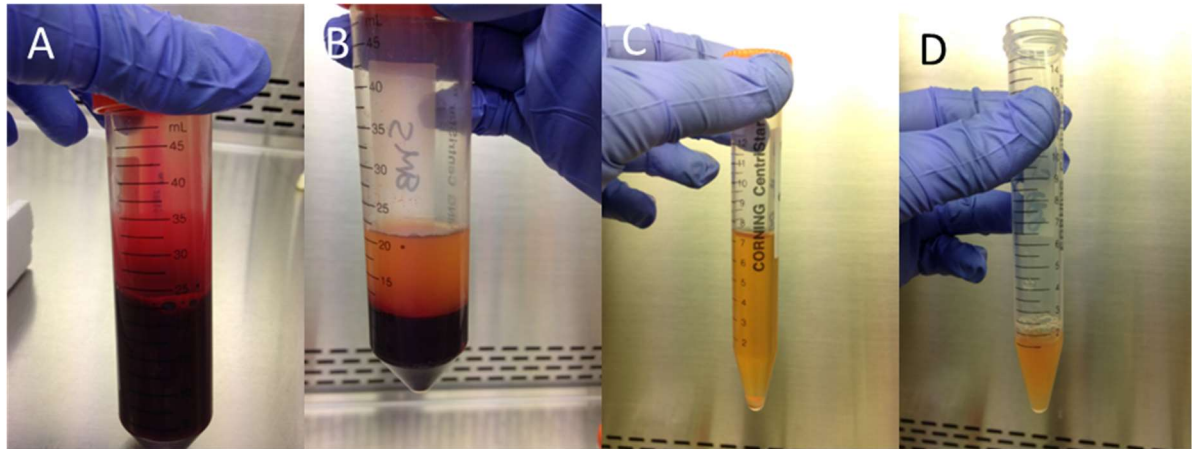


Figure 30: Making PRP uses a donor's blood (A), which is centrifuged into two distinct layers (B). The supernatant is collected (C) and centrifuged again at a higher speed. The final pellet is resuspended in 1/5th of the supernatant to make PRP (D).

5.2.2 Generating commercial PRP (C-PRP):

Patients undergoing elective orthopaedic surgery with no underlying disease (n=8, 2 females and 6 males, age range= 22-34yrs, median= 28yrs) had 60ml of their blood collected in a syringe containing 6mL ACD-A to get a final concentration of 10% ACD-A. The blood underwent a 15 minute spin step in a Biomet Biologics centrifuge (figure 31 A) to separate the C-PRP from the PPP and red blood cells the BioCUE™ Platelet Concentration System (figure 31 B). A 1mL sample of the C-PRP was collected from each donor in EDTA vacuettes, as well as 1mL of the donor-matched whole blood, for analysis using the Hematology-Analyzer (section 5.2.5). Three patients also donated 20mL of whole blood for the production of PRP as outlined in section 5.2.1 to enable donor matched comparisons between the two platelet products.

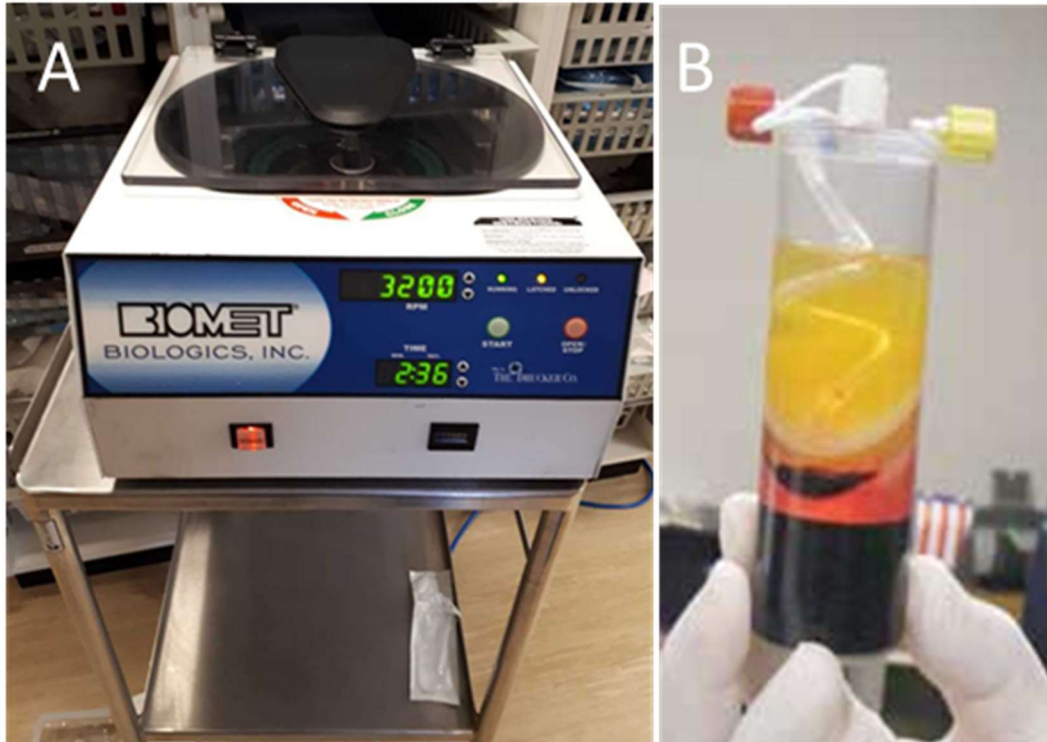


Figure 31: C-PRP was made using an in-theatre centrifuge (A) and the BioCUE™ Platelet Concentration System (B) to concentrate the platelets.

5.2.3 Generating filtered PRP (fPRP):

To remove all leukocytes from PRP (described in section 5.2.1) and generate fPRP, samples were filtered using a white blood cell syringe filter. Between 2-5 ml of sample in a syringe is allowed to pass through the filter via gravity allowing the entrapment of leukocytes whilst the filtered PRP is collected below the syringe barrel for further processing. 100 μ L of filtered samples were analysed using the haematology analyser as described in section 5.2.5.

5.2.4 Leukocyte and platelet stability assay:

PRP products from three healthy donors were prepared according to section 5.2.1 in both EDTA and sodium citrate vacuette tubes. Once made, the PRP products were incubated at 37°C in sealed falcon tubes for 14 days whilst 100 μ L aliquots were collected on days 1, 4, 7 and 14 for analysis using the haematology analyser.

5.2.5 Analysing blood and PRP samples:

To quantify cell populations in PRP, fPRP and C-PRP 100µL of each sample was analysed using the haematology analyser. White blood cells (WBC), red blood cells (RBC), platelets (PLT) and leukocyte percentages of lymphocytes (LYM), basophils and eosinophils (MXD), and neutrophils (NEUT) were quantified in each sample based on each cell type's electrical impedance. 100µL of donor-matched whole blood was also analysed and its cell counts were used as the baseline to calculate fold enrichment or depletion in each of the platelet products.

5.2.6 Generating PL and C-PL and fPL:

To generate the lysed products for *in vitro* assays, PRP, fPRP and C-PRP were processed through three freeze-thaw cycles which involved freezing at -80°C for at least one hour followed by defrosting at 37°C for 10 mins [28]. Lysis of the products changed their nomenclature from PRP, fPRP and C-PRP, to platelet lysate (PL), filtered platelet lysate (fPL) and clinical platelet lysate (PL). The products were then centrifuged at 2700 xg to separate the supernatant from intact cells and debris in the pellet. The supernatants were then stored at -80°C in aliquots of 1mL to be used in BM-MSC proliferation and migration assays (sections 5.2.7 and 5.2.8).

5.2.7 BM-MSC XTT Proliferation assay:

In order to ensure the optimal platelet product is loaded onto the membrane, the efficacy of different products (PL, C-PL and fPL) for supporting BM-MSC proliferation was first tested using the *in vitro* XTT assay. Cultured BM-MSCs up to passage four were seeded at a density of 500 cells/well in Stem Macs media in a 96-well plate and incubated. After 24 hours the wells were rinsed with PBS and replaced with 200µL of treatment media. The treatment medias were made up using a base media of DMEM, 1% Penicillin/Streptomycin and 2 I.U./mL heparin (to prevent clotting of the sample) supplemented with either 10% FCS (positive control), 10% mesencult serum (positive control), 5% or 10% platelet product (test media), or 10% DMSO (negative control). Cells were cultured in supplemented media for five days with a half media change on day three before finally staining with XTT reagent according to section 2.9.

5.2.8 Migration assays:

As well as proliferation, the optimum PL product loaded onto the membrane must also effectively induce BM-MSc migration. The chemotaxis transwell assay was used to test the efficacy of PL, C-PL and fPL's ability to induce BM-MSc migration. First, cultured cells up to passage four were serum-starved for 12 hours before the assay. Serum starving involved washing the attached cells in PBS, replacing the media with DMEM only (no FCS), and incubating overnight. Following overnight serum starving, the cells were trypsinised off the flasks as described in section 2.7 and suspended in DMEM containing 1% FCS (as opposed to 10% used for standard cell culture). The cells were centrifuged at 500 xg for 5 mins before being resuspended in DMEM.

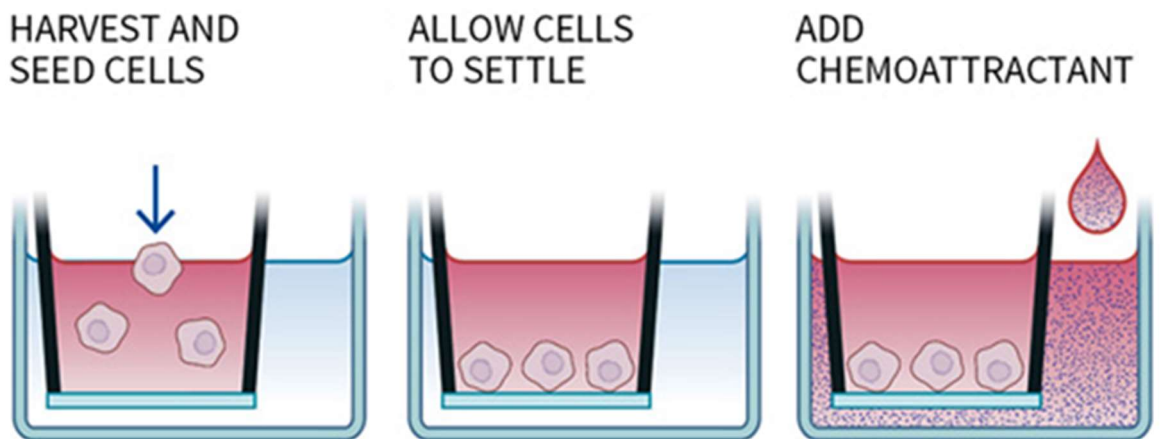


Figure 32: BM-MSCs were harvested and seeded into the transwell insert before allowing to settle at ambient temperature for 15 mins. Once cells settled, the chemoattractant was added to the bottom reservoir chamber and the plate placed inside the Incucyte device for imaging. Images adapted from the Incucyte chemotaxis cell migration quick guide [29].

In a 96 transwell plate, 600 cells in 60 μ L DMEM media were seeded per well in triplicate on the top transwells as illustrated in figure 32. In the bottom wells, 200 μ L of supplemented media was pipetted including: 10% FCS in DMEM (positive control), DMEM with no FCS (negative control) and 10% PL in DMEM (test). All medias contained 1% Penicillin/Streptomycin and 2 I.U./mL heparin. The plates were incubated for 15 mins to reduce condensation and were then moved into the IncuCyte for imaging. Migration was analysed using phase-contrast imaging of the bottom of the transwell as cells migrate along the chemotactic gradient. The transwell pores measure 8 μ m in diameter to allow single cells to move across but ensure the concentration gradient is maintained. The bottom of the wells were imaged every 30 mins and a mask was generated for each BM-MSc donor to

improve accuracy of the cell counting. The mask was made using up to six representative images of the wells on which the processing definition was created – this specified the growth threshold, minimum and maximum cell size, as well as the minimum and maximum eccentricity of each cell (how defined the cell needs to be to be recognised). Figure 33 demonstrates an example mask.

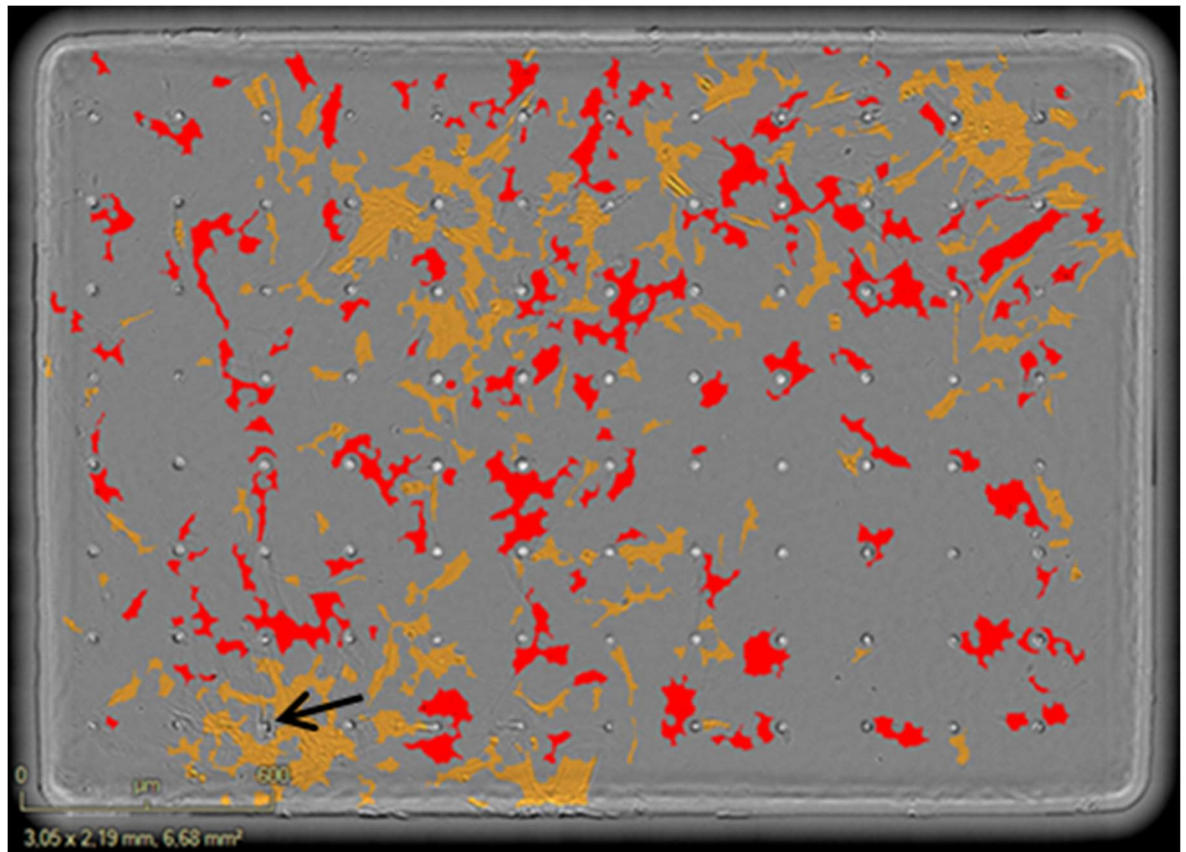


Figure 33: Example of the mask used to quantify cells, cells on top of the well are orange, on the bottom of the well are red whilst a black arrow points to an uncounted cell in grey.

5.2.9 Statistics

Statistical analyses were carried out on datasets that consisted of at least three independent experiments using a paired student's t test when comparing two groups from the same donor and an unpaired student's t test when donors weren't matched. One-way ANOVA with Tukey's multiple comparison test was used when comparing more than two groups or two-way ANOVA with Tukey's multiple comparison test for nonparametric results with GraphPad Prism software. All data are expressed as mean \pm standard deviation. * $P < 0.05$, ** $P < 0.01$, *** $P < 0.001$, and **** $P < 0.0001$ defined statistical significance.

5.3 Results:

To test the hypothesis that leukocytes in PRP have a negative effect on BM-MSc proliferation and migration, the cellular composition of the PRP were analysed (section 5.31) and their platelet and leukocyte stability were assessed (5.32). A proliferation experiment was optimised using an XTT assay (5.33) and the platelet product's proliferative capacities were tested (5.34). The IncuCyte migration assay was optimised (5.35), and the platelet products migratory capacities were tested (5.36). To test the second hypothesis that PRP prepared in-house will induce more proliferation and migration than PRP made using a commercial device (C-PRP), the differences in cell composition were analysed (5.37), and their effects on proliferation (5.38) and migration (5.39) were studied.

5.3.1 Cellular composition of PRP and fPRP:

Before the two platelet products (PRP and fPRP) could be tested, they were first characterised to ensure that filtration of the leukocytes from fPRP was successful. PRP (made in-house) and fPRP (made in-house and syringe filtered) were analysed using a haematology analyser (figure 34). Fold change of cells from whole blood was calculated as:

$$\frac{(final\ value - initial\ value)}{initial\ value}$$

For cell types that were completely depleted to zero, the fold change could not be defined and so the symbol # was used in place of a value.

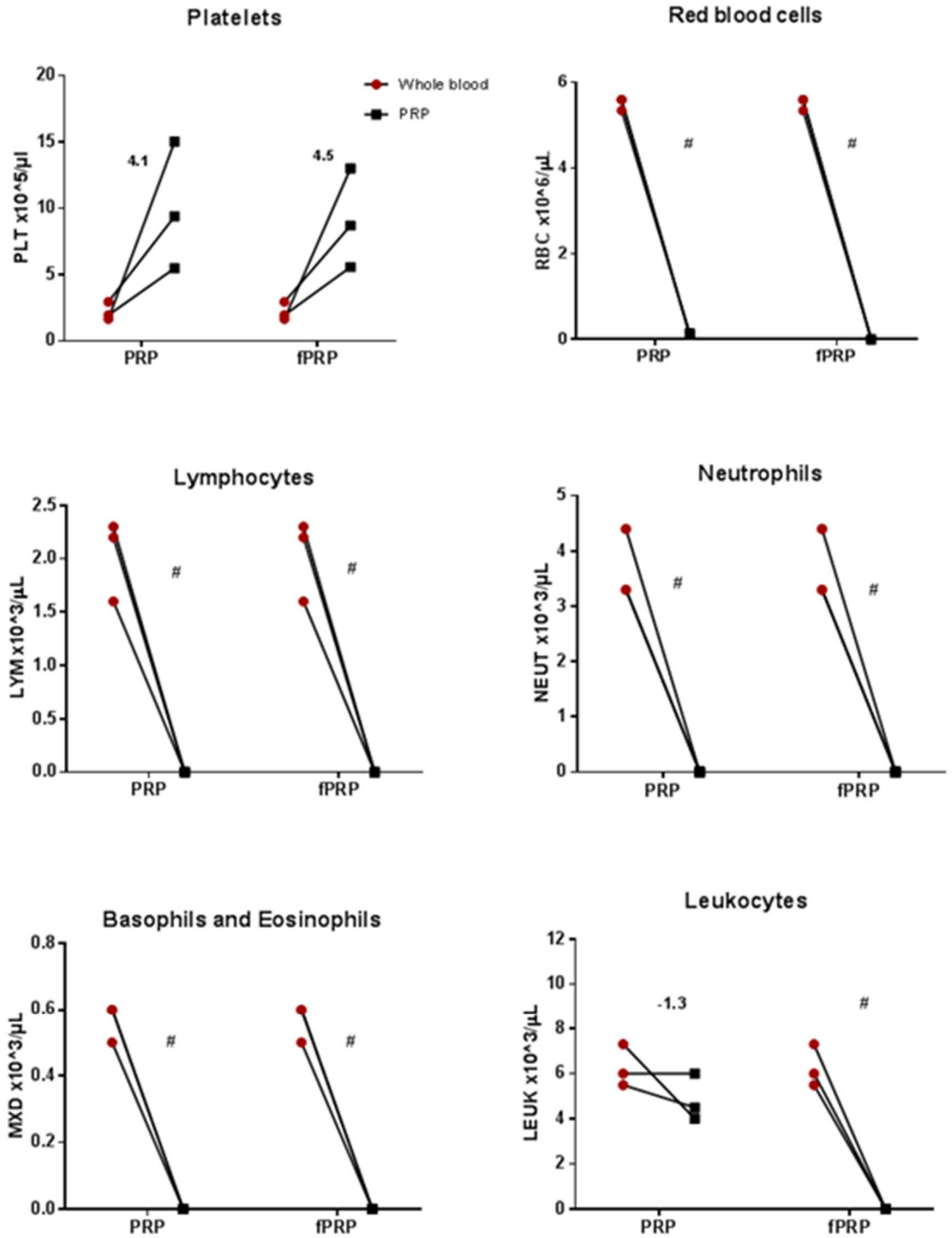


Figure 34: Comparing the changing cellular compositions from whole blood to PRP and fPRP (n=3) using a haematology analyser. Platelets, red blood cells, leukocytes, lymphocytes, basophils and eosinophils and neutrophils were counted and their fold changes from whole blood to PRP included. The numbers above each product indicate the fold change from whole blood to C-PRP/PRP, positive values indicate an average fold increase whilst a negative value indicates an average fold decrease, # indicates a complete reduction of cells to 0. Occasionally fewer than 3 data points are shown due to overlapping values forcing some data points to superimpose.

It was shown in figure 34 that filtering removes very few platelets causing PRP and fPRP to have similar platelet counts: $9.9 \pm 3.7 \times 10^3 /\mu\text{L}$ in PRP and $9.1 \pm 4.8 \times 10^3 /\mu\text{L}$ in fPRP. Looking at other cell types; red blood cells, lymphocytes, basophils, eosinophils and neutrophils, both PRP and fPRP were found to be completely depleted of them all. A paired t-test comparing all cell types in PRP and fPRP only found a significant difference in their number of leukocytes. PRP was found to reduce leukocytes by 1.3 fold from whole blood, leaving an average of $4.8 \pm 1.0 \times 10^3 /\mu\text{L}$ leukocytes whereas filtration depleted all contaminating leukocytes in fPRP. It can be concluded from this data then that the two products are the same except for their leukocyte numbers (most likely to be monocytes which the haematology analyser cannot quantify).

5.3.2 PRP stability:

To ensure the PRP products used remained consistent over the course of the assays, the stability of key cell populations (leukocytes and platelets) were analysed using the haematology analyser. Three PRP preparations made in EDTA and sodium citrate were kept at 37°C and tested on days 1, 4, 7 and 14 after preparation (figure 35). These anticoagulants were used as lab alternatives to the ACD anticoagulant used in theatre to prepare C-PRP.

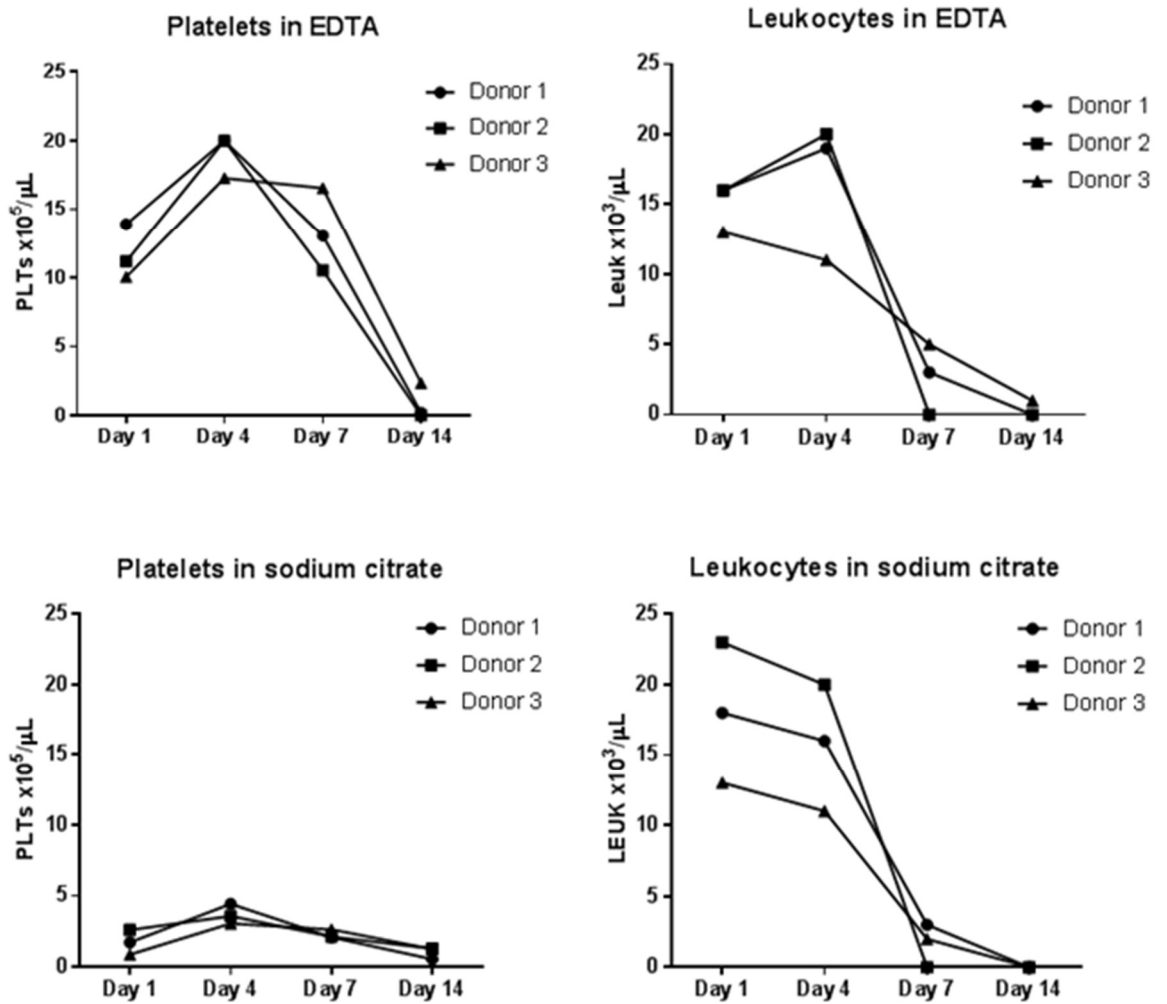


Figure 35: Comparison of the stability of platelets and leukocytes in PRP prepared in EDTA and sodium citrate over 14 days.

Although PRP made in sodium citrate resulted in lower platelet counts possibly due to their aggregation, compared to PRP made in EDTA, both anticoagulants showed a similar trend for platelet preservation. Initially, it appears that platelet numbers increase between days one to four but this is likely due to the breaking up of the cell aggregates, then, after day four, platelet numbers begin to steadily decrease as they become necrotic and lyse. A similar pattern is seen for leukocytes preserved in EDTA and sodium citrate although they appear to lyse faster than platelets, with a huge loss of intact cells by day seven. By day 14 almost all of the platelets and leukocytes in both anticoagulants have lysed. It is also noteworthy how much more varied the initial leukocyte numbers in the sodium citrate samples are compared to the EDTA samples, indicative of the impact anticoagulants have on the processing of PRP. Overall, this data demonstrates how drastically cell numbers can vary even

in the first seven days, supporting previous findings in the literature that their composition changes even after 24 hours at room temperature [30, 31]. Therefore, all proliferation and migration assays will use the lysed form of PRP, platelet lysate (PL), to ensure consistency of product.

5.3.3 Optimising XTT proliferation assay:

To optimise the XTT assay, 10% and 5% solutions of different control supplements were tested on cultured BM-MSCs for four days to decide the optimal concentration to dose the basal media DMEM with. FCS and Mesencult serum were chosen as positive controls and DMSO was chosen as the negative control whilst three individual BM-MSC cultures were used up to passage four at a seeding density of 500 cells/well in a 96 well plate. Across all three cultures, it was seen that there was a clear distinction between both positive and negative controls at both concentrations and the seeding density met the acceptance criteria as the mean OD₄₅₀ of the positive control was greater than 0.2 so no further optimisation was necessary. As expected, there was also a clear trend of 10% FCS and 10% Mesencult serum inducing more proliferation than their 5% counterparts. As well, it was seen that 10% DMSO killed more cells than 5% and so was a more reliable negative control. These results support findings in the literature that 10% is generally considered the optimum dose [32-34]. 10% will therefore be used as the concentration in all media for these assays.

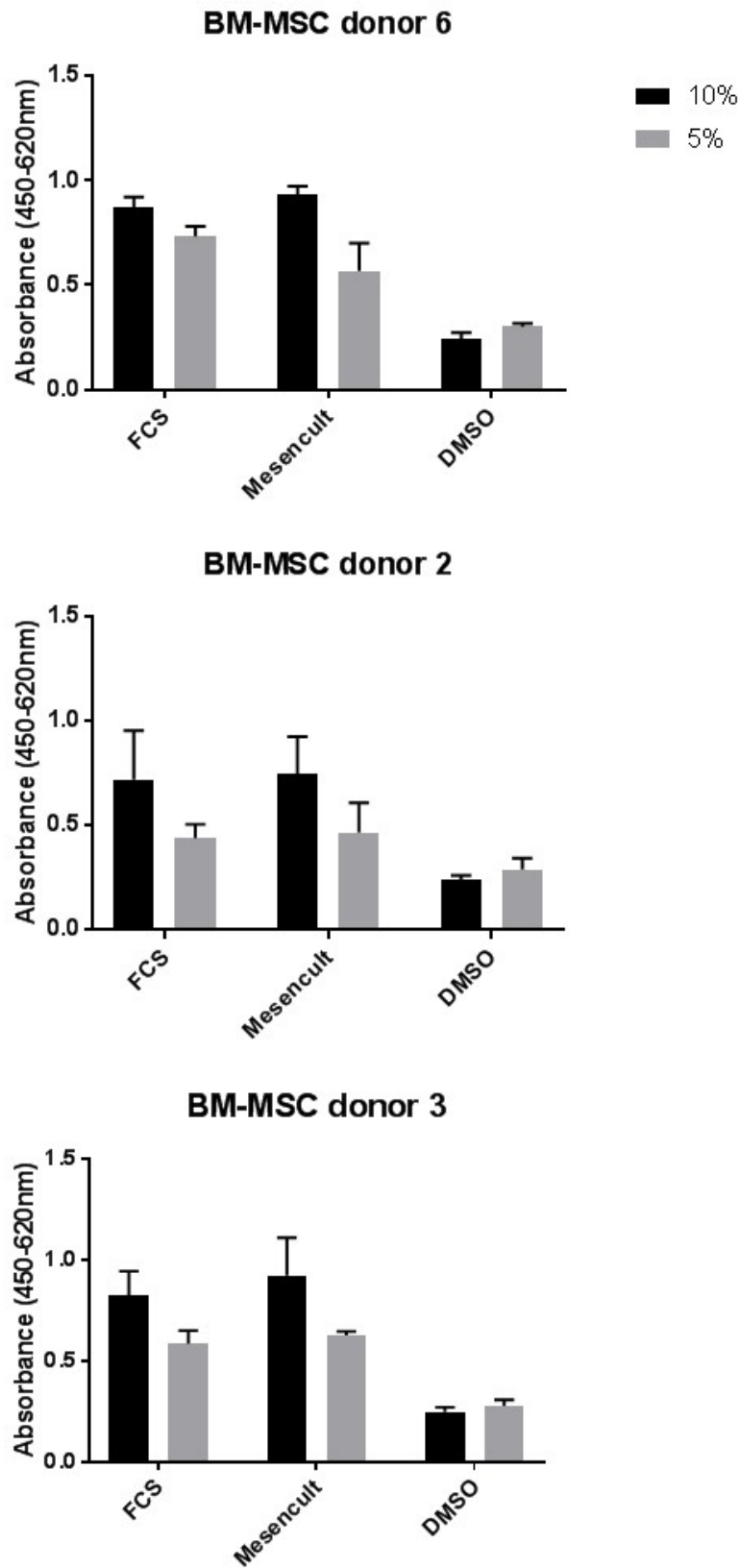


Figure 36: Comparing BM-MSc proliferation after exposure to 10% and 5% doses of control supplements; FCS, Mesencult and DMSO on cultured BM-MSCs (n=3) whilst standard error bars indicate variance between technical replicates in the XTT assay.

To assess BM-MSC culture variation, the controls were further tested on five BM- MSC cultures and it was seen that both FCS and Mesencult consistently induced proliferation (figure 37). As all the cultures demonstrated a similar response to the supplements, their results were combined as an average and a one way ANOVA test with multiple comparisons found that FCS and Mesencult both induced significantly more proliferation than the negative control DMSO ($P < 0.001$) supporting their use as appropriate controls for this experiment. Due to the similarity in response of the BM-MSCs to FCS and Mesencult serum, only FCS was carried forward as the positive control. 10% DMSO was also found to be a very reliable negative control and so was unnecessary to repeat in future experiments.

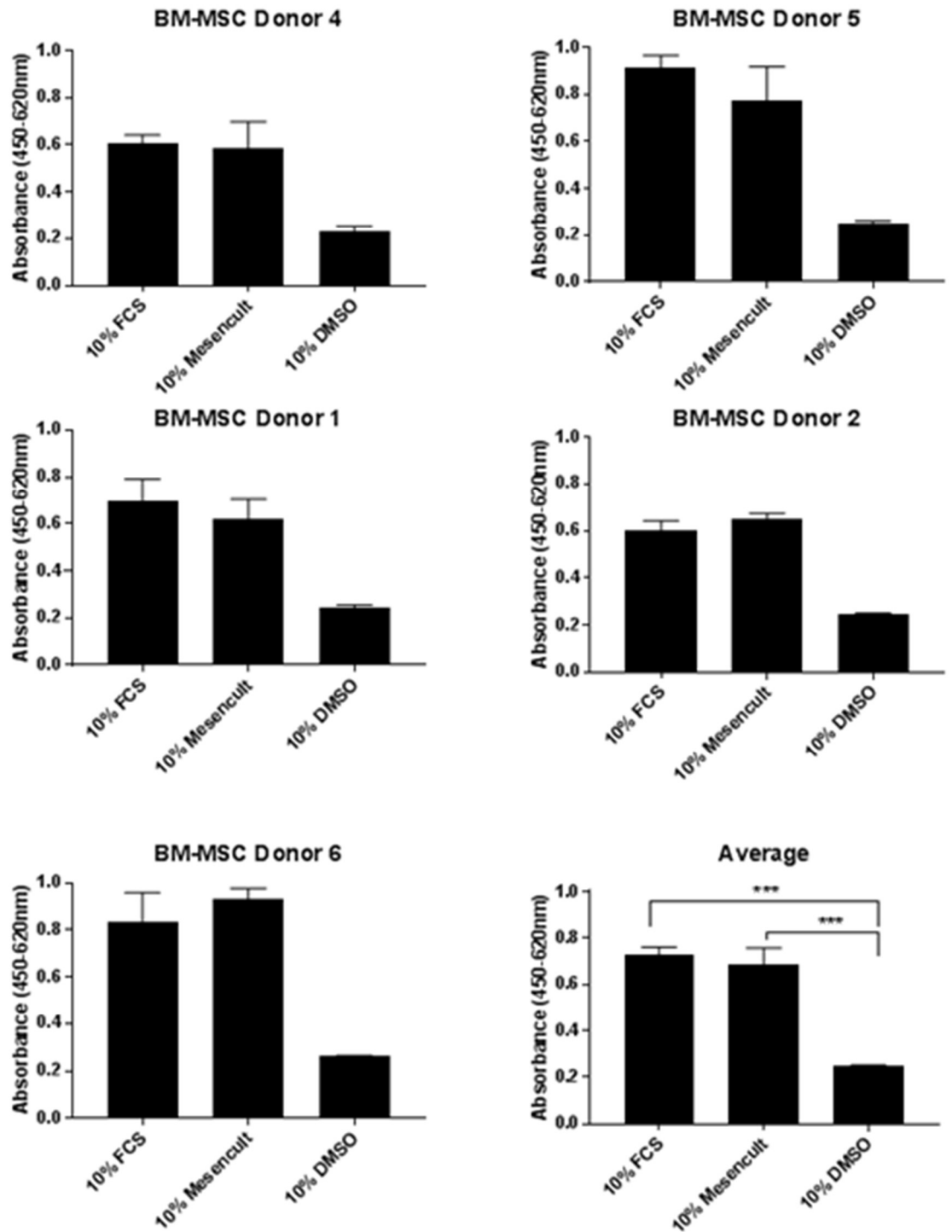


Figure 37: Testing 10% FCS, 10% Mesencult serum and 10% DMSO as potential positive and negative control supplements for doping basal media (BM-MSC n=5, *** indicate significance $P < 0.001$). Error bars for the individual donors indicates technical variation between replicates whilst error bars for the average graph indicates variation between culture averages.

Based on the findings in figure 35, that leukocytes in PRP aren't stable at 37°C past 24 hours days, PL will be used instead of PRP for proliferation and migration assays. To investigate whether BM-MSCs responded in the same way to PL as to PRP was necessary to ensure that the potency of the platelet's and leukocyte's releasate wasn't diminished in the freeze-thawing process. To carry out this experiment, the PRP from one donor was split into two; one half kept as PRP whilst the other half was prepared as PL by freeze-thawing to extract the platelet releasate-containing supernatant. Both these products were then tested on three BM-MSC cultures (figure 38). This experiment found no significant difference between the proliferative response of BM-MSC cultures to PL and PRP. This finding further supports the use of PL in place of PRP for these assays. The lack of significant difference between both platelet products and FCS in figure 38 is also noteworthy, as, despite a slight trend of lower proliferative capacity in the PL supplemented media, both PL and PRP are able to support as much BM-MSC proliferation as FCS. As all three BM-MSC cultures showed the same response to PL and PRP, the results for the three cultures were normalised to FCS and collated to allow for statistical analysis which found no significant difference between FCS, PL or PRP using an unpaired t-test (figure 38, bottom right).

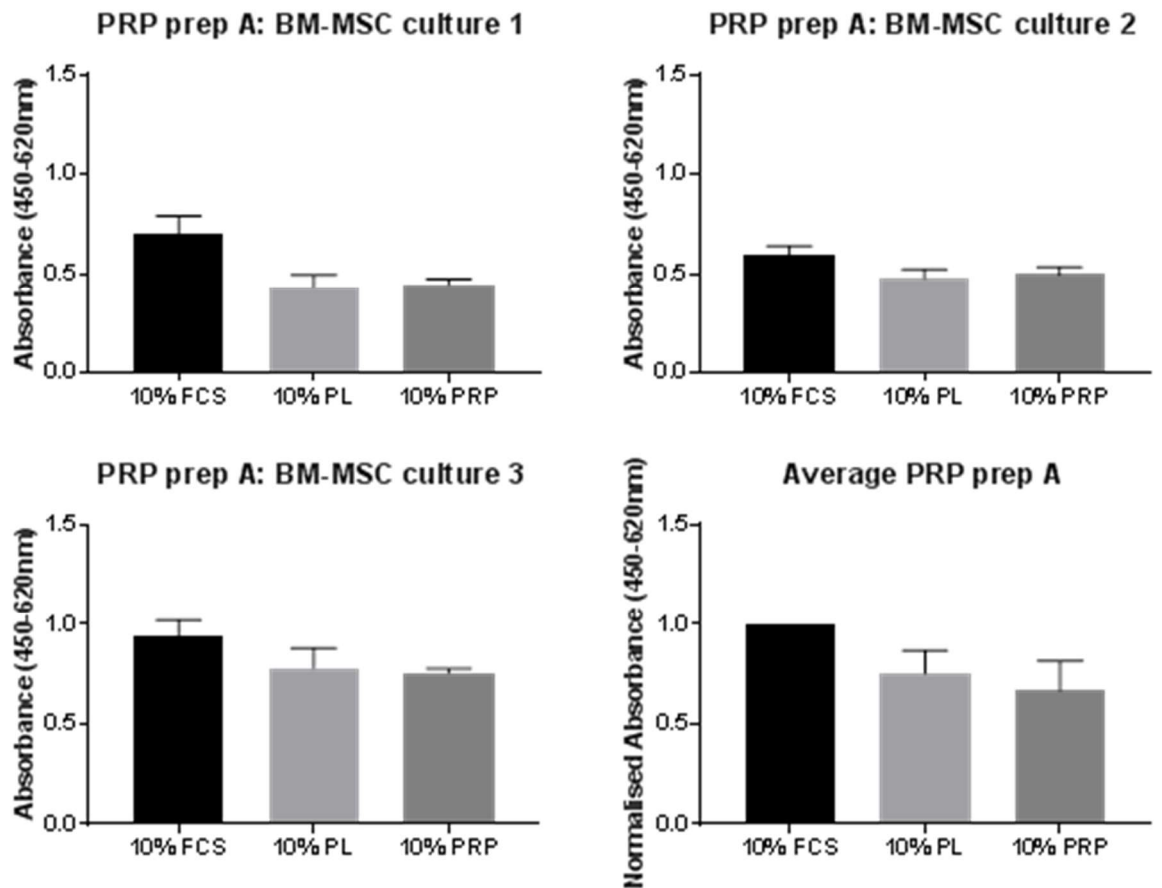


Figure 38: Comparing the proliferative capacity of PL and PRP preparation A on individual cultured BM-MSCs and their normalised average (n=3). Error bars for culture 1-3 indicate technical variation between replicates whilst error bars for the average (bottom right) indicates variation between culture averages normalised to FCS.

This effect was further tested on two more platelet preparations (preparation B and C) whereby each tested on three BM-MSC cultures as shown in figure 39. Looking first at platelet preparation B, despite a slight trend of more proliferation in PRP than FCS and PL the differences weren't found to be significant. Similar results were observed in platelet preparation C where, despite BM-MSC culture one showing slightly more proliferation when dosed with PRP over PL and FCS, no significant difference was found between the supplements. Overall, although there appeared to be a minor trend of more proliferation when BM-MSCs were cultured in PRP instead of PL, the trend was not found to be significant which validates the use of PL as a representative surrogate of PRP.

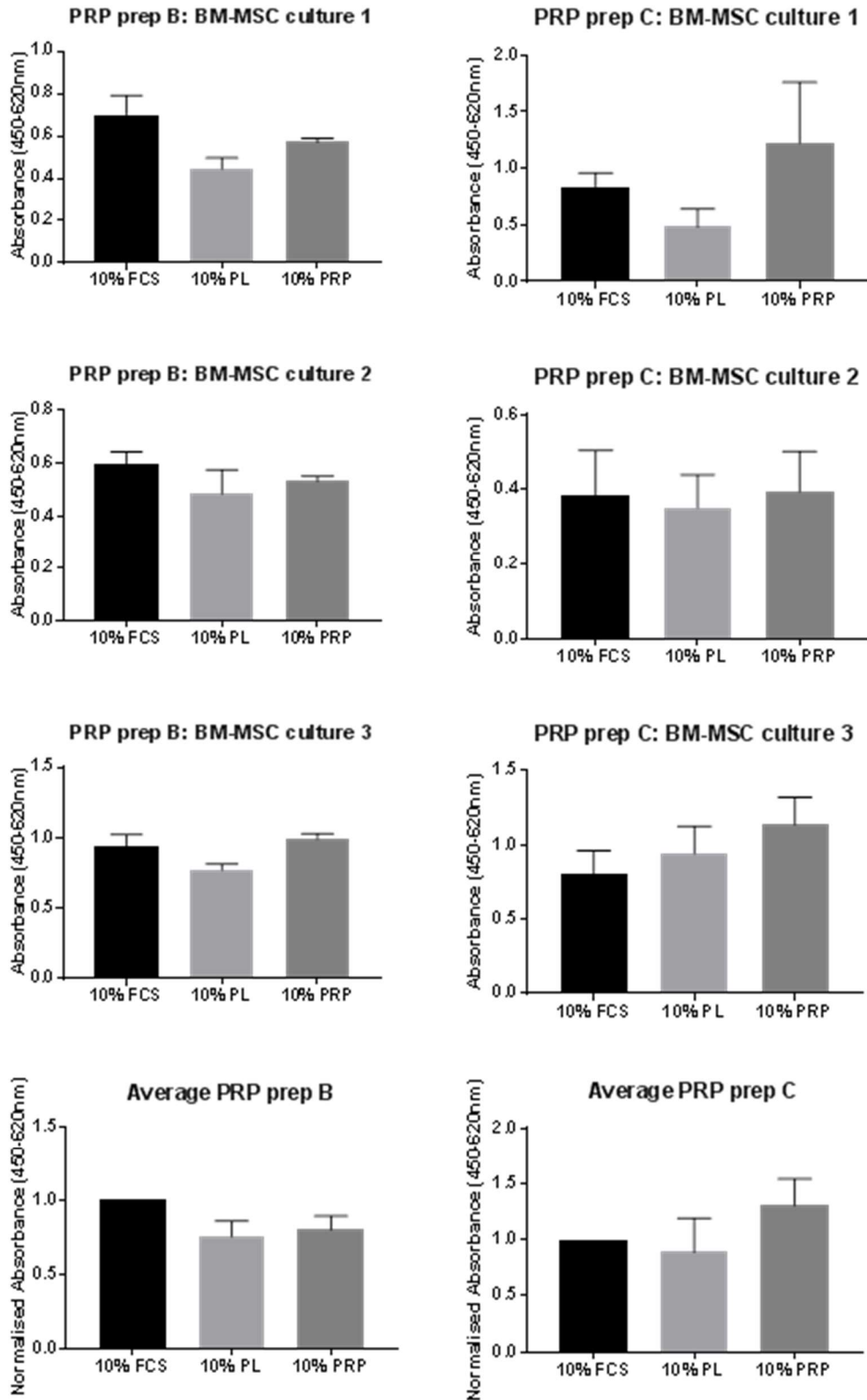


Figure 39: Comparing the proliferative capacity of PL and PRP preparation B and C on individual cultured BM-MSCs and their normalised average (n=3). Error bars for culture 1-3 indicate technical variation between replicates whilst error bars for the average (bottom right) indicates variation between culture averages normalised to FCS.

Through these optimisation studies, it can be concluded that 10% FCS and DMSO are appropriate control supplements for the XTT assay, and that PL can be used as a representative surrogate for PRP. As well, these findings indicate that PRP and PL are equal to FCS in supporting BM-MSC proliferation.

5.3.4 Comparing PL's vs fPL's ability to induce BM-MSC proliferation:

To investigate the effect of leukocytes in PL on BM-MSC proliferation, three BM-MSC cultures were treated with 10% PL, 10% fPL and 10% PPP (platelet poor plasma). To clarify, 10% PL is PRP generated in-house that contained $4.5 \pm 1 \times 10^3/\mu\text{L}$ leukocytes and was lysed, 10% fPL is 10% PL that has been filtered to remove all leukocytes (whilst maintaining the same platelet number), and 10% PPP is the plasma-only by-product which contains no cellular content and is therefore used as a negative control for these experiments. Since PPP is simply plasma containing proteins and growth factors [35] (including those involved in supporting BM-MSC proliferation), the PL products can be considered PPP with added growth factors that are released from the lysis of platelets and leukocytes. These three products were each generated from two PRP donors (PRP preparations D and E). Due to the importance of ensuring that fPRP had no contaminating leukocytes but had similar platelet numbers to PRP, as well as ensuring the PPP contained neither cell type, their platelet and leukocyte counts were analysed (figure 40) before lysing into their PL counterparts. As expected, filtration resulted in only a minor loss of platelets from PRP to fPRP, whereas leukocytes are completely depleted in both preparations. PPP was also found to contain neither platelets nor leukocytes.

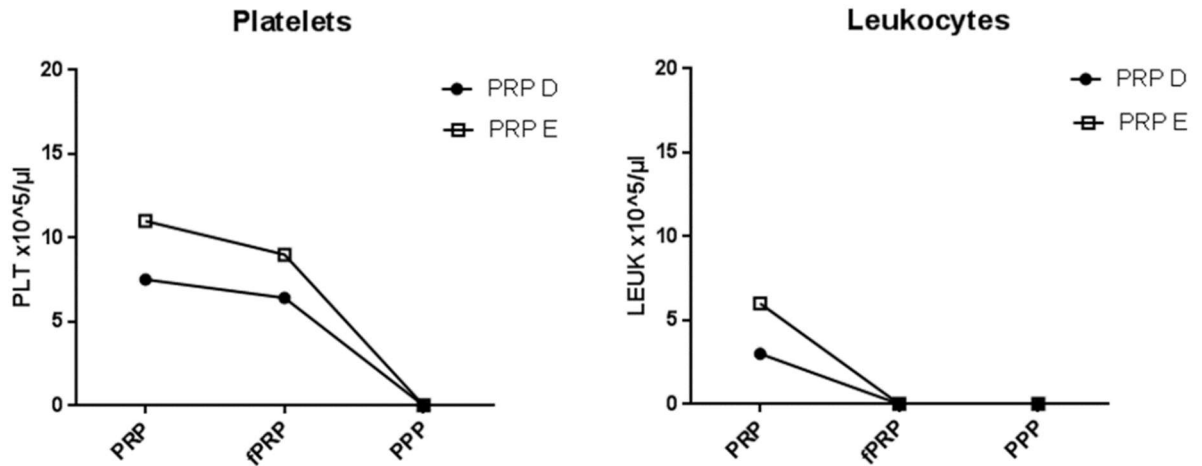


Figure 40: Counted using the haematology analyser, individual platelet (PLT) and leukocyte (LEUK) counts for PRP preparation D and E were plotted as well as their corresponding PPP cell numbers.

The results in figure 40 supports the use of these products in the proliferation assay to investigate the effect of leukocytes on BM-MSC proliferation (figure 41). Contrary to our initial hypothesis, across three cultures, both PL preparations induced a similar proliferation response from the BM-MSCs and in most cases induced equal to or greater proliferation than FCS. As expected 10% PPP appeared to induce only half the amount of proliferation than its platelet- and leukocyte-containing counterparts. This suggests the platelet content plays an important role in supporting proliferation that is absent in plasma alone. The consistency in response across all cultures meant that the results could be collated and normalised to 10% FCS to allow for statistical analysis. A two-way ANOVA analysis of the results found that in both PL preparations, PL and fPL were found to induce statistically the same level of BM-MSC proliferation. Furthermore, both preparations induce the same amount of proliferation as the positive control 10% FCS and, in the case of fPL prep E, significantly more proliferation than FCS. These findings suggest that leukocytes don't have a significant negative impact on BM-MSC proliferation and, unexpectedly, appear to have a positive role in supporting proliferation. It was also demonstrated that whilst PPP was able to induce some proliferation, the presence of growth factors from the platelets and leukocytes in PL and fPL significantly increased their ability to support proliferation. This supports the hypothesis that the cellular contents of platelets and leukocytes play a key role in BM-MSC proliferation.

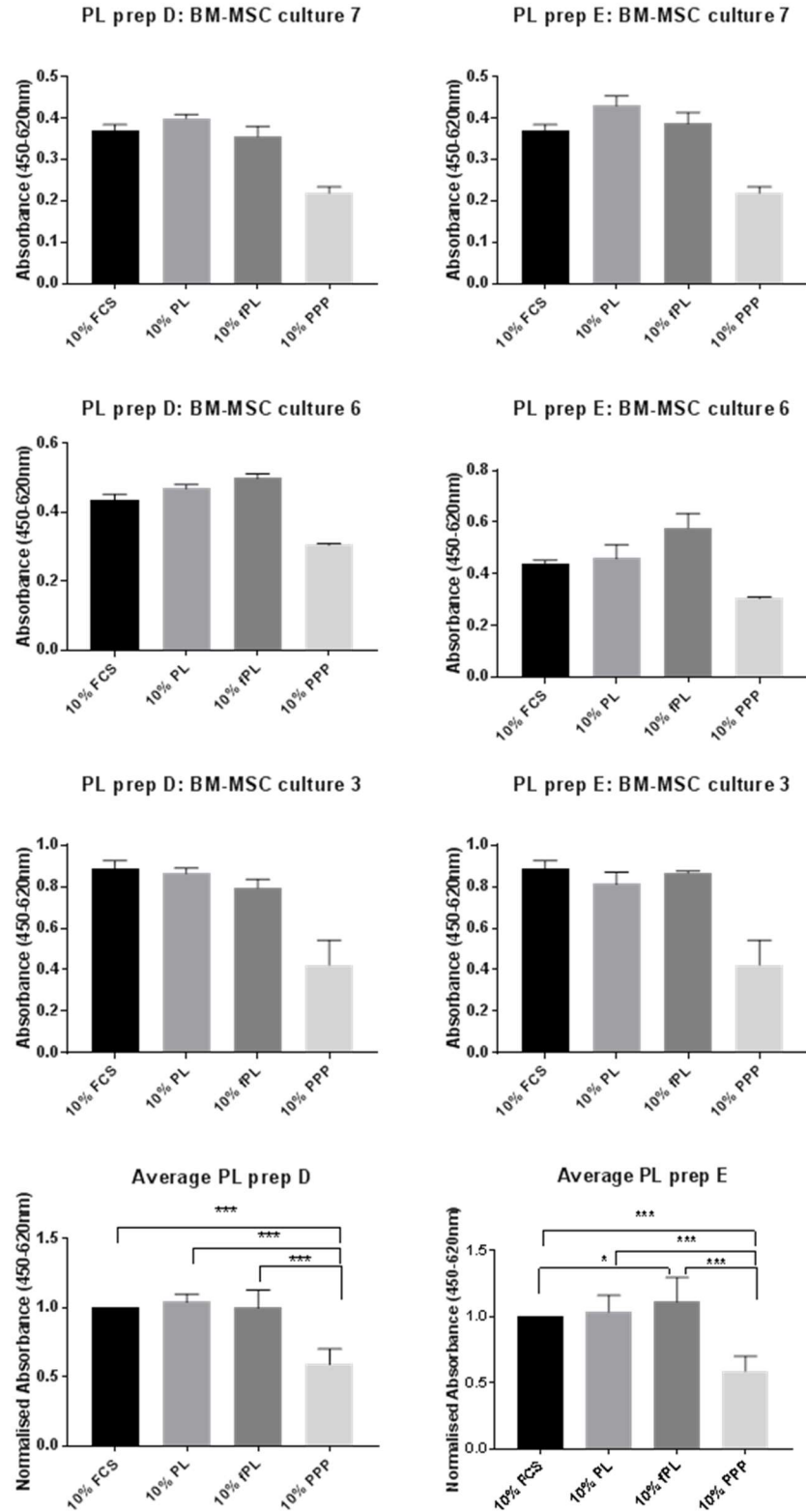


Figure 41: Comparing the proliferative capacity of PL, fPL and PPP from two PL preparations (D and E) on individual cultured BM-MSCs and their normalised average (n=3). Error bars for cultures 7, 6 & 3 indicate technical variation between replicates whilst error bars for the average (bottom row) indicates variation between culture averages normalised to FCS. * $P < 0.05$, ** $P < 0.01$, *** $P < 0.001$.

5.3.5 Developing a migration assay towards PL supplemented media using the IncuCyte device:

To investigate BM-MSC migration a few techniques are available, however these often require either manipulation of the cells (fluorescent tagging for the Ouchterlony-type assay) or an *in vivo* model (Boyden chamber assay), or they cannot precisely differentiate migration from proliferation (scratch wound assay). Transwell migration assays are considered an *in vitro* solution to the Boyden chamber and involve cells migrating along a chemotactic gradient toward the stimulant of interest through a porous transwell where they can be counted. Despite their efficacy, transwell assays are limited by the lack of live cell imaging [36, 37] and their short duration (usually 4 hours) [38]. A recent advancement of the transwell assay incorporates time-lapse phase contrast imaging of the transwell throughout the assay and a processing software to quantify cells. The 8µm diameter of the transwell pores ensures only actively migrating cells are quantified as well as maintaining a stable chemotactic gradient for 48 hours [39]. This method is also thought to be more accurate as regular imaging of individual wells throughout the experiment reduces the risk of technical error. For these reasons the Incucyte was chosen as the assay to quantify BM-MSC migration towards different PL preparations, specifically investigating the effect leukocytes play on BM-MSC migration.

Measuring PL's impact on BM-MSCs using the Incucyte is a novel technique that has not yet been published in the literature, and so required thorough optimisation including; overnight cell starving, cell seeding density, dose of media supplement and assay duration. Overnight cell starving is necessary in some migration assays to increase the cellular response and reduce the effect any residual serum from the growth media may have. Optimisation of seeding density was needed to ensure there are as many cells as possible available to migrate but not so many that they prevent the software from accurately identifying individual cells. The dose of PL needed optimising to maximise migration as well as ensure high quality images were captured as there was a risk that the density of the solution would compromise image quality at higher concentrations. And finally, whilst the Incucyte transwells are able to maintain a stable gradient for 48 hours (however due to limited access, assays were conducted up to 36 hours) the assay duration still needed optimising to ensure BM-MSCs would stay viable and migrate in that time. For these experiments, PL was again used as a surrogate for PRP not only due to platelet and leukocyte instability, but also to improve imaging of the transwells as it was found that the presence of intact cells in PRP prevented clear image capture of

the cells. In these experiments, as outlined in methods section 5.2.8, cells were seeded on top of the transwell in serum-free media and allowed to migrate towards a serum- or PL-supplemented media in the bottom chamber for up to 36 hours. Over the course of the experiment, a camera captured multiple phase-contrast images of the top and bottom of the transwell and a 'mask' is created that quantifies the BM-MSCs as they migrate along the chemotactic gradient. The main data output from this assay is the total area of the bottom of the transwell that is covered by BM-MSCs (object area $\mu\text{m}^2/\text{well}$).

Initially, to optimise seeding density and the effect of overnight starving; starved and unstarved BM-MSCs from three cultures were seeded at densities of 250, 500 and 1000 cells/well in triplicate in a 96 well with 10% FCS (positive control) and 0.5% FCS (negative control) supplemented media in the bottom wells.

As shown in figure 42, row A, 1000 cells/well was too confluent for making an accurate mask to quantify cell migration so were excluded from the analysis. Analysis of the controls first shows that, at both 250 and 500 cells/well seeding densities, starved and unstarved, 10% FCS induced an increase in the object area of the bottom of the well (indicative of migration) more than 0.5% FCS which produced a minimal migratory response. The clear distinction in response to the positive and negative controls supports their suitability for these migration experiments. Furthermore, whilst the top panel in column B shows that unstarved cells seeded at 250 cells/well and 500 cells/well exhibit the same total migration, a more distinct difference was seen in the starved cells (bottom panel, column B). More of the starved cells migrated, they did so at a faster rate towards 10% FCS, and as expected, more migration was induced from 500 cells/well than from 250 cells/well. In the top panel of column C, whilst starving the cells made no obvious difference to the rate or amount of migration at 250 cells/well, starving 500 cells/well (bottom panel, column C) increased the rate and total amount of migration. Based on these findings, starved cells, seeded at 500 cells/well were chosen for future experiments alongside 10% and 0.5% FCS as the positive and negative controls.

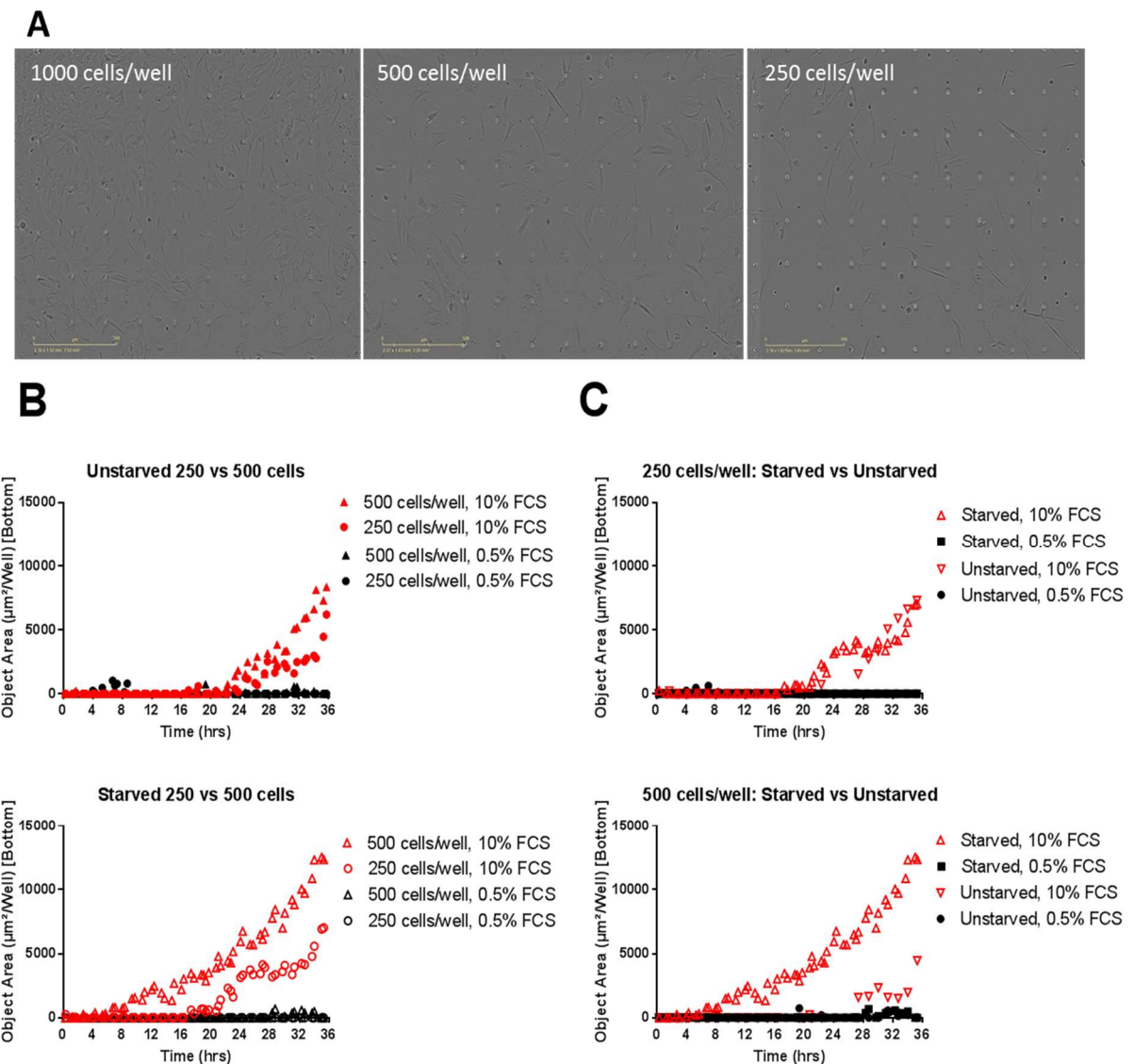


Figure 42: Example of seeded wells at 1000, 500 and 250 cells/well in the top panel A. Results from the IncuCyte migration assay comparing unstarved seeding densities (top of column B) and starved seeding densities (bottom of column B) as well as the effect of starving cells overnight at 250 cells/well (top of column C) and 500 cells/well (bottom of column C).

Following optimisation of the seeding density, the concentration of PL then had to be optimised to maximise migration and ensure image clarity. 20%, 10% and 5% PL concentration in base media was tested on three BM-MSC cultures (figure 43). Data for 20% PL was excluded as the high concentration of lysate made the media too cloudy for accurate image capture and analysis. Across all three cultures it was shown that, up to 12 hours the both 10% and 5% PL induce a similar response from the cells as 10% FCS. However, after 12 hours, both PL concentrations appear to

induce more migration than 10% FCS. As well, 10% PL appeared to induce the most total migration in all three cultures and, in two of the three cultures, 10% PL also had the steepest curve indicative of a faster migratory response. It is also noteworthy to mention that, although 10% FCS does not appear to induce any more migration than the 0.5% FCS in figure 43, a closer look at the data in figure 43 demonstrates how its migratory effect is made negligible in comparison to the substantial response both 10% and 5% PL bring about.

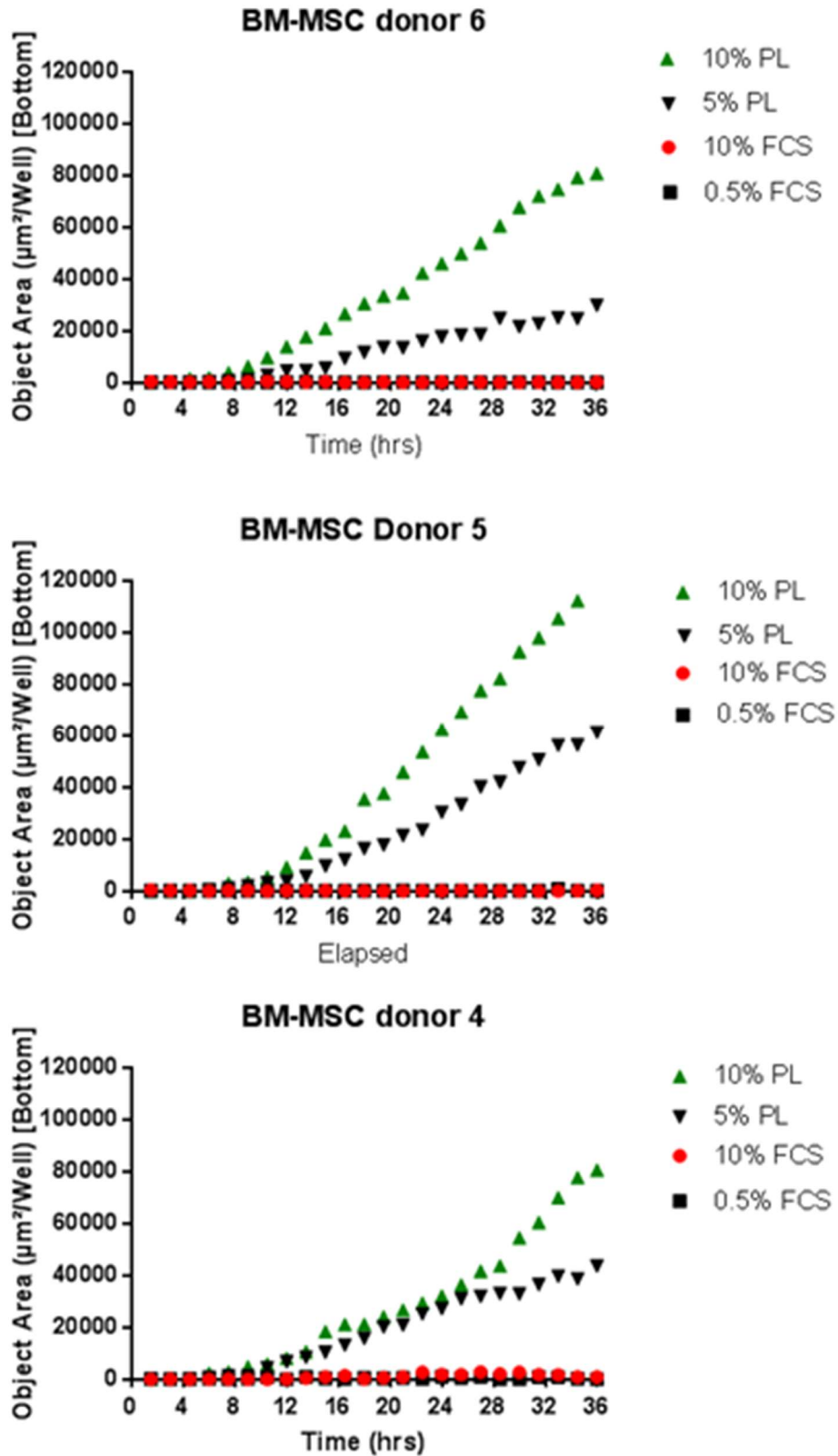


Figure 43: Compares the effect of 10% PL and 5% PL on cultured BM-MSCs (n=3) using the IncuCyte migration assay.

To enable statistical analysis of the supplement's effects on BM-MSC migration, three time-points were chosen; 12, 24 and 36 hours and the results of which are shown in figure 44. Occasionally statistics comparing 0.5% FCS to the other conditions could not be carried out because the mean migration for 0.5% FCS was not greater than zero. It was observed that after just 12 hours, in all three cultures, 10% PL had already induced significantly more migration than 10% and 0.5% FCS. As well, in two of the three cultures, 10% PL induced significantly more migration than 5% PL. At 24 hours the same trend continued with 10% PL still inducing significantly more migration than 5% PL as well as 10% and 0.5% FCS in all three cultures. Although cells weren't as responsive to 5% PL as they were to 10% PL, 5% PL was still found to induce significantly more migration than the positive FCS control. At 36 hours, BM-MSCs were found migrating towards 0.5% FCS in two of the three cultures which could be indicative of the assay reaching its limit of accuracy. Despite this, 10% PL was still found to induce significantly more migration than both 5% PL and 10% FCS, with 5% PL again inducing more migration than either of the FCS controls. Overall, 10% PL was found to consistently induce the most migration across all three time points and all three BM-MSC cultures, and that, despite being the positive control, 10% FCS was consistently outperformed by both PL concentrations demonstrating PL's strong chemotactic properties.

To optimise this experiment, it would have been preferential to test PL from more than one donors but due to the precious nature of the samples, the limited volume harvested and the clarity of the results, only one donor was tested. This assay also demonstrated culture variability as BM-MSC culture 4 appeared much more migratory than the other cultures. These cells might possess an inherently more migratory phenotype which could include; higher expression of the GTPases Rac and Cdc42 which control actin assembly and cell protrusions such as pseudopodia and enable motility, possessing more GF receptors on their membranes such as CXCR4 which binds SDF-1 and FGFR which binds FGF [40] which makes them more responsive to the growth factors in the media, or they could have weaker cell-cell adhesions which could also contribute to faster migration [41, 42]. This demonstrates how varied the BM-MSCs responses can be to the same PL preparation and indicates that BM-MSC variability is almost as significant as PL variability. In highly migratory cells it appears that the addition of PL, whilst it still has a positive effect the strength of the effect is not as significant as seen in less migratory cells.

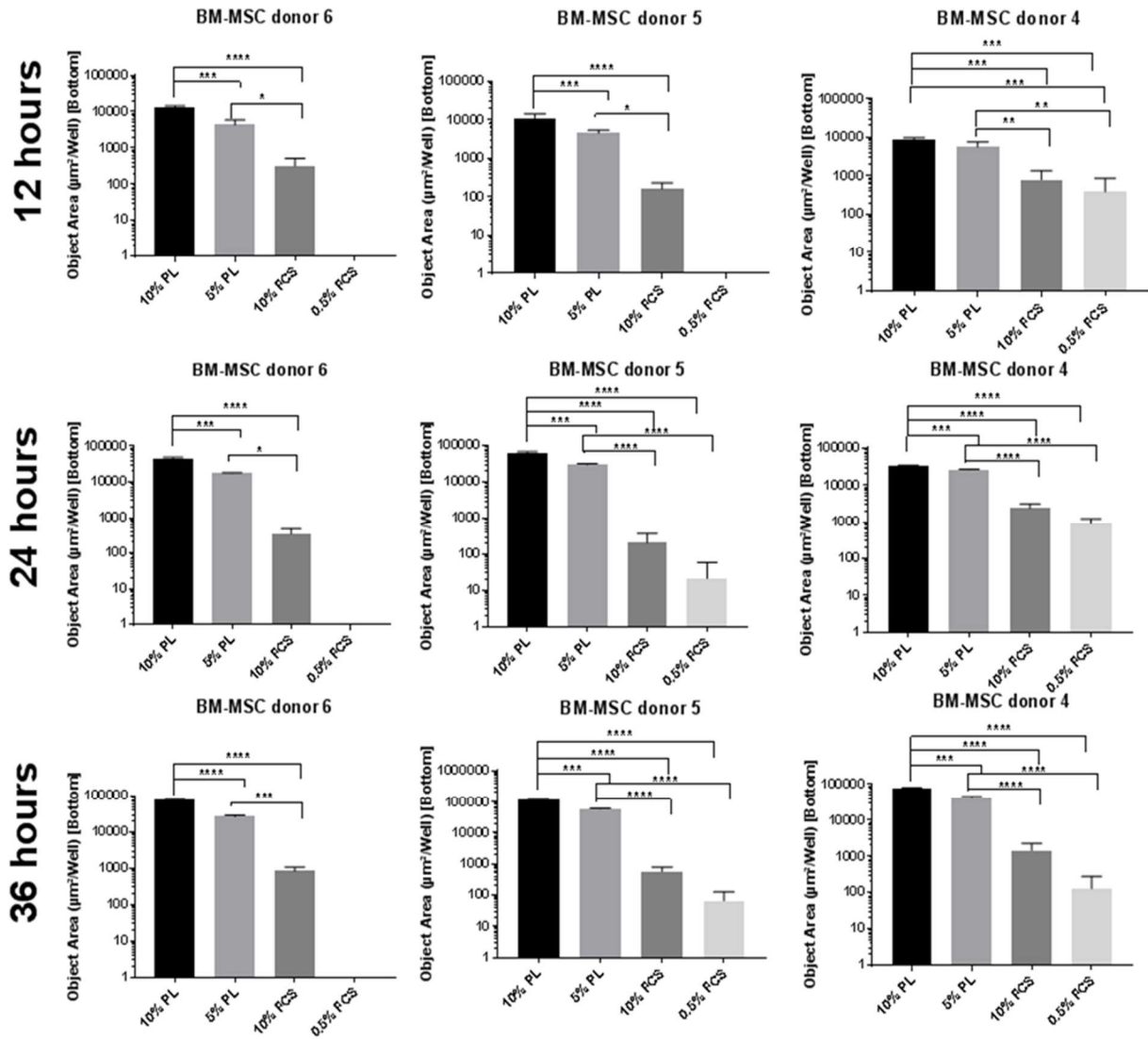


Figure 44: Migration towards 10% PL, 5% PL using the IncuCyte assay which measures total cell area on the underside of the well against time at time-points: 12, 24 and 36 hours. One PL prep was used ($n=1$) on cultured BM-MSCs ($n=3$). The error bars represent the standard errors of the technical replicates, * $P < 0.05$, ** $P < 0.01$, *** $P < 0.001$.

In regards to time-points, figure 44 shows how, across the three BM-MSCs cultures, cells steadily migrate towards the chemoattractant up to 36 hours and that 12, 24 and 36 hour time-points are appropriate to demonstrate the overall migration patterns.

10% PL time course

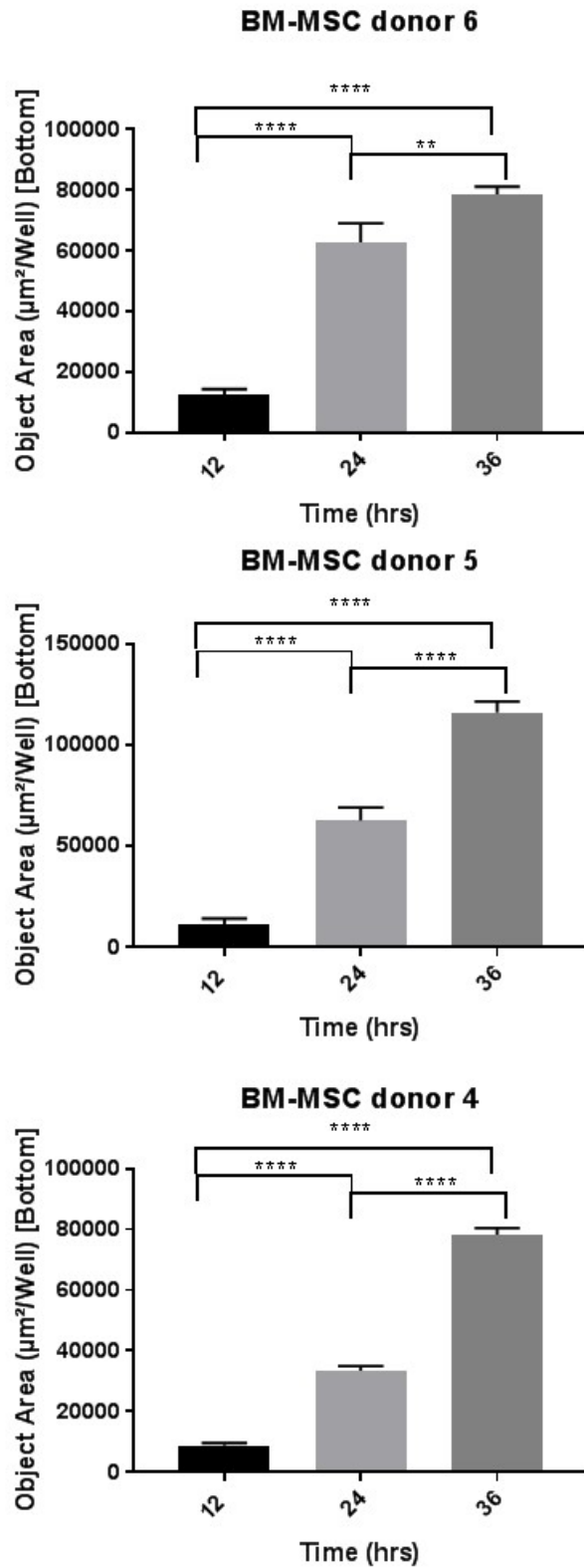


Figure 45: BM-MSC (n=3) migration towards 10% PL at the three time points; 12, 24 and 36 hours to demonstrate steady migration over the course of the assay. The error bars represent the standard errors of the technical replicates, * $P < 0.05$, ** $P < 0.01$, *** $P < 0.001$, **** $P < 0.0001$.

From this data it can be concluded that 10% PL will be used alongside 10% FCS and 0.5% FCS in future experiments on 500 starved cells/well, over the course of a 36 hour-long assay.

5.3.6 Comparing PL's and fPL's ability to induce migration in BM-MSCs:

Once the Incucyte migration assay was optimised, the effect of leukocytes on BM-MSc migration was tested using three PL preparations (preparation D, F and G) that were generated from three female donors aged between 24-34 years. Each PL preparation was divided into two and one half was kept as PL whilst the other half was filtered to remove all leukocytes to produce fPL. Both PL and fPL preparations were tested on BM-MSc cultures from three healthy donors. Figure 46 shows the individual migratory responses of three BM-MSc cultures as well as their averaged trend of migration towards the different PL preparations. Looking at PL preparation D (left hand column, figure 46), except for BM-MSc donor 6, there appeared to be little difference between either 10% PL, 10% fPL or 10% FCS. Removal of leukocytes from PL preparation D was not found to have a consistently positive effect. PL preparation F (middle column, figure 46) showed that the complete removal of leukocytes did appear to reduce BM-MSc's migratory response in all three BM-MSc cultures. Finally, with regards to PL preparation G (right column, figure 46) both PL and fPL induced similar migratory responses from BM-MScs except for culture 9 which showed a trend of increased migration towards the leukocyte-and platelet-containing PL over fPL. Overall, looking at the average response of the three BM-MSc cultures to the individual PL preparations (bottom row, figure 46) it can be seen that both 10% PL and fPL are consistently as good as, if not better than, 10% FCS at inducing BM-MSc migration, consistent with the optimisation data shown in figure 45.

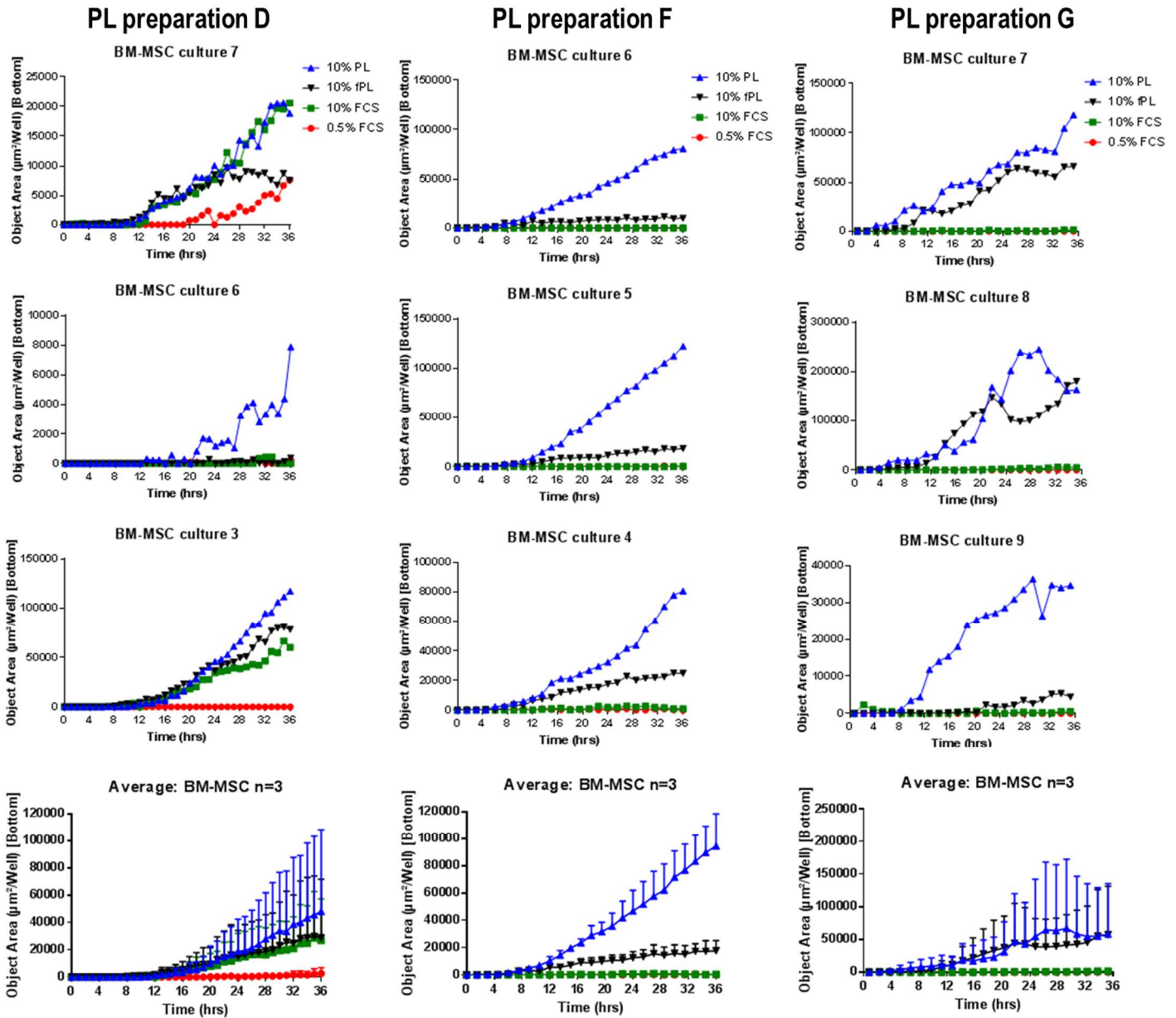


Figure 46: A representative real-time trace of total cell area on the underside of the well against time comparing 10% PL with 10% fPL's ability to induce migration using the IncuCyte migration assay using PL preparations (D,F and G, n=3) cultured BM-MSCs. Error bars indicate the variation between BM-MSCs cultures for each PL preparation.

To better compare the different platelet preparations, three time-points at 12, 24 and 36 hours were chosen for statistical analysis of each PL preparation's average (BM-MSCs n=3) as shown in figure 47. It was seen that, after 12 hours, despite a trend of PL and fPL inducing more migration than FCS, the difference was only found to be significant in PL preparation F between 10% PL and 10% FCS. Again at 24 hours, despite a trend of PL and fPL inducing more migration than 10% FCS in

all three cultures only in PL preparation F were PL and fPL found to be significant. The trend continued up to 36 hours with no significant difference found in PL preparations D and G, but in PL preparation F both PL and fPL were found to significantly outperform 10% FCS. Towards the end of the assay cells were also found to start migrating towards 0.5% FCS in PL preparations D and F. The combined results from figure 46 and 47 indicate that removal of leukocytes does not significantly improve migration and indeed their presence, in the case of PL preparation F, may even be beneficial.

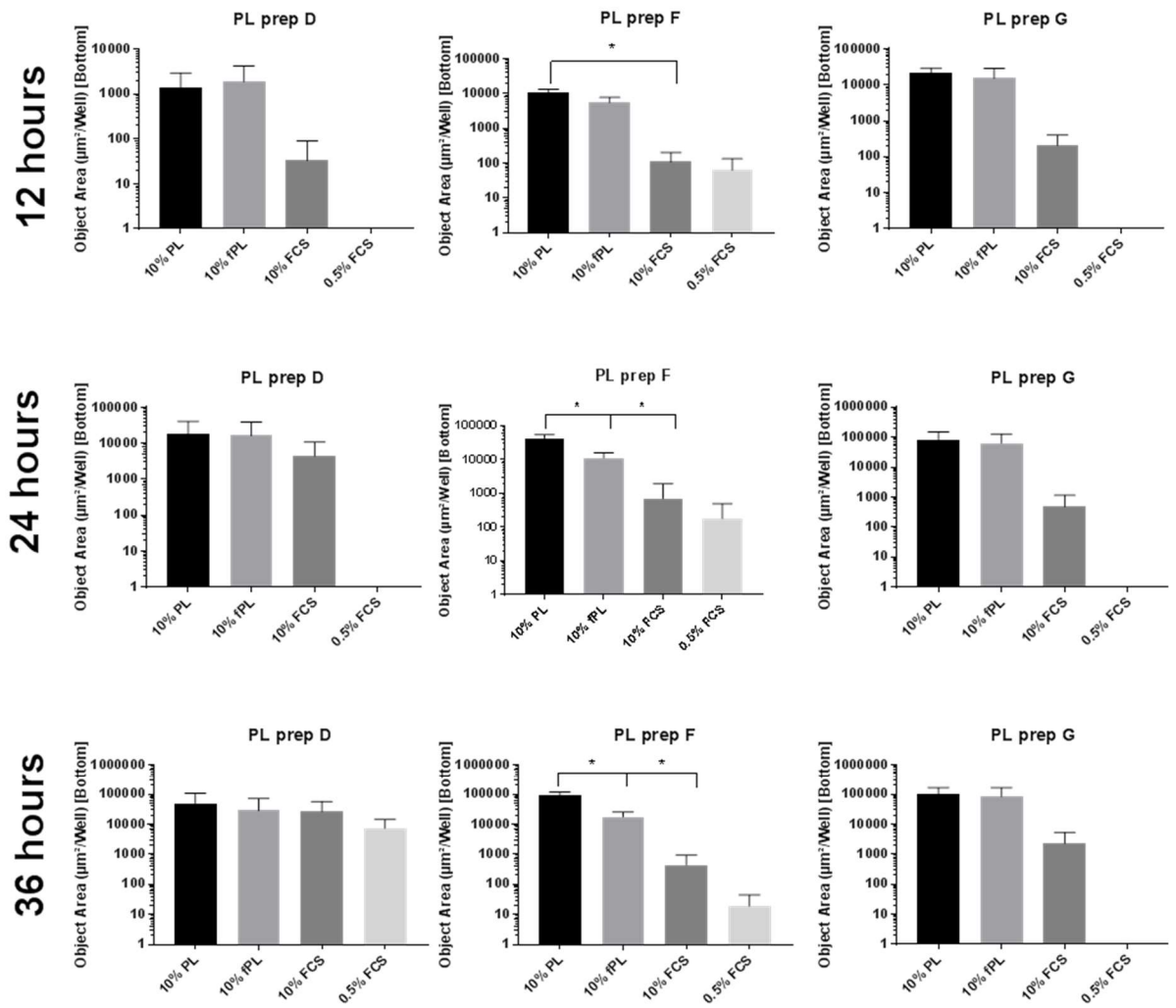


Figure 47: Migration towards 10% PL, 10% fPL, 10% FCs and 0.5% FCS using the IncuCyte assay which measures total cell area on the underside of the well against time at time-points: 12, 24 and 36 hours. PL preparations D, F and G were used (n=3) on cultured BM-MSCs (n=3). The error bars represent the standard errors of the technical replicates, * P < 0.05, **P < 0.01, ***P < 0.001.

To explain the variability between BM-MS-C cultures, the total cell seeding density at time point zero was checked to ensure equal cell loading (figure 48). Cell seeding densities between cultures were found to be consistent therefore ruling out unequal seeding as a potential explanation for the difference in migratory response. Despite what appears to be a strong chemotactic gradient for some BM-MS-C cultures was found to have much lower migratory effect on others, demonstrating the impact BM-MS-C variability has on the success of PL to induce migration. Due to the distinct difference between BM-MS-C culture's total migration, the y-axis for object area ($\mu\text{m}^2/\text{well}$) can be considered a representative unit and was not normalised between cultures.

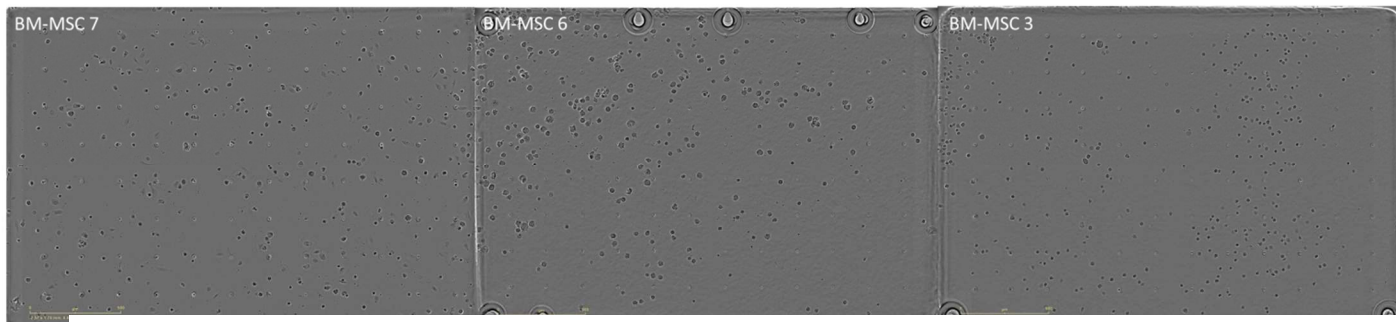


Figure 48: Representative phase-contrast images of the top of the wells seeded with 500 cells/well.

Because the units for this assay are only representative, it is difficult to compare different BM-MS-C cultures and PL preparations, however, looking at all three PL preparations averages, PL preparation F appears to induce the most consistent migratory response from cells. Looking at the preparation's cell numbers (table 10) might explain the differences observed. PL preparation D had the biggest difference in platelet numbers between PL and fPL ($100 \times 10^3/\mu\text{L}$ fewer platelets in fPL) as well as $3 \times 10^3/\mu\text{L}$ fewer leukocytes, and whilst PL appeared to induce more migration than fPL, the trend wasn't found to be significant. Both the PL and fPL products of preparation F were found to have the most platelets and least leukocytes of the three preparations and the dramatic difference between PL and fPL is considered to be due to the loss of either $50 \times 10^3/\mu\text{L}$ platelets or $2.3 \times 10^3/\mu\text{L}$ leukocytes from PL to fPL. Because of its cell composition, fPL of preparation F is likely to reflect the role of leukocytes. Preparation G's PL and fPL had to lowest platelet numbers and highest leukocytes numbers and yet the difference between PL and fPL is maybe the least distinct of the three preparations.

Table 10: Platelet and Leukocyte numbers of PL and fPL preparations D, F & G as analysed on the haematology analyser.

PL preparation			fPL preparation	
Sample:	Platelets ($\times 10^3/\mu\text{L}$)	Leukocytes ($\times 10^3/\mu\text{L}$)	Platelets ($\times 10^3/\mu\text{L}$)	Leukocytes ($\times 10^3/\mu\text{L}$)
D	752	3	652	0
F	843	2.3	793	0
G	555	5	500	1

Overall it appears that, like in the proliferation assays in section 5.34, leukocytes in PL have no significant detrimental effect on BM-MSc migration and, based on the results of PL preparation F (figures 46 and 47), could even play a positive role. As well, the consistency of effect from each PL preparation over time suggests their stimulatory effects have longevity *in vitro*.

5.3.7 In-house and commercial PRP cell compositions:

Following on from the initial hypothesis; that leukocytes would be detrimental to BM-MSc proliferation and migration, despite no significantly detrimental effect of leukocytes was found it was also hypothesised that the purer PRP prepared in-house (PRP) will induce more proliferation and migration than PRP made using a commercial device (C-PRP). To test this, the two products were analysed using the haematology analyser to identify the differences in their cellular compositions (figure 49). PRP had significantly higher numbers of platelets ($15.9 \pm 5.6 \times 10^5$ PLT/ μL) in comparison to C-PRP ($6.4 \pm 3.4 \times 10^5$ PLT/ μL) as well as significantly lower leukocyte numbers ($1.5 \pm 1.4 \times 10^3$ LEUK/ μL) compared to C-PRP ($20.6 \pm 8.5 \times 10^3$ LEUK/ μL). Furthermore, whilst both preparations depleted red blood cells, PRP was found to have significantly fewer than C-PRP. Basophils and eosinophils were analysed together based on their similar cell size and again, C-PRP enriched both cell types, with the exception of one donor, whilst PRP significantly reduced them. C-PRP's neutrophil numbers showed the least consistency, but on average C-PRP had a 1.8 fold enrichment of neutrophils whereas PRP completely depleted them. Significant variation in starting numbers between the products were also

observed for red blood cells, leukocytes and neutrophils. This is likely due to the different anticoagulants used and differences in their ability to preserve cells for accurate cell counting, however the final differences between the PRP and C-PRP are so significant that these initial variations are made negligible. Based on these findings, PRP made in-house can be classified using the PAW classification system^[43] as P4-B- β which describes its platelet count as 'super' with a greater than six fold increase of platelets from baseline (using whole blood counts as the baseline value) and more than 1,250,000 platelets/ μ L (P4), as well, its white blood cells count is below the baseline (B) as is its neutrophil count (β). C-PRP made using the commercial device can be categorised as P2-A- α based on its moderate platelet count (defined as being greater than baseline up to 750,000 platelets/ μ L) and a fold increase of platelets between 1-4 times above baseline (P2). C-PRP also has a greater than baseline white blood cell count (A) and greater than baseline neutrophil count (α). Overall, the data shows a clear trend of PRP's ability to reduce leukocytes and enrich platelets significantly more so than C-PRP, whilst C-PRP non-specifically enriched all cell types except for red blood cells. It is also of note that whilst the commercial device that makes C-PRP refers to the final product as 'PRP', it actually enriches leukocytes and lymphocytes as much as it does platelets, and in some cases, even more so.

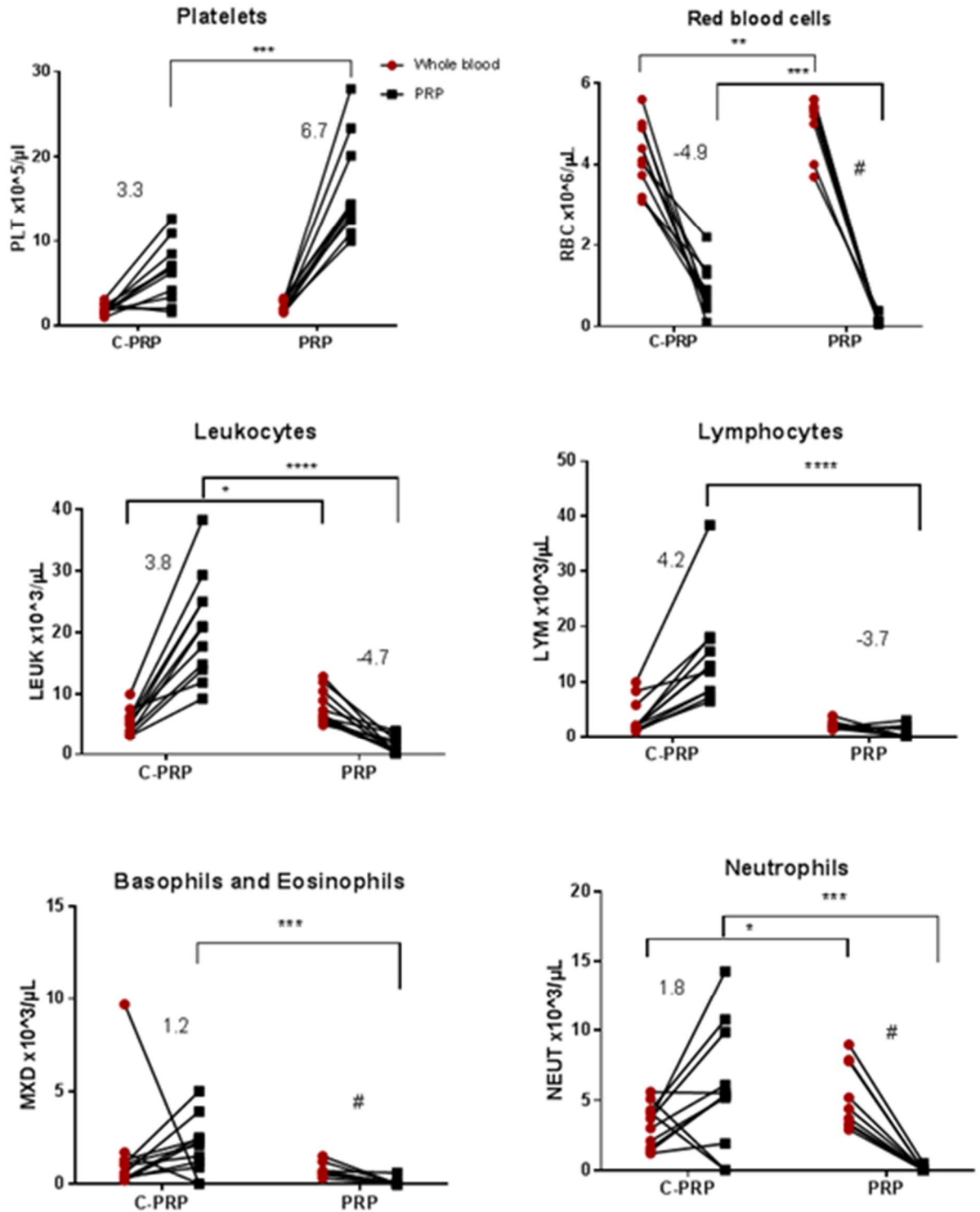


Figure 49: Compares the changing cell compositions from whole blood to C-PRP and PRP (n=11 each). The numbers above each product indicate the fold change from whole blood to C-PRP/PRP, positive values indicate an average fold increase whilst a negative value indicates an average fold decrease, # was used to indicate a complete reduction of cells to 0. An unpaired t-test was used to compare C-PRP and PRP whilst a paired t-test was used to compare each product after platelet concentration: * = $P < 0.05$, ** = $P < 0.01$, *** = $P < 0.001$, **** = $P < 0.0001$.

The observed differences in figure 49 indicate that the final differences in cell populations between C-PRP and PRP could be due to the different anticoagulants used, as well as the different centrifugation protocols. Therefore, to test the role of anticoagulants, the protocol used to generate PRP was carried out with two different anticoagulants: ACD-A (used to make C-PRP in theatre) and EDTA (used to make PRP in-house) and the cells of the subsequent PRPs were quantified using the haematology analyser (figure 50).

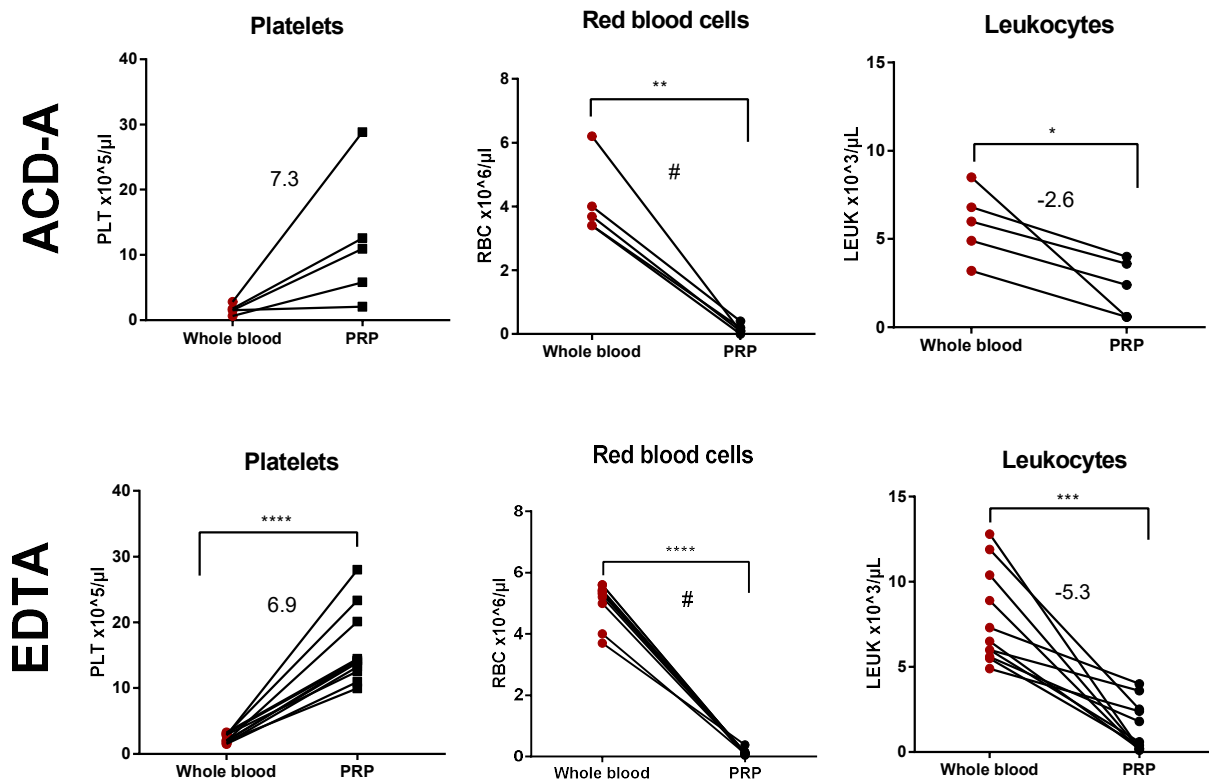


Figure 50: Compares the role ACD-A and EDTA have on enriching and depleting the key cell populations from whole blood to PRP ($n=5$ for ACD-A and $n=11$ for EDTA). The numbers above each product indicate the fold change from whole blood to C-PRP/PRP, positive values indicate an average fold increase whilst a negative value indicates an average fold decrease. A paired t-test was used to compare each product after platelet concentration: * = $P < 0.05$, ** = $P < 0.01$, *** = $P < 0.001$, **** = $P < 0.0001$.

Generating PRP is process that can damage the cells whilst the repeated pelleting and re-suspending requires a strong anticoagulant that prevents the cells from aggregating. Looking first at platelets the results show that; when using the same protocol, both anticoagulants are able to preserve and enrich platelets to a similar extent. Despite ACD-A enriching on average slightly more platelets (7 fold increase

compared to 6.9 fold increase in EDTA) EDTA seems to produce a more consistent product, however the larger sample size for EDTA than ACD-A could have partially contributed to the differences observed. Both anticoagulants were found to equally deplete red blood cells to zero. The biggest difference between the two anticoagulants however is seen in the effect they have on leukocytes. Using ACD-A and the in-house PRP producing method, it was found that leukocytes were depleted only 4.9 fold whilst using EDTA decreased leukocytes 11.1 fold. It is of note that EDTA's average fold depletion of leukocytes observed in figure 50 is much greater than the average seen in figure 49 likely due to donor variability and more of the PRP samples in figure 50 having their leukocyte numbers depleted to less than 1. The differences these anticoagulants have on different cell populations is likely due to the difference in strength of anticoagulation, whilst both involve the chelation of circulating calcium cations, EDTA has a stronger bond to the calcium ions whereas ACD-A's attachment is weaker and reversible. Therefore, whilst ACD-A may be suitable for the commercial PRP protocol, it may not be strong enough anticoagulant to withstand the extensive manipulation of the in-house method resulting in less distinction between buffy coat layers and higher contamination of leukocytes. This data suggests that the type of anticoagulant contributes to the difference in leukocyte numbers between C-PRP and PRP and that the different processing protocols contribute to the difference in platelet and red blood cell numbers, however, as it wasn't possible to test blood collected in EDTA in the commercial device it cannot be confirmed which, the anticoagulant or the processing protocol, makes the most significant difference.

5.3.8 Comparing PL's and C-PL's ability to induce BM-MSC proliferation:

Analysis of PL and C-PL confirmed that they are significantly different in terms of platelet and leukocyte numbers and so it was hypothesised that they would have significantly different effects on BM-MSC proliferation. To test this hypothesis the optimised XTT assay (section 5.3.3) was used to test 10% C-PL (n=5) and 10% PL (n=5) with 10% PPP and 10% FCS (as controls) on cultured BM-MSC cultures (figure 51). To account for BM-MSC variation, each data point was normalised to its BM-MSC's average response to 10% FCS. One PL preparation (PL: J) was also tested on donor matched BM-MSCs. It was seen that in four out of the five PL preparations, 10% PL was found to induce significantly more BM-MSC proliferation than its leukocyte-rich counterpart C-PL. Furthermore, in three of the PL donors, C-

PL was found to induce significantly less proliferation than 10% FCS. Surprisingly, PPP was found to induce as much proliferation as FCS and C-PL, and, despite a consistent trend of PL inducing more proliferation than PPP, the difference was not found to be significant. This indicates that the growth factors found in PPP (as opposed to those that have been lysed from the leukocytes and platelets in PL and C-PL) are able to support some proliferation. Lysing the mostly-platelets in PL was found to significantly increase BM-MSCs' proliferative capacity, at least to the level of FCS, whereas lysing the platelets combined with leukocytes in C-PL doesn't improve the base-line proliferation provided by PPP and in some cases, hinders proliferation. This suggests that the growth factors responsible for supporting proliferation are found in the plasma and platelets, which C-PL has fewer of than PL. Importantly, these trends were seen in PL preparation J that was donor matched, which indicates that the trends observed are likely to occur in the clinical setting using autologous PL.

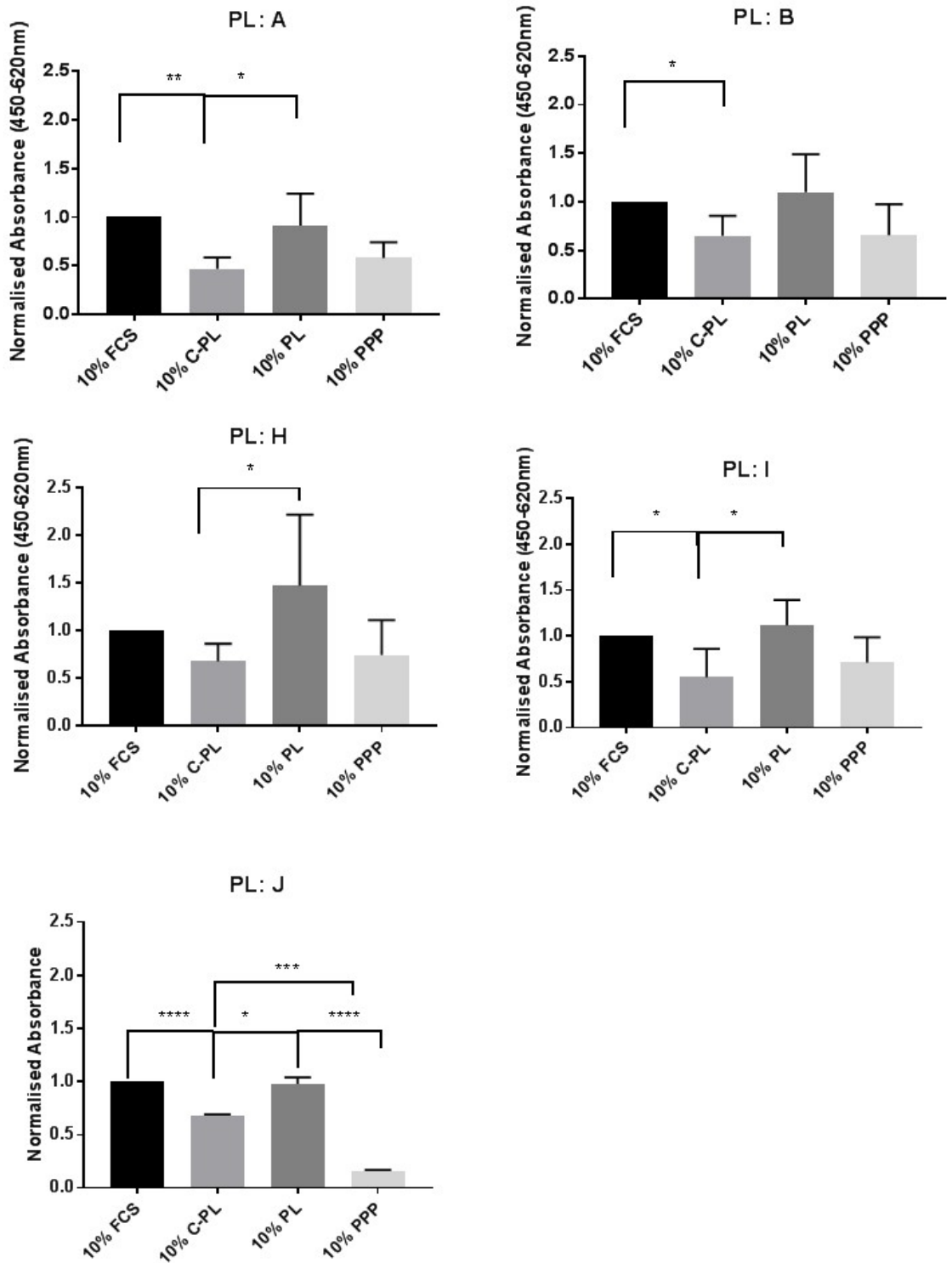


Figure 51 compare the effect of leukocytes on BM-BMSC proliferation using the XTT assay to test 10% PL and 10% C-PL ($n=5$) against 10% FCS and 10% PPP. All PL preparations were tested on $n=4$ BM-MSCs except for PL J which was tested on $n=1$ autologous matched BM-MSCs. Error bars indicate variation between BM-MSC donors (PL A, B, H, & I), error bars for PL J indicate technical error between replicates. One-way ANOVA with Tukey's multiple comparison test was used to identify significance * $P < 0.05$, ** $P < 0.01$, *** $P < 0.001$, **** $P < 0.0001$.

5.3.9 Comparing PL and C-PL's ability to induce BM-MSC migration:

PL and C-PL were also tested on BM-MSC migration, with the same IncuCyte migration assay that was optimised in section 5.35, using two PL preparations (H and I) each tested on three BM-MSC cultures (figure 52). It is of note that, due to condensation forming on the plate at 28 hours, data after that point could not be analysed. Looking first at PL preparation H, BM-MSC cultures 6 and 5 responded similarly to PL and C-PL; both induced an increase in the total phase object area on the underside of the well indicative of more total migration than the positive control. Both PL and C-PL show similar trends of migration, with PL appearing to bring about a faster initial migratory response. BM-MSC culture 3 responds differently to the platelet products; despite being the most static of the cultures, it initially begins to migrate towards PL but its' response plateaus off and by 28 hours its response is equal to C-PL and FCS. BM-MSC culture 3's response is more inconsistent than the other cultures but this is likely because its total migration is so low that any variation in the mask between scans appear more exaggerated than in other cultures that migrated more. The average of all three cultures' response to the PL H platelet products shows that, despite a faster initial response to PL, after 28 hours there is no difference between PL and C-PL's total migration and both are far more inductive of migration than FCS. Looking next at PL preparation I, BM-MSCs from culture 6 and 5, after 16 hours, begin to migrate rapidly towards PL and C-PL making the migration towards FCS appear negligible by comparison. The BM-MSCs continue to migrate towards PL and C-PL at a consistent rate up to 28 hours. Interestingly, PL induces a strong consistent migratory response from BM-MSCs in culture 3 whereas C-PL induces a much weaker response which plateaus after 24 hours and is only marginally better than FCS. Despite some variation in the responses of the three BM-MSC cultures to PL preparation I, both PL and C-PL induce a strong migratory response at least equal to, if not greater than, FCS. Considering the significantly higher numbers of leukocytes in C-PL, these findings indicate that the presence of leukocyte-derived proteins is not a detriment to BM-MSC migration and potentially contribute towards improved migration. To find out whether these trends are significant or not, statistics were carried out at three time points (figure 53).

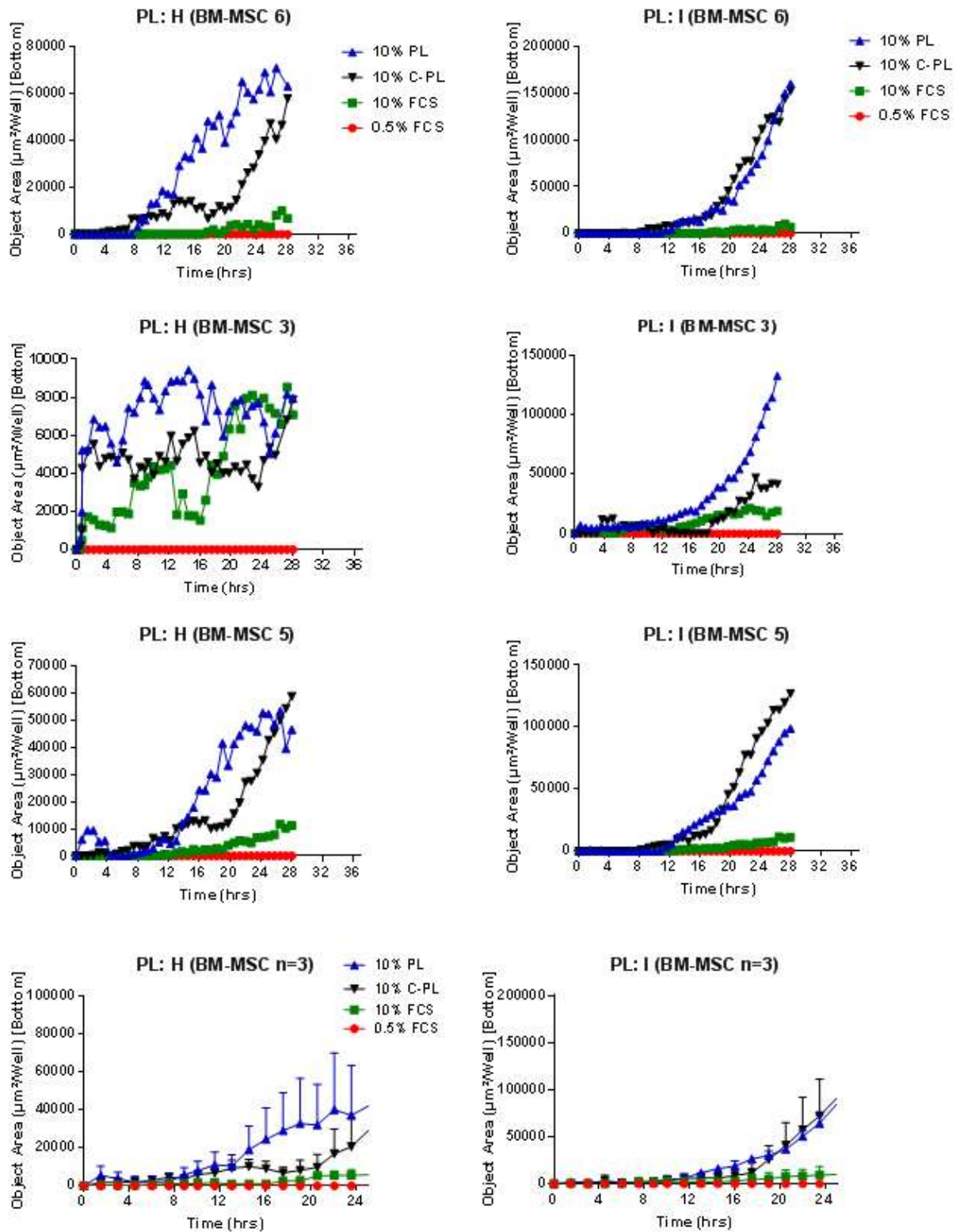


Figure 52 compares the ability of PL and C-PL (n=2) to stimulate migration in BM- MSC cultures (n=3) using the IncuCyte migration assay. Error bars indicate the variation between BM- MSC cultures for each PL preparation.

In figure 53, it can be seen that after just 12 hours, both PL and C-PL show much more migration than 0.5% FCS and despite a slight trend of PL inducing more migration than 10% FCS, they are not significantly different. By 24 hours, PL has induced significantly more migration than the controls in both preparations as does C-PL in one preparation (PL preparation I). Across both time points there was a clear trend of both PL and C-PL inducing as much migration as FCS, and often, more. This supports the finding in figure 52 that both platelet products are effective options for inducing migration and that leukocytes do not have a significantly inhibitory effect.

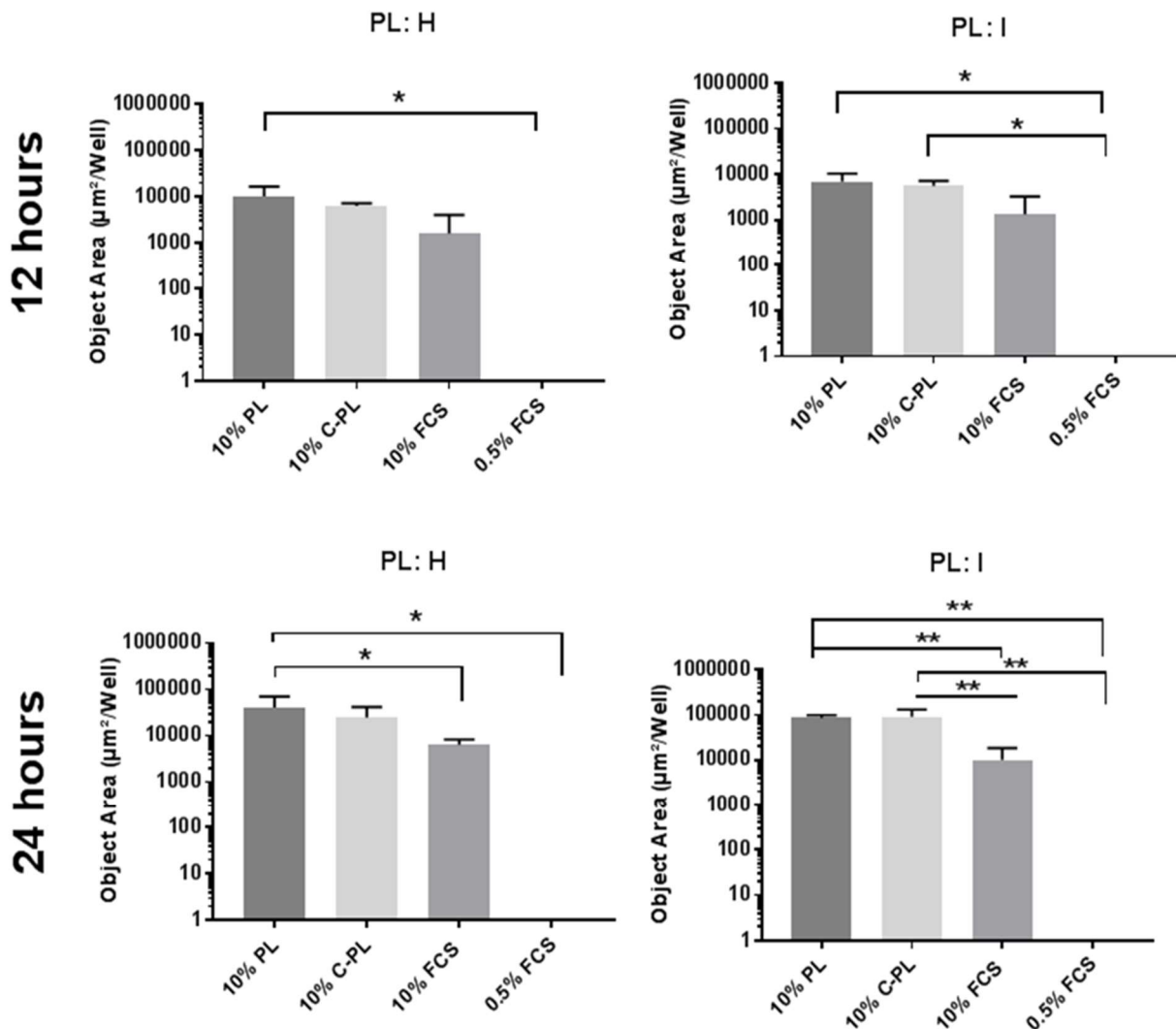


Figure 53 shows the amount of BM-BMSC migration towards 10% PL, 10% C-PL, 10% FCS and 0.5% FCS using the IncuCyte assay at time-points: 12 and 24 hours. All PL preparations (n=2) were tested on n=3 BM-MSCs. The error bars represent the standard errors of the means, * $P < 0.05$, ** $P < 0.01$, *** $P < 0.001$.

5.4 Discussion:

In order to attract and amplify BM-MSCs to the site of injury, a collagen membrane loaded with PRP will be used. However, whilst the clinical effectiveness of PRP is generally accepted, due to the lack of quality control, the variation in manufacturing, processing, delivery and its different applications (e.g. rotator cuff repair [44] and osteoarthritis [45, 46]), the 'optimal' composition of PRP is still hotly debated.

The main issue with lack of standardisation is exemplified by one study which found that PRP had no significant effect on bone healing [47], however, a closer look at the platelet numbers used in the study found that some of the PRP tested had over 16-fold more platelets than other PRP. Despite the vast differences in platelet numbers and omitted leukocyte numbers, these products were all classified under the same umbrella term 'PRP'. This is commonplace across the literature, whereby, the absence of standardised nomenclature, quality control, as well as thorough analysis of cellular contents, makes it difficult to draw clear conclusions. According to Delong et al.'s [43] platelet number, activation method and white blood cell number (PAW) classification system, C-PRP is classified as P2-A- α (which identifies the increase of platelets as 'moderate' and the leukocytes as 'enriched above baseline') whilst PRP is classified as P4-B- β (which identifies the platelet concentration as 'highly enriched' above baseline and leukocytes depleted below baseline). Platelet activation of PRP is most commonly used to initiate the formation of a gel for confined delivery of growth factors [48] as well as to ensure platelet lysis. Exogenous activators such as thrombin and calcium chloride weren't used in this research as they are not used as standard in current orthopaedic applications of PRP, and it has been well described that exposure to collagen at the site of injury induces similar activation and release of growth factors as thrombin [43, 48, 49]. As well as variation in platelet concentrations, the lack of regulation also instils concern in the scientific community over the use of highly concentrated leukocytes, their associated pro-inflammatory cytokines (specifically TNF- α and IL-1 β), and the risk that they could counteract the platelet's beneficial effects and impede bone regeneration [24]. TNF- α and IL-1 β are known to induce inflammation causing a biphasic physiological response; whilst inflammation is necessary for healing [50], in excess it is thought to activate the NF κ B pathway [24] inhibiting osteogenesis and promoting osteoclastogenesis [51]. However, more recently, these proinflammatory cytokines have been linked to increased osteogenesis [52], BM-MSC migration [53] and proliferation [38] indicative of the lack of consensus in the field.

This study addressed these concerns by better defining platelets and leukocyte's roles in the two key physiological processes of bone regeneration: BM-MSc proliferation and BM-MSc migration. With regards to proliferation, once the assay was optimised, it was first found that both PRP and PL induce as much proliferation as FCS, supporting their use as *in vitro* xeno-free media supplements providing an alternative to FCS and contributing to the development of autologous cell expansion for tissue engineering purposes [16]. Removing leukocytes from PL to make fPL did not further improve their ability to induce proliferation whilst direct comparison of PL and C-PL found C-PL to be suboptimal at supporting BM-MSc proliferation. This response from the BM-MScs was also observed using donor-matched platelet products, proving that the response from the cells was not due to the allogeneic nature of the platelet products. Collectively this data points to C-PL's poor performance compared to PL and fPL is likely due to its lower number of platelets rather than its higher number of leukocytes as originally thought– both of which are theories that have been reported to reduce proliferation in the literature [24, 43, 54, 55]. This suggests that, in our experimental conditions, the cytokines released from leukocytes neither enhanced nor inhibited BM-MSc proliferation and that platelets are most likely responsible for releasing the predominant growth factors involved in supporting BM-MSc proliferation. Due to the limited volume of samples collected, these results are limited by the lack of a direct comparison between fPL and filtered C-PL. Due to the bigger difference in leukocyte number between the two products, if no significant difference was observed this would have supported the theory that it is platelets, rather than leukocytes, that determine major outcomes in BM-MSc proliferation. Future work in this area should also include 'spiking' experiments whereby fPL is dosed with increasing numbers of leukocytes to measure any dose-dependent response from the cells.

With regards to BM-MSc migration, all three platelet products; PL, C-PL and fPL induced significantly more migration than FCS. This result supports two previous studies that used BM-MScs seeded onto transwells [24, 56] and another that used BM-MScs seeded in a Boyden chamber [57] which all found 10% PRP to outperform FCS. PRP and PL's significant chemotactic effects are thought to be a result of their greater concentration of cytokines and chemokines, such as VEGF and SDF-1, that are released from platelet's α -granules [58, 59]. As was seen in the proliferation experiments, removing leukocytes from PL did not further enhance its effect on BM-MSc migration, but even seemed to reduce it. Whilst there is no precedent for the use of platelet products in BM-MSc migration studies, the current data supports previous literature of platelet products outperforming FCS [24, 56].

The methods used are also unique in that, not only is the total migration shown, but also the increased rate of cell migration towards the platelet products. Furthermore, these findings suggest that whilst platelet and leukocyte numbers contribute towards BM-MSC migration, it is likely that most of the cytokines that induce migration are present in the plasma component of PRP (i.e. PPP) – and so any additional platelet or leukocytes make no significant difference. Unfortunately PPP wasn't tested in migration experiments due to the limited number of wells the IncuCyte device could capture at each time point.

Interestingly, the two platelet products (H and I) bring about notably different responses from BM-MSC culture 3. Whilst BM-MSC culture 3 appears to be the most static culture tested, the platelet products of preparation H induce as much migration as FCS whilst the platelet products of preparation I induce considerably more migration. This indicates there is donor variation platelet product donors as well as between BM-MSC donors. Although both products have seemingly similar platelet and leukocyte numbers, PL preparation I's success could be due to the slightly higher platelet count ($1,162 \times 10^3$ PLTs/ μ L for PL I compared to $1,000 \times 10^3$ PLTs/ μ L for PL H). Another possible cause for the difference could be PL preparation I's plasma (PPP) simply contains higher concentrations of chemokines. Whilst the impact of donor age on PRP functionality has not yet been investigated specifically, research by Evanson *et al.* found a negative correlation with age and growth factor concentrations in PRP preparations [60] which could also explain variability between donors aside from platelet and leukocyte numbers.

Based on these findings it could be proposed that, with regards to migration, the compositions of both PL and C-PL can be characterised as 'high quality' based on their ability to induce BM-MSC migration, whilst for proliferation, PL is a suitable product whereas C-PL is suboptimal. This suggests that to generate a high quality product for both BM-MSC proliferation and migration should simply focus on enriching platelets without regard for leukocytes – this could be easily achieved by decreasing the final volume to yield a more concentrated platelet product. However the excessive enrichment of platelets faces the risk paradoxically inhibiting cell proliferation, viability and migration [43]. A therapeutically effective 'window' of platelet concentration is likely to be the case rather than a specific pure concentration. This therapeutically optimum platelet concentration could be identified by testing the functionality of PPP (plasma only) that has been treated with a range of platelet concentrations to identify the therapeutic concentration range.

Whilst BM-MSC donor variation was expected [61, 62], measuring the surface expression of specific growth factor receptors such as CD140a and CD140b for PDGF [63] on BM-MSCs could indicate how responsive donor's BM-MSCs will be to PRP treatment. Variation in PRP donors is an overlooked issue in the literature and acts as a bottleneck for its therapeutic standardisation – therefore, developing the best PRP protocol is key as well as assaying PRP and BM-MSC quality before use will equally contribute towards successful treatment outcomes.

This study also supports the notion that the specific clinical application and desired outcome should be considered for defining best formulations of platelet products for bone regeneration. If cell proliferation is thought to be limiting regeneration, for example in elderly patients that have low numbers of autologous BM-MSCs [64], then C-PL will be sub-optimal and PRP with higher concentrations of platelets should be used. If however, the surgeon's priority is to induce BM-MSC migration to the site of injury, for example to attract BM-MSCs towards an unpopulated bone scaffold, then the current clinical standard C-PL may be sufficient. Although the work presented here gives insight into the role of platelets and leukocytes, it does not address which specific growth factors and cytokines are involved. Future work should be directed at defining the growth factor profile of 'high quality' PRP samples based on their ability to induce BM-MSC proliferation and migration as a means of quality control. As well, what affect these products have on inducing chondrogenesis and osteogenesis would provide a better insight into their long-term clinical use.

In conclusion, this study found that both PL and fPL induce as much BM-MSC proliferation as FCS and that low platelet number, rather than high leukocyte number, hinders C-PL's performance with regard to proliferation. Promisingly, with regards to migration, all platelet products induced significant, sustained responses from BM-MSCs up to 24 hours, regardless of their cell composition. This data demonstrates that PL is an effective product to load membranes with to maximise BM-MSC proliferation and migration at the site of injury. To confirm this, membranes loaded with PL (and C-PL as the clinical control product), will be tested in chapter 6.

5.5 References:

1. Tzioupis, C. and P. Giannoudis, *Prevalence of long-bone non-unions*. Injury, 2007. **38, Supplement 2**: p. S3-S9.
2. Calori, G.M., et al., Treatment of long bone non-unions with polytherapy: Indications and clinical results. Injury, 2011. **42**(6): p. 587-590.

3. Santolini, E., R. West, and P.V. Giannoudis, Risk factors for long bone fracture non-union: a stratification approach based on the level of the existing scientific evidence. *Injury*, 2015. **46 Suppl 8**: p. S8-s19.
4. Giannoudis, P.V., T. Einhorn, and D. Marsh, *Fracture healing: the diamond concept*. *Injury* 2007. **4**: p. 3-6.
5. Giannoudis, P.V., et al., Masquelet technique for the treatment of bone defects: Tips-tricks and future directions. *Injury*, 2011. **42**(6): p. 591-598.
6. Dimitriou, R., et al., *Bone regeneration: current concepts and future directions*. *BMC Medicine*, 2011. **9**: p. 66-66.
7. Krishnakumar, G.S., et al., Clinical application of bone morphogenetic proteins for bone healing: a systematic review. *International Orthopaedics*, 2017. **41**(6): p. 1073-1083.
8. Moghaddam-Alvandi, A., et al., *Results of nonunion treatment with bone morphogenetic protein 7 (BMP-7)*. *Unfallchirurg*, 2012. **115**(6): p. 518-526.
9. Lyon, T., et al., Efficacy and safety of recombinant human bone morphogenetic protein-2/calcium phosphate matrix for closed tibial diaphyseal fracture: a double-blind, randomized, controlled phase-II/III trial. *J Bone Joint Surg Am*, 2013. **95**(23): p. 2088-96.
10. Ristiniemi, J., et al., RhBMP-7 accelerates the healing in distal tibial fractures treated by external fixation. *J Bone Joint Surg Br*, 2007. **89**(2): p. 265-72.
11. Babiker, H., M. Ding, and S. Overgaard, *Demineralized bone matrix and human cancellous bone enhance fixation of porous-coated titanium implants in sheep*. *Journal of Tissue Engineering and Regenerative Medicine*, 2016. **10**(3): p. 245-251.
12. Li, X.F., D.X. Xu, and Y.Z. Chen, Teriparatide as a nonoperative treatment for tibial and femoral fracture nonunion A case report. *Medicine*, 2017. **96**(16).
13. Tall, M., *Treatment of aseptic tibial shaft non-union without bone defect*. *Orthopaedics & Traumatology-Surgery & Research*, 2018. **104**(1): p. S63-S69.
14. de Grado, G.F., et al., Bone substitutes: a review of their characteristics, clinical use, and perspectives for large bone defects management. *Journal of Tissue Engineering*, 2018. **9**.
15. Alsousou, J., et al., The biology of platelet-rich plasma and its application in trauma and orthopaedic surgery: a review of the literature. *J Bone Joint Surg Br*, 2009. **91**(8): p. 987-96.
16. Bieback, K., Platelet Lysate as Replacement for Fetal Bovine Serum in Mesenchymal Stromal Cell Cultures. *Transfusion Medicine and Hemotherapy*, 2013. **40**(5): p. 326-335.
17. Altaie, A., H. Owston, and E. Jones, *Use of platelet lysate for bone regeneration - are we ready for clinical translation?* *World Journal of Stem Cells*, 2016. **8**(2): p. 47-55.
18. Moreira Teixeira, L.S., et al., The effect of platelet lysate supplementation of a dextran-based hydrogel on cartilage formation. *Biomaterials*, 2012. **33**(14): p. 3651-61.
19. Oliveira, S.M., R.L. Reis, and J.F. Mano, *Assembling Human Platelet Lysate into Multiscale 3D Scaffolds for Bone Tissue Engineering*. *ACS Biomaterials Science & Engineering*, 2015. **1**(1): p. 2-6.
20. Moojen, D.J., et al., Antimicrobial activity of platelet-leukocyte gel against *Staphylococcus aureus*. *J Orthop Res*, 2008. **26**(3): p. 404-10.
21. Boswell, S.G., et al., *Platelet-rich plasma: a milieu of bioactive factors*. *Arthroscopy*, 2012. **28**(3): p. 429-39.
22. Robert, Z., et al., Different preparation methods to obtain platelet components as a source of growth factors for local application. *Transfusion*, 2001. **41**(10): p. 1217-1224.
23. Xu, Z., et al., Comparative evaluation of leukocyte- and platelet-rich plasma and pure platelet-rich plasma for cartilage regeneration. *Scientific Reports*, 2017. **7**: p. 43301.
24. Yin, W., et al., Advantages of pure platelet-rich plasma compared with leukocyte- and platelet-rich plasma in promoting repair of bone defects. *Journal of Translational Medicine*, 2016. **14**: p. 73.

25. Shih, D.T. and T. Burnouf, Preparation, quality criteria, and properties of human blood platelet lysate supplements for ex vivo stem cell expansion. *N Biotechnol*, 2015. **32**(1): p. 199-211.
26. Bowen, R.A. and A.T. Remaley, Interferences from blood collection tube components on clinical chemistry assays. *Biochem Med (Zagreb)*, 2014. **24**(1): p. 31-44.
27. Mussbacher, M., et al., Optimized plasma preparation is essential to monitor platelet-stored molecules in humans. *PLOS ONE*, 2017. **12**(12): p. e0188921.
28. Strandberg, G., et al., Standardizing the freeze-thaw preparation of growth factors from platelet lysate. *Transfusion*, 2017. **57**(4): p. 1058-1065.
29. Essen, B. *Chemotaxis application*. Chemotaxis cell migration quick guide 2018 [cited 2018 28/08/18].
30. Bausset, O., et al., *Formulation and Storage of Platelet-Rich Plasma Homemade Product*. *BioResearch Open Access*, 2012. **1**(3): p. 115-123.
31. Zini, G., Stability of complete blood count parameters with storage: toward defined specifications for different diagnostic applications. *International Journal of Laboratory Hematology*, 2013. **36**(2): p. 111-113.
32. Soleimani, M. and S. Nadri, A protocol for isolation and culture of mesenchymal stem cells from mouse bone marrow. *Nat Protoc*, 2009. **4**(1): p. 102-6.
33. Tropel, P., et al., Isolation and characterisation of mesenchymal stem cells from adult mouse bone marrow. *Experimental Cell Research*, 2004. **295**(2): p. 395-406.
34. Pittenger, M.F., *Mesenchymal Stem Cells from Adult Bone Marrow*, in *Mesenchymal Stem Cells: Methods and Protocols*, D.G.P. D.J. Prockop, and B.A. Bunnell, Editor. 2008, Humana Press: Totowa, NJ. p. 27-31.
35. Cho, H.S., et al., Individual Variation in Growth Factor Concentrations in Platelet-rich Plasma and Its Influence on Human Mesenchymal Stem Cells. *The Korean Journal of Laboratory Medicine*, 2011. **31**(3): p. 212-218.
36. Justus, C.R., et al., *In vitro Cell Migration and Invasion Assays*. *Journal of Visualized Experiments : JoVE*, 2014(88): p. 51046.
37. Hulkower, K.I. and R.L. Herber, *Cell Migration and Invasion Assays as Tools for Drug Discovery*. *Pharmaceutics*, 2011. **3**(1): p. 107-124.
38. El-Zayadi, A.A., et al., Interleukin-22 drives the proliferation, migration and osteogenic differentiation of mesenchymal stem cells: a novel cytokine that could contribute to new bone formation in spondyloarthropathies. *Rheumatology*, 2017. **56**(3): p. 488-493.
39. Lindy O'Clair, M.R., Maria Tikhonenko, Clare Syzbut, Nicola Bevan, Kirk Schroeder and Daniel M. Appledorn *Quantification of Cell Migration and Invasion Using the IncuCyte® Chemotaxis Assay*, in *Essen BioScience - Application Note*, M. Ann Arbor, USA and Welwyn Garden City, Hertfordshire, UK, Editor. 2017: Michigan, USA.
40. Friedl, P. and D. Gilmour, *Collective cell migration in morphogenesis, regeneration and cancer*. *Nature Reviews Molecular Cell Biology*, 2009. **10**: p. 445.
41. Kedrin, D., et al., *Cell motility and cytoskeletal regulation in invasion and metastasis*. *J Mammary Gland Biol Neoplasia*, 2007. **12**(2-3): p. 143-52.
42. Friedl, P., *Prespecification and plasticity: shifting mechanisms of cell migration*. *Current Opinion in Cell Biology*, 2004. **16**(1): p. 14-23.
43. DeLong, J.M., R.P. Russell, and A.D. Mazzocca, *Platelet-Rich Plasma: The PAW Classification System*. *Arthroscopy: The Journal of Arthroscopic & Related Surgery*, 2012. **28**(7): p. 998-1009.
44. Randelli, P., et al., *Regenerative Medicine in Rotator Cuff Injuries*. *BioMed Research International*, 2014. **2014**: p. 9.
45. Sanchez, M., et al., Intraosseous infiltration of platelet-rich plasma for severe knee osteoarthritis. *Arthrosc Tech*, 2014. **3**(6): p. e713-7.

46. Dai, W.L., et al., Efficacy of Platelet-Rich Plasma in the Treatment of Knee Osteoarthritis: A Meta-analysis of Randomized Controlled Trials. *Arthroscopy*, 2017. **33**(3): p. 659-670.e1.
47. Joo, M.W., et al., The Effect of Autologous Platelet-Rich Plasma on Bone Regeneration by Autologous Mesenchymal Stem Cells Loaded onto Allogeneic Cancellous Bone Granules. *Cells Tissues Organs*, 2017. **203**(6): p. 327-338.
48. Cavallo, C., et al., Platelet-Rich Plasma: The Choice of Activation Method Affects the Release of Bioactive Molecules. *BioMed Research International*, 2016. **2016**: p. 7.
49. Fufa, D., et al., *ACTIVATION OF PLATELET-RICH PLASMA USING SOLUBLE TYPE I COLLAGEN*. *Journal of oral and maxillofacial surgery : official journal of the American Association of Oral and Maxillofacial Surgeons*, 2008. **66**(4): p. 684-690.
50. Glass, G.E., et al., *TNF- α promotes fracture repair by augmenting the recruitment and differentiation of muscle-derived stromal cells*. *Proceedings of the National Academy of Sciences of the United States of America*, 2011. **108**(4): p. 1585-1590.
51. Lacey, D.C., et al., Proinflammatory cytokines inhibit osteogenic differentiation from stem cells: implications for bone repair during inflammation. *Osteoarthritis and Cartilage*, 2009. **17**(6): p. 735-742.
52. Croes, M., et al., Proinflammatory Mediators Enhance the Osteogenesis of Human Mesenchymal Stem Cells after Lineage Commitment. *PLoS ONE*, 2015. **10**(7): p. e0132781.
53. Tomchuck, S.L., et al., Toll-like receptors on human mesenchymal stem cells drive their migration and immunomodulating responses. *Stem Cells*, 2008. **26**(1): p. 99-107.
54. Doucet, C., et al., Platelet lysates promote mesenchymal stem cell expansion: a safety substitute for animal serum in cell-based therapy applications. *J Cell Physiol*, 2005. **205**(2): p. 228-36.
55. Muraglia, A., et al., Combined platelet and plasma derivatives enhance proliferation of stem/progenitor cells maintaining their differentiation potential. Vol. 17. 2015. 1793-1806.
56. Murphy, M.B., et al., Adult and umbilical cord blood-derived platelet-rich plasma for mesenchymal stem cell proliferation, chemotaxis, and cryo-preservation. *Biomaterials*, 2012. **33**(21): p. 5308-5316.
57. Lykov, A.P., et al., Comparative Effects of Platelet-Rich Plasma, Platelet Lysate, and Fetal Calf Serum on Mesenchymal Stem Cells. *Bull Exp Biol Med*, 2017. **163**(6): p. 757-760.
58. Crespo-Diaz, R., et al., Platelet Lysate Consisting of a Natural Repair Proteome Supports Human Mesenchymal Stem Cell Proliferation and Chromosomal Stability. *Cell Transplantation*, 2011. **20**(6): p. 797-812.
59. Cuthbert, R.J., et al., Induced periosteum a complex cellular scaffold for the treatment of large bone defects. *Bone*, 2013. **57**(2): p. 484-492.
60. Evanson, J.R., et al., Gender and age differences in growth factor concentrations from platelet-rich plasma in adults. *Mil Med*, 2014. **179**(7): p. 799-805.
61. Siegel, G., et al., Phenotype, donor age and gender affect function of human bone marrow-derived mesenchymal stromal cells. *BMC Medicine*, 2013. **11**(1): p. 1-20.
62. Phinney, D.G., et al., Donor variation in the growth properties and osteogenic potential of human marrow stromal cells. *J Cell Biochem*, 1999. **75**.
63. Tan, H.B., et al., The systemic influence of platelet-derived growth factors on bone marrow mesenchymal stem cells in fracture patients. *BMC Medicine*, 2015. **13**: p. 6.
64. Block, T.J., et al., Restoring the quantity and quality of elderly human mesenchymal stem cells for autologous cell-based therapies. *Stem Cell Research & Therapy*, 2017. **8**: p. 239.

6 Functionality testing of scaffolds

6.1 Introduction:

Following the design and fabrication of a novel collagen-PCL membrane, the next step in development is to elucidate its viability as an effective GBR device by characterising specific functions. As well as mechanical strength (which has already been tested in chapter 4), these desired functions include; the ability to absorb and release platelet products at the site of injury, to be biocompatible and support BM-MSC proliferation, a degradation time that is long enough to achieve bone building before membrane disintegration and finally; once loaded with PL, to support rare BM-MSC colony formation. Since the healing of bone is dependent on the influx and proliferation of BM-MSCs, this chapter focuses on ensuring the membrane developed can support these rare cells for maximum reossification.

As of yet, collagen membranes have not been used in orthopaedics due to the absence of a stable and mechanically sound enough product [1, 2]. This research aims to incorporate novel ES techniques to manufacture stable, biocompatible collagen scaffolds to retain grafted material at the site of injury in long bone defects. It is hypothesised that this approach will optimise current fracture repair treatments based on two key factors; 1) the success of the guided bone regeneration approach in the masquelet technique, whereby the presence of a protective biological membrane enhances bone healing [3, 4], and 2) the successful application of collagen membranes in oral biology, whereby the scaffold is used as a flap to segregate the defect and protect it from soft tissue ingrowth that would impair healing [5-7]. Despite anatomical differences, the use of collagen membranes in dentistry provides a useful insight into their potential success if translated into long bone fracture.

Promisingly, commercial scaffolds such as Bio-Gide used in dentistry have also been found to induce ossification in rabbits and humans undergoing bilateral root resection and even demonstrated better bone healing compared to the collagen solution only control (no membrane) [8]. Another commercial product used in dentistry is Mucograft, which is used for oral soft tissue regeneration, however, it has also recently been associated with bone healing in rat calvarial defects [9]. Despite these scaffold's successful use in small bone defects, their direct translation into orthopaedics, and non-union fractures specifically, is impeded by their rapid degradation. The minimum time needed for complete bone healing is

thought to be around 12 weeks [10, 11] depending on fracture location, however Mucograft has been described to completely degrade after 7 days [2] and Bio-Gide was found to degrade by 80% after 9 weeks [1]. This rapid degradation time means that the scaffold is not able to provide structural support or biomechanical stability until the new bone is fully formed. As well as their short degradation profiles, an optimal scaffold for bone repair must be able to absorb and release growth factors, stable enough to be handled and retain the grafted material, as well as be pliable enough to mould around the defect. These desired properties have been collated from over two decades of GBR research and development [6, 12] as well as from demand from the clinical orthopaedic community [4], for an alternative solution to the existing methods such as bone grafts, bone substitutes, bone marrow aspirate, and the already described two-stage masquelet technique.

Delivering PRP to the site of injury is a common step in the treatment of most bone fractures, however it is often administered through the soaking synthetic bone chips and bone grafts [13]. Despite PRP being a key contributor to bone healing [14], the volumes supplied to the site of injury are limited by the delivery method and it was hypothesised that this volume can be increased by using the absorbent collagen membrane as another means of delivery to maximise bone generation. Whilst some success has been attributed to alternative methods of PRP delivery, such as injections which was found to increase bone formation around hydroxyapatite dental implants in dogs [15], generally this is an inaccurate method that does not ensure confinement of the PRP to the site of injury or consistent distribution around the defect [13].

Developing a novel membrane poses a challenge to effectively test its functionality due to the lack of pre-existing standard protocols. To address this, assays had to be adapted; including the incorporation of a PRP loaded membrane into the CFU-F assay for BM-MSC colony formation, the development of a protein release assay to quantify its release kinetics, alongside standard protocols for measuring *in vitro* cytotoxicity and proliferation (ISO 10993-5:2009), and absorption capacity (BS EN 13726-1:2002).

This chapter focuses on testing the key functions of the prototype electrospun 70:30 collagen:PCL scaffold compared against the PCL only control scaffold.

6.2 Specific Methods:

Unless specified, all scaffolds were dried for 12 hrs at 40°C before use to ensure all solvent had fully evaporated before testing.

6.2.1 Scaffold eluate XTT cytotoxicity assay:

Scaffold eluates were prepared from PCL and 70:30 scaffolds (n=2 from each scaffold type) according to the ISO standard: ISO 10993-12:2007 part 12. Sample preparation and reference materials were prepared by macerating 600 mg of the scaffold sample into 6 ml of basal DMEM media (not containing FCS) in a sterile bijou which was incubated at 37°C for 72 hours. The solution was centrifuged at 180 xg to remove the scaffold sections and the extract media was frozen at -4°C. Once the eluate was prepared, cytotoxicity was evaluated according to ISO: 10993-5:2009(E) part 5: Tests for in vitro cytotoxicity. Cells from three BM-MSC cultures (n=3) were each seeded in triplicate in 200 µL basal media at densities of 10,000 cells/well in a 96 well plate for 24 hrs. After 24 hrs incubation, the basal media was removed and replaced with 200 µl of the thawed treatment media containing either the scaffold eluate, the negative control (basal media with 10% DMSO), or the positive control (basal media). Cells were then incubated in treatment media for another 24 hrs before adding the XTT reagents.

6.2.2 Scaffold eluate proliferation assay:

To assess the impact scaffold eluates would have on BM-MSC proliferation, an extended adaptation of the XTT assay outlined in section 5.2.7 was used. First, scaffold eluates were prepared in the same way as in section 6.2.1, followed by seeding cells at a density of 500 cells/well in a 96 well plate for 24 hrs in basal media (not containing FCS). After 24 hrs, the basal media was removed and replaced with 200 µl of treatment medium containing either the scaffold eluate, the negative control (basal media with 10% DMSO), or the positive control (basal media). Cells were cultured for five days, during which, the media was replenished at the start of day three. After five days, the XTT assay was carried out and analysed as described in section 2.8 to quantify cell proliferation compared to the positive control.

6.2.3 Scaffold absorbance of PL:

Folded scaffolds roughly 1 cm² in size were measured using a thickness gauge (and dried at 40°C for 12 hrs before weighing them (weight_{dry}). Once weighed, each scaffold was placed in 1 ml of 100% human PL from Cook Regentec. Because of the large volumes needed, commercially sourced PL was used in this assay for consistency. Scaffolds were soaked in PL at room temperature for 15 mins to mimic the clinical setting [16, 17]. After soaking, the scaffolds were removed and the excess CRPL was allowed to drip-off for 30 seconds. Finally, the PL-soaked scaffolds were weighed again (weight_{soaked}) to calculate their percent weight increase, as an indicator of absorption capacity using equation 4. Whilst the percent weight increase of each scaffold was then normalised to the initial area of the sample using equation 5.

$$\text{Weight increase (\%)} = \left(\frac{\text{Weight}_{\text{soaked}}(\text{g}) - \text{Weight}_{\text{dry}}(\text{g})}{\text{Weight}_{\text{dry}}(\text{g})} \right) \times 100$$

Equation 4: Formula used to calculate the percent increase in weight of the PL soaked scaffolds

$$\text{Area}(\text{cm}^2) = 2 (lw + wh + hl)$$

$$\text{Normalised Absorption capacity (g/cm}^2\text{)} = \frac{\text{Weight}_{\text{soaked}}(\text{g}) - \text{Weight}_{\text{dry}}(\text{g})}{\text{Area (cm}^2\text{)}}$$

Equation 5: Formula used to first calculate the surface area of each scaffold where l equals length, w equals width and h equals height of each sample. Using the area, the weight increase of the soaked scaffolds can then be normalised.

The volume absorbed was also calculated to ensure the weight increase was accurately representative of the volume absorbed using equation 6. Because of the different shapes and sizes of the scaffolds, this volume was normalised to each scaffold's area.

$$\text{Normalised absorbed volume (\mu L/cm}^2\text{)} = \frac{\text{Total volume}(\mu\text{L}) - \text{Unabsorbed volume}(\mu\text{L})}{\text{Area (cm}^2\text{)}}$$

Equation 6: Formula used to calculate the volume absorbed by the scaffolds normalised to their area

6.2.4 Scaffold release of PL:

To measure the rate at which the scaffolds release the growth factors in PL this assay was designed which mimics the *in vivo* setting *in vitro*. It employs three main

steps which will be outlined below:

- 1) Sample collection
- 2) BCA assay
- 3) Analysis

6.2.5 Scaffold release of PL – sample collection

Following absorbance measurements (section 6.2.3), the PL soaked scaffolds were incubated in 3mL of simulated body fluid (SBF) at 37°C. Two samples were used for each scaffold type group, as well as an unloaded control group (not soaked in PL). Fluid samples were collected sacrificially at regular time points whereby 60µL/time point was extracted and replaced with an equal volume of SBF (appendix 1). The time points were collected every five minutes for the first two hours, then hourly for the following 10 hours, then every 12 hours for up to 64 hours. After 64 hours, the scaffolds were removed and suspended to remove excess solution before being moved into fresh SBF for one hour before 60 µL was extracted again. The aim of this final extraction was to quantify any protein that remained bound to the scaffold by creating a maximum diffusion gradient (to ensure protein released into the SBF hadn't reached equilibrium). The 60µL aliquots were stored in sealed eppendorf tubes at 4°C until all time points were collected and ready for the BCA assay.

6.2.6 Scaffold release of PL – Bicinchoninic acid (BCA) assay:

The BCA assay is a colorimetric assay which enables quantification of protein in a sample using a bovine serum albumin (BSA) standard curve. First, the BSA standard was established with a final working range of 0-2000 µg/mL made up using 2 mg/mL BSA diluted in SBF following a dilution series outlined in table 11. SBF composition is outlined in appendix 1 [18]. 25 µL of each standard and test samples was pipetted in duplicate in a 96-well plate followed by 200 µL of the BCA working reagent. The plate was covered and agitated on a microplate shaker for 30 seconds before incubation at 37°C for 30 mins. The absorbance was subsequently measured at 570 nm using a microplate reader. The average blank (SBF) absorbance was subtracted and the protein concentration (µg/mL) of the unknown samples was measured by comparing with a standard curve ($R^2 = 0.9936$) obtained from the BSA standards (figure 54).

Table 11: The dilution series used to make the range of BSA concentrations for the standard curve

<u>Vial</u>	<u>Volume of Diluent</u> <u>(μL)</u>	<u>Volume and Source of BSA</u> <u>(μL)</u>	<u>Final BSA Concentration</u> <u>($\mu\text{g}/\text{mL}$)</u>
A	0	300 of Stock	2000
B	125	375 of Stock	1500
C	325	325 of Stock	1000
D	175	175 of vial B dilution	750
E	325	325 of vial C dilution	500
F	325	325 of vial E dilution	250
G	325	325 of vial F dilution	125
H	400	100 of vial G dilution	25
I	400	0	0 = Blank

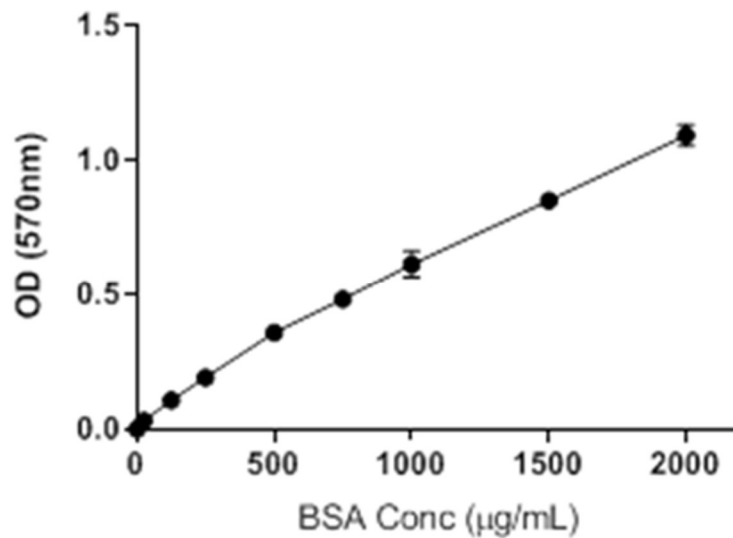


Figure 54: The standard curve produced from the albumin standards outlined in table 11 and their corresponding optical density (OD). Error bars indicate variation between technical replicates.

6.2.7 Scaffold release of PL – Analysis

To quantify the amount of proteins released from the scaffolds, the average blank (SBF only) OD reading was subtracted from each time point's OD reading. Due to the sacrificial nature of the release assay, each blank-corrected OD reading was divided by the dilution factor which was calculated for each sample using equation 7.

$$\text{Dilution factor} = \frac{\text{Final volume (mL)}}{\text{Solute volume (mL)}}$$

Equation 7: Formula used to calculate the dilution factor for each time point of the release assay where the final volume is the final volume of the well and the solute volume is the volume left in the well after each sample has been collected and before it is replenished with fresh SBF.

The protein concentration was then quantified by dividing each blank-corrected, dilution-corrected OD value by the linear regression of the BSA standards ($y=0.0005958x+0$) as outlined in equation 8.

$$\text{Protein concentration } (\mu\text{g/mL}) = \left(\frac{\text{OD}}{\text{linear regression}} \right) \div \text{volume of SBF (mL)}$$

Equation 8: Formula used to calculate the protein concentration based on the optical density (OD), linear regression of the standard curve and the volume of simulated body fluid (SBF) in each well.

The percent of protein concentration released for each time point was calculated as a fraction of the total amount of protein initially absorbed as described in equation 9.

$$\text{Total protein absorbed } \left(\frac{\mu\text{g}}{\text{mL}} \right) = \text{Volume absorbed } (\mu\text{L}) \times \left(\frac{\text{OD of } 1\mu\text{L pure PL}}{\text{linear regression}} \right)$$

$$\text{Protein released } (\%) = \frac{\text{Protein released } (\mu\text{g/mL})}{\text{Total protein absorbed } (\mu\text{g/mL})} \times 100$$

Equation 9: Formulas used to calculate the percent of protein released from the scaffolds based on the total amount that was absorbed [19].

6.2.8 Protein quantification in 10% PL:

To test whether the PL loaded scaffold released as much protein as is found in 10% PL (which had been previously optimised for cell proliferation in section 5.33) the protein quantities in 10% PL were analysed. C-PL products from 4 donors were diluted 1:10 in SBF alongside the BSA standards. The BCA assay was carried out on each PL product in triplicates using the microplate reader. As well, the average blank OD reading was subtracted from each OD reading. The same equations as outlined in section 6.2.7 were used to quantify the protein concentrations in the PL products.

6.2.9 Degradability:

To monitor scaffold degradation, roughly 1 cm² sections of single, unfolded sheets of 70:30 were cut up in triplicate and placed into 2 ml PBS in a 6 well plate. The plates were photographed, incubated at 37°C for up to 4 weeks, before analysing under SEM and photographed again.

6.2.10 PRP loaded scaffold CFU-F proliferation assay:

An adaptation of the CFU-F assay was used to quantify how C-PL-loaded membranes (70:30 and PCL) affected the proliferation and migration capacity of uncultured BM-MSCs. As in previous assays (section 5.2.7 and 5.2.8), PL was used in place of PRP to ensure consistency of product. First, fresh BMA from three donors underwent red blood cell lysis after which a total of 5×10^5 cells were plated in 15mL expansion media to adhere over 24 hrs. After initial attachment and a PBS wash, the media was replaced with either 15 mL expansion media containing 2 I.U/mL sodium heparin solution (control) or 15 mL DMEM media (no serum) containing 2 I.U/mL sodium heparin solution (test). 1 cm² square sections, 400 µm thick, of UV-sterilised 70:30 and PCL scaffolds were soaked in 2 mL of C-PL from one donor for 15 mins until saturated before being placed in the centre of the test dishes (figure 55). The dishes were incubated for a further 19 days with a half-media change in the second week. After 21 days, the dishes were washed in PBS, fixed in 10% (v/v) formalin and stained in 1% (w/v) methylene blue. All colonies were imaged using a plate scanner at 1200 dpi. Colony area, integrated density and number per dish was quantified using ImageJ whereby scanned images were converted to 8-bit greyscale and a threshold mask was applied before colonies were analysed and measured.

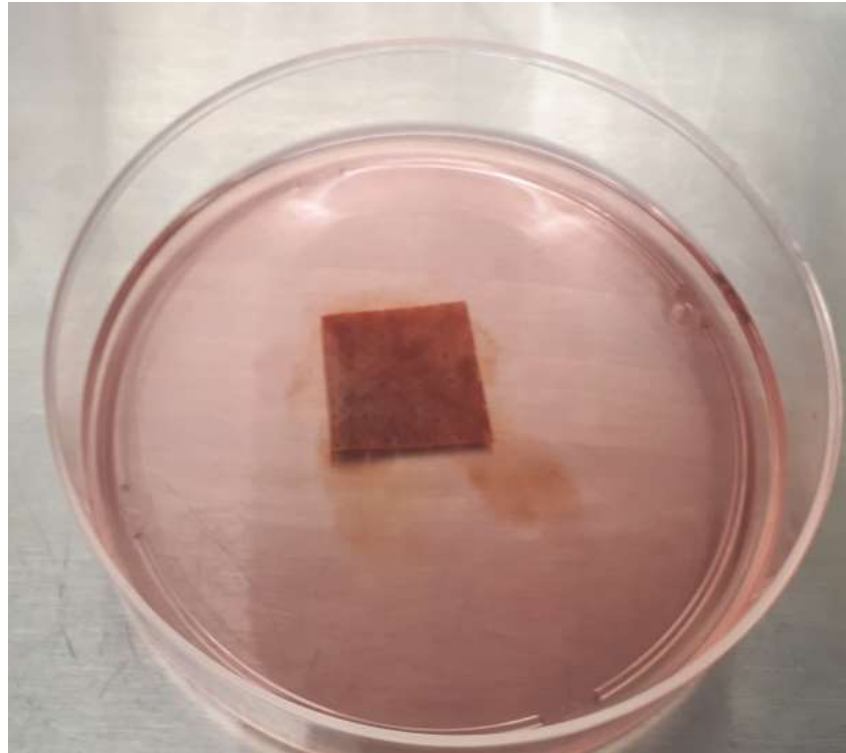


Figure 55: An example CFUF dish with a PL loaded 70:30 membrane.

6.2.11 Statistics

Statistical analyses were carried out on datasets that consisted of at least three independent experiments using a paired student's t test when comparing two groups from the same donor and an unpaired student's t test when donors weren't matched. One-way ANOVA with Tukey's multiple comparison test was used when comparing more than two groups or two-way ANOVA with Tukey's multiple comparison test for nonparametric results with GraphPad Prism software. All data are expressed as mean \pm standard deviation. * $P < 0.05$, ** $P < 0.01$, *** $P < 0.001$, and **** $P < 0.0001$ defined statistical significance.

6.3 Results:

Creating a novel scaffold requires testing its specific functions depending on the desired application, testing its functionality in these early phases of development ensures the ideal scaffold is fabricated by identifying potential weaknesses and strengths. This chapter used the XTT assay to assess the scaffold's effect on BM- MSC cytotoxicity and proliferation, as well as an adapted BCA assay to quantify protein absorption and release. Degradability was also assessed qualitatively and the CFU-F assay was used to test whether the loaded scaffold could support *in vitro*

BM-MSC proliferation. 70:30 was the scaffold chosen for this work as optimised in chapter 4, PCL only scaffold is used here as a control scaffold.

6.3.1 Cytotoxicity:

As outlined in ISO 10993-5:2009 (tests for in vitro cytotoxicity), 1×10^4 BM-MSCs/well were seeded in a 96 well plate in triplicate and exposed to either basal media (positive control), basal media containing 70:30 scaffold extract (test), or basal media containing 10% DMSO (negative control) for 24 hrs to identify the scaffold extract's effect on BM-MSC viability. Three individual BM-MSC cultures were used up to passage four and their average absorbance is shown in figure 56. The test at 1×10^4 BM-MSCs/well met the acceptance criteria as the mean OD_{450} of blanks was greater than 0.2 [20] so no further optimisation was necessary. As expected, there was a significant difference found between both the negative and positive controls ($P < 0.05$), and the negative and test media ($P < 0.05$). The scaffold extract containing media was found to be statistically similar to the basal media indicating no cytotoxic effect of the scaffold extract on BM-MSCs.

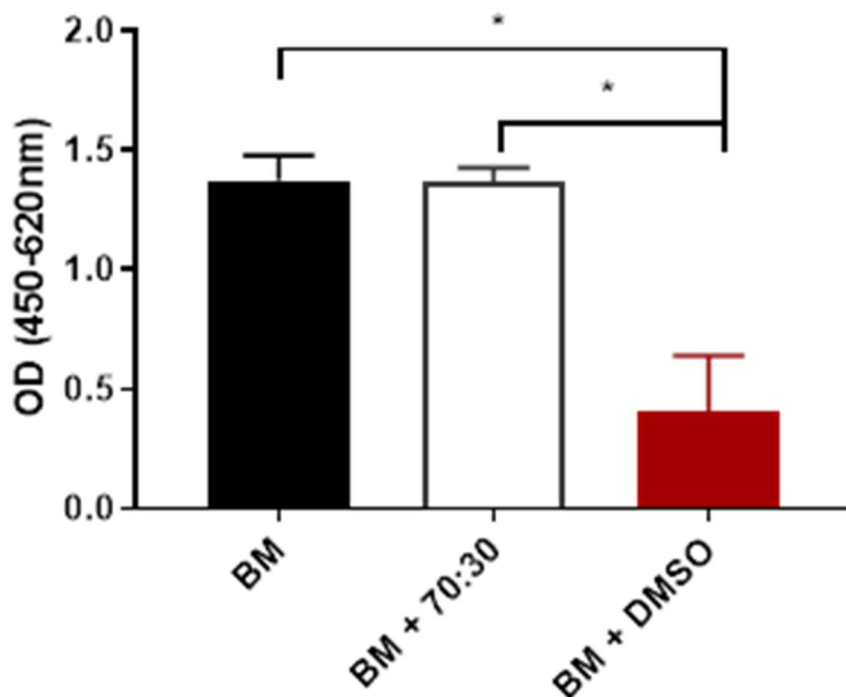


Figure 56: Average cytotoxicity results of three BM-MSC cultures exposed to basal media (BM), basal media containing 70:30 scaffold extract (BM+70:30), and basal media containing 10% DMSO (BM+DMSO). Standard error bars indicate variation between cultures ($n=3$).

6.3.2 Effect of the scaffold on BM-MSC proliferation:

Whilst the short 24 hr assay outlined in section 6.3.1 is useful to assess the effects of 70:30 scaffold's extract on BM-MSC survival a longer assay of 5 days exposure to the extract containing media is useful to assess its effect on BM-MSC proliferation. BM-MSCs were exposed to either basal media (positive control), basal media containing scaffold extract (test) or basal media containing 10% DMSO (negative control). Although no significant difference was found between the negative control and either the positive or test media, a clear trend of increased proliferation was observed in the basal media and extract containing media. The scaffold extract was found to have no significant negative effect on BM-MSC proliferation.

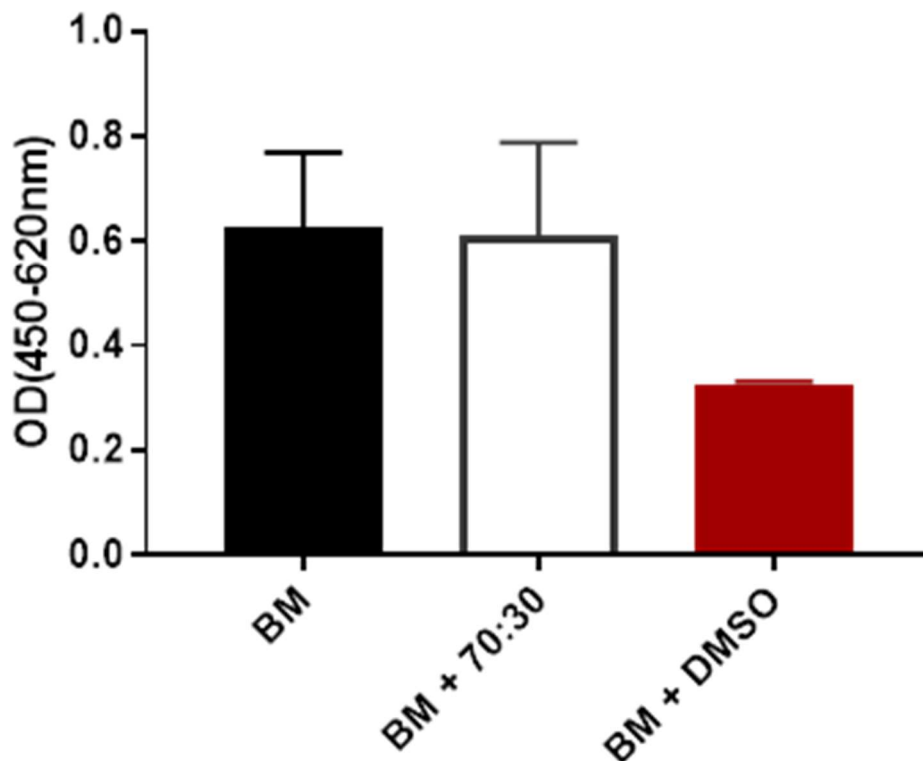


Figure 57: Average proliferation results of three BM-MSC cultures exposed to basal media (BM), basal media containing 70:30 scaffold extract (BM+70:30), and basal media containing 10% DMSO (BM+DMSO). Error bars indicate variation between cultures (n=3).

6.3.3 Measuring the scaffold's ability to absorb PRP:

To quantify 70:30 scaffold's ability to absorb PRP, the absorption capacity (weight increase normalised to area) and absorbed volume (normalised to area) were quantified for 70:30 scaffolds, control PCL scaffolds, and the current commercial control scaffold Mucograft (Geistlich). Due to limited samples available of the Mucograft scaffold only one sample was tested, whereas three scaffolds of 70:30 and PCL were tested, this discrepancy in numbers prevented statistical analysis. Despite the absence of statistics, it is apparent that both the in-house manufactured scaffolds (PCL and 70:30) appeared to have a much higher absorption capacity than Mucograft. The normalised volume absorbed suggests the scaffolds are more similar to one another than the absorption capacity data alone would indicate. This promising finding has demonstrated how the 70:30 scaffold performs at least as well as the commercial equivalent, if not better, as it appears to outperform Mucograft despite being made up of less than half its size.

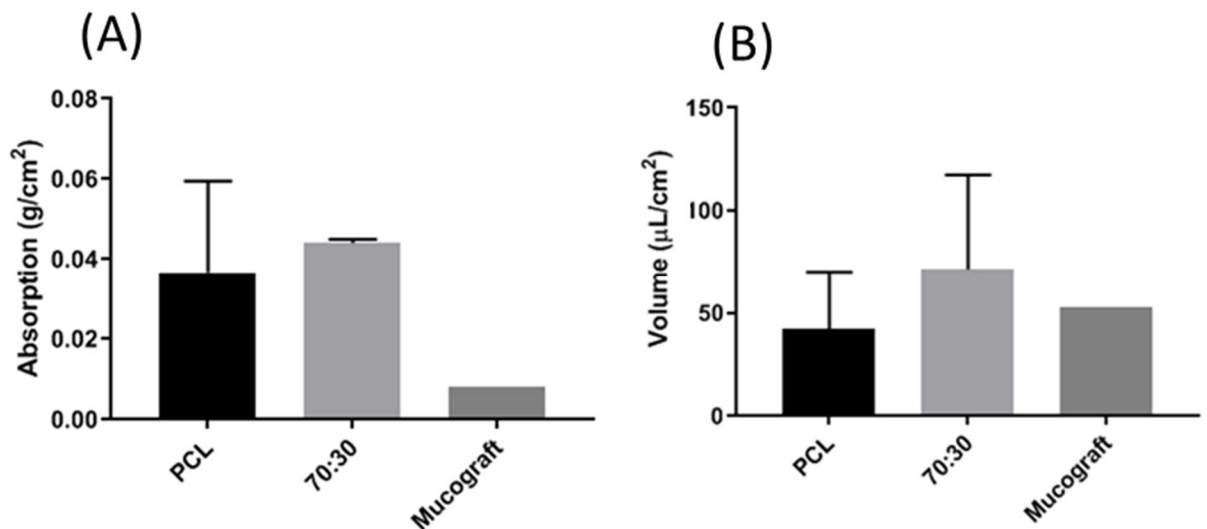


Figure 58: The results of the scaffold's average absorption capacity (A) and volume absorbed (B) both normalised to the scaffold's area. Standard error bars show variation between repeats (PCL and 70:30 n=3, Mucograft n=1).

6.3.4 Release:

To first validate the BSA assay for this application and investigate whether the albumin standard could be used as a representative surrogate for quantifying protein in PL its standard curve was compared to different concentrations of PL diluted in simulated body fluid (SBF); 1:1, 1:5 and 1:10. It can be seen in figure 59 that the standard curve of PL 1:10 provides the most reliable linear coefficient

correlation and almost directly overlays the albumin standard. This validates the albumin standard as an effective way to calculate protein concentrations in PL and demonstrates that the protein concentrations in PL can be reliably calculated using this method.

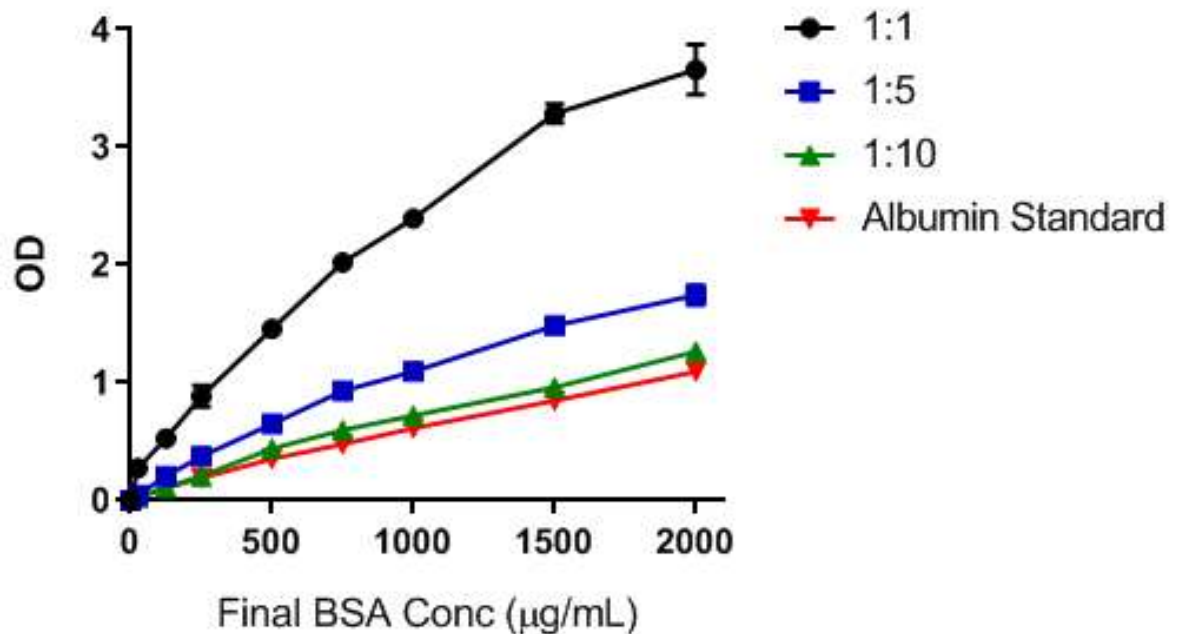


Figure 59: Optimisation of serial dilutions of PL diluted in simulated body fluid (SBF) with starting concentrations of 1:1 (PL:SBF), 1:5, and 1:10, alongside the BSA albumin standard concentrations. Error bars indicate variation between technical replicates. OD is read at 570nm.

Following protein absorbance, it was important to understand how the scaffold would release the absorbed proteins; whether the proteins would be released gradually, or rapidly as a 'burst' release. The cumulative release of PL loaded scaffolds over 60 hours is shown in figure 60 A and shows how most of the release occurs in the first 2 hrs before plateauing. As the first 2 hrs appears to be the most critical in the release kinetics, the data is shown separately in more detail (figure 60 B). It can be seen that whilst the PCL scaffolds show the most variation, they also appear to initially release most of the protein indicative of lower absorption of the PL into the scaffold and suggestive of a more superficial coating compared to 70:30 and Mucograft. The 70:30 scaffolds appear to release PRP more consistently than PCL as their data points overlay each other, the release profile compared to PCL also appears to be more gradual indicative of more absorption into the scaffold.

Although only one Mucograft scaffold was tested, it showed the most gradual release of PRP which was expected due to its sponge-like structure.

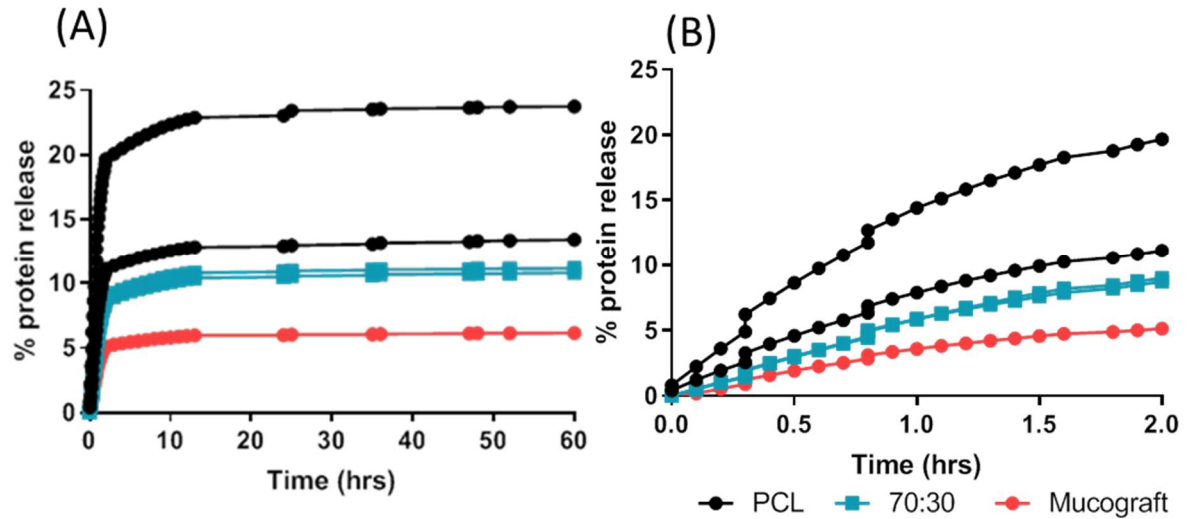


Figure 60: The cumulative protein released from the scaffolds as a percentage of the initial amount absorbed shown over 60 hours (A) and the first 2 hours (B). Each scaffold tested is shown separately; PCL $n=2$, 70:30 $n=2$, Mucograft $n=1$.

To ensure the loaded scaffolds could absorb and release enough protein to support BM-MSC proliferation, the cumulative amount released from each scaffold in the first hour was compared against the amount of protein in 10% PL (as has previously found to induce sufficient BM-MSC proliferation in the literature [21, 22] and section 5.33), the results are shown in figure 61. The amount of protein released in 10% PL (dotted line in figure 61) was found to equal $1552.5 \pm 325.1 \mu\text{g/ml}$ and all three scaffold types were found to surpass this amount with the 70:30 scaffolds releasing $2709.1 \pm 21.3 \mu\text{g/ml}$ in the first hour. The unloaded 70:30 scaffold was also included to confirm that negligible protein was released from the scaffold itself ($85.3 \mu\text{g/ml}$).

Protein conc ($\mu\text{g}/\text{mL}$) released in first hour

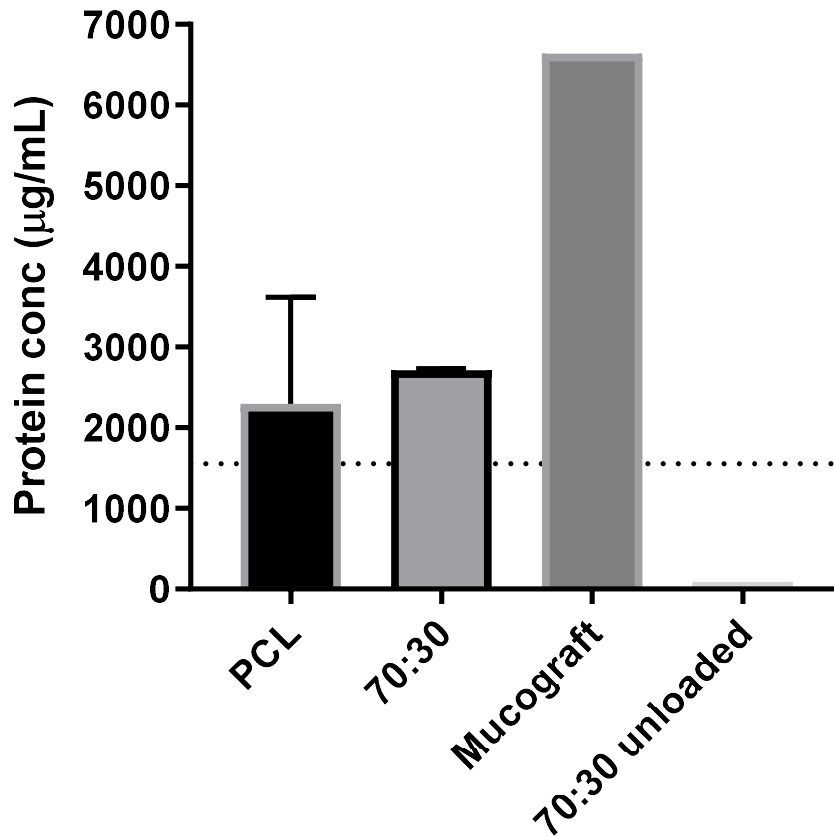


Figure 61: The results of the average cumulative amount of protein released in the first hour from PCL ($n=2$), 70:30 ($n=2$), Mucograft ($n=1$) and an unloaded 70:30 control scaffold ($n=1$).

6.3.5 Assessment of the scaffold's degradation profile:

For the initial assessment of the scaffold's degradation profile, macroscopic analysis of the membranes after 30 days hydrated in PBS was carried out (figure 62). After 30 days, no observable change to their structure or composition was found.

SEM analysis of the scaffolds showed that after 30 days, morphological changes in the fibres were prevalent (figure 63). Fibres appeared swollen and were less distinct after soaking in SBF for 30 days. Despite this expected change in the membranes' microarchitecture, the scaffolds were still found to be very much intact and resilient. This qualitative preliminary finding supports the use of the scaffolds in the modified

CFU-F assays where the scaffolds need to stay intact for over 2 weeks at 37°C in media.

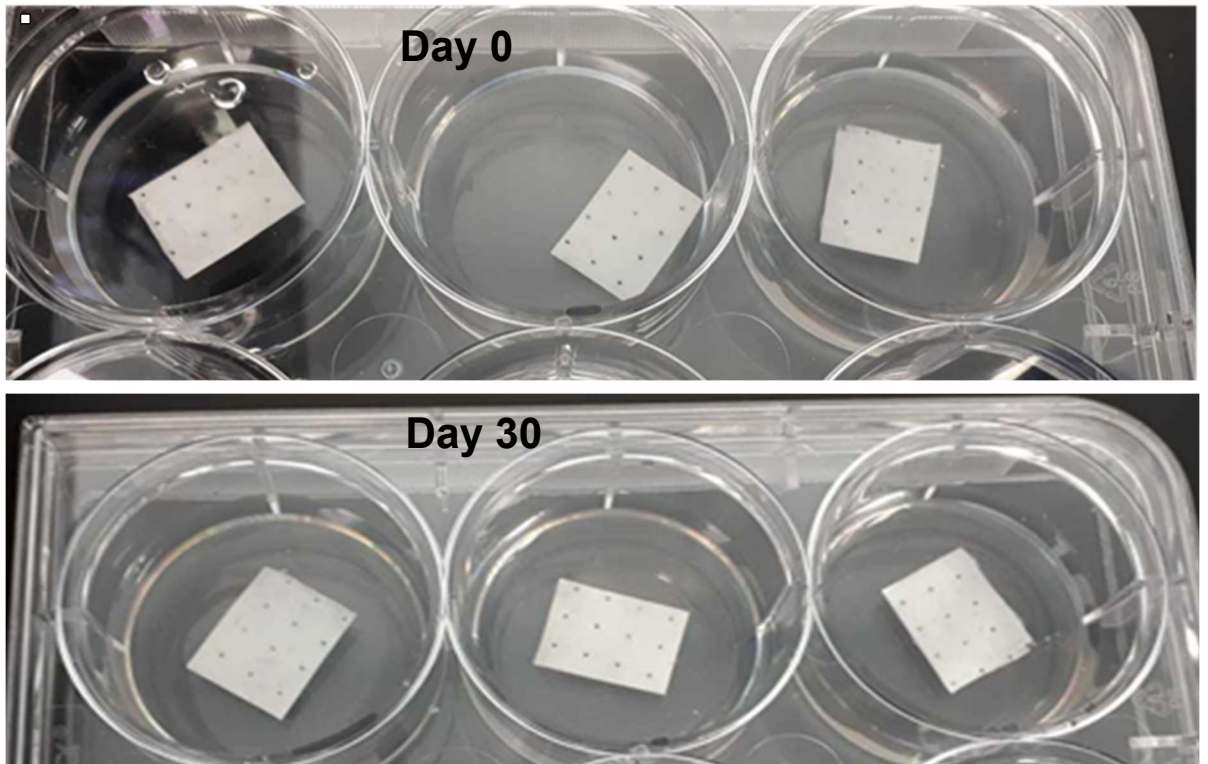


Figure 62: Degradation assay in SBF. Image shows 70:30 scaffold samples soaked in SBF at day 0 and day 30 (n=3).

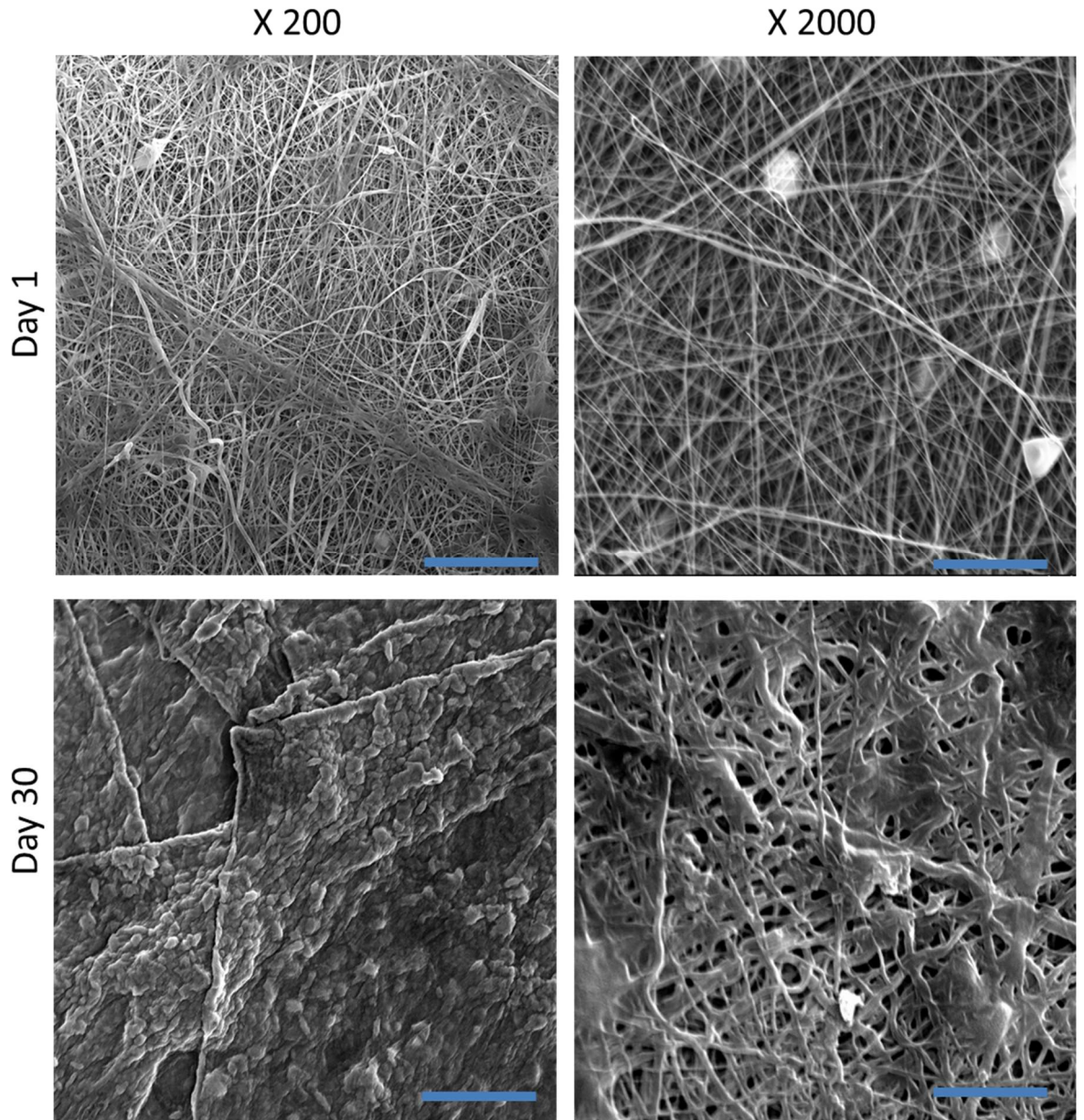


Figure 63: Degradation SEM images. SEM analysis of the 70:30 scaffolds hydrated in SBF at 37°C after 1 day and 30 days. Representative images at x200 and x2000 magnification are shown. Scale bars show 100 μm at x200 and 10 μm at x2000.

6.3.6 Loaded scaffold ability to support colony formation:

Once it was confirmed that the loaded scaffolds could absorb and release similar amounts of protein as was found in 10% PL (figure 61), and the scaffolds would stay intact over the course of the assay (figure 62 and 63), their ability to support BM-MSC colony formation was then investigated using the modified CFU-F assay. To mimic the clinical application, uncultured BM-MSCs from BM aspirates were used in these experiments. BM-MSCs were cultured in dishes containing either

standard Stem Macs expansion media (control) or basal serum-free media with the addition of a clinically approved PL (C-PL)-loaded membrane (test). Both PCL and 70:30 loaded scaffolds were tested and colony formation was observed in all test dishes. The colonies observed all had similar morphologies as shown in figure 64, and using ImageJ analysis, the colonies' area, density and number were quantified. Whilst analysis of the PCL loaded scaffolds appeared to induce fewer colonies than the control expansion media, this difference was not found to be significant and whilst fewer colonies were counted, the PCL-loaded membrane appeared to result in larger and denser colonies. A similar trend was observed in the 70:30 loaded scaffolds whereby, although no significance was found, the fewer colonies that grew were often larger and denser than the colonies in the control expansion media. These findings demonstrate how C-PL loaded membranes (both PCL and 70:30) can support the formation of rare BM-MSK colonies from BMA at least as well as expansion media, if not better.

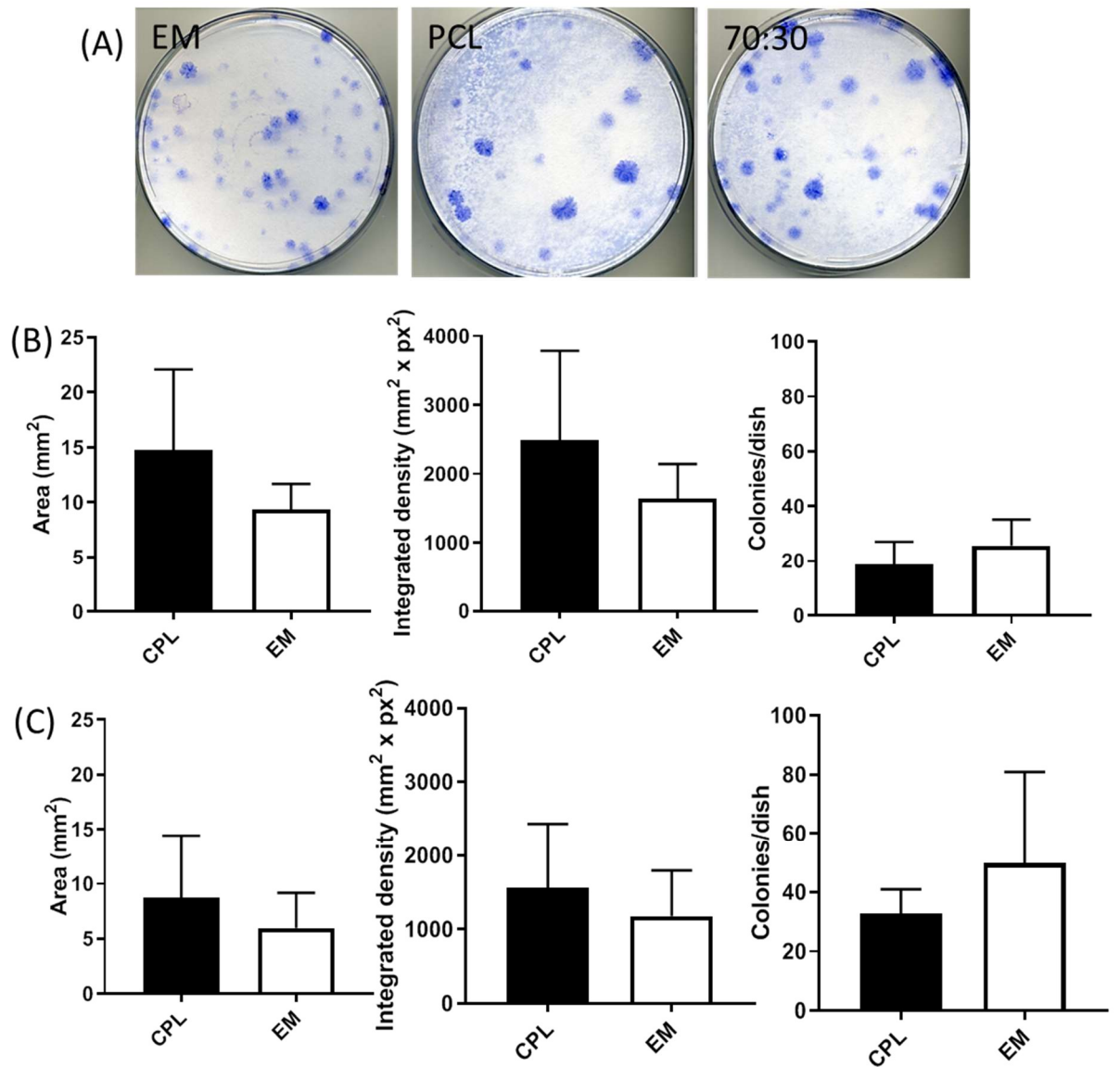


Figure 64 Modified CFU-F assay to incorporate loaded scaffolds. A) representative dishes of colonies grown in expansion media (EM), C-PL loaded PCL membrane (PCL), and a C-PL loaded 70:30 membrane (70:30). B) shows the characterisation of colonies exposed to PCL loaded membranes (n=3) whilst C) shows the characterisation of colonies cultured with 70:30 loaded scaffolds (n=3). Error bars indicate the standard error between cultures.

6.4 Discussion:

In order to test the key functions of the prototype electrospun 70:30 collagen:PCL scaffold, this exploratory pilot study investigated its cytotoxic and proliferative characteristics, as well as its ability to absorb and release proteins, its degradation profile, and its ability to support colony formation.

Promisingly, this study found the scaffold induced no cytotoxic effects on BM-MSCs nor did it inhibit BM-MSC proliferation. These characteristics are fundamental in the development of a biomaterial so were tested according to industry standard protocols. Further investigation would have included direct contact cytotoxicity, however it is accepted that eluate cytotoxicity is a reliable indicator of a material's cytotoxic effects [23, 24].

Whilst the normalised absorption capacity and volume showed some discrepancy (likely due to lack of accuracy in detecting such small changes in weight and volume), both indicate that 70:30 is as least as good as Mucograft, with regard to its ability to absorb PL, if not better, despite being less than half the size. The success of both scaffolds suggest that their structures provide sufficient mechanisms for protein uptake[25]. Furthermore, as both 70:30 and PCL scaffold have similar absorption capacities, this unexpectedly indicates that the presence of collagen doesn't significantly increase its absorption despite its hydrophilicity [26, 27]. Again, this is likely because, at this scale, it is the highly porous structure of the scaffolds that contributes to its absorption capacity, rather than its composition. It is predicted that the hydrophilic effect of collagen in 70:30 scaffolds would show significantly higher absorptive capacity than PCL only scaffold if larger samples were tested.

Although no significant difference was found between 70:30 and PCL with regards to their ability to absorb PL, their release profiles show slightly different trends. PCL has a faster release profile suggestive of a superficial coating of PL which sits in the pores rather than true absorption into the fibres of scaffold. 70:30's slower release correlates to its hydrophilic collagen content enabling absorption into the fibres and a more gradual release. Collectively, this absorbance and release data support 70:30's structure and composition as the optimum delivery material for this scaffold.

With regards to scaffold degradation, this initial qualitative assessment found that, despite some morphological changes of the fibres as was expected, overall the scaffolds were found to remain intact over the course of the assay. Further quantitative characterisation work is needed on the rate of scaffold degradation long-term and ensuring that it is able to survive the 12-week minimum regeneration

period required for bone healing. The risk of incorporating collagen into a biomaterial is that it will degrade too quickly for thorough in vitro characterisation and even more concerning, that it will degrade before it has induced sufficient tissue regeneration [26, 28]. Collagen's poor mechanical properties have restricted its use in commercial bone scaffolds where mechanical stability is required [29] however, here it has been shown that when manufactured as a composite material with PCL the scaffold has sufficient stability for in vitro testing and characterisation. Further analysis of how much collagen remains at the end of this degradation assay is needed and if the data suggests that a significant proportion of the collagen is lost and does degrade other post-manufacture processing techniques can be incorporated to enhance its longevity such as cross-linking [30]. As mentioned previously, more in-depth analysis of the scaffolds degradation profile will include measuring changes in weight over longer incubation periods as well as using EDX analysis and Sirius red staining [31] to monitor changes in composition. Incorporating cells and collagenase into future degradation assays will also result in a more accurate representation of the in vivo setting and the interaction of cells and enzymes on the scaffold as has been demonstrated by Gaspar et al [32].

Most promising of this study was the data collected from the CFUF assay which not only further validated the cytocompatibility and proliferation results, as well as demonstrated sufficient absorption and release of functional PL to support BM-MSC growth, but also confirmed practically how the loaded scaffolds could support rare BM-MSC colony formation. Both the loaded 70:30 and PCL scaffolds were found to perform at least as well as the expansion media (EM) controls and even appeared to induce larger and denser colonies which is widely believed to indicate faster proliferation [33, 34]. Because of BM-MSCs key role in bone regeneration, inducing their faster proliferation, as was observed in this study, is a valuable characteristic for a scaffold's clinical application. Despite some concerns in the literature over HFIP's toxic effects [35], this study shows how they can be overcome, alleviating any risk of cytotoxicity by allowing complete solvent evaporation.

It is of note that due to the novelty of this work, Mucograft was the only commercial scaffold that was comparable for use as a control. And due to its high cost, only a limited amount was sourced for experiments. Ideally more control scaffolds would be tested as controls alongside the prototype membranes to get a better understanding of their novelty and the role their structure and composition have on the functioning of the prototypes. Limited sample volumes were also an issue when loading the scaffolds with PL as they exceeded the volume of clinical samples available. As a solution, human PL was sourced commercially from Cook Regentec.

However as this product comes already lysed, its platelet, leukocyte and growth factor content cannot be determined and direct comparisons to the PL products tested in chapter 5 are restricted. Future development of this work would include characterisation of scaffolds loaded with 'in-house' PL and 'in-theatre' C-PL for a more accurate replication of the clinical setting.

Importantly, this chapter investigates the success of a novel ES prototype collagen-containing scaffold compared to a PCL-only control. It was found that, as both scaffolds performed well with regards to absorbance and release of PL and their ability to support colony formation, there is no distinct advantage to incorporating collagen. However, despite no significant difference observed from these assays, it is believed that the advantage of collagen's presence is still vital to scaffold properties that were not possible to investigate in this pilot study. Time constraints prevented; 1) cell attachment analysis which a study by Sousa *et al.* showed is significantly enhanced in the presence of collagen [36], 2) a more in-depth study of the scaffold's degradation profile since a PCL-only scaffold is more likely to need removal in a second surgery, whereas collagen is fully biodegradable [37],3) and enhanced vascularity [38]. The incorporation of chloroallantoic membrane (CAM) assays and subcutaneous implantation into animal in vivo models [39] are the next stages to demonstrate the need for collagen for optimal integration and biocompatibility.

Whilst more in-depth functional characterisation work is needed on the prototypes, this pilot study has demonstrated the potential application of this scaffold and fulfilled the initial criteria set out for a successful guided bone regeneration device. The work contributes towards optimised bone healing and the development of future scaffolds.

6.5 References:

1. Kozlovsky, A., et al., Bio-degradation of a resorbable collagen membrane (Bio-Gide) applied in a double-layer technique in rats. *Clin Oral Implants Res*, 2009. **20**(10): p. 1116-23.
2. Stankovic, D., et al., *Use of acellular collagen matrix for the closure of the open oral wound in bone regeneration*. *Journal of Stomatology, Oral and Maxillofacial Surgery*, 2018. **119**(5): p. 446-449.
3. Christou, C., et al., The Masquelet Technique for Membrane Induction and the Healing of Ovine Critical Sized Segmental Defects. *PLOS ONE*, 2014. **9**(12): p. e114122.
4. Dimitriou, R., et al., The role of barrier membranes for guided bone regeneration and restoration of large bone defects: current experimental and clinical evidence. *BMC Medicine*, 2012. **10**: p. 81-81.

5. Jepsen, K., et al., Treatment of gingival recession defects with a coronally advanced flap and a xenogeneic collagen matrix: a multicenter randomized clinical trial. *J Clin Periodontol*, 2013. **40**(1): p. 82-9.
6. Dahlin, C., et al., *Healing of bone defects by guided tissue regeneration*. *Plast Reconstr Surg*, 1988. **81**(5): p. 672-6.
7. Dahlin, C., et al., Healing of maxillary and mandibular bone defects using a membrane technique. An experimental study in monkeys. *Scand J Plast Reconstr Surg Hand Surg*, 1990. **24**(1): p. 13-9.
8. Schlegel, A.K., et al., Preclinical and clinical studies of a collagen membrane (Bio-Gide®). *Biomaterials*, 1997. **18**(7): p. 535-538.
9. Ramalingam, S., et al., Efficacy of Mucograft vs Conventional Resorbable Collagen Membranes in Guided Bone Regeneration Around Standardized Calvarial Defects in Rats: A Histologic and Biomechanical Assessment. Vol. 36 Suppl. 2016. s99-s107.
10. Shan, X. and D. Hu, *Bone engineering by cell sheet technology to repair mandibular defects*. *Experimental and therapeutic medicine*, 2017. **14**(5): p. 5007-5011.
11. Giannoudis, P.V., et al., Simultaneous bilateral femoral fractures: systemic complications in 14 cases. *Int Orthop*, 2000. **24**(5): p. 264-7.
12. Noritake, K., et al., Development of a New Barrier Membrane for Guided Bone Regeneration: an in Vitro and in Vivo Study. *Journal of Oral Tissue Engineering*, 2011. **9**(2): p. 53-63.
13. Rodriguez, I.A., et al., Platelet-rich plasma in bone regeneration: engineering the delivery for improved clinical efficacy. *Biomed Res Int*, 2014. **2014**: p. 392398.
14. Giannoudis, P.V., T. Einhorn, and D. Marsh, *Fracture healing: the diamond concept*. *Injury* 2007. **4**: p. 3-6.
15. Yun, J.H., et al., Effects of bone marrow-derived mesenchymal stem cells and platelet-rich plasma on bone regeneration for osseointegration of dental implants: preliminary study in canine three-wall intrabony defects. *J Biomed Mater Res B Appl Biomater*, 2014. **102**(5): p. 1021-30.
16. Giannoudis, P.V., et al., Restoration of long bone defects treated with the induced membrane technique: protocol and outcomes. *Injury*, 2016. **47**: p. S53-S61.
17. Douras, P., T. Tosounidis, and P.V. Giannoudis, Application of the 'diamond concept' with fast bone marrow aspirate concentration for the treatment of medial malleolus non-union. *Injury*, 2018. **49**(12): p. 2326-2330.
18. Sung-Baek Cho, K.N., Tadashi Kokubo, Naohiro Soga, Chikara Ohtsuki, Takashi Nakamura, Toshiaki Kitsugi, Takao Yamamuro, *Dependence of apatite formation on silica gel on its structure: effect of heat treatment*. *J Am Ceram Soc*, 1995. **78**: p. 1769-974.
19. Kamath, M.S., et al., Polycaprolactone scaffold engineered for sustained release of resveratrol: therapeutic enhancement in bone tissue engineering. *International journal of nanomedicine*, 2013. **9**: p. 183-195.
20. Swinehart, D.F., *The Beer-Lambert Law*. *Journal of Chemical Education*, 1962. **39**(7): p. 333.
21. Soleimani, M. and S. Nadri, A protocol for isolation and culture of mesenchymal stem cells from mouse bone marrow. *Nat Protoc*, 2009. **4**(1): p. 102-6.
22. Pittenger, M.F., *Mesenchymal Stem Cells from Adult Bone Marrow*, in *Mesenchymal Stem Cells: Methods and Protocols*, D.G.P. D.J. Prockop, and B.A. Bunnell, Editor. 2008, Humana Press: Totowa, NJ. p. 27-31.
23. Oshima, H. and M. Nakamura, *A study on reference standard for cytotoxicity assay of biomaterials*. *Biomed Mater Eng*, 1994. **4**(4): p. 327-32.
24. Van Tienhoven, E.A., et al., In vitro and in vivo (cyto)toxicity assays using PVC and LDPE as model materials. *J Biomed Mater Res A*, 2006. **78**(1): p. 175-82.
25. Abdal-hay, A., et al., Fabrication of Highly Porous Biodegradable Biomimetic Nanocomposite as Advanced Bone Tissue Scaffold. Vol. 10. 2016.

26. Brett, D., A Review of Collagen and Collagen-based Wound Dressings. *Wounds*, 2008. **20**(12): p. 347-56.
27. Tronci, G., The application of collagen in advanced wound dressings. 2018.
28. Guan, J., J.J. Stankus, and W.R. Wagner, Development of Composite Porous Scaffolds Based on Collagen and Biodegradable Poly(ester urethane)urea. *Cell transplantation*, 2006. **15**(Suppl 1): p. S17-S27.
29. Parenteau-Bareil, R., R. Gauvin, and F. Berthod, *Collagen-Based Biomaterials for Tissue Engineering Applications*. *Materials*, 2010. **3**(3): p. 1863-1887.
30. Davidenko, N., et al., Control of crosslinking for tailoring collagen-based scaffolds stability and mechanics. *Acta Biomaterialia*, 2015. **25**: p. 131-142.
31. Lattouf, R., et al., Picosirius red staining: a useful tool to appraise collagen networks in normal and pathological tissues. *J Histochem Cytochem*, 2014. **62**(10): p. 751-8.
32. Gaspar, A., et al., *Collagen-based scaffolds for skin tissue engineering*. *Journal of medicine and life*, 2011. **4**(2): p. 172-177.
33. Gothard, D., J.I. Dawson, and R.O.C. Oreffo, Assessing the potential of colony morphology for dissecting the CFU-F population from human bone marrow stromal cells. *Cell and Tissue Research*, 2013. **352**(2): p. 237-247.
34. Cuthbert, R., et al., Single-platform quality control assay to quantify multipotential stromal cells in bone marrow aspirates prior to bulk manufacture or direct therapeutic use. *Cytotherapy*, 2012. **14**(4): p. 431-40.
35. Nam, J., et al., Materials selection and residual solvent retention in biodegradable electrospun fibers. *Journal of Applied Polymer Science*, 2008. **107**(3): p. 1547-1554.
36. Sousa, I., A. Mendes, and P.J. Bártolo, *PCL Scaffolds with Collagen Bioactivator for Applications in Tissue Engineering*. *Procedia Engineering*, 2013. **59**: p. 279-284.
37. Gentile, P., et al., Biosynthetic PCL-graft-Collagen Bulk Material for Tissue Engineering Applications. *Materials (Basel, Switzerland)*, 2017. **10**(7): p. 693.
38. Bertram, U., et al., Vascular Tissue Engineering: Effects of Integrating Collagen into a PCL Based Nanofiber Material. *BioMed research international*, 2017. **2017**: p. 9616939-9616939.
39. Singh, S., B.M. Wu, and J.C.Y. Dunn, *Delivery of VEGF using collagen-coated polycaprolactone scaffolds stimulates angiogenesis*. *Journal of biomedical materials research. Part A*, 2012. **100**(3): p. 720-727.

7 Conclusions

As outlined at the start, the aim of this project was to design and develop a biomimetic collagen-based membrane, modelled on the IM, to act as a guided bone regeneration device for long bone fracture repair. The key properties of the pilot membrane were for it to be biocompatible, have appropriate mechanical strength, to absorb and release PRP, and to support BM-MSC proliferation.

To begin the design process, the IM tissue that was to be mimicked had to be characterised. Using histological techniques, the IM was found to be thicker than periosteum, to have less distinct layers than expected and to drastically vary in blood vessel size and overall thickness between donors. These differences are thought to be due to differences in age, anatomical location and fracture severity between donors. Despite a small sample size of 7 donors these findings were translated into the design process by widening the acceptance criteria of the scaffold's thickness, porosity and fibre diameter. As well, due to the rarity of human IM samples, this analysis contributed to the relatively small amount of existing literature on the human IM's structure and microarchitecture. Analysis of the IM's birefringence was particularly novel and revealing of the collagen fibrils organisation. If further defined in a larger study with a wider donor pool, this information could enhance our understanding of optimal fibre orientation of manufactured scaffolds.

Based on the samples that were harvested and characterised, it was decided that the biomimetic scaffold would be made of a blend of collagen and PCL to meet the criteria of biocompatibility and mechanical properties. Needleless electrospinning was also chosen with clinical translation in mind as well as its ability to manufacture highly porous scaffolds. This technique was found to successfully produce consistent scaffolds composed of up to 70% collagen with sub-micron fibre diameters. The small fibre diameter contributed to a dense construct with over 80% of pores being smaller than 4 μm . As has been outlined, PCL was chosen as the polymer of choice because of its prevalent use in existing biomedical devices however, future development of this project would incorporate a larger polymer library. Co-polymers also pose an interesting avenue to pursue, for example PLGA which is made from a blend of poly lactic acid and glycolic acid, the ratios of which can be adjusted to tailor the final scaffold's degradation and hydrophilicity [1]. Other more novel scaffolds could be investigated such as polyurethane which has, elastic properties that could be interesting to incorporate [2] and composites such as poly

lactic acid blended with hydroxyapatite particles which have already shown promising results [3].

Although some manufacturing problems were encountered, for example; the thinner than designed membranes and the small inherent pore size, the multidisciplinary aspect of the project resulted in innovative solutions such as heat-treating, folding and laser cutting. As well, despite these problems being not initially expected they were not entirely negative results. For example, the sub-micron pore sizes of the scaffold could be useful in drug-delivery applications or wound healing where barrier membranes with high surface area are desirable [4, 5]. Furthermore, laser cutting the pores into the scaffolds proved to further improve their strength by acting as anchoring points between the layers and annealing the construct overall.

In order to attract and amplify BM-MSCs to the site of injury, chemoattractants and growth factors from platelet lysate (PL) were analysed. It was decided that, as BM-MSC proliferation and migration were fundamental in ensuring optimal bone healing, these two functions would be the focus of analysing PL's success. Promisingly, PL was found to induce as much BM-MSC proliferation as FCS (the standard culture medium supplement) as well as out-perform FCS at inducing BM-MSC migration regardless of its cell composition. The main conclusion that can be drawn from this body of work is that low platelet numbers, rather than high leukocyte numbers, are responsible for limiting PL's proliferative and migratory effects. These findings contribute towards the development of xeno-free cell culture techniques specifically useful for tissue engineering applications. Whilst leukocytes were not found to have any observable negative effects, a future study could include 'doping' filtered pure plasma with known numbers of leukocytes and platelets to be truly certain of their roles.

To bring all the research together, the manufactured collagen membrane was functionally tested with clinical translation in mind using industry standard protocols where possible. The scaffold was found to have no harmful cytotoxic effects nor limit BM-MSCs proliferation capacities compared to standard culture media. As well, the scaffolds were found to sufficiently absorb and release proteins sourced from PL, withstand initial degradation assays as well as support colony formation. Although this pilot data is *in vitro* based, it still provides a promising indication into the scaffold's ability to endure future *in vivo* testing. Most exciting was the 70:30 scaffolds absorption capacity that was found to be similar to a commercial scaffold despite being less than half its size. Collectively, this absorbance and release data

support the structure and composition of the 70:30 scaffold as the optimum delivery material.

Previously, collagen's poor mechanical properties have restricted its use in commercial scaffolds where mechanical stability is required however, here it has been shown that when manufactured as a composite material with PCL the scaffold has sufficient stability to withstand *in vitro* testing. Further characterisation work is needed on the rate of scaffold degradation long-term and ensuring that it is able to survive the 12-week minimum regeneration period required for bone healing [6, 7]. How much collagen is retained over the course of a degradation assay could also be carried out using a picro Sirius red assay in parallel to the degradation assay using sacrificial samples at time points throughout the experiment. If the data suggests that a significant proportion of the collagen is lost and does degrade other post-manufacture processing techniques can be incorporated to enhance its longevity (such as cross-linking) [8, 9].

The final experiment of this research brought together all the aspects studied throughout using CFU-F assay with a PL-loaded scaffold. This data not only validated the absence of any cytotoxic effects of the scaffold, but also demonstrated the ability to absorb and release sufficient PL to support rare BM-MSC colony formation. Both the loaded 70:30 and PCL scaffolds were found to perform at least as well as the standard culture media and even appeared to induce faster proliferation (indicated by larger, denser colonies). However, interestingly, no significant difference was observed between the 70:30 and PCL scaffolds in their ability to induce colony formation. This lack of difference between the scaffolds could result from the assay not being a direct contact assay, where the cells are cultured directly onto the scaffold. Cell attachment and proliferation on the scaffold would be a useful indicator for how the cells interact with, and are supported by the scaffold, and would be a priority experiment in the next stage of this work. Because of BM-MSCs key role in bone regeneration, inducing their faster proliferation, as was observed in this study, is a valuable characteristic for a scaffold's clinical application. Despite concerns over HFIP's toxic effects, this study found no cytotoxic effect caused by the scaffolds, indicative of complete solvent evaporation, however residual HFIP would be a priority to test and quantify before any clinical translation. To fully test the abilities of this scaffold, importantly its cell attachment and *in vivo* vascularisation, intergration and degradation profile chlorioallantoic membrane (CAM) assays [10, 11] and subcutaneous implantation into animal *in vivo* models [11, 12] are the next stages of research. Further study into the effect of different pore sizes and densities on the scaffolds mechanical properties would also

be carried out as well as incorporation of post-processing techniques, such as plasma treating the surface of the scaffold, to enhance hydrophilicity and cell attachment.

Collectively, this work has advanced the field of tissue engineering by developing and applying a novel technique and a novel material to successfully create a biomimetic scaffold with quantities of collagen that was initially not thought possible at the start of this project. The continuation of this work, and its translation into clinical manufacturing would result in the streamlining of a two-stage surgical procedure into a single-stage procedure resulting in significant savings to the NHS, faster healing times for patients, shorter hospital stays, and time saved for surgeons. The interactions between cells, growth factors and scaffolds are also now better understood which would have a wider impact on the field of tissue engineering as a whole, outside of orthopaedics, and the ability to manufacture scaffolds in this way could result in the production of dermal patches, cartilage implants, corneal scaffolds to name a few.

This study has demonstrated the potential application of a biomimetic collagen-PCL scaffold and fulfilled the initial criteria set out to create a guided bone regeneration device. The work contributes towards optimised bone healing and the development of future scaffolds.

7.1 References:

1. Franco, R.A., T.H. Nguyen, and B.-T. Lee, Preparation and characterization of electrospun PCL/PLGA membranes and chitosan/gelatin hydrogels for skin bioengineering applications. *Journal of Materials Science: Materials in Medicine*, 2011. **22**(10): p. 2207-2218.
2. Guan, J., J.J. Stankus, and W.R. Wagner, Development of Composite Porous Scaffolds Based on Collagen and Biodegradable Poly(ester urethane)urea. *Cell transplantation*, 2006. **15**(Suppl 1): p. S17-S27.
3. Shim, J.-H., et al., Fabrication of Blended Polycaprolactone/Poly (Lactic-Co-Glycolic Acid)/ β -Tricalcium Phosphate Thin Membrane Using Solid Freeform Fabrication Technology for Guided Bone Regeneration. *Tissue Engineering. Part A*, 2013. **19**(3-4): p. 317-328.
4. Jun, I., et al., Electrospun Fibrous Scaffolds for Tissue Engineering: Viewpoints on Architecture and Fabrication. *Int J Mol Sci*, 2018. **19**(3).
5. Ding, Y., et al., Electrospun Fibrous Architectures for Drug Delivery, *Tissue Engineering and Cancer Therapy*. Vol. 29. 2019. 1802852.
6. Dimitriou, R., et al., *Bone regeneration: current concepts and future directions*. *BMC Medicine*, 2011. **9**: p. 66-66.
7. Sousa, C.P., et al., Evaluation of bone turnover markers and serum minerals variations for predicting fracture healing versus non-union processes in adult sheep as a model for orthopedic research. *Injury*, 2017. **48**(8): p. 1768-1775.

8. Arafat, M.T., et al., Biomimetic wet-stable fibres via wet spinning and diacid-based crosslinking of collagen triple helices. *Polymer*, 2015. **77**: p. 102-112.
9. Davidenko, N., et al., Control of crosslinking for tailoring collagen-based scaffolds stability and mechanics. *Acta Biomaterialia*, 2015. **25**: p. 131-142.
10. Rameshbabu, A.P., et al., Polycaprolactone nanofibers functionalized with placental derived extracellular matrix for stimulating wound healing activity. *Journal of Materials Chemistry B*, 2018. **6**(42): p. 6767-6780.
11. Singh, S., B.M. Wu, and J.C.Y. Dunn, *Delivery of VEGF using collagen-coated polycaprolactone scaffolds stimulates angiogenesis*. *Journal of biomedical materials research. Part A*, 2012. **100**(3): p. 720-727.
12. Van Tienhoven, E.A., et al., In vitro and in vivo (cyto)toxicity assays using PVC and LDPE as model materials. *J Biomed Mater Res A*, 2006. **78**(1): p. 175-82.

8 Appendix 1

8.1 Standard solutions:

Cell freezing media

90% FCS, 10% DMSO

Formaldehyde

4% formalin solution (v/v) in PBS

Methylene blue solution

1% (w/v) methylene blue dissolved in 10mM disodium tetraborate (pH 8)

Basal media

DMEM, 1% Penicillin/Streptomycin (v/v)

Expansion media

Stem Macs media, 1% Penicillin/Streptomycin (v/v)

Simulated body fluid

dH₂O 1000ml, Sodium chloride (NaCl) 8.04g, Sodium bicarbonate (NaHCO₃) 0.36g, Potassium chloride (KCl) 0.23g, Potassium Hydrogen Phosphate Trihydrate (K₂HPO₄ 3H₂O) 0.23g, Magnesium Chloride (MgCl₂ 6H₂O) 0.31g, 1.0_M Hydrochloric acid (HCL) 39ml, Calcium chloride (CaCl₂) 0.29g, Sodium sulphate (Na₂SO₄) 0.07g, Tris(hydroxymethyl)aminomethane 6.12g, adjust to pH 7.4 with 1.0_M-HCL.

9 Appendix 2:

9.1 Consumables:

Consumables	Manufacturer
Acrodisc white blood cell strainer	Pall Life sciences
Cell Strainer (70 mm)	BD Falcon
CFU-F dish (15mm)	Corning
Cryovials (1.8 mL)	Nunc
Eppendorf tubes	Eppendorf
Falcon Tubes (15 mL, 50 mL)	Corning
Flat bottom well plates – (6, 12, 24, 48, 96 well)	Corning
Histology Slide Covers	Thermo Scientific
Mr Frosty Freezing Container	Thermo Scientific
Mucograft scaffold	Geistlich
Non Tissue Culture Treated Plates (6, 12 well)	Cellstar
Pipette Tips (10 mL, 1000 mL)	Anachem
Scalpel	Swann Morton
SEM Specimen Stubs and Mounts	Agar Scientific
Strippete (5 mL, 10 mL, 25 mL)	Corning
SuperFrost Plus Histology Slides	Thermo Scientific
Syringe (10 mL)	BD Biosciences
Tissue Culture Flasks (25 cm³)	Corning
Tissue Culture Round Dishes (100 mm or 60 mm diameter)	Corning
Vacurette blood tubes (EDTA and ACD-A)	Greiner Bio-one

9.2 Equipment:

Equipment	Manufacturer
Auto Sputter Coater	Agar Scientific
AL54 Scales	Mettler Toledo
Attune 2 Laser System Flow Cytometer	Applied Biosystems
Attune software	Applied Biosystems
Bevel Tipped Trocar	Stryker
Centrifuge 5415D	Eppendorf
Centrifuge 5810R	Eppendorf
CKX41/BX45Microscope	Olympus
Class II Laminar Flow Biological Safety Cabinet	Nuaire
CO₂ Incubator InCuStage	Sanyo
Epsom 3590 Photo Scanner	Epsom
Freezer (-80 C)	New Brunswick Scientific
Gilson Pipette	Gilson
GX Microscope	GX Microscope
Haematology analyser	Sysmex
Haemocytometer	Hawksley
Hitachi 5-3400N SEM	Hitachi
Hitachi 5-3400N SEM Software	Hitachi
Hot Plate	Stuart Scientific
ImageJ Software	ImageJ
IncuCyte	Essen
Infinity 1 Camera	Lumenera
Infinity Image Acquisition software	Lumenera
Laser cutter FB700	FB series

Mucograft	Geistlich
NanoSpider NS Lab	Elmarco
Porolux 100FM	Porometer
ProGage Thickness Tester	Thwing-Albert Instrument Company
Tissue Processor – ASP200	Leica
Tensile Testing Machine	James Heal

9.3 Solutions:

Solution	Supplier
1.0M Hydrochloric acid (HCL)	Sigma Aldrich
2-Propranolol	Sigma-Aldrich
Acetic acid	Sigma Aldrich
Albumin standard 2mg/mL	Thermo Scientific
Alcian blue	Sigma-Aldrich
Ammonium Chloride Solution	Stemcell Technologies
BCA	Thermo Scientific
Calcium chloride (CaCl ₂)	Thermo Scientific
Dimethyl sulfoxide Hybri-Max	Sigma-Aldrich
DNase	Sigma life science
DPX mountant	Dako
Dulbecco's modified eagles medium (DMEM)	Sigma-Aldrich
Eosin	VWR international
Ethanol	Fisher Scientific
Faetal calf serum	Bio Sera
Formaldehyde (37%)	Fisher Scientific
Haematoxylin	VWR international
Haematoxylin Weigerts (solution A)	Atom Scientific
Haematoxylin Weigerts (solution B)	Atom Scientific
Heparin Sodium 1000 IU/ml	Fannin
HFIP (purity > 99.0%)	Sigma
Human platelet lysate	Cook Regentec
Magnesium Chloride (MgCl ₂ 6H ₂ O)	Sigma Aldrich
Magnesium Sulphate	Sigma
Mesencult serum	Stemcell Technologies
Methyl Blue 2% in 2.5% Acetic Acid	Atom Scientific
Paraffin Wax	Cell Path
PCL (Mn: 80 000 g mol ⁻¹)	Sigma
Penicillin/Streptomycin	Thermo Fisher

Perfluoroether	Galpore
Phosphate buffered saline (PBS)	Sigma-Aldrich
Phosphotungstic Acid (1%)	Atom Scientific
Ponceau Fuchsin (Masson)	Atom Scientific
Potassium chloride (KCl)	Thermo Scientific
Potassium Hydrogen Phosphate Trihydrate (K₂HPO₄ 3H₂O)	Sigma Aldrich
Scott's Tap Water	Sigma-Aldrich
Sirius Red Powder	Atom Scientific
Sodium Bicarbonate	Sigma
Sodium bicarbonate (NaHCO₃)	Sigma Aldrich
Sodium chloride (NaCl)	Sigma Aldrich
Sodium hydroxide	Sigma Aldrich
Sodium sulphate (Na₂SO₄)	Sigma Aldrich
Stem Macs	Miltenyi Biotec
Tris(hydroxymethyl)aminomethane	Thermo Scientific
Trypan Blue Solution (0.4%)	Sigma-Aldrich
Trypsin	Gibco
XTT Cell Viability Assay	Thermo Scientific
Xylene	Atom Scientific

10 Appendix 3

10.1 Patient Consent form

The Leeds Teaching Hospitals 
NHS Trust

PATIENT CONSENT FORM

Collec

Prof Peter Giannoudis

Patient Name:

Patient Identification Num

Please circle as appropriate

- 1. I have read the patient information sheet for the above study. Yes/No
- 2. I have had the opportunity to ask questions about the study and to discuss it with family and friends if I so wish to. Yes/No
- 3. I understand the purpose of the study, and how I will be involved. Yes/No
- 4. I understand, and accept, that if I take part in the study I may not gain direct personal benefit from it. Yes/No
- 5. I understand that all information collected in the study will be held in confidence and that, if it is presented or published, all my personal details will be removed. Yes/No
- 6. I give permission for responsible individuals from regulatory authorities to have access to my medical notes where it is relevant to my taking part in the research. This is on the understanding that no personal details which might identify me will be presented or published without my permission. Yes/No
- 7. I confirm that I will be taking part in this study of my own free will, and I understand that I am free to withdraw from the study at any time without giving a reason and without affecting my future care or legal rights. Yes/No
- 8. I have spoken to Dr P Giannoudis
- 9. I agree to take part in this research study.

PATIENT:

Signed:

Date: 23/3/16

Name (BLOCK CAPITALS):

Investigator/Sub-investigator

I have explained the study to the above named participant and he/she has indicated his/her willingness to participate

Signed: [Signature] Date: 23/3/16

Name (BLOCK CAPITALS): P Giannoudis